Tectonic and fluvial geomorphology of the Zagros fold-and-thrust belt

AHMED KADHIM OBAID

Tectonic and fluvial geomorphology of the Zagros fold-and-thrust belt

Ahmed Kadhim Obaid B.Sc., M.Sc.

A thesis submitted in partial fulfilment of the requirements for the degree of Doctor of Philosophy at Durham University

Department of Earth Sciences, Durham University

September 2018

Contents

List of figures

List of tables

Abstract

The Zagros-fold-and thrust belt has been selected to explore landscape responses to tectonic and climatic drivers using river profile steepness (k_{sn}), relief from topography, and basin scale Hypsometric Index (HI) extracted from Shuttle Radar Topography Mission (SRTM) 30 m dataset. There are differences in the k_{sn} and the HI value from one area to another across the Zagros range. The northeastward presence of high HI values with respect to the seismicity cut-off in the combined Dezful/Bakhtyari region is attributed to wetter conditions, in turn driven by high strain and high topographic gradients in the Bakhtyari region. Drier climate and low power rivers in the Fars region promote plateau growth, and high HI values occur south of the thrust seismicity cut-off. In spite of the regional differences in k_{sn} and HI, there is a similarity in the integrated relief along swath profiles, consistent with the similar rate of strain and total strain across different parts of the Zagros.

Digital Elevation Model (DEM)-based geomorphic indices; Hypsometric Index (HI), Surface Roughness (SR) and their combination Surface Index (SI) have been applied to quantify landscape maturity in the Kirkuk Embayment of the Zagros. Landscape maturity suggests out of sequence deformation towards the hinterland in opposite sense to classical 'piggyback' thrusting model. The SI shows new previously undiscovered anticlines of hydrocarbon potential. New balanced cross-section indicates shortening in the order of ~5% in the Zagros foreland.

Basin-scale values of HI exhibit sharp boundary of the low/high HI transition in the south of the Himalaya consistent with the zone of the Main Himalayan Thrust (MHT), and indicate the controls of the MHT on Himalayan topography. Smaller magnitude increases in HI value across the physiographic transition (PT_2) do not support the out-of-sequence model of active deformation of Himalayan tectonics.

Point-counting technique was conducted for modern river sand from the Zagros suture and the Neogene sandstones of the Zagros foreland. Results show recycled orogen provenance and litharenite composition and spatial increase in quartz content towards the northwest, which might refer to provenance change and/or drainage reorganization. The more lithic composition of river sand and the Neogene sandstone refers to an uplift of the Zagros suture area, which is partly caused by the out-of sequence deformation of the Mountain Front Fault.

Declaration

The proposed work in this thesis has not been submitted previously for an academic degree in this or any other university. The thesis entirely is my own work and includes no outcome which is done by others except where reference is made to previously published or unpublished work.

Ahmed Kadhim Obaid

Department of Earth Sciences

Durham University

September 2018

Acknowledgments

First and foremost I would like to express my great thanks and appreciation to my supervisors, Professor Mark B. Allen and Professor Kenneth McCaffrey for their guidance and support. I owe a great deal to Mark Allen for his great guidance, motivation, very fruitful discussion during my Ph.D. study and other scientific and personal support, which built my skills in the academic research field. His notes and deep focusing on the minor things will be kept in my mind forever. According to my culture, I pray to him to be in a full health and happiness in his future life.

My gratitude goes to the Ministry of Higher Education and Scientific Research (MOHSR) in Iraq for funding my Ph.D. study.

Many thanks to my best colleagues in the Institution of Geological Survey in Iraq (GEOSURV), Ahmed T. Shihab, Ahmed F. Al-Maamar and Dr. Arsalan A. Othman for their help and discussions. Special thanks to my friend Ahmed T. Shihab, Professor Diary M. Ameen (head of Earth Sciences department in the University of Sulaimaniya, Kurdistan, Iraq), Dr. Sarkawt G. Salar (Department of Geography, Garmian University, Kurdistan, Iraq and Mr. Othman Aljaf for their help and elimination of fieldwork difficulties.

I would like to thank the very friendly reviewers' team (Associate Professor Stuart Jones and Professor Gillian Foulger) who put my Ph.D. project in the right path. Also, I like to thank Associate Professor Sarah Boulton in the school of Geography, Earth and Environmental Sciences, Plymouth University for her generous help in the installation of the Stream profiler software and her discussion during the events of the BSG conferences.

I will never forget to thank my friends, the Iraqi PhD students Ali Lilo, Jaafar Jotheri, Amjed Qais, Sinan Azzawi and Omar Saleh for maintainings our weekly meeting and enjoyable times which helped me so much during my Ph.D. study. All colleagues from the Department of Earth Sciences, University of Durham deserve my gratitude and specifically Chimaobi Nwachukwu, Elizabeth Atar, Sean O'Neill and Dimitrios Michelioudakis for their very kind attitude.

In addition, I’m grateful to the researchers who reviewed the manuscripts included in this thesis; their comments and suggestions enriched the results of this study

My gratitude goes to researchers from different universities and institutions that provided supporting maps contained in this thesis. Those are Mozhgan Ahmadi (Islamic Azad University, Iran), John Cannon (Houston University, USA) and Victoria Stevens (California Institute of Technology, USA).

Finally, I have to thank my family and especially my wife (Lamees) who did her best to be a wife, mother of two kids and a Ph.D. student at the same time.

This thesis is dedicated to the memory of my mother

Ahmed

Chapter 1

1. Introduction

1.1 Rationale

The Zagros region is an important area for studies of continental deformation as it forms part of the active Arabia-Eurasia collision zone. Therefore, approaches using geomorphology, seismicity and geodesy can be used, which are not applicable in ancient and inactive regions of deformation like the Caledonides or the Alps. The Arabia-Eurasia collision is due to the northward movement of the Arabian Plate that resulted in the closure of the Neotethys ocean (Alavi 2007; Blanc et al. 2003; Ghasemi and Talbot 2006; Vera and Gines 2009; McQuarrie 2004). The exact time of initial collision is not well constrained, but most recent estimates put it in the range 25-35 Ma (McQuarrie and van Hinsbergen 2013; Allen and Armstrong 2008). There has been several hundred kilometres of continental convergence after initial collision (Mouthereau et al. 2012), which has been accommodated within an area covering much of southwest Asia, and specifically the territory of Iran, Turkey, Iraq and neighbouring countries.

As well as these academic considerations, the Zagros is also important because it host natural resources – mainly oil and gas – and because the active tectonics mean that the area is affected by devastating earthquakes. These have included the *M* 7.3 12 November 2017 Iran-Iraq earthquake, in the border region between the two countries, which killed over 600 people.

One of the most important aspects of tectonic studies is exploiting geomorphology to understand landscape response to tectonic signals, which are expressed by geomorphic indices (Keller and Pinter, 2002). These geomorphic indices have become popular and effective tools in tectonic studies due to the evolution of the quality (resolution) of digital elevation models (DEMs) (Burbank and Anderson, 2012; Kirby and Whipple, 2012). For the purposes of studying neotectonic activity in terms of detecting its preserved signals in the landscape of the Zagros fold-and-thrust belt, this study uses quantitative geomorphic indices in map form: surface roughness, hypsometric index, and surface index (González et al. 2015; Grohmann 2004; Mahmood and Gloaguen 2012; Shahzad and Gloaguen 2011b; Siddiqui 2014). Further geomorphic indices include the normalised channel steepness index (k_{sn}) and

its corollary knickpoint along river profiles, Hypsometric index of a basin and regional swath topographic profiles. All of these approaches have been used on a regional scale to understand their relation with major structures along and across the strike of the Zagros. A further factor brought into the study is climate, which varies across different regions of the Zagros: structural and climatic interactions are a major focus for tectonic studies at the present time.

A separate but complementary study was based around reconnaissance level fieldwork in northern Iraq: this has allowed modern river sediment and Miocene sandstone petrology to be investigated, to understand the provenance of sedimentation and consequent implications for the tectonics of the NW Zagros (i.e. Kirkuk Embayment).

Although the bulk of the thesis is about the Zagros fold-and-thrust belt, one chapter applies the geomorphic approaches to study the Himalayan fold-and-thrust belt, with the same aim of understanding the relations between tectonics, climate and landscape. By studying both the Zagros and the Himalayas it is possible to compare and contrast the processes which might control the landscape (e.g. convergence rate, structural style, lithology and climate).

1.2 Thesis aims

The Zagros region has a scientific and economic importance as it comprises one of the most active collisional fold-and-thrust belts in the world and contains a large number of hydrocarbon reservoirs. The geopolitical situation played an important role in not conducting detailed fieldwork studies to understand the tectonic history of the Zagros and specifically the Iraqi part of the Zagros. This thesis attempts to answer the following questions: 1) can remotely sensed data and geomorphic indices be used to quantify deformation, and specifically relative timing of fold growth? 2) do the tectonic and climatic records left in landscapes represents useful tools to investigate regional deformation of fold-and-thrust belts? and 3) do modern river sediments give information in regards to Zagros foreland tectonics? Therefore, this study uses remotely-sensed data to overcome the difficulties of non-accessible areas in addition to a single reconnaissance level fieldtrip. The initial aim of the project was to study the Iraqi sector of the Zagros. This work is largely presented in Chapter 3. It became clear through the course of the work that there was the opportunity to

study the entire Zagros beyond the political boundaries of Iraq, and this led to the regional Zagros study, mainly presented in Chapter 2: the chapters are presented in this order so that the regional picture is given before focusing on the more local study area. Having analysed the entire Zagros in this way, the next step was to apply the same techniques and approaches to the Himalayas, thereby covering both great, active, Eurasian continental collision zones. The remaining chapter covers the results arising from brief fieldwork and sampling in the Iraqi Zagros. Whilst this chapter is somewhat separate from the other studies, it shows the potential for future work integrating fieldwork, sample analysis and remote sensing studies.

Specific components of this study are summarized as follows:

- Analyse geomorphic indices and assess their implications for Zagros tectonics, both for the entire range, and for a more detailed study in the Kirkuk Embayment.
- Perform a similar geomorphic analysis for the Himalayas, with the additional aspect that the Himalayan and Zagros tectonic geomorphology can then be compared and contrasted.
- Analyse the modern river sand of the Zagros suture region, in addition to the analysis of Late Miocene formations of the Zagros foreland, NE part of the Kirkuk Embayment. This will help in understanding the provenance of the sediment sources, and shed light on the tectonic evolution of the NW segment of the Zagros fold-and-thrust belt.

1.3 Thesis layout

This thesis is designed to be six chapters; four core research chapters (2-5) are presented in paper structure with their own methodologies.

- Chapter one outlines the thesis aims and rationale and provides a regional review of the tectonics of the Zagros fold-and-thrust belt. It also contains previous work, subdivisions of tectonic zones and tectonostratigraphy of the Zagros.
- Chapter two focusses on the use of geomorphic indices including normalised channel steepness index (k_{sn}), relief and basin scale hypsometric index (HI) to investigate how the landscape responds to tectonic and climatic drivers in the

Zagros fold-and-thrust belt, and shows how geomorphology can be a sensitive indicator of tectonic processes.

- To deal with difficulties in finding the most suitable moving window and the limitations of computer efficiency for regional scale geomorphic analysis of the Zagros, Chapter three deals with local scale maturity index mapping techniques.
- Chapter three focuses on the use of landscape maturity analysis in understanding anticline growth in the Kirkuk Embayment. The Digital Elevation Model (DEM)-based geomorphic indices Hypsometric Index (HI), Surface Roughness (SR) and their combination Surface Index (SI) have been applied to quantify landscape maturity and show accordingly out-of-sequence retreat deformation in the Zagros foreland basin. This chapter is published in Tectonophysics (2017), 717**,** 27– 40.

  After analyzing geomorphic indices locally and regionally across the Zagros, the Himalayan orogen has been chosen for basin scale HI analysis to investigate the similarities and differences between the two orogenic belts in Chapter four.
- Chapter four focuses on the use of the basin scale hypsometric index (HI) to investigate the relationships between the main tectonic structures and changes in the HI value in the Himalayas, both across and along the strike of the range.

  Geomorphic indices show good results in regard to the Zagros tectonics, and then a simple petrological study for modern river sediment in the Zagros Suture has been carried out in Chapter five. This technique helps in opening new research windows for future provenance studies in the Zagros wherever possible.
- Chapter five analyses the petrology of modern river sand in the upstream area of the Lesser Zab River basin (Zagros suture zone), downstream sediments of the Diyala River basin and Late Miocene sandstones for the purpose of provenance identification. This chapter builds on a contribution made to a paper published in Earth-Science Reviews (2016), **162**, 107–128.

- Chapter six is the discussion chapter, and the principal results of all the main chapters and recommendations for future research are highlighted. The conclusions are contained in this chapter.

1.4 Contributions

Through the duration of the Ph.D. there have been the following presentations and papers.

1.4.1 Conferences

1- TSG, 2016 conference, UCL-Birkbeck, London (poster presentation).
2- BSG, 2016 conference, University of Plymouth, Plymouth, UK (poster presentation).
3- Annual conference of the Earth Sciences department 2016, Durham University, UK (poster presentation).
4- TSG, 2017 conference, University of Liverpool, UK (poster presentation).
5- EGU, 2017 conference, Vienna (poster presentation).
6- BSG, 2017 conference, University of Hull, UK (poster presentation).
7- TSG, 2018 conference, University of Plymouth, UK (poster presentation).
8- EGU, 2018 conference, Vienna (poster presentation).

1.4.2 Papers

1- Co-author of a paper published in Earth-Science Reviews (2016) **162**, 107–128: 'The Euphrates-Tigris-Karun river system: Provenance, recycling and dispersal of quartz-poor foreland-basin sediments in arid climate' http://dx.doi.org/10.1016/j.earscirev.2016.09.009.
2- First author of a paper published in Tectonophysics (2017) **717,** 27–40: 'Landscape maturity, fold growth sequence and structural style in the Kirkuk Embayment of the Zagros, northern Iraq' http://dx.doi.org/10.1016/j.tecto.2017.07.006.

1.5 Regional Tectonics of the Zagros

As a part of the Arabia-Eurasia collision zone, the Zagros fold-and–thrust belt (ZFTB) (Fig. 1.1) extends for ~1800 km from south-east Turkey, passing through the north and north-east of Iraq, across southern Iran and ending at the Oman Line (Alavi 2007; Vera and Gines 2009). The Zagros fold-and-thrust belt is built over what was the

northern, passive continental margin of the Arabian Plate before its collision with Eurasia. The Zagros region has been subjected to a series of compressional and extensional phases during its geological history that have initiated and later reactivated a series of basement faults (Ameen 1992; Jassim and Goff 2006; Stern and Johnson 2010; Burberry 2015). The Arabia-Eurasia collision is only the latest of these events. GPS data suggests that the region accommodates a northward movement of the Arabian Plate at a rate of ~16-26 mm/yr (Vernant et al. 2004), with the rate increasing eastwards. GPS studies have focused on territory in Turkey and Iran rather than Iraq.

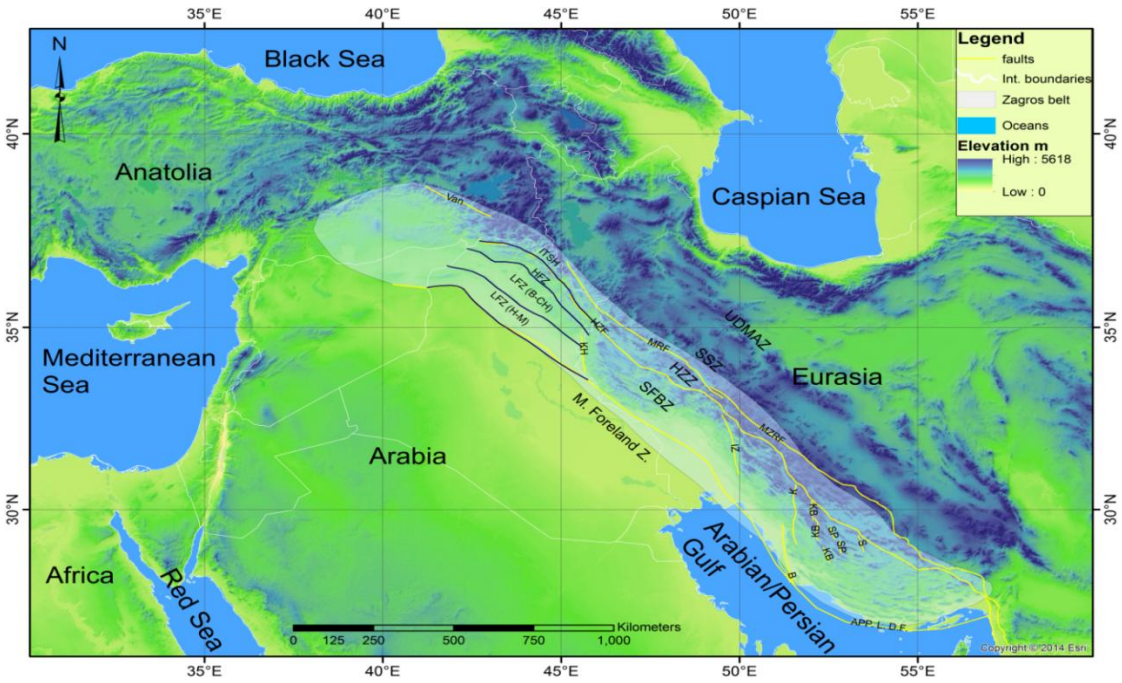

Fig. 1.1. Regional tectonic map of the Zagros fold-and-thrust belt shows the major faults system. Abbreviations: MZRF = Main Zagros Reverse Fault; HZF = High Zagros Fault; MRF = Main Recent Fault; B = Borazjan Fault; Iz = Izeh Fault; K = Kazerun Fault; KB = Kareh Bas Fault; Kh = Khanaqin Fault; S = Sarvestan Fault; SP = Sabz-Pushan Fault; Van = Van Fault; UDMA = Urumieh-Dokhtar Magmatic Arc; SSZ = Zagros Suture Zone; HZZ = High Zagros Zone; ZFBZ = Zagros Fold Belt Zone; ITSH = Imbricate and Thrust Sheet Zone; HFZ = High Folded Zone; LFZ (B-CH) = Low Folded Zone (Butmah-Chemchemal Zone); LFZ (M-H) = Low Folded Zone (Makhool-Himreen Zone). The shaded polygon is the Zagros belt.

The timing of the initial collision of Arabia-Eurasia is a controversial issue, however recent estimates put it as: 1) Late Cretaceous/Paleocene (Mazhari et al., 2009), 2) Early Miocene (Fakhari et al., 2008; Okay et al., 2010) and 3) Mid/Late Miocene (Guest et al., 2006). There is geological evidence that indicates a Late Eocene (~35 Ma) initial collision (Allen and Armstrong 2008; Perotti et al., 2016) roughly at the Eocene-Oligocene boundary. This evidence includes an unconformity detected via seismic data for the Arabian/Persian Gulf, and the shutdown of arc magmatism across SW Asia. McQuarrie and van Hinsbergen (2013), Mouthereau et al. (2012) and Saura et al. (2015) suggested a Late Oligocene-Early Miocene timing of initial collision, based on plate reconstructions and the timing of molasses sedimentation in the evolving foreland. Estimates for earlier initial collision (Late Cretaceous, or Cretaceous-Tertiary boundary) are related to the timing of pre-collision ophiolite obduction onto the Arabian Plate, and may be discounted (Allen and Talebian, 2011).

There are variations in the level of exhumation, relief and surface elevation along the strike of the Zagros from northwest to southeast, which divide the range along the tectonic strike into a number of zones, commonly referred to as embayments and salients. The terms are misleading, given that the deformation front of the Zagros is roughly linear in the north where the Kirkuk and Dezful embayments occur, and does not step back from the margins of the intervening Pusht-e Kuh Arc (salient). The Fars region forms the remainder of the Zagros to the southeast, and has a curved deformation front, convex to the south (Berberian 1995).

The origins of the two embayments are of interest for hydrocarbon geology in the region, as they contain numerous oil and gas fields in both Kirkuk (Iraq) and Dezful (Iran). These divisions of the Zagros indicate a different distribution of strain along the strike of the range, despite an apparently smooth and continuous convergence pattern of Arabia with Eurasia at the regional scale (McQuarrie et al. 2003; Vernant et al. 2004). Low strains within the embayments are probably complemented in each case by high strain zones to the northeast (McQuarrie 2004; Allen and Talebian 2011); this is consistent with the observed geology of the Bakhtyari Culmination to the north of the Dezful Embayment, but there are not yet equivalent studies in Iraq, north of the Kirkuk Embayment. The Dezful Embayment has been related to the pre-continental collision of the Arabian Plate margin, and the irregular distribution of

Cretaceous ophiolites upon it (Allen and Talebian 2011). However, it is not clear whether this model applies to the Kirkuk Embayment.

The Iraqi sector of the Zagros is commonly mapped as having northeast-southwest trending basement faults (e.g. Jassim and Goff 2006 and references therein). However, it is unclear to what extent these faults are active (Kent 2010; Burberry 2015), or even exist as mapped. As they do not appear to offset the prominent northwest-southeast anticlines that are the focus of chapter three, we do not consider them further.

Based on its geomorphology, seismicity and exposed geology, the Zagros belt has been divided into sub–parallel tectonic units in a number of different ways by different authors (e.g. Berberian, 1995). Generally the Zagros consists of three main parallel tectonic units (Fig. 1.1). From the northeast to the southwest, the subduction-related Urumieh-Dokhtar Magmatic Arc (UDMA), the Sanandaj-Sirjan Zone and the Zagros fold-and-thrust belt. The major faults of the Main Zagros Reverse Fault (MZRF) and the High Zagros Fault (HZF) divided the ZFTB itself into three main structural zones. These zones are the High Zagros Zone (HZZ), the Simply Folded Belt Zone (SFBZ) and the Mesopotamian Foreland and Gulf Zone (MFGZ) towards the southwest (Fig 1.1). A simple division is to treat everything southwest of the High Zagros as a part of the Simple Folded Belt, as the boundaries between the lower elevation areas are hard to define consistently along the entire length of the fold-and-thrust belt (Allen et al. 2013).

The Iraqi part of the Zagros has been studied by many researchers (e.g. Fouad, 2015; Jassim and Goff, 2006; Lawa et al., 2013; Numan, 2000). Jassim and Goff (2006) proposed a sub-classification for the suture, the simply folded belt tectonic zones and the remainder of Arabia to the southwest in Iraq into two main zones (“Unstable” and “Stable”), each sub-divided into a number of sub-zones (Fig. 1.2).

The boundary between the two main zones is the current Zagros main deformation front, although subtle Cretaceous-Cenozoic structures appear to the south of this line (including oil and gas fields).

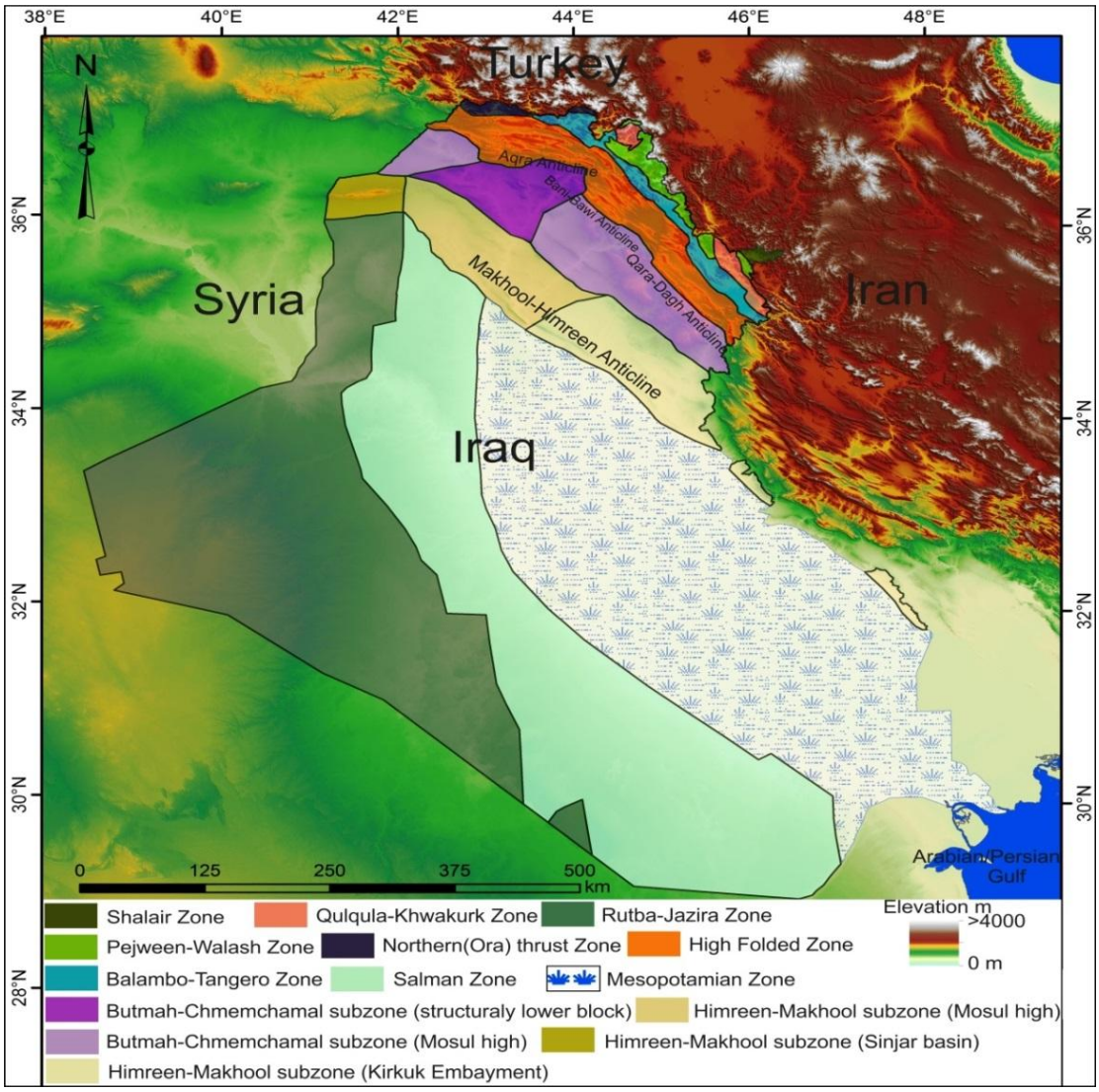

Fig. 1.2. SRTM 30 m topography, overlain by tectonic sub-division of the Iraqi Zagros (redrawn after Jassim and Goff, 2006).

The pre-collisional significance of the boundary is unclear, but likely relates to differences in the Palaeozoic-Mesozoic rifting history of the Arabian Plate, associated with the opening of Tethys. The “Unstable” and “Stable” terms relate to differences in the pre-Cenozoic history and stratigraphy. The zones and subzones of the Iraqi Zagros are described in the following sections. This is provided as a reference guide, should readers need to relate the features described in later chapters to one or more these conventional sub-divisions of Iraqi geology. A unified geology map of the Zagros, going across political borders, has been compiled and is presented as Fig. 1.3. Several regional studies of the Zagros stratigraphy are compiled and presented as Fig. 1.4.

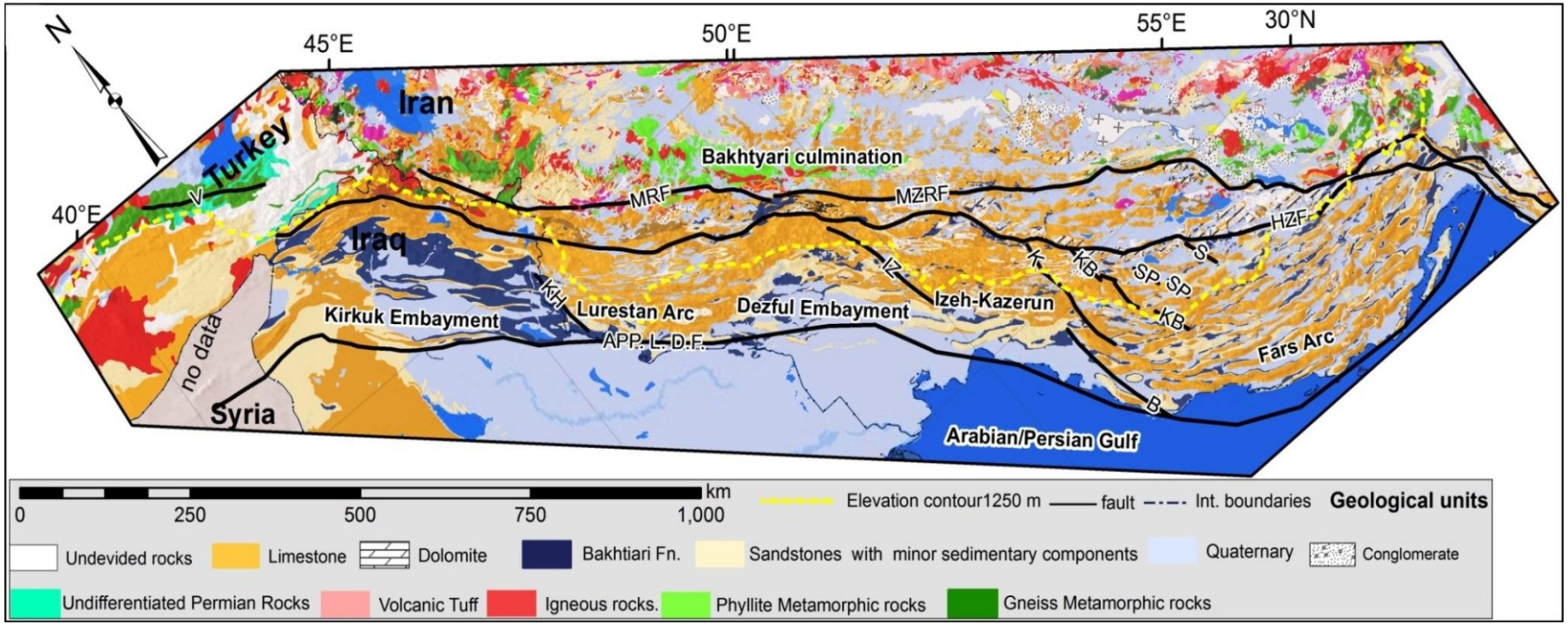

Fig. 1.3. Geological map of the Zagros shows the exposed lithologies of the Zagros fold-and-thrust belt (redrawn after 1) the geological map of Turkey 1:2,000,000; 2) Sissakian, 2000 and 3) Afaghi and Salek, 1975; 1977; Afaghi et al., 1978).

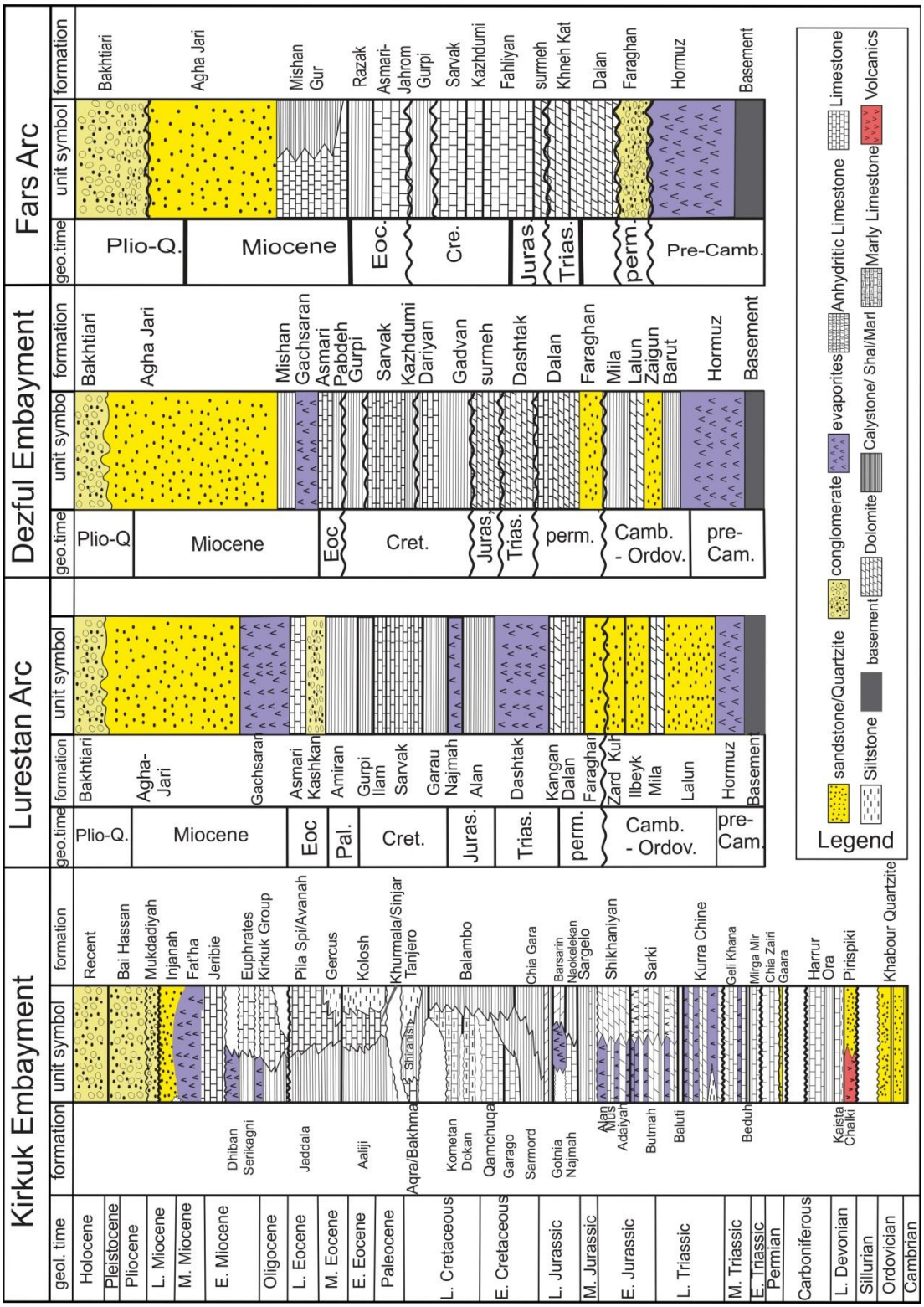

Fig.1.4. Stratigraphic columns across of the Zagros fold-and-thrust belt show the changes in the sedimentary basins across the Zagros since the Precambrian (redrawn after Jassim and Goff, 2006; Molinaro et al., 2005; Sherkati at al., 2005; Casciello at al., 2009; English et al., 2015).

1.5.1 Folded Zone or Unstable Zone

The IZ comprises the most deformed part of the north-eastern margin of the Arabian plate during the ophiolite obduction in the late Cretaceous and the main continental collision of Miocene-Recent age. It is characterised by anticlinal structures parallel to the Taurus-Zagros (Arabia-Eurasia) suture. The Taurus anticlines group takes the direction of E-W exemplified by Aqra Anticlines (Fig. 1.2). The second anticlinal group is the Zagros group, which is represented by Qara-Dagh and Bani-Bawi anticlines (Fig. 1.2). This folded (unstable) zone is classified into four subzones.

1.5.1.1 Zagros Suture Zone (ZSZ)

In the Late Cretaceous and Mio-Pliocene, the obduction and collision phases caused the thrust of the Zagros suture units over the Arabian plate. The ZSZ consists of three further subzones (Fig. 1.2). First is the Qulqula-Khwakurk subzone, which deformed in the Cenomanian. The deposition of conglomerates with chert pebbles within this subzone is attributed to folding and uplifting in the eastern inner zone. The basement depth is about 14 km beneath this subzone and located along the southeastern margin of the Neo-Tethys, according to the NE increase of volcanics in the chert sequences. Recumbent and isoclinal folds and thrust and reverse faults are the dominant structural features (Jassim and Goff, 2006 and reference therein).

Second, the Penjween-Walash subzone comprises a belt along the Iraq-Iran border and a thrust mass over Qulqula-Khwakurk and Balambo-Tanjero subzones. The Penjween-Walash subzone is characterized by three thrust sheets, from the highest to the lowest: Qandil, Walash and Naopurdan. Third, the Shalair (Sanandaj-Sirjan) subzone takes its name from the outcrops in Shalair valley. It is considered as a higher structurally thrust sheet in Iraq (Jassim and Goff, 2006). During the Cretaceous, high-grade metamorphism affected the rock of the Shalair subzone. It is characterised by several transversal and longitudinal faults and E-W transversal anticlines (Jassim and Goff, 2006 and reference therein).

1.5.1.2 Imbricated Zone (IZ)

This consists of two subzones (Fig. 1.2). First, the Balambo-Tanjero subzone seems to be a narrow zone (25 km wide) trending NW-SE and characterised by thrust sheets. To the south of Greater Zab River, the highly intense folding and faulting often caused the anticlines to over-ride the synclines. Second, the Northern (Ora)

Thrust Zone, trends E-W about 15 km wide. In the Iraqi part of the Zagros, this subzone is considered allochthonous and the majority of its basement lies in the north of Iraq which can be found at a depth of 10 km (Jassim and Goff, 2006 and reference therein).

1.5.1.3 High Folded Zone (HFZ)

This zone borders from the south by the Qara-Dagh and Aqra anticlines, previously interpreted to overlie a deep-seated fault (Fig. 1.2). Also, it is known as the Simply Folded Belt and covers most of northern Iraq with a width in the order of 25 to 50 km. The anticlines are harmonic, uplifted intermittently during the Cretaceous and the Paleogene with high deformation during the Late Tertiary and Quaternary. These anticlines consist of Mesozoic limestone in their cores and Paleogene / Neogene clastics and limestone in their flanks. In general the trend of anticlines is NW-SE, and the zone has an elevated basement of up to 8 km compared with the Low Folded Zone (LFZ) (Jassim and Goff, 2006 and reference therein).

1.5.1.4 Low Folded Zone (LFZ)

The SW flank of Himreen, Makhool (Fig. 1.2) and Pusht-e-Khu anticlines along the Himreen-Makhool Fault (HMF) is considered as the SW border of this zone, which is also known as the foot-hill zone. The depocenter within this zone occurred in the Kirkuk Embayment (KE), which refers to the deepest Precambrian basement at approximately 13 km (Jassim and Goff 2006). This idea is supported by the high maturity of the KE source rock as a result of fault reactivation (Burberry, 2015). This zone consists of the Himreen-Makhool and the Butmah-Chemchemal subzones (Fig. 1.2) which exhibit a big difference in the length of their anticlinal structures and thickness of the sedimentary sequences. The length of anticlines in the Mosul High increases towards the KE. The line of the Qara-Dagh and Aqra anticlines comprises the NE boundary of this zone (Jassim and Goff, 2006 and reference therein).

1.5.2 Unfolded Zone or Stable Zone

1.5.2.2 Rutba –Jazera Zone

This consists of two subzones. First, the Al-Jazera subzone which is mostly outcrops by the Middle Miocene Fat'ha (Lower Fars) and the Late Miocene Injana (Upper Fars) formations, in addition to the Late Oligocene outcrop of the Kirkuk Group. Second, the Rutba subzone which is characterised by the most prominent feature

named the Ga'ara Depression, unconformably overlain the Jurassic fluviatile and shallow marine strata with the Late Triassic carbonates to the SE. Other unconformities occurred between Early Permian sediments and the Late Cretaceous, and between the Paleocene and Eocene sediments (Jassim and Goff, 2006 and reference therein).

1.5.2.2 Salman Zone

This subzone consists of outcrops of Middle-Late Eocene strata in the west and in the east there are the Early and Middle Miocene strata, with Miocene strata to the south. The central part of the zone is dominated by NW-SE transversal faults with a frequent occurrence of N-S trending faults. Fewer faults are seen in the northern part of this zone (Jassim and Goff, 2006 and reference therein).

1.5.2.3 Mesopotamian Zone

This comprises the proximal eastern termination of the stable shelf. Supposedly, it was uplifted during the Hercynian deformation and subsided in the Late Permian. It comprises a low topographic gradient area (10 cm/km) and is mostly covered by Quaternary sediments due to the activity of the Tigris, Euphrates and Diyala Rivers (Jassim and Goff, 2006 and reference therein).

2. Landscape expressions of tectonics in the Zagros fold-and-thrust belt

2.1 Introduction

Landscape evolution is influenced by tectonics and climate, but can also be a sensitive record of tectonic processes. Active tectonism has been widely investigated using multiple geomorphic indices because the ability of the latter to detect the landscape response to tectonic forces (El Hamdouni et al., 2008; Keller and Pinter, 2002). In addition, these indices provide measurements which help in the quantitative assessment of the relative roles of crustal displacement and the variation in rock resistance during landscape development (Walcott and Summerfield, 2008). In this chapter, I use the hypsometric index (HI) of drainage basins, longitudinal river profiles and topographic swath profiles to examine the geomorphology, and help understand interactions of tectonics, climate and landscape in the Zagros.

One of the major tectonic events of the Cenozoic was the closure of the Neo-Tethys Ocean. A consequence of this closure was the Arabia-Eurasia collision, which initiated the Zagros fold-and-thrust belt as one of the largest and most active mountain ranges in the world (Stampfli and Borel, 2002; Mouthereau et al., 2012). The Zagros fold-and-thrust belt extends over 1800 km (Fig.2.1A). It has accommodated part of the Arabia-Eurasia convergence (Blanc et al. 2003; McQuarrie, 2004; Ghasemi and Talbot, 2006; Alavi, 2007;Vera and Gines, 2009) since at least the Early Miocene (Fakhari et al., 2008). The timing of initial collision is debated. Recent estimates include the Eocene-Oligocene boundary (~35 Ma) (Allen and Armstrong, 2008; Perotti et al., 2016) and the Late Oligocene-Early Miocene (McQuarrie and van Hinsbergen, 2013; Mouthereau et al., 2012; Saura et al., 2015). The Zagros collision zone includes the folded sedimentary cover of the Arabian Plate and its underlying basement. The Zagros is divided into the High Zagros Zone (HZZ), Zagros Simply Folded Zone (ZSFZ) and the Mesopotamian Foreland Zone (MFZ) (Fig.2.1A).

Many folds have developed as a consequence of the Arabia-Eurasia collision. These are the classic “whaleback” structures of the Zagros, which trend NW-SE along the greater part of the range. Anticlines in the far north western part of the Zagros and in

the Fars region in the SE deviate from the NW-SE orientation, and have more E-W trends. The High Zagros Fault (HZF) separates the High Zagros to the north from the Simply Folded Belt to the south. Other structural divisions have been described across the strike of the orogen, but these are secondary, and bounded by features such as the Mountain Front Fault that may not be continuous along the length of the range.

Along the strike of the Zagros there are variations in the degree of exhumation, topographic elevation, relief, stratigraphy, position of the deformation front and structural style changes along strike (Talbot and Alavi, 1996). These along-strike changes divide the range into several domains, referred to as salients and embayments, adjacent to the higher elevation Turkish-Iranian Plateau to the northeast (Fig. 2.1A). These domains are the Kirkuk Embayment, Lurestan (Pusht-e Kuh) Arc, Dezful Embayment and Fars Arc, from the northwest to southeast (Casciello et al., 2009; Lacombe et al., 2006). There are differences in the strain distribution within the Zagros related to the occurrence of these embayments (e.g. low strain in the Dezful Embayment complemented by high strain in Bakhtyari Culmination) (McQuarrie, 2004; Allen and Talebian, 2011). Out-of-sequence deformation of the Zagros has been discussed in the northeast of the Kirkuk Embayment by Koshnaw et al. (2017), and the southwest by Obaid and Allen (2017). The Zagros represents an area with a wide range of exposed geology, but mainly sedimentary rocks from the Jurassic to the Holocene (Fig. 2.1B).

Whereas there is pronounced crustal deformation within the Zagros, witnessed by the abundant seismicity and shortening across the range, the Turkish-Iranian Plateau represents a region of the collision zone where there is little active convergence, relatively low relief, and subdued seismicity (mainly strike-slip). The boundary between the tectonic plateau and the active fold-and-thrust belt is debatable, but there is a marked cut-off in thrust seismicity at the 1250 m elevation contour. Most thrust events confined in low elevation part of the simply folded belt below the 1250m elevation contour and such events are very rare beyond this elevation; possibly because of difference in strength and depth of basement (Nissen et al., 2011). Elevations continue to climb to the northeast, but with little indication of active shortening, at least at upper crustal levels (Allen et al., 2013). The seismicity cut-off is therefore an important marker for studies of landscape response to tectonism.

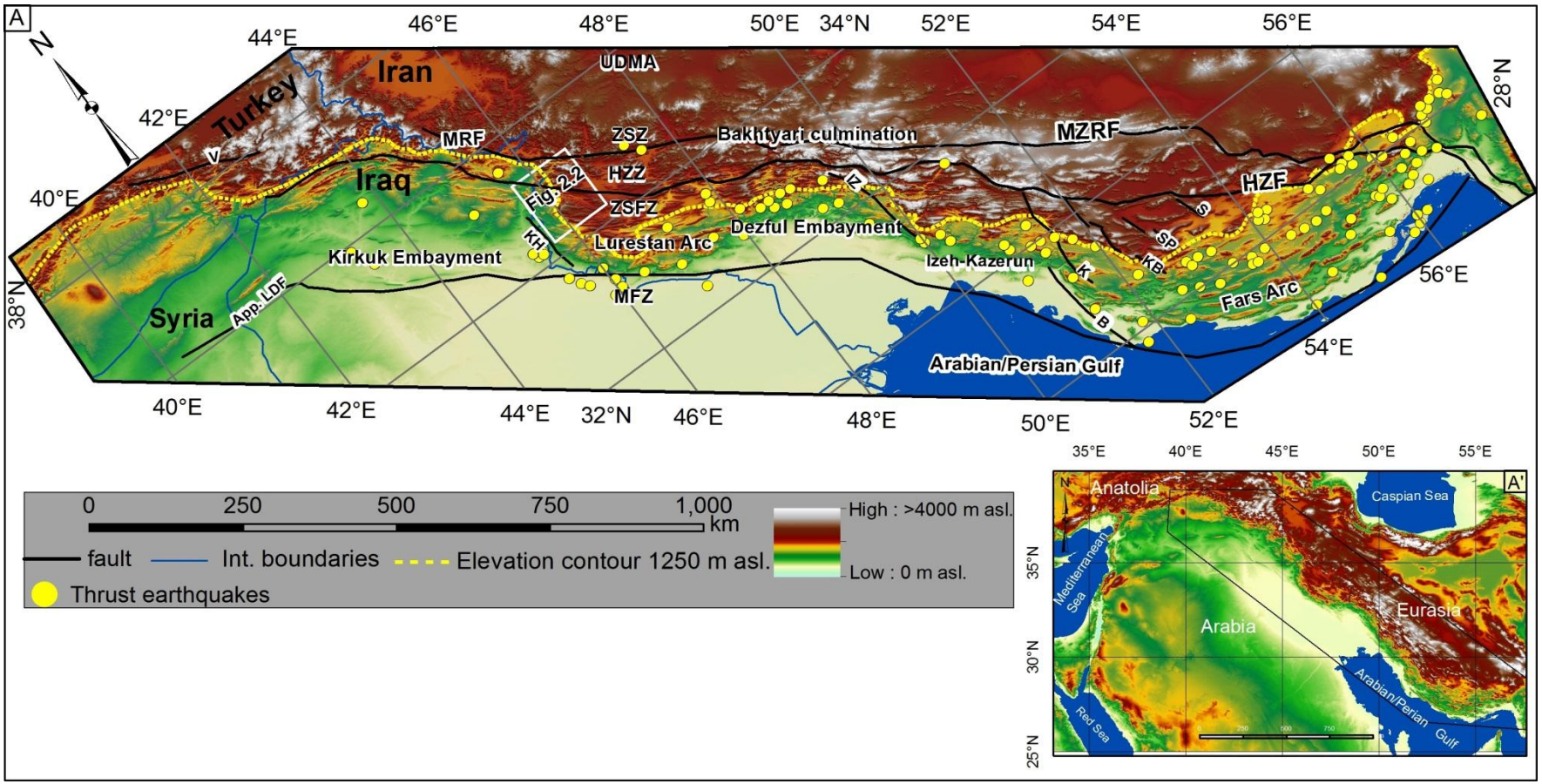

Fig. 2.1. A, Regional tectonics of the Zagros fold-and-thrust belt shows the topography and location of the studied area.

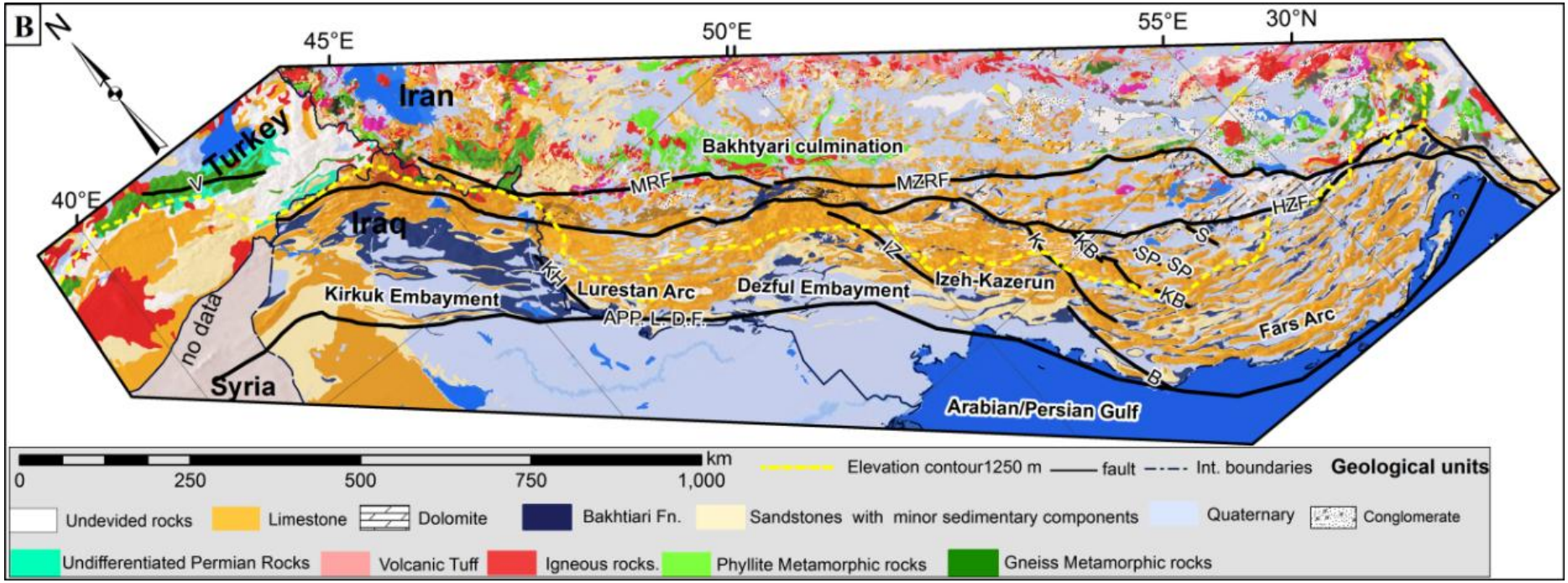

Fig. 2.1. B, Exposed lithologies of the Zagros fold-and-thrust belt (redrawn after 1) the geological map of Turkey 1:2,000,000; 2) Sissakian, 2000 and 3) Afaghi and Salek, 1975; 1977; Afaghi et al., 1978). Abbreviations: MZRF = Main Zagros Reverse Fault; HZF = High Zagros Fault; MRF = Main Recent Fault; B = Borazjan Fault; Iz = Izeh Fault; K = Kazerun Fault; KB = Kareh Bas Fault; Kh = Khanaqin Fault; S = Sarvestan Fault; SP = Sabz-Pushan Fault; V = Van Fault; UDMA = Urumieh-Dokhtar Magmatic Arc; ZSZ = Zagros Suture Zone; HZZ = High Zagros Zone; ZSFZ = Zagros Simply Fold Zone; MFZ = Mesopotamian Foreland Zone; App. LDF = Approximate Limit of Deformation Front.

2.2 Methods and data

2.2.1 Topographic swath profiles, drainage analysis

Swath profiles represent topographic variation by maximum, mean and minimum elevations across the swath width. 25 swath profiles oriented NE-SW, have been analysed, using the Shuttle Radar Topography Mission (SRTM) 30 dataset (https://www2.jpl.nasa.gov/srtm/). The width of swaths was fixed to 25 km on either side of the swath centre. The difference between the maximum and minimum elevations is the relief across the swath profile (called incision by Andreani et al., 2014; although there is no requirement that a previous surface is incised). Across-profile relief values were integrated to give an indication of overall relief for the range within each profile area.

River network and river characteristics such as river incision, river divergence and deflection can be used to investigate concealed underlying geological structures (Holbrook & Schumm 1999). Also, drainage patterns can preserve folds and faults kinematics (Jackson et al. 1998). River course behaviour can be used to investigate whether the lateral growth or fold linkage occurs in the fold-and-thrust belt by the means of the ancestral drainage pattern on fold flanks (Ramsey et al. 2008). This chapter includes an analysis of this type for the Zagros, focusing on areas of the Iraqi sector that have not been covered by previous studies. No automated process was used to perform this analysis.

2.2.2 River profiles

The landscape has been used as a source of information of the present and past tectonics. The field of tectonic geomorphology is simply the use of signs of deformation from landforms remnants to characterise active deformation in both folds and faults (Behr et al., 2010; Lave and Avouac, 2000; Zielke at al., 2010). A dynamic equilibrium is required between the two competitive parameters; the rate of rock uplift and the rate of terrain removal to preserve tectonic signals in the landforms (Dietrich et al., 2003) although such preservation is very hard in erosional mountains.

Landscape relief is set by the river channel network (Whipple et al., 1999). Thus, past and present tectonic patterns can be interpreted from information contained in the drainage network of an area. Features of active deformation can be recognised

using the sensitivity of river profiles to uplift processes (Seeber and Gornitz, 1983). Tectonic geomorphology methods focus on the analysis of steady state river long profile (e.g., Kirby et al., 2003; Snyder et al., 2000; Whipple and Tucker, 1999; Wohl and Merritt, 2001) or methods which reflect a change in base level (e.g., Boulton and Whittaker, 2009; Whipple, 2004; Whipple and Tucker, 1999, 2002; Whittaker and Boulton, 2012; Whittaker et al., 2007, 2008).

The shape of longitudinal river profiles dictates topographic relief. Changes in the slope of river profiles can be recognized by the occurrence of knickpoints, both in slope-area or elevation-distance plots (Fig. 2.2). Such knickpoints develop in response to tectonic effects (i.e. uplift caused by folding and/or faulting), or changes in base level (Goldrick and Bishop, 2007; Kirby and Whipple, 2012; Wobus et al., 2006a). Knickpoint distribution has been used to identify tectonic forcing in active orogens (Miller et al., 2012; Schildgen et al., 2012; Morell et al., 2012; Olivetti et al., 2012).

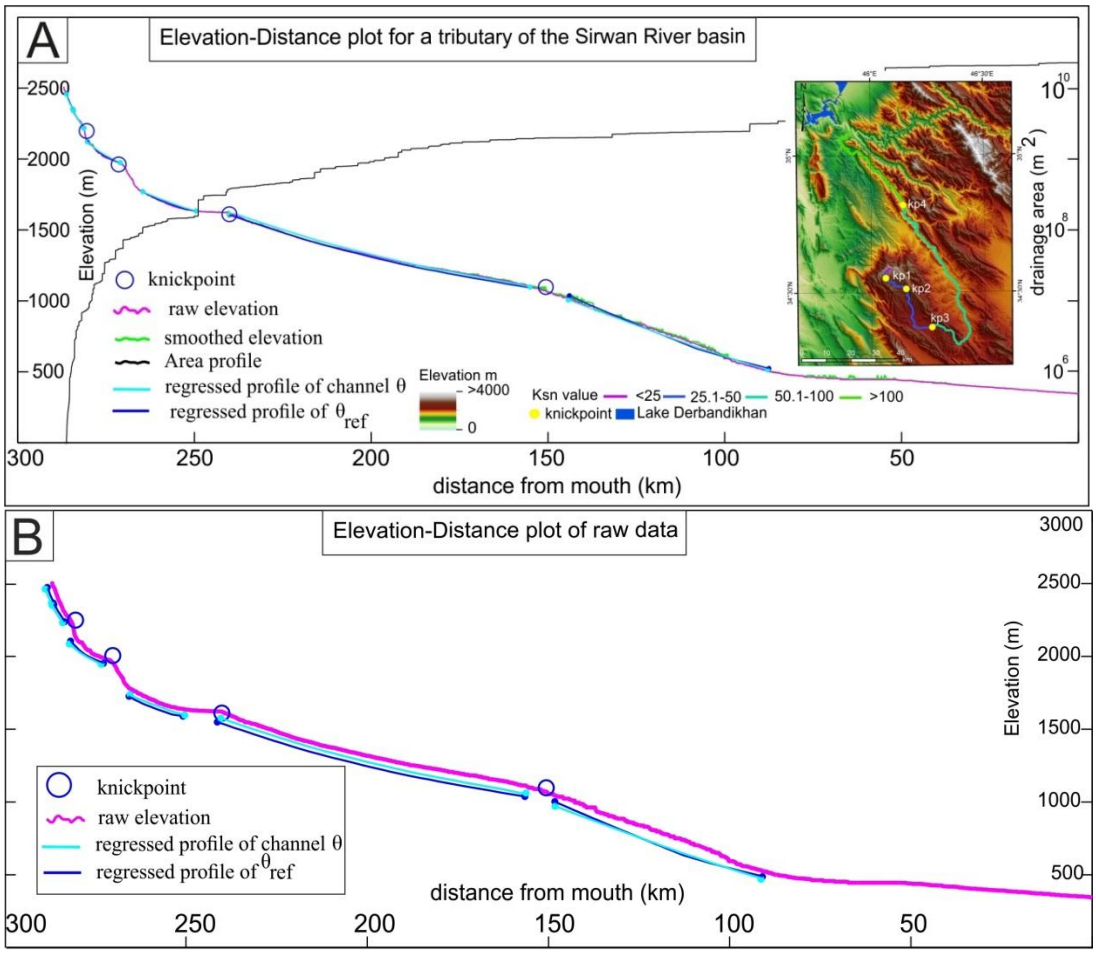

(Continued with caption on next page)

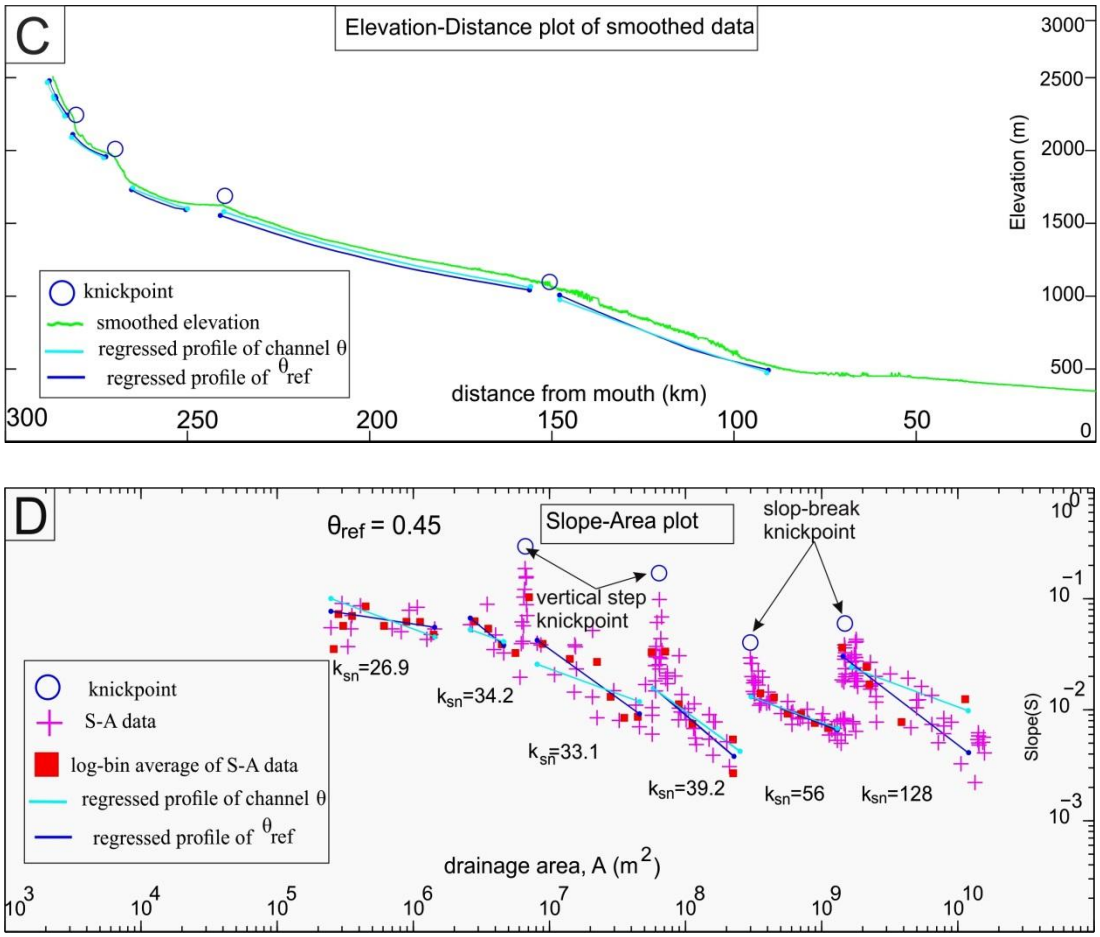

Fig. 2.2. Calculation method of river Normalized steepness index (k_{sn}) and the determination of knickpoints for a tributary of the Sirwan River Basin/north-eastern Iraq (Fig. 2.1a). A) Elevation-Distance plot as exported from Stream Profiler software (http://geomorphtools.geology.isu.edu/Tools/StPro/StPro.htm). B and C represent the Elevation-Distance plot for the raw and smoothed elevations respectively, showing the limits of regressed profile segments and the location of knickpoints on the profile and D) Slope-Area plot for the selected river shows the k_{sn} value using reference concavity (0.45).

Tucker and Whipple (2002) and Whipple and Tucker (2002) described fluvial erosion in three models. These models are 1) detachment-limited which is representing bedrock river where erosion is equal to uplift, where fall in base level or regional uplift and substrate erodibility control the gradient of river. 2) Transport-limited model, where channel gradient is determined by the capability of a river to transfer sediments load and so, this river is an alluvial river characterised by loose sediments and banks and bars. 3) The third model is the hybrid river where substrate erodibility and sediment flux control the gradient of a channel. All these models can foresee the relationship between local slope of river channel (S) and upstream area (A) known as power low (Hack (1957).

$$S = k_s\, A^{-\theta} \qquad (2.1)$$

Where k_s and θ are the steepness index and concavity index respectively (Hack, 1957; Flint, 1974).

Slope-area plots allows the extraction of both S and A directly from DEMs using the regression of slope and area data. Accordingly the concavity index, θ, and the steepness index, ks, can be calculated. The concavity index (θ) in Eq. (2.1) describes the change in slope along stream profile (Wobus et al., 2006). Thus, significant deviation from a smooth concave up form of stream profile reflects transient response to tectonic uplift or subsidence (Boulton and Whittaker, 2009; Snyder et al., 2000; Larue, 2008), rock structures and their resistance differences (Larue, 2008; Phillips and Lutz, 2008) and other changes in base level and landscape (Bowman et al., 2007; Harmar and Clifford, 2007). Although the concavity index shows significant variability in natural streams, in a steady state it often has a value within the range ~ 0.4-0.6 (Kirby and Whipple, 2001; Snyder et al., 2000; Whipple, 2004; Wobus et al., 2006a).

The steady state condition means that the differences in lithology, climate, and the rate of rock uplift along the length of channel are uniform. This uniformity leads to the insensitivity of concavity index to the factors mentioned above. In contrast, steepness index exhibits changes in value along the segmented profile dependent on these factors. Steepness index considers the change in channel slope and drainage area, to overcome systematic variations in river gradient index as a result of changes in basin shape and discharge (Goldrick and Bishop, 2007).

To overcome the dependence of longitudinal profile on the basin shape, linear regression of gradient against drainage area should be applied on a log slope-log area plot. However, wide variation in k_s (regression intercept) can be the corollary of a small variation in θ (regression slope). So, relying on the assumption of restricted range of concavity index in a steady state ($0.4 \leq \theta \leq 0.6$) (Kirby and Whipple, 2001; Kirby and Whipple, 2012; Snyder et al., 2000; Wobus et al., 2003; Wobus et al., 2006a), normalized steepness index (k_{sn}) can be determined by evaluating slope-area regression using a reference concavity (θ_{ref} = 0.45) in Eq. (2.2).

$$S = k_{sn}\, A^{-\theta ref} \qquad (2.2)$$

Here, the variation in drainage area can be surmounted and effective comparison between streams profiles can be achieved, regardless of their catchment areas. In equilibrium landscapes, similar concavity for multiple segments of stream profile can be recognised, but not similar steepness. Uplift results in steepened rivers, and accordingly the steepness index will vary (Dietrich et al., 2003; Snyder et al., 2000). Thus, k_{sn} can be used as a suitable metric in tectonic geomorphology studies (Kirby and Whipple, 2001; Wobus et al., 2006a). 340 rivers have been selected randomly across the Zagros to perform river profile analysis.

Discontinuities on river long profile (convexities) are very importand features which represent a breaks in the pwer-low scaling on slope-area plot to identify either slop-break or vertical step knickpoint (Fig. 2.3). This occurrence of knickpoint indicate in general, the undergoing transient response of river to perturbation as a transition wave of incision where knickpoint migrate over time towards upstream (Bishop et al., 2005; Crosby and Whipple, 2006; Wobus et al., 2006). Landslides, debris flow and locally resistant substrate will generate vertical-step knickpoint recognised as spike in slop value on slop-area plot and has no tectonic significance. Contrary, slop-break knickpoint of tectonic origin which is generate from continual change in forcing maybe due to faulting or change in the rate of fault slip (Kirby and Whipple, 2012).

If slop-break knickpoints show linear arrangment it will lead to identify geological structures which have not recognised previously (i.e., Kirby and Ouimet, 2011; Wobus et al., 2003) as well as it might refer to the rate of uplift changes across unknown structures (Hoke et al., 2007; Kirby et al., 2007). Also these class of knickponts migrate generally upstream at a nearly constant vertical rate (Neimann et al., 2001; Whipple and Tucker, 1999) but their horizontal swiftness could be a function drainage area, thus the velocity of knickpont migration and drainage area will decrease (Crosby and Whipple, 2006; Harkins et al., 2007; Whipple and Tucker, 1999). Therefore, knickpoints of a nearly constant elevation could be the corollary of continuous changes in rock uplift and assuming an equilibrium state of drainage network prior perturbation (Harkins et al., 2007; Wobus et al., 2006). However, one should consider the variation in climate and the rate of uplift, or the absence of pre-existing steady-state which cause a dispersion and differences of knickpoint

elevation and celerity respectively ((Boulton and Whittaker, 2009; Castillo et al., 2013; Harkins et al., 2007; Schildgen et al., 2012; Whittaker and Boulton, 2012).

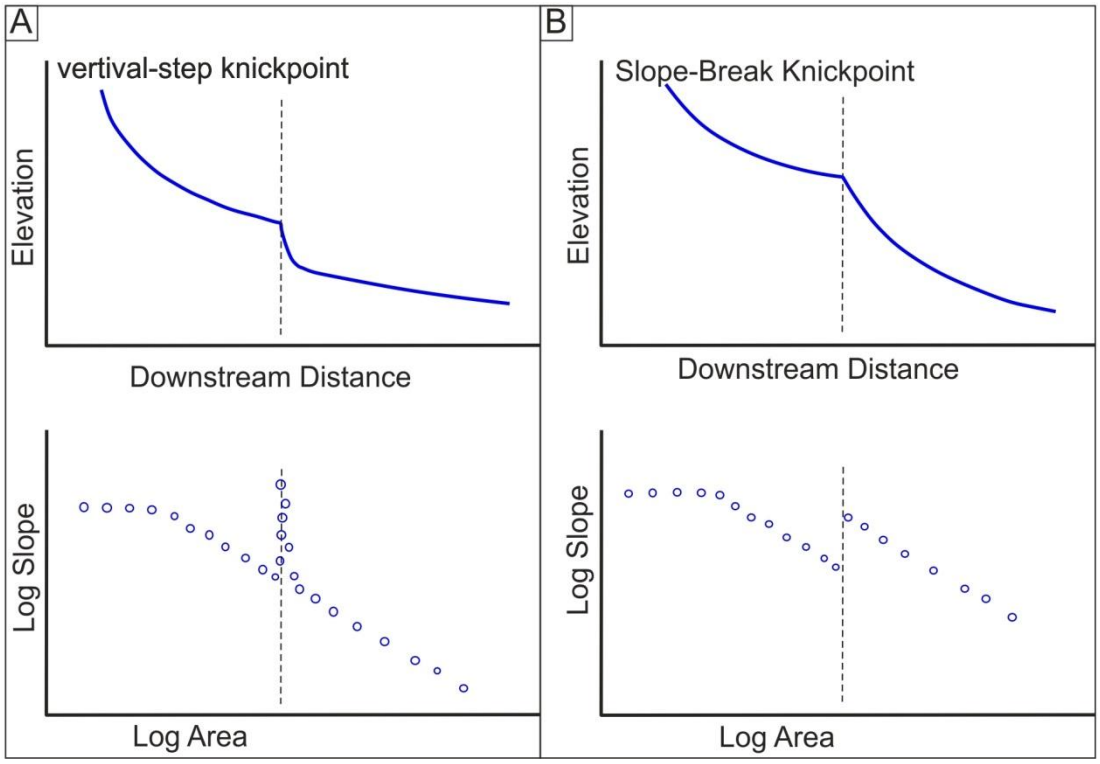

Fig.2.3. knickpoint classifcation shows the difference between knickpoints on log slope -log area scaling (after Kirby et al., 2012).

2.2.3 Hypsometric Index (HI)

The idea of hypsometry was first used to express the forms of drainage basins (catchments) and their slopes (Langbein, 1947). Each individual basin consists of different intervals of elevation bounded different areas between them. These intervals of elevations and areas form the hypsometric curve (Strahler, 1952) which integrated into a value known as hypsometric index, or integral (Fig. 2.4 A and B).

For a given drainage basin HI refers to the amount of residual terrain above the lowest horizontal plane of a basin and it can be used as a proxy for the erosional stage and landform development (Strahler, 1952; Schumm, 1956). Thus high HI values (close to 1) means that the terrain removal is in the lowest stage (the uplift is greater than erosion) and the land surface is in a youth stage, while low HI values (close to 0) means high amount of terrain removal (erosion is greater than uplift) and

the land surface is in a mature stage. This dimensionless form enables the comparison between different basins regardless of their areas.

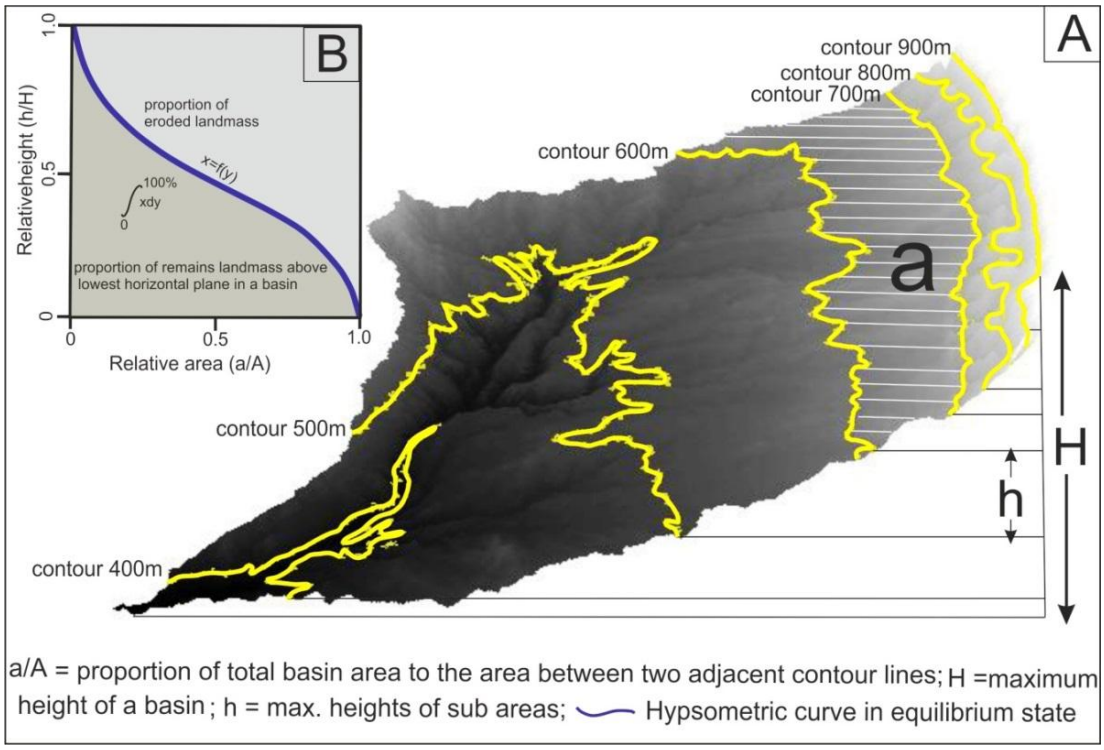

Fig. 2.4. The basics of hypsometric index calculation. A) Sub-basin of the lesser Zab River north of Iraq shows the calculation method of the relative elevation and the relative area. Inset B (after Strahler, 1952) is the equilibrium state of the hypsometric curve, showing the proportion of the eroded and the remaining land masses associated with the equilibrium state.

HI is a powerful tool to investigate the relative tectonism of an area, by characterizing the topographic dissection of a basin (Keller and Pinter, 2002). Due to the development of Digital Elevation Models (DEMs), HI can be calculated automatically using Eq. (2.3) (Pike and Wilson, 1971; Keller and Pinter, 2002).

$$HI = \frac{H_{mean} - H_{min}}{H_{max} - H_{min}} \quad (2.3)$$

I adopt the approach of Gao et al (2016), who measured HI for drainage basins of a particular stream order to map out regional variations. This differs from approaches that apply moving windows to calculate HI across a landscape (see Chapter 3). The rationale is that drainage basins are naturally-defined areas that reflect both tectonics and lithology, and so align with changes in one or both of these parameters (e.g. slip and uplift on active faults). I used the threshold of 0.3 to classify the HI value into relatively low <0.3 and relatively high >0.3 as the highest HI value of the area is 0.5.

2.2.4 Data and sensitivity testing

The SRTM 30 dataset was used for the purpose of drainage network extraction, using MATLAB-based TecDEM software (Shahzad and Gloaguen, 2011a). The D8 algorithm (Jones, 2002) was applied to calculate flow directions. The parameters of Equation 2.3 were obtained directly from DEM data and HI was calculated automatically using TecDEM 2.2 MATLAB-based and standard ArcGIS 10.3.1 software (Fig. 2.5A). The HI data were converted into raster mode using the polygon to raster function within the ArcGIS 10.3.1 to extract swath profiles for the HI data across different regions in the Zagros.

For river profile extraction process, a minimum threshold of 10^5 m^2 contributing area was chosen to ensure fluvial dominated channel flow (Kirby and Whipple, 2001; Montgomery and Foufoula, 1993; Wobus et al., 2006a). Using Stream Profiler software, the k_{sn} value was calculated for the whole Zagros (Fig. 2.5B) using a reference concavity of θ_{ref} = 0.45 (Wobus et al., 2006a) to overcome lithological effects on the concavity index, and consequently the steepness index. Results were compared with exposed lithologies to determine whether knickpoint and HI values are affected by active tectonic or lithological changes.

Rainfall data from the Tropical Measurement Mission satellite TRMM 3B43 (https://mirador.gsfc.nasa.gov/) were analysed for the time series 1998-2016 (resolution 0.25˚* 0.25˚~25*25 km) to investigate climatic effects on the geomorphic indices (Section 2.3.6).

The final part of the results section contains an analysis of the sensitivity of the methods described in the above sections, in particular the robustness of the stream profile extraction and the effects of looking at basin scale HI at different drainage basin orders.

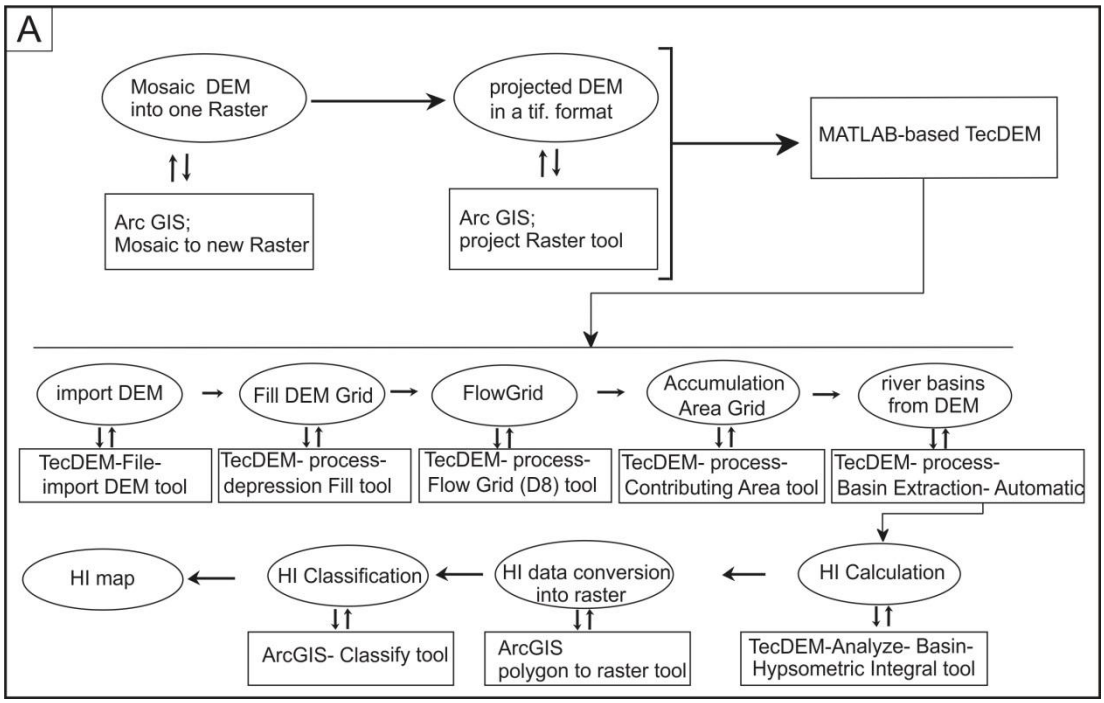

Fig. 2.5A. Summary of work flow adapted in the methodology shows data processing using TecDEM 2.2 for the extraction of the HI value of a drainage basin.

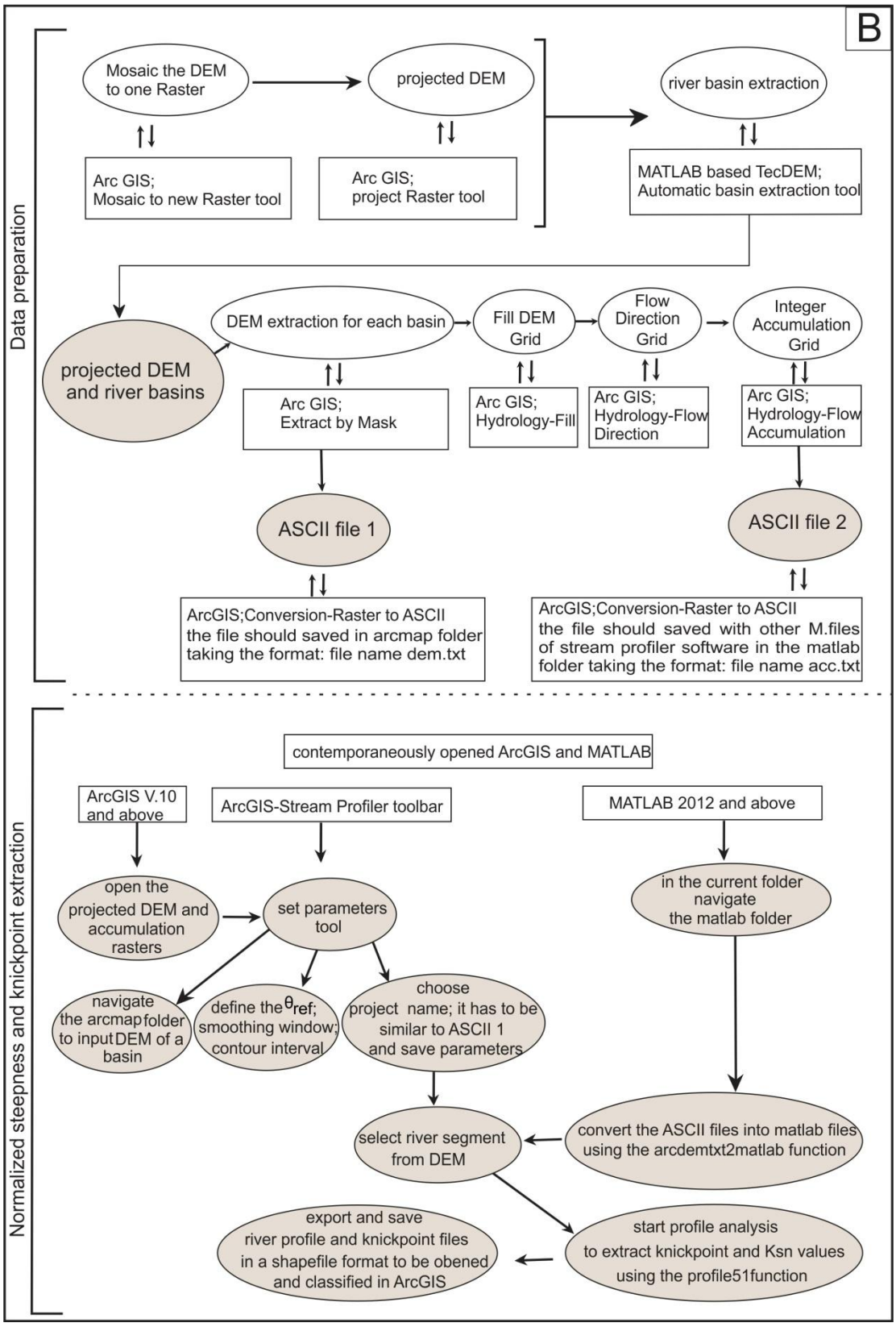

Fig. 2.5B. Summary of work flow adapted in the methodology shows data processing, software and the functions used to calculate k_{sn} and identify knickpoints.

2.3 Results

2.3.1 Climate

The climate of the Zagros is classified as arid to semi-arid with hot dry summer and cold arid winter (Kottek et al., 2006). The interaction between the Mediterranean and Sudan Lows synoptic systems with different elevations across the Zagros Mountains produces precipitation variability in space and time (Boroujerdy et al., 2013). The Tropical Measurement Mission (TRMM) satellite 3B43 data for 1998-2016 have been analysed. Results show high variability in precipitation across different regions of the Zagros (Fig. 2.6). The maximum precipitation (0.2 m/year) is in the Bakhtyari Culmination, Lurestan and the northeast of the Kirkuk Embayment. The minimum precipitation (0.05 m/year) was in the central and eastern Fars regions, the interior of the Turkish-Iranian Plateau and in the foreland.

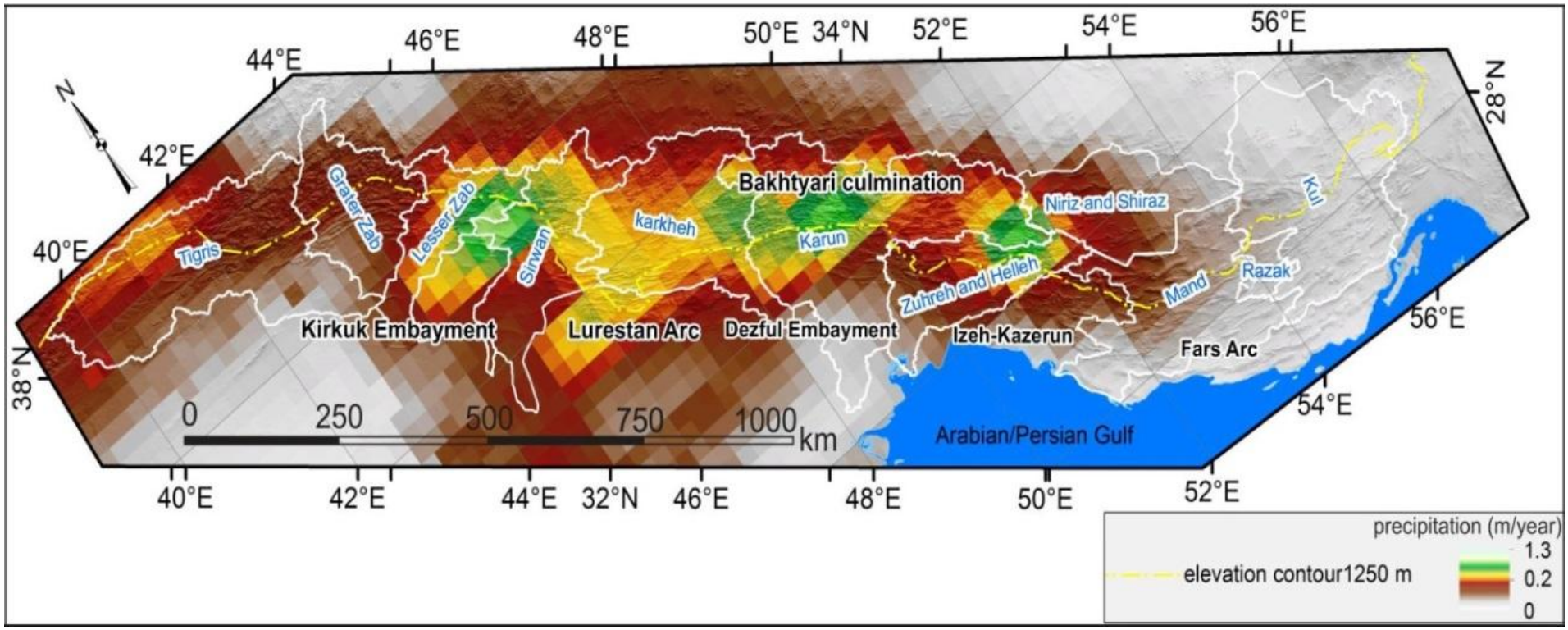

Fig. 2.6. SRTM 30 m shaded relief map of the Zagros, overlain by the mean annual precipitation from the Tropical Measurement Mission satellite TRMM 3B43 for the period 1998-2016 with resolution 0.25˚ * 0.25˚~ 25*25 Km. Note the big difference in precipitation between the Fars and the Dezful/Bakhtyari.

2.3.2 Zagros topography

The Zagros consists of different topographic regions: the high topography and low relief of the Turkish-Iranian Plateau to the east and northeast, the low relief and low topography of the Zagros foreland to the west and southwest, and the high relief areas of the Zagros fold-and-thrust belt between the plateau and the foreland (Fig. 2.7). It is a question as to what rate the plateau is growing outwards as the collision continues, and whether the rate and process is the same in different areas of the Zagros with different climatic or structural regimes (Allen et al., 2013). Plateau growth continues southwest in the Fars arc, and probably in the Lurestan arc, but may be retarded to the northeast in the Dezful/Bakhtyari region. The growth of the Turkish-Iranian Plateau is plausibly in a relation with crustal thickening, and the seismicity cut-off limit below the 1250 m elevation (Nissen et al., 2011; Allen et al., 2013). The location of the seismicity cut-off is therefore of importance to examine landscape's response to tectonism. The reasons for the Zagros topographic differences are debated and some geomorphic analysis may shed light on these differences.

Swath profiles across the Zagros in a width of 50 km (Fig. 2.7) show variations in topography across different regions of the Zagros. The difference in elevation ranges from ~ < 50 m in the Dezful Embayment to > 2500 m in the Bakhtyari Culmination. Some profiles exhibits gradual decline in elevation towards the foreland such as the Sinjar and Kirkuk profiles. Others drop sharply towards the foreland such as the Lurestan and Dezful (Fig. 2.7-a). The increase in elevation and gradient towards the hinterland mark the limit of seismogenic thrusting at 1250 m elevation (Allen et al., 2013) in both the Lurestan and Dezful sections. A very gentle change in elevation in the Fars region occurs even when passing through the cut-off of seismicity and the High Zagros Fault (Fig. 2.7-a). The difference between the maximum and the minimum elevations within the swaths (relief) shows how and where river networks dissect the landscapes.

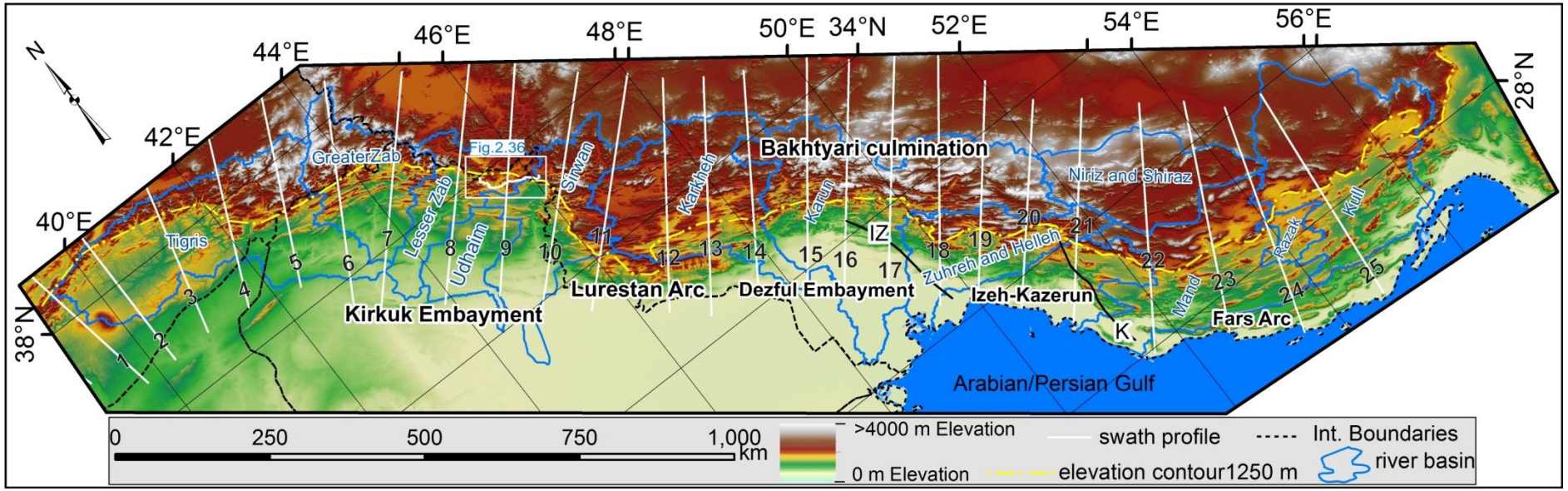

Figure 2.7a (Continued with caption on next page)

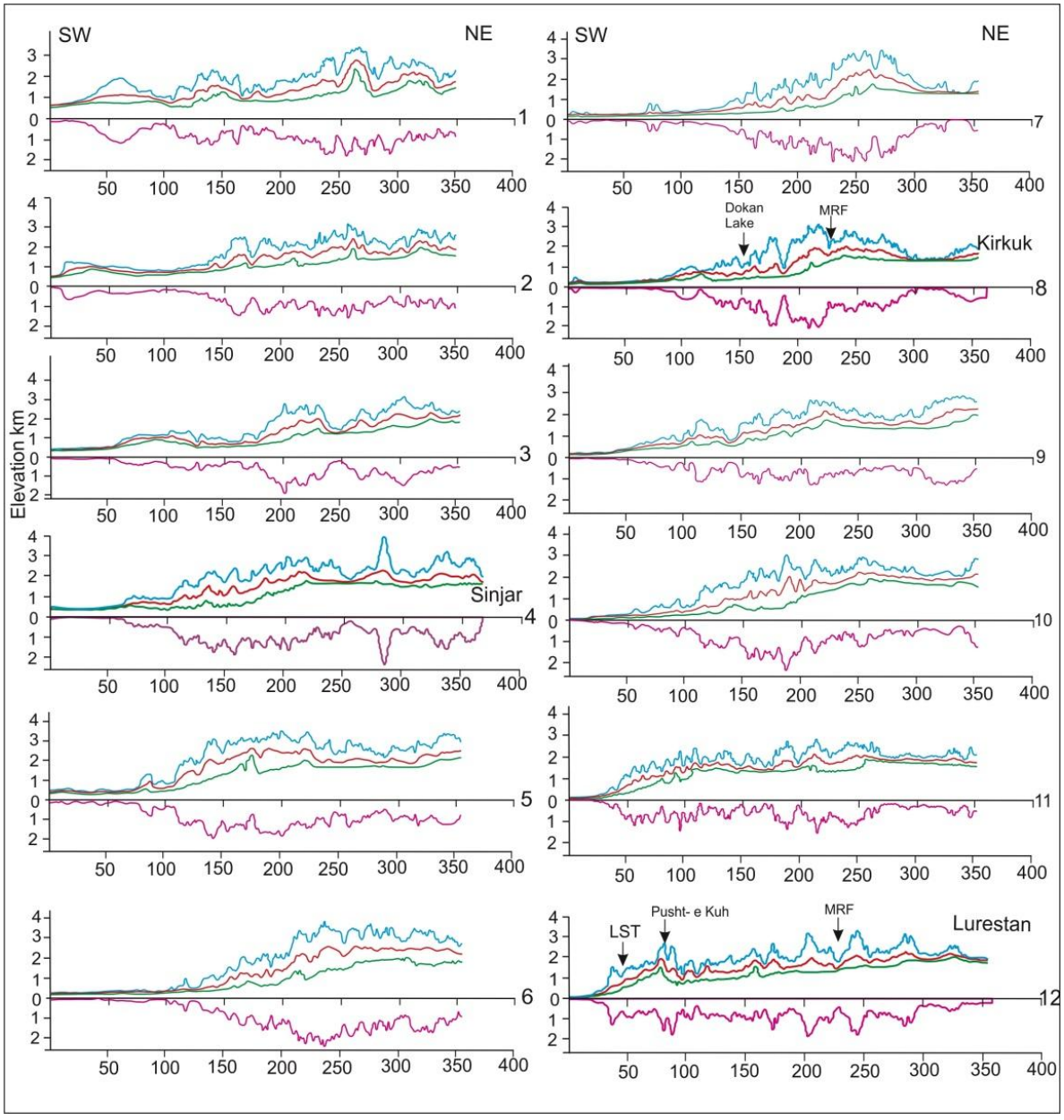

Figure 2.7a (Continued with caption on next page)

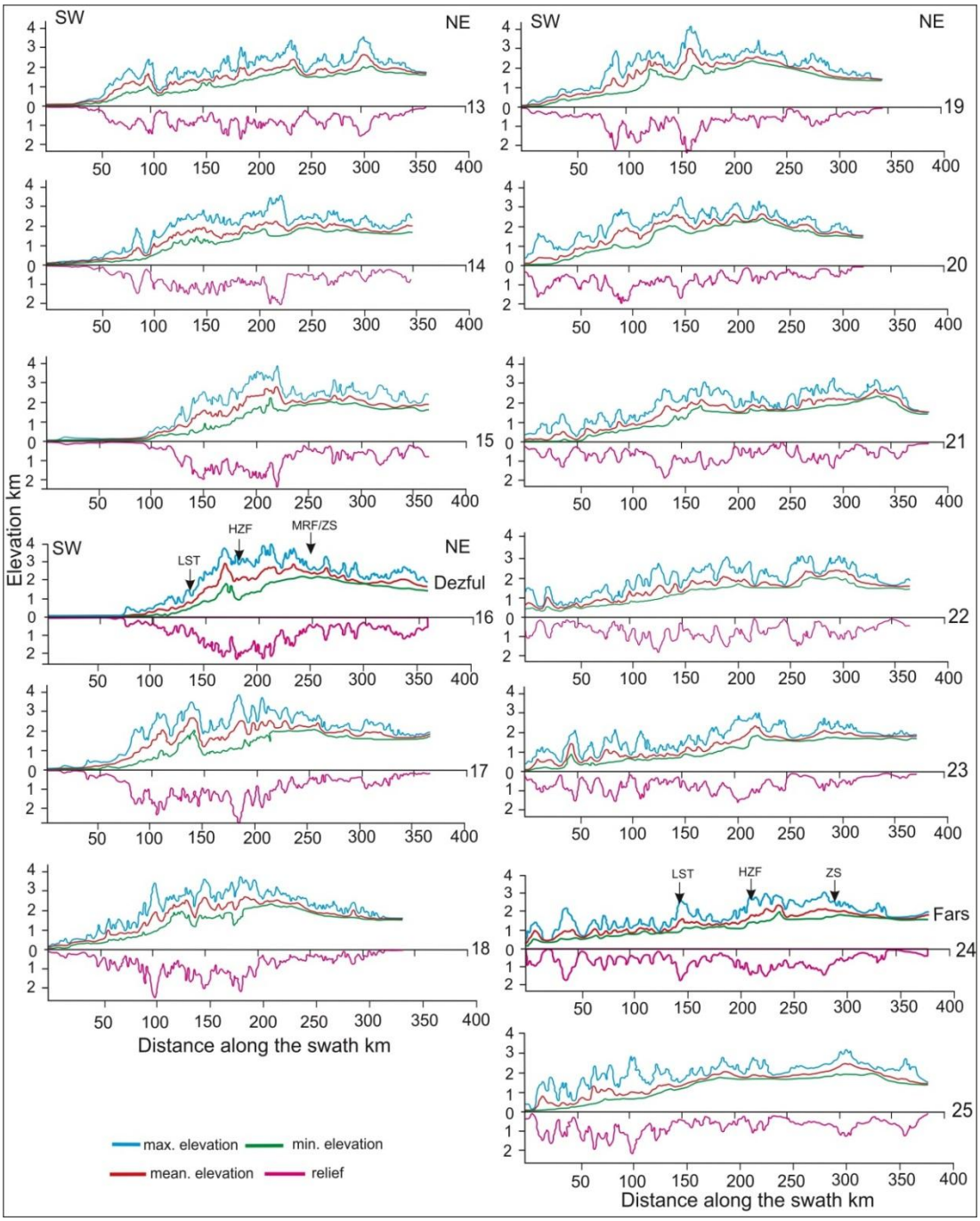

Fig. 2.7a. SRTM 30 m topography of the Zagros fold-and-thrust belt shows the major river basins in the Zagros. 25 Swath profiles centred on the section lines in the location map at the start of the figure show the patterns of topography and the changes in elevation and relief across different regions of the Zagros.

Five different regions across the Zagros have been selected to integrate their relief (Fig. 2.7b). A cumulative difference between the maximum and minimum elevations (shaded areas in Fig. 2.7b) exhibits a difference of ~20% (Fig. 2.57b), which is nearly similar for the selected five profiles in spite of the difference in along strike parameters of the Zagros.

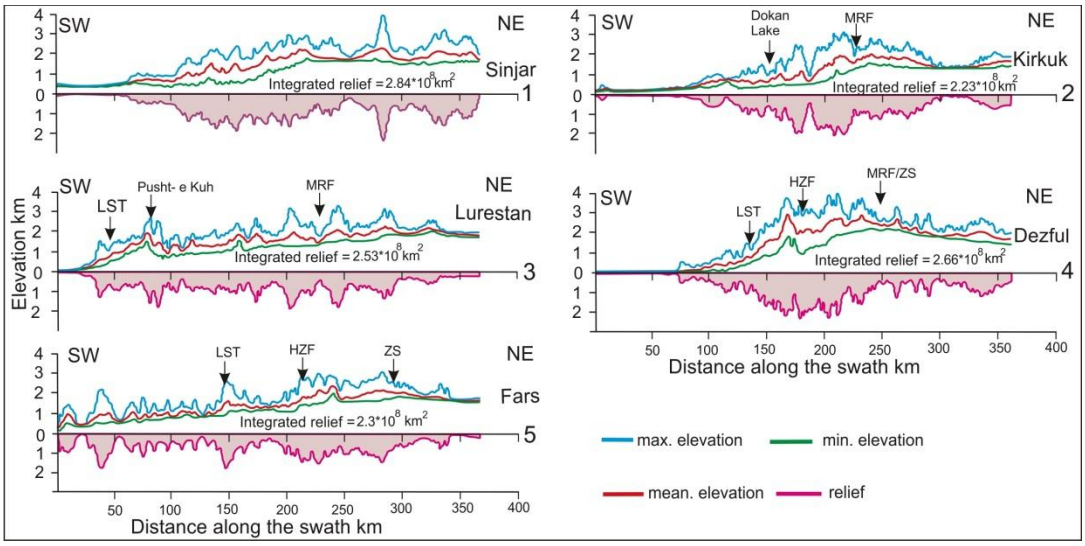

Fig. 2.7b. Integrated relief graphs show a limited relief difference in the order of ~20% between representative swath profiles. LST = Limit of seismogenic thrusting and ZS = Zagros Suture.

2.3.3 Zagros drainage basins

Owing to the structural growth, Zagros rivers have a specific configuration: generally they flow south, southeast, and some intermontane rivers flow northwest especially in the NW of the Zagros. From the north, the major rivers of the Zagros are: the Tigris, Greater Zab (GZ), Lesser Zab (LZ), Udhaim, Sirwan, Karkheh, and Karun rivers, and, to the southeast, the Mand and Kul rivers (Fig. 2.7a).

The Greater Zab River and Lesser Zab River converge with Tigris upstream of the Himreen/Makhool anticline while the Udhaim and Sirwan (Diyala) rivers continue southward and converge with the Tigris in Balad district and southern Baghdad city respectively. The drainage network of the Greater Zab, Lesser Zab, Udhaim and Sirwan river basins converge in the Kirkuk Embayment. Other smaller and ephemeral streams also flow towards the Tigris basin draining the area of the western side of the Lurestan arc. The Karkheh River converges with Karun River in the Dezful Embayment to join the main and large drainage system of the Tigris in the Sutt Al-Arab, preceded by 80 km of another confluence between the Tigris and the

Euphrates in Al-Qurnah. These river basins have many streams interacting with the anticlinal structures of the Zagros in different patterns, which may reflect the differences in an individual anticline's growth and/or the differences in tectonics from one area to another.

2.3.4 River-fold interaction of the Zagros

The study of river-fold interaction in the Zagros had been dealt with by local studies without comparisons between different regions along strike of the Zagros (e.g. Bahrami, 2013; Bretis et al., 2011; Burberry et al., 2008, 2010; Ramsey el al., 2008; Walker et. al., 2011; Zebari and Burberry, 2015). There are differences in the cross-cutting relationships between the folds and river in the Zagros from one region to another, which might relate to the differences in topographic uplift and the differences in climate. Figures 2.8 and 2.9 show how rivers cross most of anticlines in the Dezful/Bakhtiari region and north of the Kirkuk Embayment respectively, which are characterised by high relief and high topographic uplift. In contrast, the Fars region shows a general tendency of river deflection and the Fars rivers rarely cross anticlines, which could be the result of a relatively drier climate and relatively low topography (Fig. 2.10) (see also descriptions and discussion later in this chapter). The NW of the Zagros has both patterns; some rivers cross anticlines and the rest divert or exploit the relay zones between anticlines, which might refer to the differences in the levels of uplift of folds in this region (Fig. 2.9).

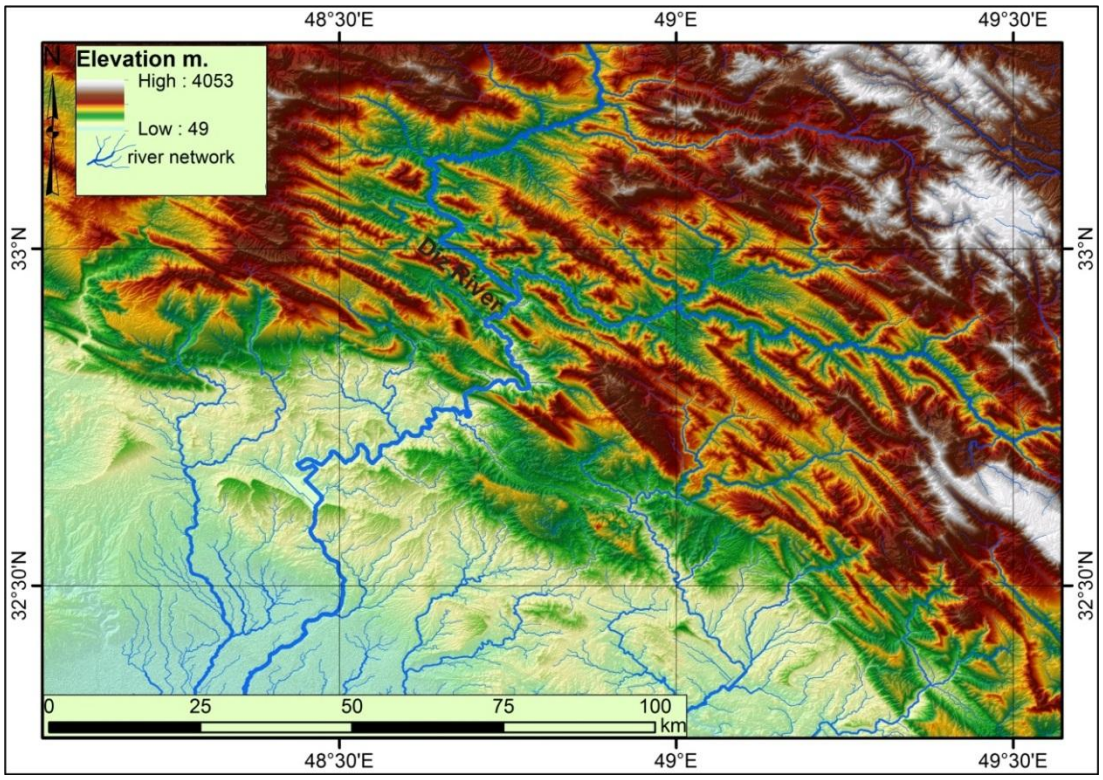

Fig. 2.8. SRTM 30 m topography shows the interactions between the river network and folds in the Dezful region; the active tectonics and youthful landscape means that elongate topographic ridges correspond to anticline crests.

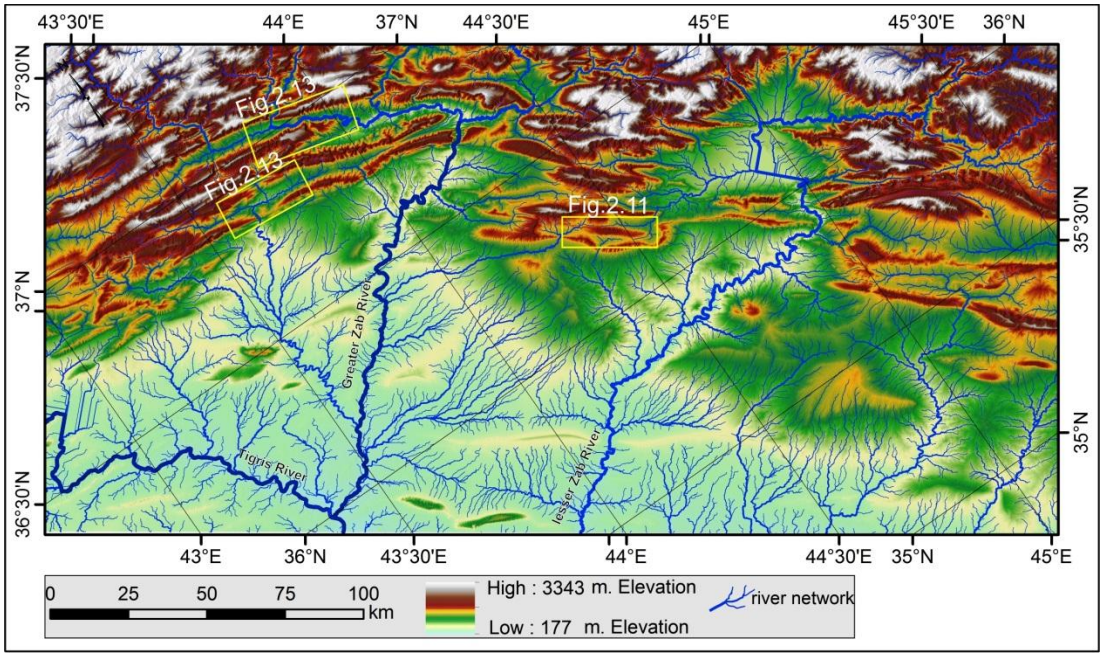

Fig. 2.9. SRTM 30 m topography shows the interactions between rivers and folds in the NW of the Zagros (Kirkuk Embayment/Iraq).

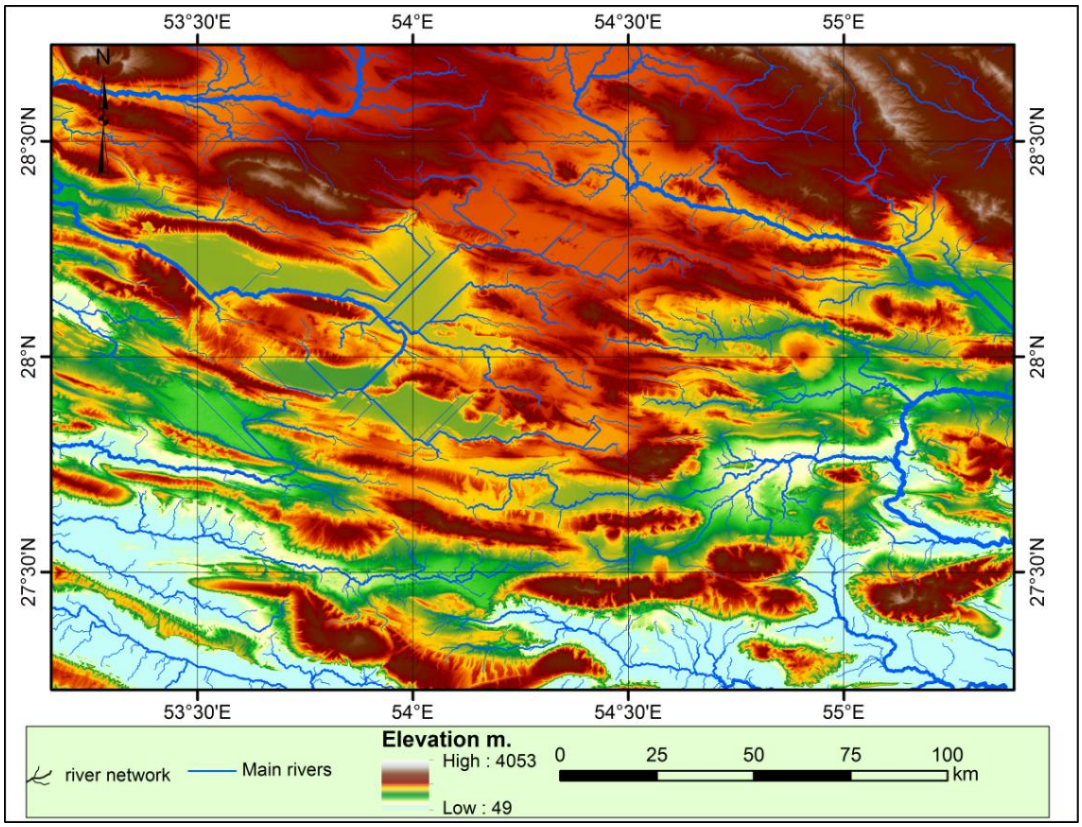

Fig.2.10. SRTM 30 m topography shows the interactions between river networks and folds Fars region. Straight river segments are artefacts, where the drainage extraction algorithm interprets a segment across a low-gradient region in error. Such regions are typically lakes or playa lakes.

The occurrence of wind and water gaps relates to fold growth (Bretis et al., 2011; Ramsey el al., 2008). In this section I highlight some examples of lateral fold growth from different areas of the Zagros. Some of these anticlines show a single wind gap and other show multiple wind gaps. It is worth noting that many folds show no wind gaps: Figure 2.11 shows the topography of the Bani-Bawi Anticline, which has side valleys related to consequent stream channels that flow in opposite directions down the flanks of the fold, to join axial rivers concentrated along the synclinal valleys between the anticlines in this region. These side valleys do not align with each other across the Bani-Bawi fold crest, and so there is no indication that they are remnants of a previous river channel across the whole structure as was previously interpreted by Bretis et al. (2011).

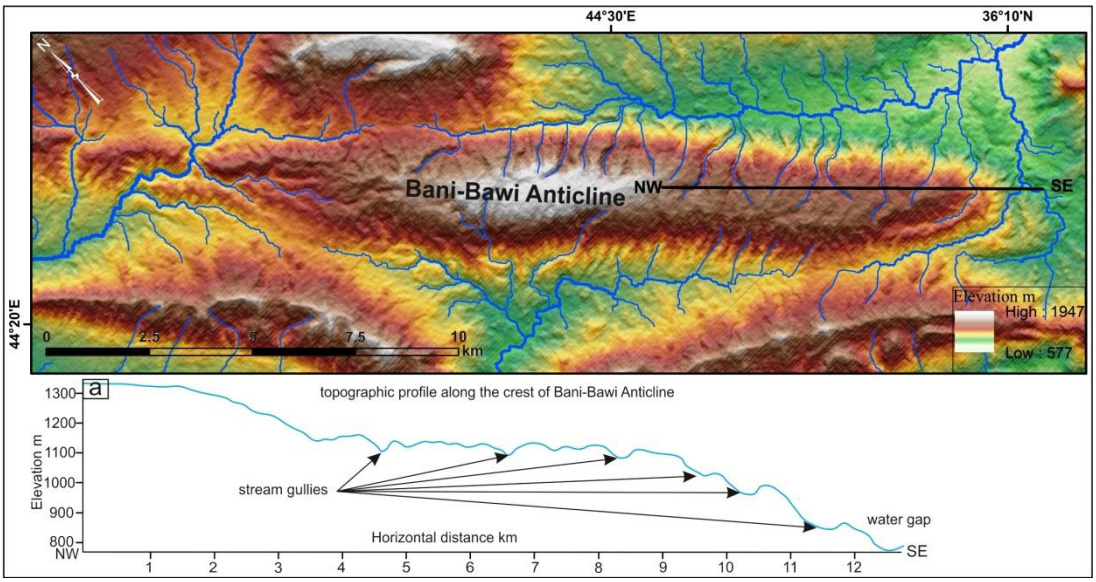

Fig.2.11. SRTM 30 m topography of Bani-Bawi anticline (Fig.2.9) rotated 45˚ anticlockwise shows consequent streams on the anticline's crest, which misinterpreted by Bretis et al. (2011) as wind gaps. (a) Topographic profile along the northeastern fold flank shows a series of stream gullies developed as the fold has grown over time.

In contrast, the Garya Anticline in the High Folded Zone of the Iraqi Zagros shows growth in its SE tip. This growth defeated one of the biggest rivers in the region, which is the Greater Zab River, and has left a wind gap in a valley with relief of 500 m, which is unlikely to be caused by the low-order river (first order) stream that partially occupies the Garya wind gap at present (Fig. 2.12). The crest of the wind gap is ~ 400 m above the present course of the Greater Zab (Fig. 2.12), which gives an indication of the surface uplift since the gap was abandoned as the active channel. The timing of abandonment is not constrained, so there is no constraint on the surface uplift rate.

To the south of Garya Anticline there are wind and water gaps that carve into the hinge line of the Aqra Anticline (Fig. 2.13), which consists of 3 to 4 anticlines connected due to the activity of a long major segmented thrust referred to as the Mountain Front Fault (MFF). The MFF separates the High Folded Zone from the Low Folded Zone (Jassim and Goff, 2006). For this segment of the train of anticlines the lateral fold growth is from B to A (Fig. 2.13) according to the wind and water gap occurrences.

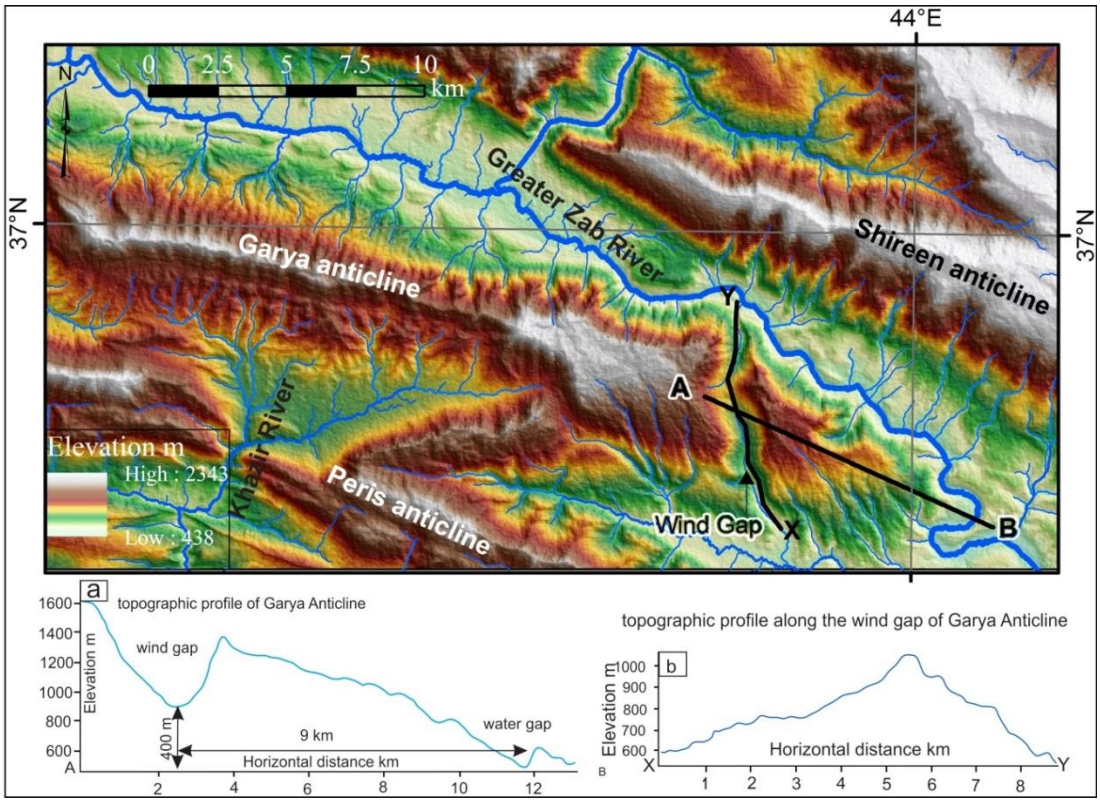

Fig. 2.12. SRTM 30 m topography of the Garya Anticline (Fig. 2.9) shows the deflection of Greater Zab River to the ESE. (a) A-B Profile along the SE tip of Garya Anticline shows 9 km distance of river segment deflection, leaving a 400 m difference in elevation between wind and the current drainage path across the fold (water gap). (b) Profile X-Y along the wind gap of Garya Anticline approximates an asymmetric convex curve (shown by the blue line) that demonstrates the fold uplift.

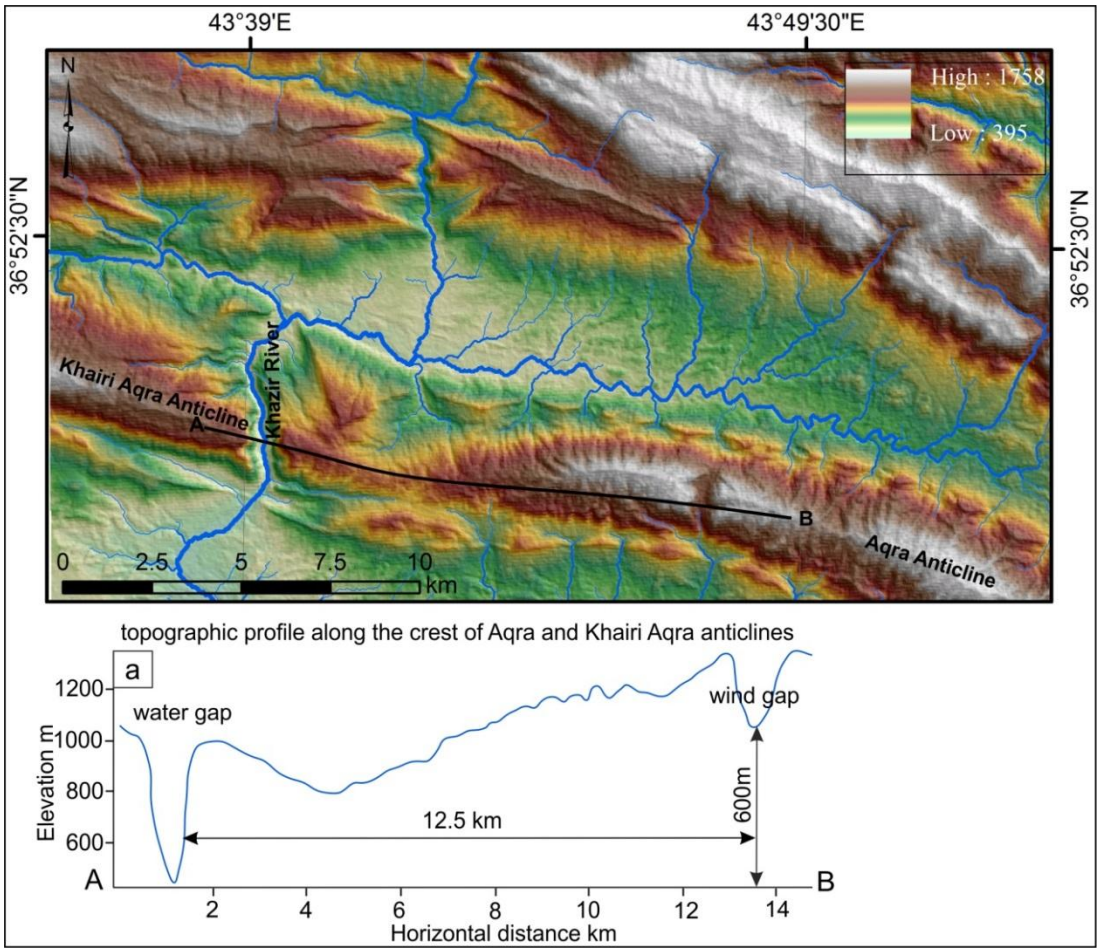

Fig. 2.13. Colour-coded 30 m SRTM topography shows the deflection of two tributaries linked to the Khazir River that cuts through the Aqra Anticline (Fig.2.9). a) A graph shows a 600 m elevation difference between wind and water gaps that were left after 12.5 km of river diversion to the west. The connection point between the Aqra Anticline and the Khairi Aqra Anticline to its west was exploited by the Khazir River at the relay zone between them.

The Kerned Garb Anticline (Fig. 2.14), an example from the Lurestan Arc, shows an eastward growth of the fold and clearly shows curved wind gaps. In the Fars region, wind gaps may be found in a few anticlines, because rivers have lower discharge than other regions of the Zagros because of the dry climate (Boroujerdy et al., 2013) and rivers are mostly diverted around anticlines. The Khonj Anticline exemplifies the lateral growth of fold in the Fars region (Fig. 2.15) (Ramsey et al., 2008); it has four wind gaps and one water gap exploiting the relay zone between the eastern Khonj and western Khonj anticlines.

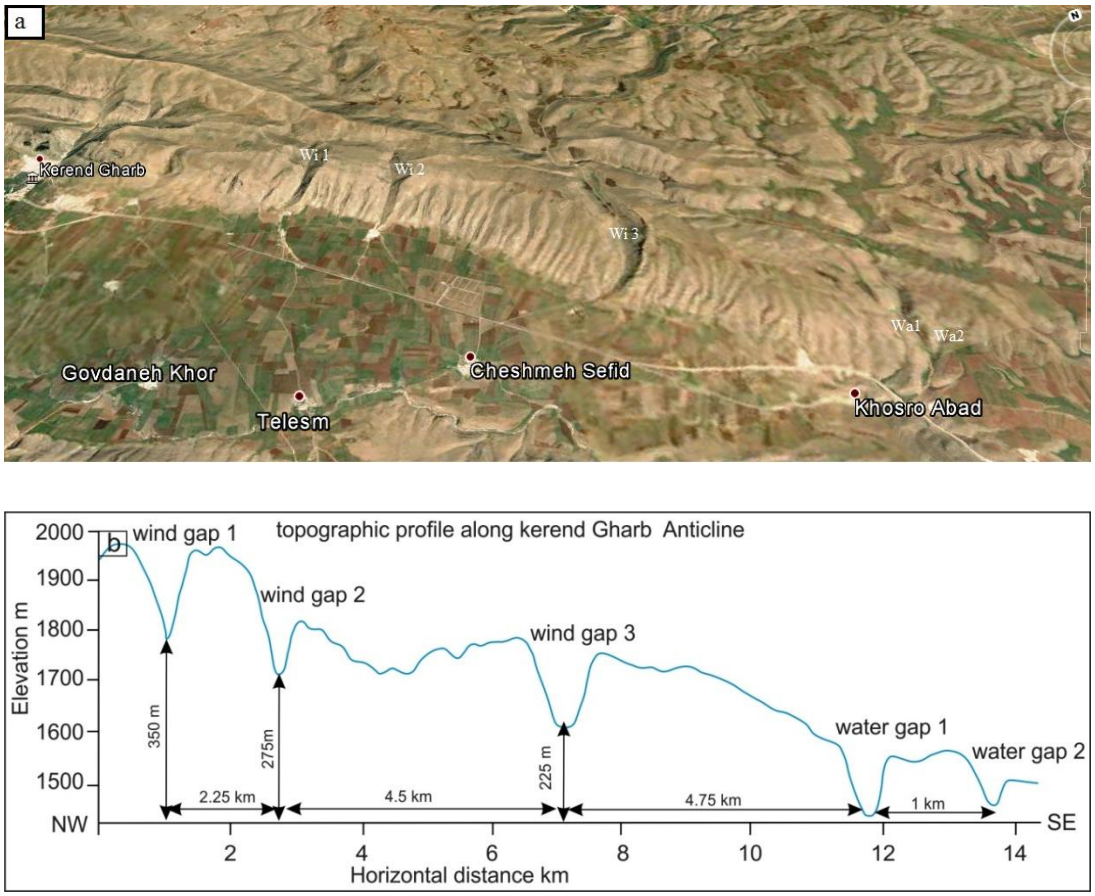

Fig. 2.14 (a) Google Earth image of the Kerend-Gharb Anticline in Lorestan, Iran, shows the development of the curved wind gaps. (b) A graph extracted from SRTM 90 m shows the evolution of water and wind gaps due to fold growth.

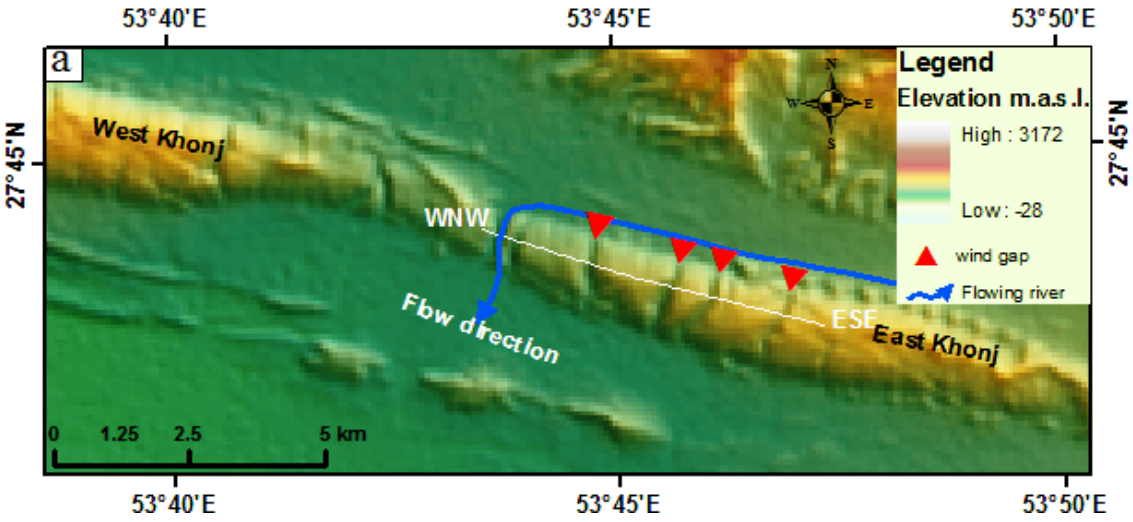

Fig. 2.15a. SRTM 90 m shows the topography of the Khonj Anticline as an example of lateral growth from the Fars region, and the deflected river around the WNW tip of the eastern part of the anticline.

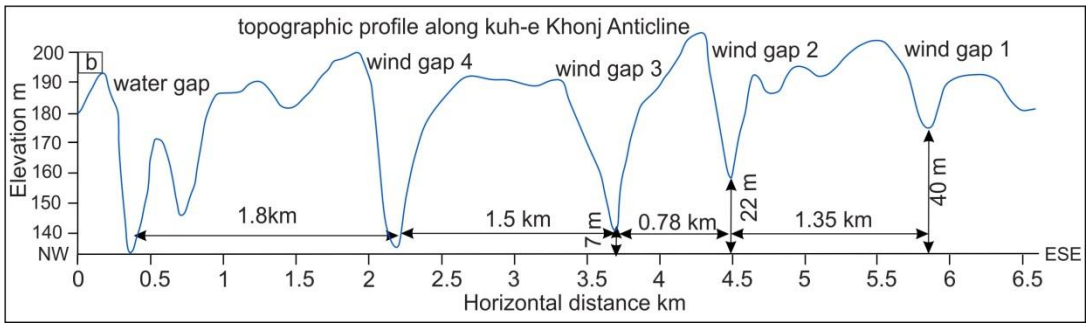

Fig. 2.15b. A graph shows the elevations and distances of four wind gaps along the crest of the East-Khonj Anticline. Note: the first, third and fourth distance intervals are nearly equally spaced except for the second interval, which may reflect episodic changes in hydrological/climatic or tectonic conditions.

2.3.5 River profiles

Longitudinal profiles were generated for 340 rivers within the Zagros. Reaches of k_{sn} <50 $m^{0.9}$ are distributed across the Iranian plateau, the foreland, intermontane rivers and Fars region (Fig. 2.16). Knickpoints generated from the regional analysis are shown in Fig. 2.17. Ranges of $50 \leq k_{sn} \leq 100$ $m^{0.9}$ occur in the high relief areas of the Bakhtyari Culmination, Sirwan River basin, and in terrain at close the 1250 m elevation contour in the NW Zagros, near the Iraq-Turkey border (Fig. 2.16). Similar distribution occurs across the high relief areas when considering the range of $100 \leq k_{sn} \leq 150$ $m^{0.9}$ (Fig. 2.16). The threshold of $k_{sn} \geq 150$ $m^{0.9}$ occurs only for a few river segments in the high relief areas of the Bakhtyari and the NW Zagros of Iraq and Turkey (Fig. 2.16). Reaches of the Mand River in the Fars region (Fig. 2.7a) have a relatively high k_{sn} value (51-100) regardless of the low relief of the area (Fig. 2.16). This is different than other rivers in the Fars region.

Overall, knickpoint distribution across the Zagros does not highlight any prominent, range-parallel, thrusts operating at shallow or emergent levels within the crust (Fig. 2.17). Knickpoints also occur above and below the 1250 m regional elevation contour (Fig. 2.17), i.e. both within and outside of the zone of active seismic deformation (Nissen et al., 2011). There are two zones where there are localised alignments of knickpoints, along the Main Recent Fault (MRF) and the Khanaqin Fault (KH) (Fig. 2.17), explored later in this chapter.

Figures 2.18-2.32 present lithology, knickpoint distributions, k_{sn} value above and below knickpoint and maximum and mean elevation for different regions of the Zagros, to explore their relationships in more detail for local areas of the range. Figure 2.18 shows the validation of using the standard reference value for (0.45). A comparison with the exposed lithologies of the Bakhtyari Culmination shows that changes in k_{sn} value do not correlate with changes in lithology, at least on the scale of the Bakhtyari Culmination. Areas of limestone in Fig. 2.18 show different values of k_{sn}, whilst rivers crossing varied lithologies maintain similar values of k_{sn}. A specific example from Fig. 2.18 shows that the river segments have k_{sn} values of 100-150 $m^{0.9}$ regardless of bedrock type, which includes limestone, dolomite and ophiolitic lithologies such as serpentinite (see area shaded black in Fig. 2.18). Similar pattern can be found in the Turkish-Iranian Plateau where the river crossing the metamorphic, igneous and quaternary deposits (the north east corner of Fig. 2.18) have k_{sn} value of (25-50).

In contrast, knickpoint locations in the Fars appear at first sight to show a correlation with lithology; knickpoints are commonly located over limestones (Fig. 2.19). However, this may be a coincidence: knickpoints in Fig. 2.19 are also commonly where rivers cross relay zones between folds (e.g. the Khonj Anticline; Fig. 2.15), such that the limestone has been exposed by erosion of overlying lithologies at the anticlines.

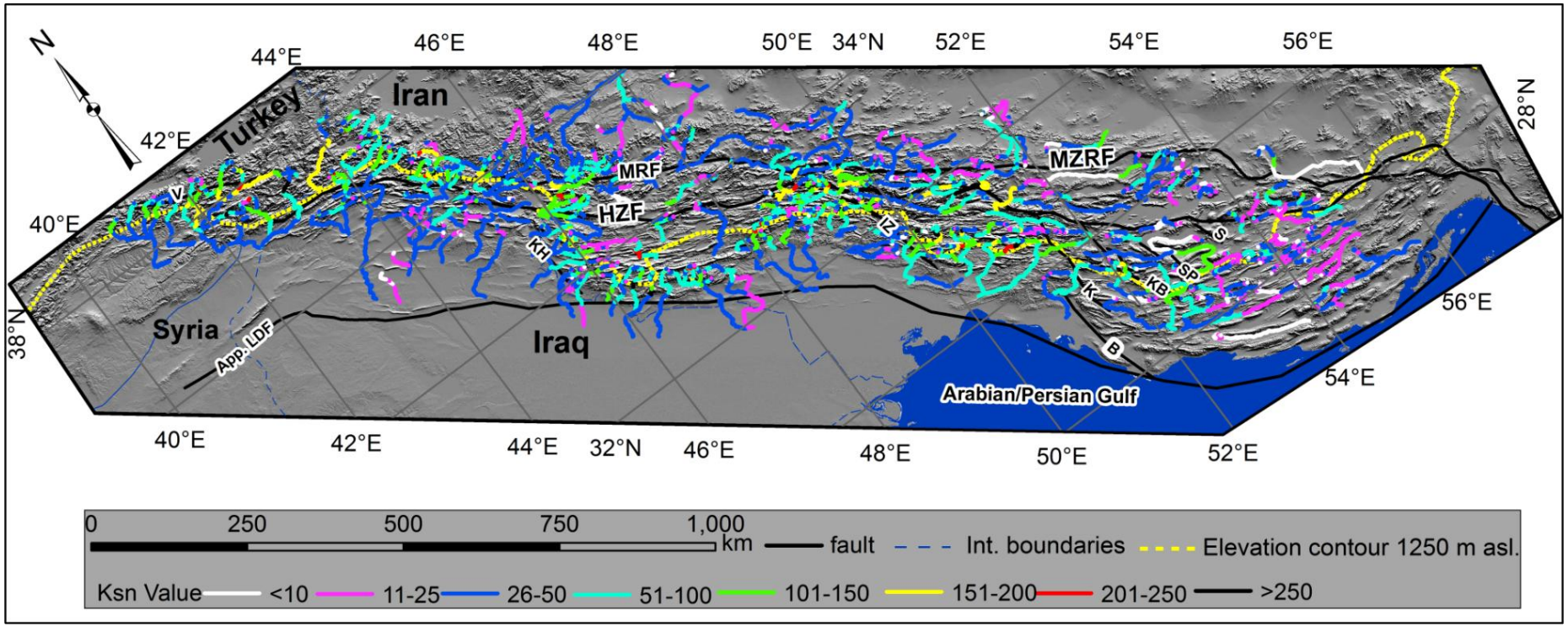

Fig. 2.16. distribution of k_{sn} value of river segments across the Zagros. High relief areas have high k_{sn} values. Note the low k_{sn} values of the Fars region.

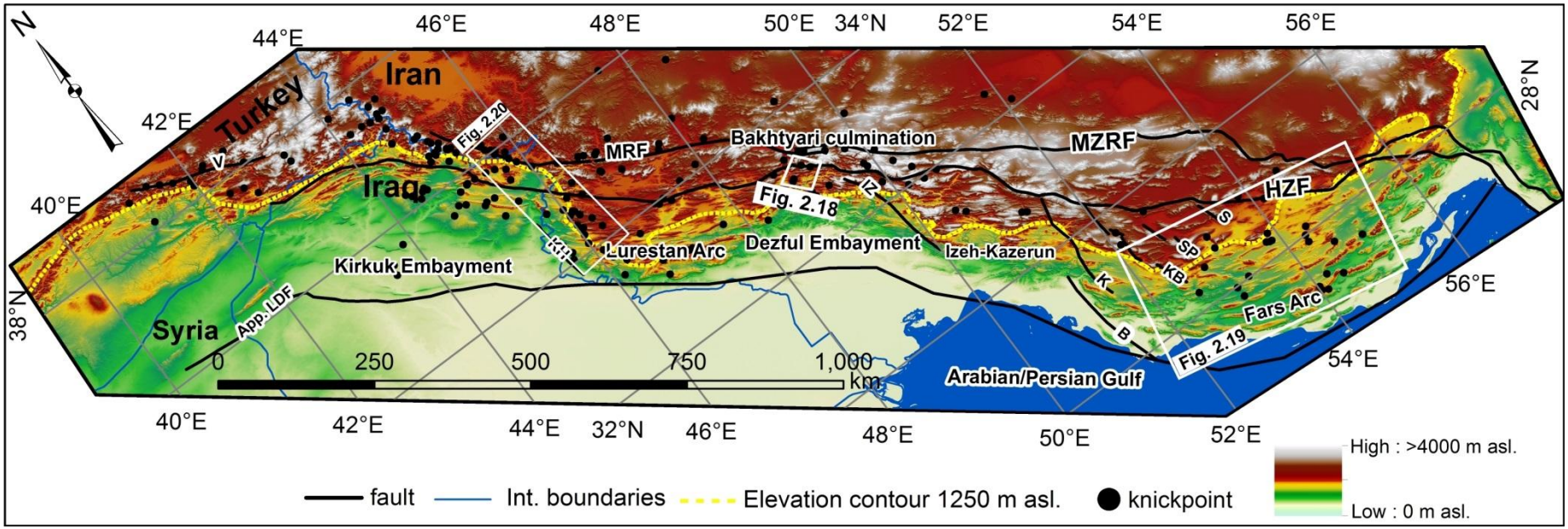

Fig. 2.17. Distribution of knickpoints across the Zagros, with no obvious patterns for the whole fold-and-thrust belt, only locally around the KH and the MRF.

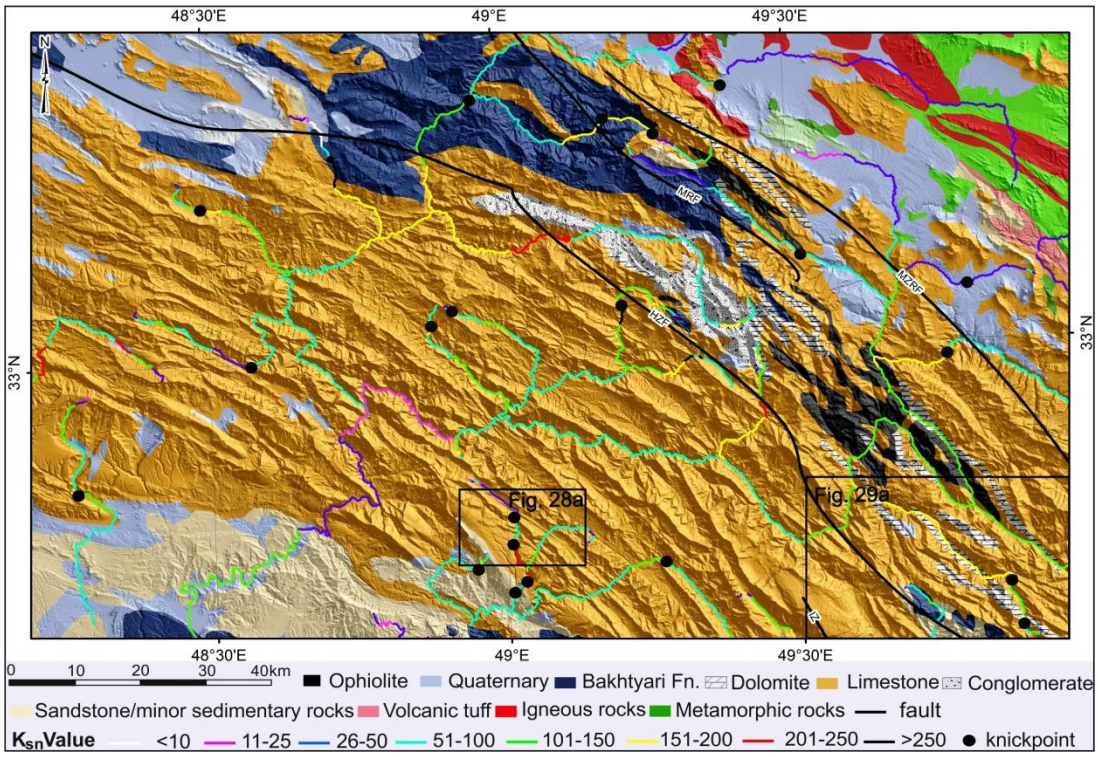

Fig. 2.18. Geological map (geology from sources in Fig. 2.1B), overlain by k_{sn} values of river segments, and knickpoints. Knickpoints across the Bakhtiari Culmination are largely independent from the lithology, although several are located at the southern limit of the regional limestone outcrop. See figure location in Fig. 2.17.

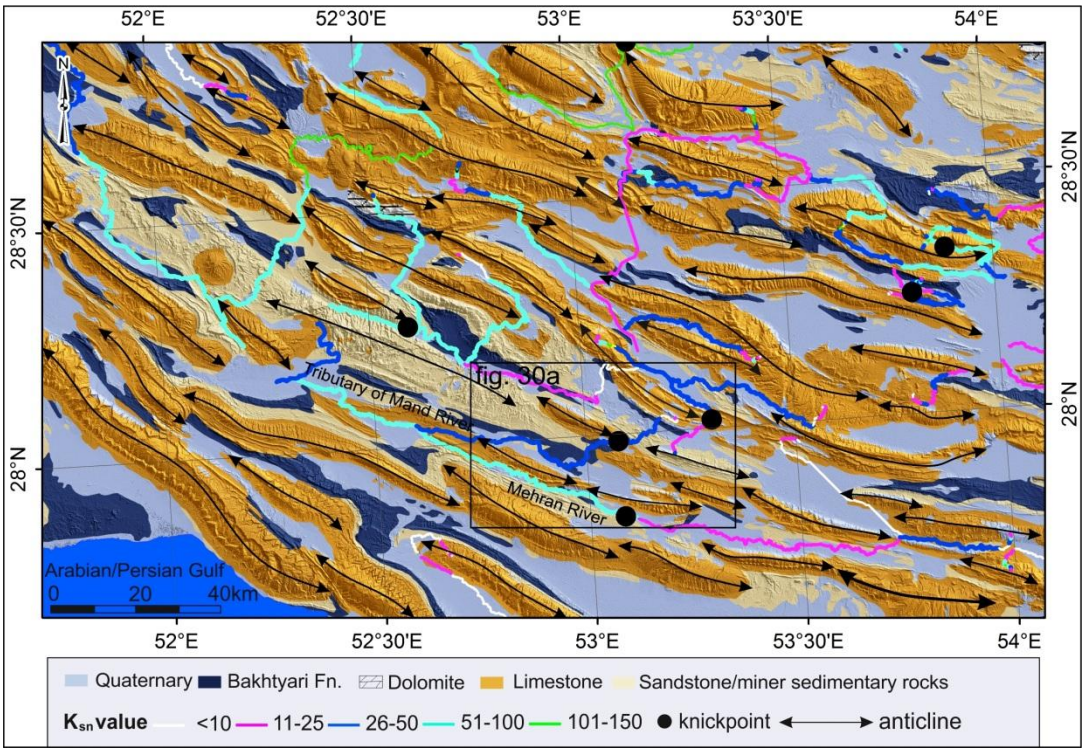

Fig. 2.19. Pattern of the k_{sn} values across the Fars Region and the relation of knickpoints with the exposed lithology (geology from sources in Fig. 2.1B). Knickpoints are generally located at zones of lithological changes, but these knickpoints probably tectonic in origin as they are lie at tips of folds. See figure location in Fig. 2.17.

Figure 2.20 shows the distributions of lithologies and knickpoints from part of the north western Zagros, including the Main Recent Fault (MRF) and the Khanaqin Fault (KH). The MRF is an active, right-lateral strike-slip fault at the northeast side of the Zagros, reactivating the Arabia-Eurasia suture. Its activity partitions oblique convergence. Figure 2.21 shows the geology, drainage network and knickpoint locations along the MRF, highlighting knickpoint alignment along the structure.

The knickpoint alignment along the MRF shown on Fig. 2.21 is shown in Fig. 2.22 to coincide with the 1350 m elevation contour, and in Fig. 2.23 with changes in river segment k_{sn} values (unsurprisingly). It shows no clear correlation with lithology (Fig. 2.21).

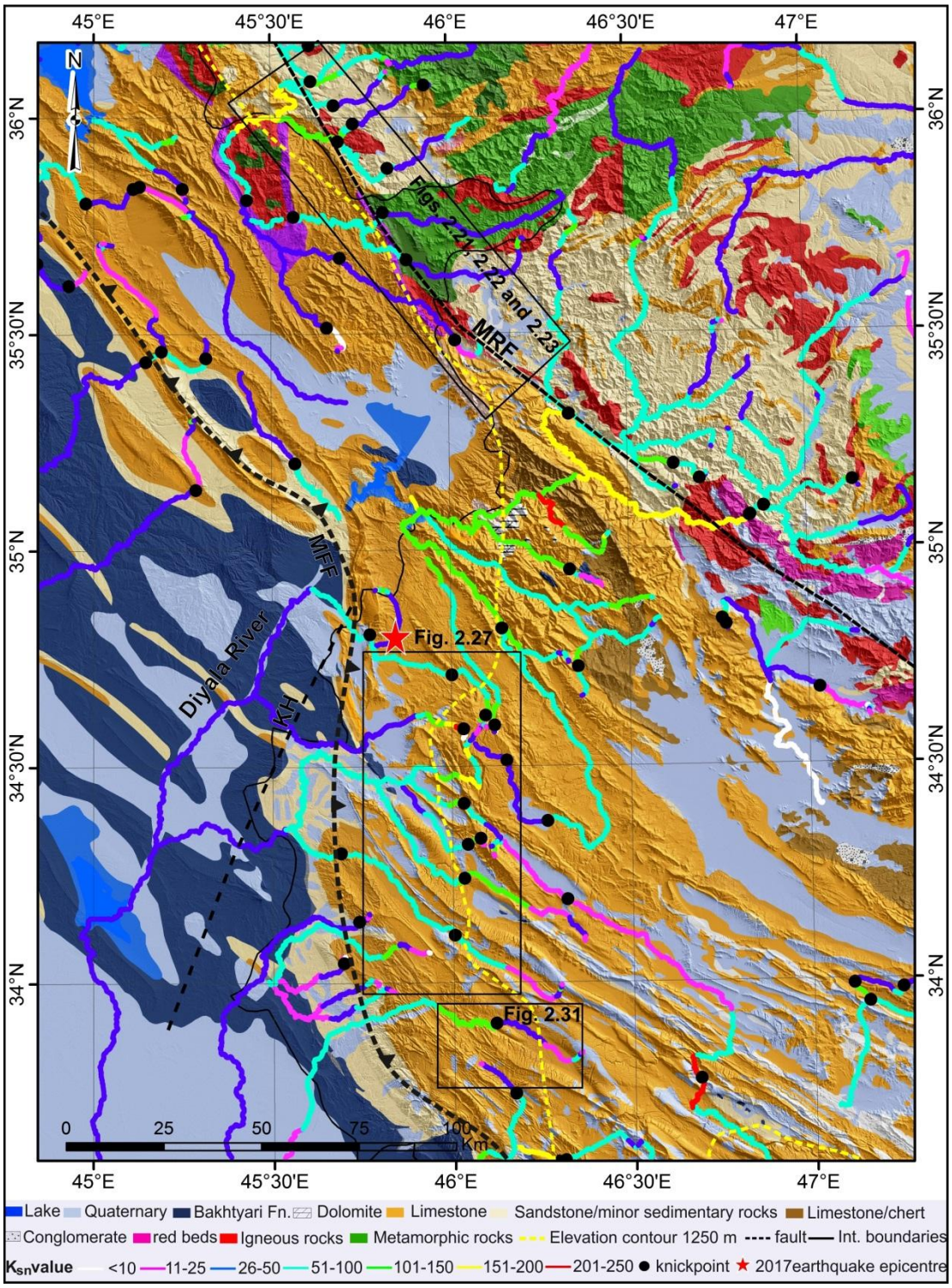

Fig. 2.20. Distribution of k_{sn} and knickpoints, northwestern Zagros. Knickpoints are aligned along the Main Recent Fault (MRF) and near to the Khanaqin Fault (KH), close to the 1250 m elevation contour (limit for seismogenic thrusting). Dashed line marks the Mountain Front Fault. The location of knickpoints shows no correlation with the exposed lithology (geology from sources in Fig. 2.1B). The star marks the epicentre of the 2017 *M* 7.3 earthquake. See figure location in Fig. 2.17

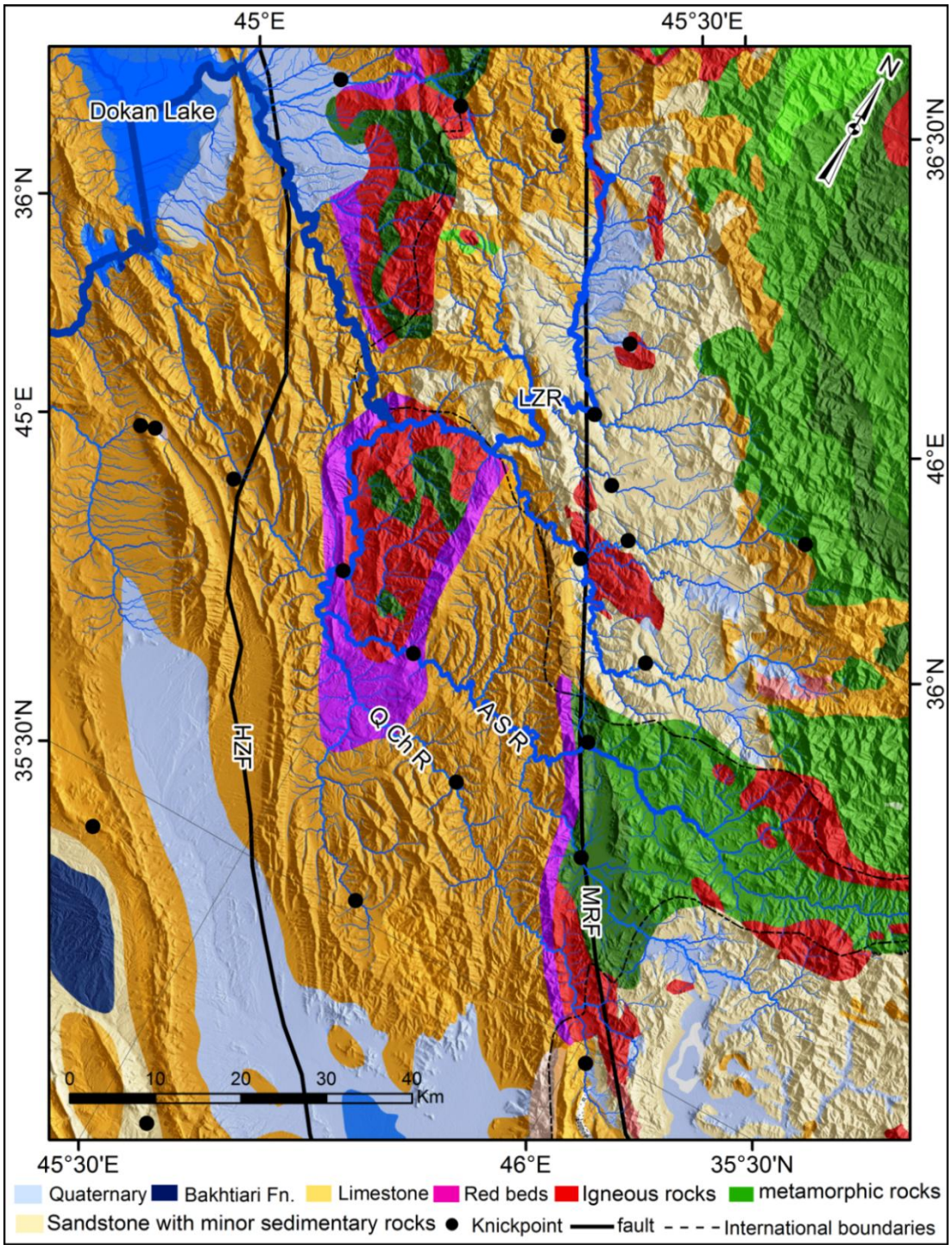

Fig. 2.21. Knickpoint location and drainage network of the Lesser Zab River basin underlain by the topography and bedrock geology (geology from sources in Fig. 2.1B). LZR = Lesser Zab River; ASR = AwaSwell River; QChR = QaraChwalan River.

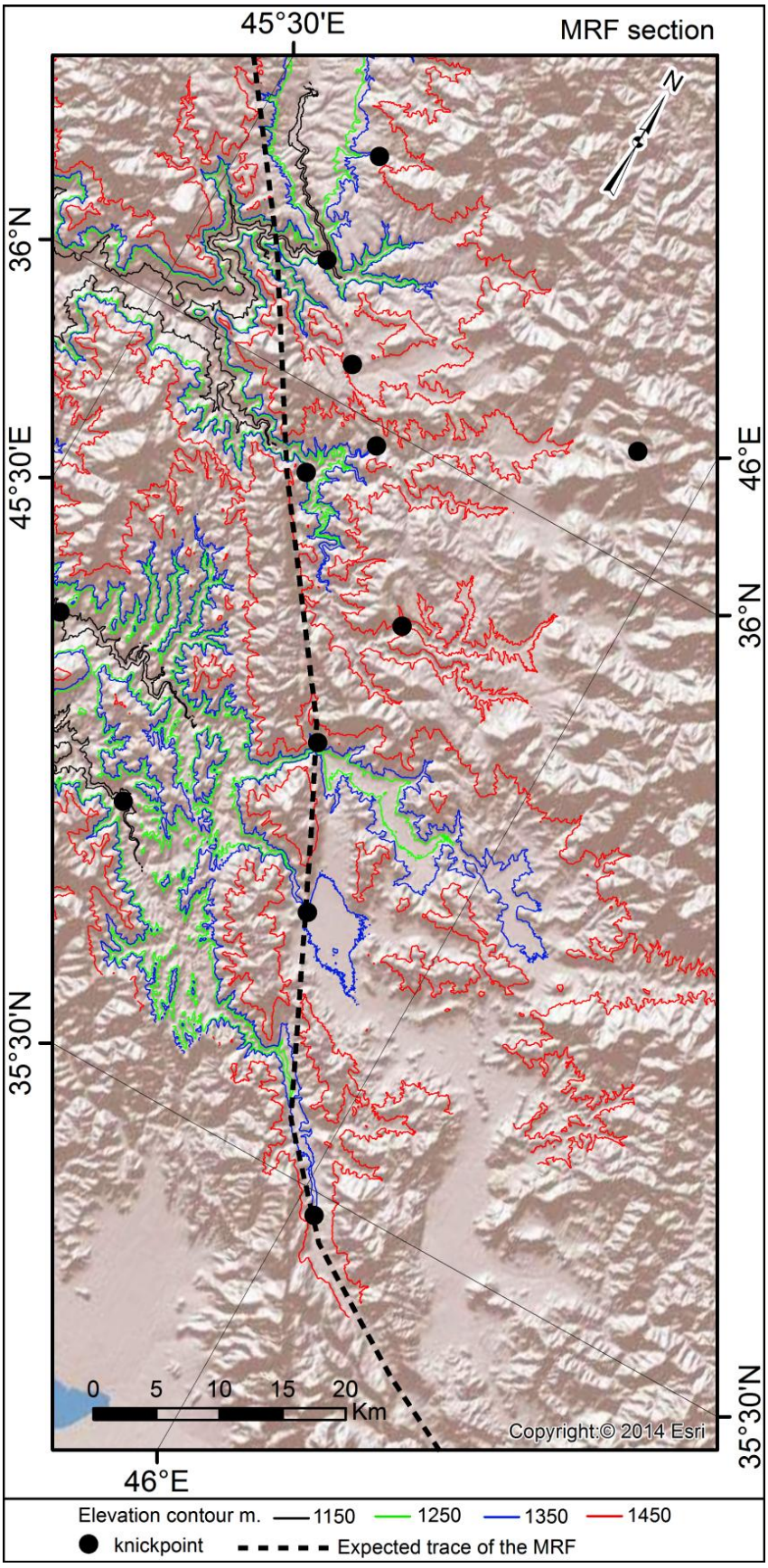

Fig. 2.22. Knickpoint alignment at roughly the 1350 m elevation contour of the Lesser Zab River basin.

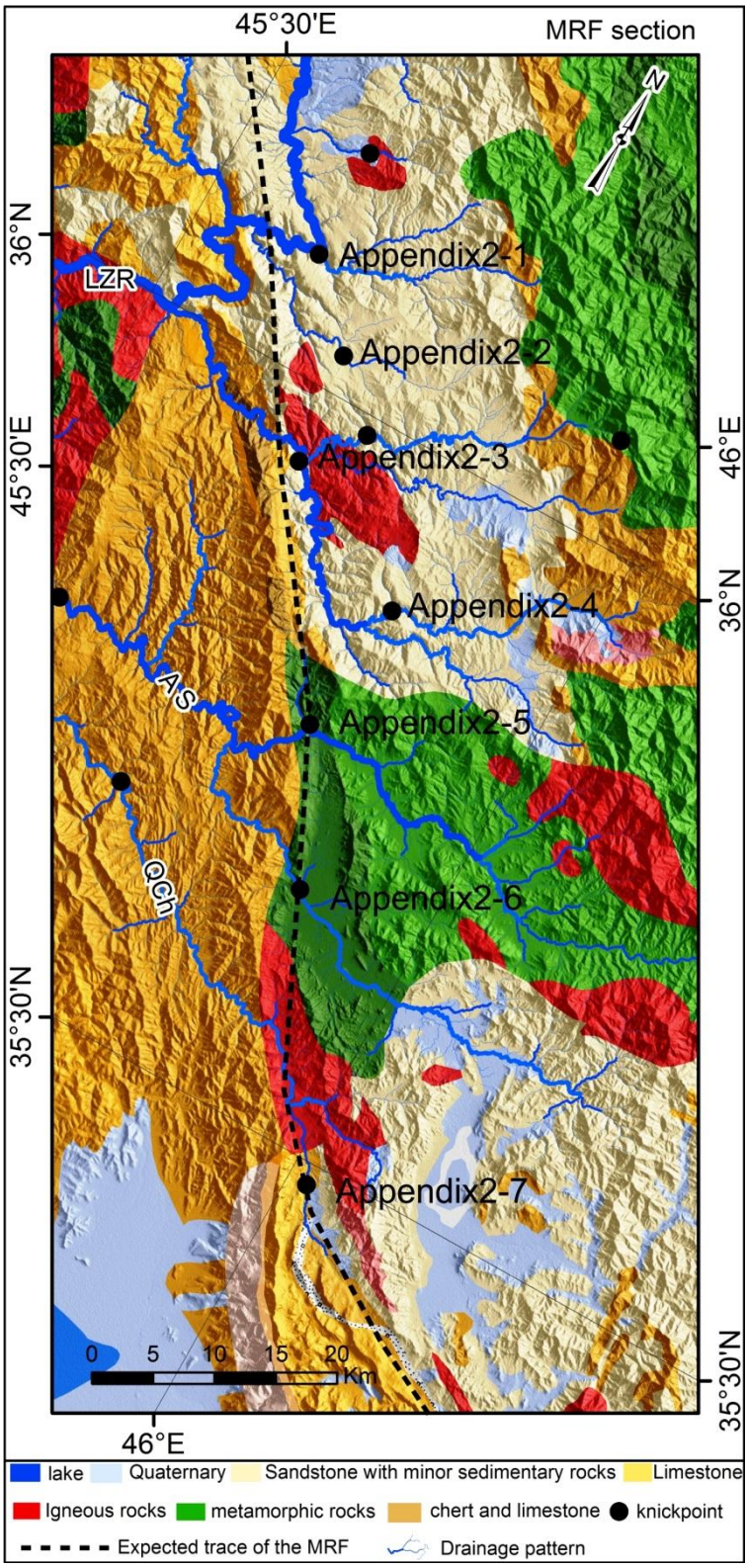

Fig. 2.23. Alignment of knickpoints on NW segment of the MRF, as for Fig. 2.21 with the addition of river segment k_{sn} values. From the SE, the 1st, 2nd and 3rd knickpoints lie within the Kuhe-e-Bistoon Formation limestone, Penjween intrusion, Giom metamorphic group respectively. The rest of knickpoints lie within sandstone and argillaceous shale (geology from sources in Fig. 2.1B). Appendices 2.1-2.7 refer to river profile analysis and knickpoints mentioned in the figure and found in appendix 2. See abbreviation in fig.2.21.

22 selected trunk rivers along the strike of the Zagros including rivers of the MRF zone and Khanaqin zone (appendix 2 and table 3.1) has been plotted with the maximum and mean topographic elevation (Fig. 2.24). Also upstream area above knickpoint and river distance below knickpoint (Fig. 2.25) has been examined to investigate whether these knickpoints were generated in the same time period (Wobus et al., 2006; Boulton et al., 2014). No potential vertical distribution has been found as shown by weak relation between downstream distance and upstream area of knickpoint (Fig.2.23) which means there is no clear evidence about the timing of knickpoint generation.

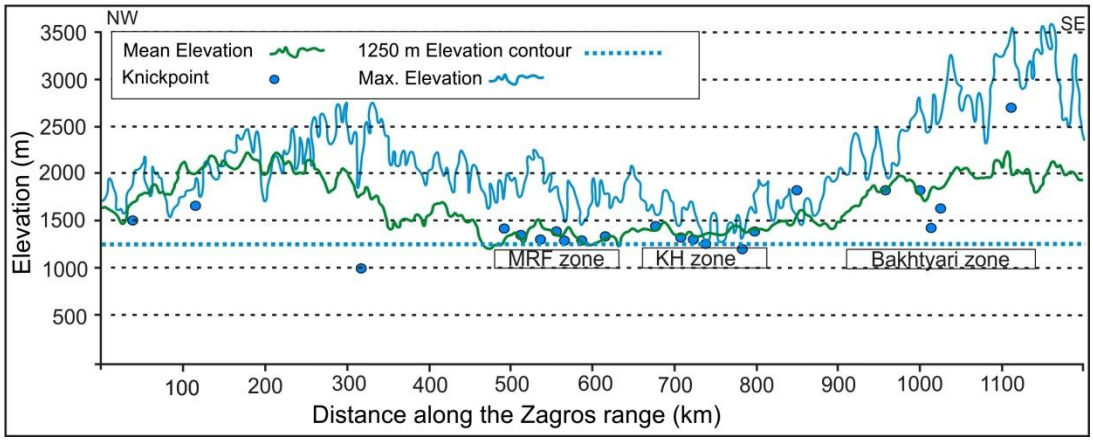

Fig.2.24. Knickpoint elevation plotted with the maximum and mean swath profile along strike of the Zagros.

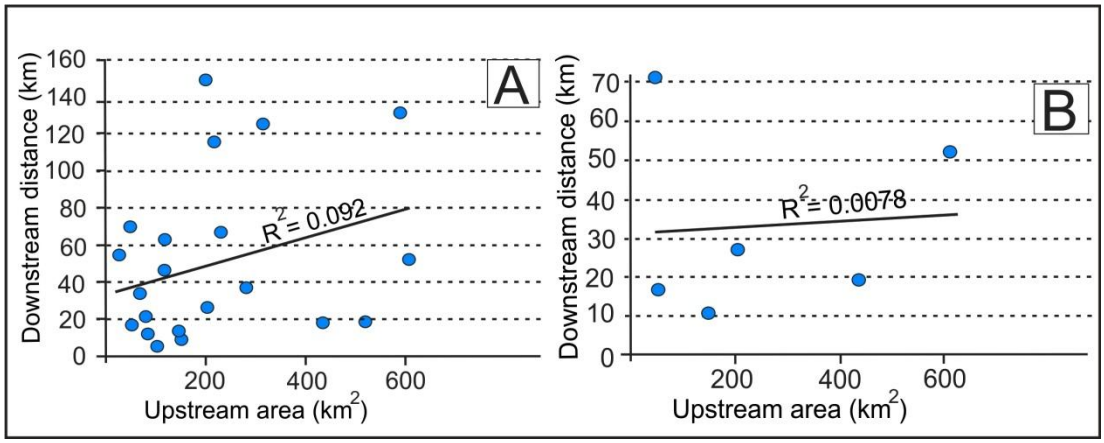

Fig. 2.25. Drainage area versus downstream distance of knickpoints: A) for all selected rivers and B) for rivers occur in the MRF zone. Weak relation shows no evidence in regards to the generation time of these knickpoints.

k_{sn} values above and below knickpoints have been plotted with the topographic relief and the 1250 m elevation contour (Fig. 2.26) to see if there is a pattern which can help in tectonic interpretation of the area. Results show no specific pattern of k_{sn} values and both above and below knickpoint k_{sn} value lie within and below the 1250 m elevation contour.

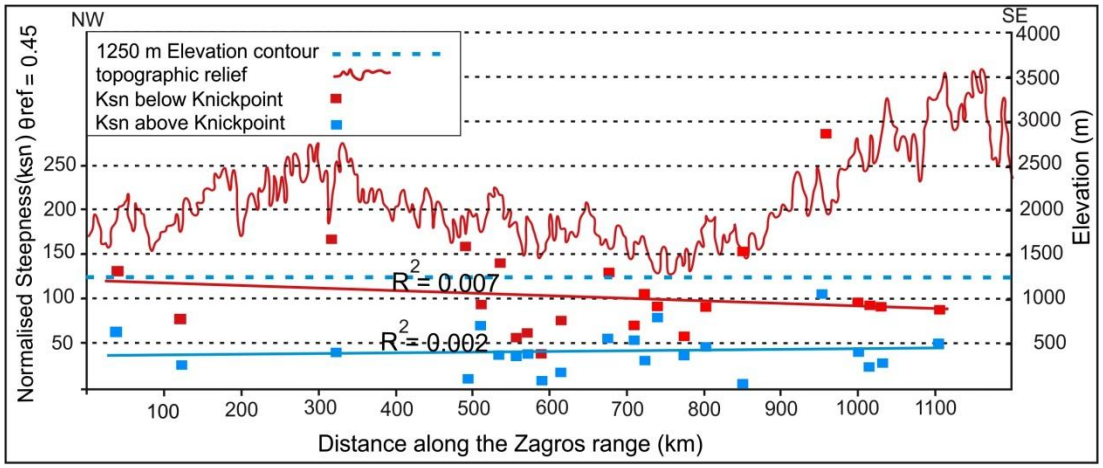

Fig.2.26. Normalised Steepness Index (k_{sn}) above and below knickpoints along strike of the Zagros plotted with the topographic relief and the 1250 m elevation contour. The best fit line for both classes of k_{sn} shows low correlation factor which cannot be considers in tectonic interpretation.

The other zone of knickpoint alignment is near the Khanaqin Fault, which lies at the transition from the lowlands of the Kirkuk Embayment to the high terrain of the Lurestan Arc (Figs. 2.20 and 2.27). Figure 2.27 shows that there is no particular correlation between the knickpoints and a lithological change. Figure 2.20 shows that the alignment is in the vicinity of the Khanaqin Fault, but not along or parallel to its commonly-drawn trace.

The Khanaqin Fault is an enigmatic structure within the Zagros, and even its trace is not consistently drawn between different publications. Clearly, there is some important structure in this region to mark the transition from the high, relatively exhumed area of the Lurestan Arc to the lowlands of the Kirkuk Embayment, but the lack of an exposed fault has hampered investigations. The *M* 7.3 2017 earthquake took place in this region (Tavani et al., 2018). This event was a low angle (16^{o}) thrust, directed towards the SW, slipping obliquely on a fault plane striking at 351^{o}.

Table 3.1: Data of river profile analysis for the selected 22 trunk river along the strike of the Zagros.

Channel number	below knickpoint		above knickpoint		upstream area (km^2)	Downstream Distance (km)
	Concavity θ	Steepness(k_{sn}) θ_{ref} = 0.45	Concavity θ	Steepness(k_{sn}) θ_{ref} = 0.45		
1	0.28 ± 0.7	129	0.45 ± 0.07	65.5	117.5	63
2	3.8 ± 2.4	72.2	0.89 ± 0.2	24.2	117.2	47
3	1.2 ± 0.5	185	0.26 ± 0.18	28.2	199.6	149
4	0.84 ± 1.8	159	0.35 ± 0.09	14.9	2913.7	28
5	0.29 ± 0.16	96.7	0.85 ± 0.18	27.2	117.5	16
6	0.43 ± 0.2	146	0.58 ± 0.16	38.6	152.2	10
7	0.15 ± 0.9	147	0.69 ± 0.4	59.6	202.3	27
8	0.35 ± 0.43	60.3	0.94 ± 0.13	37.5	437.3	19
9	0.1.2± 0.08	34.1	0.35 ± 0.2	10.7	47.2	71
10	1.4 ± 1.8	70.9	0.95 ± 0.27	21.5	610.6	52
11	1.3 ± 0.6	56	0.48 ± 0.25	33	313.5	126
12	2.6 ± 3.8	70.4	0.26 ± 0.08	55.8	234.1	66
13	1.5 ± 0.6	114	0.65 ± 0.1	21.7	588.2	131
14	0.57 ± 0.28	91.4	0.21 ± 0.15	78.5	219.1	115
15	1.0 ± 0.59	56.4	0.18 ± 0.21	36.4	283.6	36
16	0.24 ± 0.61	79.6	0.85 ± 0.6	48.7	147.1	14
17	0.78 ± 0.63	156	0.77 ± 1.5	8.6	50.8	17
18	0.78 ± 6.3	283	0.57 ± 0.16	109	58.06	12
19	3.5 ± 2.3	98.5	0.59 ± 0.7	44.3	106.3	12
20	-1.8 ± 1.6	98.6	1.5 ± 0.39	18.8	63.1	32
21	1.3 ± 1.7	96.2	0.15 ± 0.37	24.7	523.6	19
22	1.4 ± 2.2	88.6	0.1.6± 0.29	50.2	79.9	21

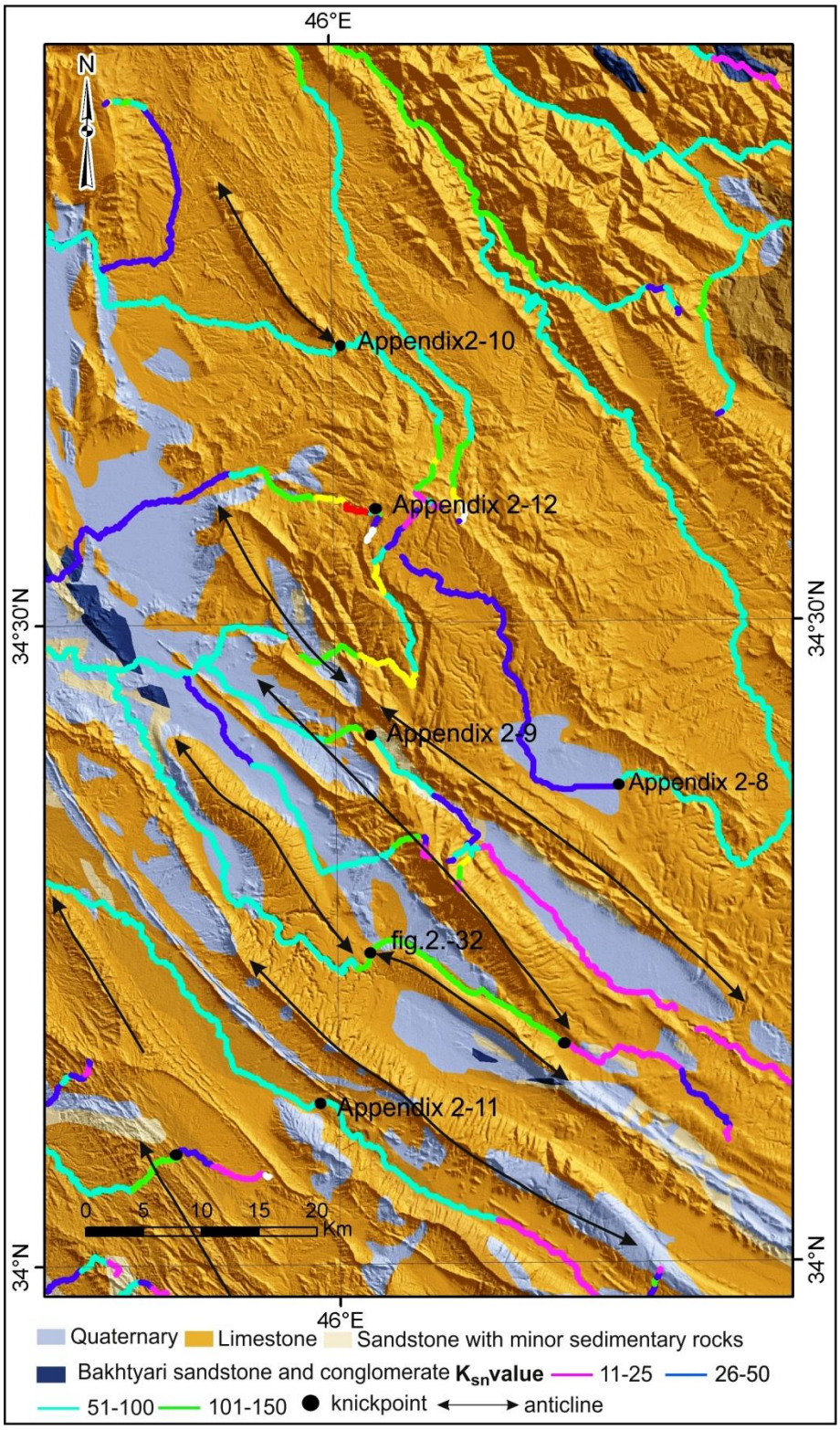

Fig. 2.27. Knickpoint distribution in the region of the Khanaqin Fault Zone and the local bedrock lithology (see Fig. 2.20 for location).

Closer inspection of Fig. 2.20 reveals two alignments of knickpoints in this area: one is along the line of the Mountain Front Fault where it runs north-south through this area, and the other is to the east, roughly at the line of the 1250 m regional elevation

contour, which, as noted, marks the upper elevation limit for major thrust seismicity in the Zagros (Nissen et al., 2011).

The remaining figures in this part of the results section (Figs. 2.28-2.32) present large scale maps of the lithologies, drainage and shaded relief for specific parts of the Zagros (part "a" of Figs. 2.28-2.32), accompanied by figures presenting the river profile analysis for each main river segment (part "b" of Figs. 2.28-2.32). Whilst not exhaustive, there is a pattern across all examples that knickpoints tend to be related to zones where rivers cross anticlines, rather than major changes in lithology, or, if the knickpoint is at a change in bedrock lithology, this is also an anticlinal zone (see the knickpoint near the centre of Fig. 2.30, along a tributary of the Mand River, as an example of this behaviour).

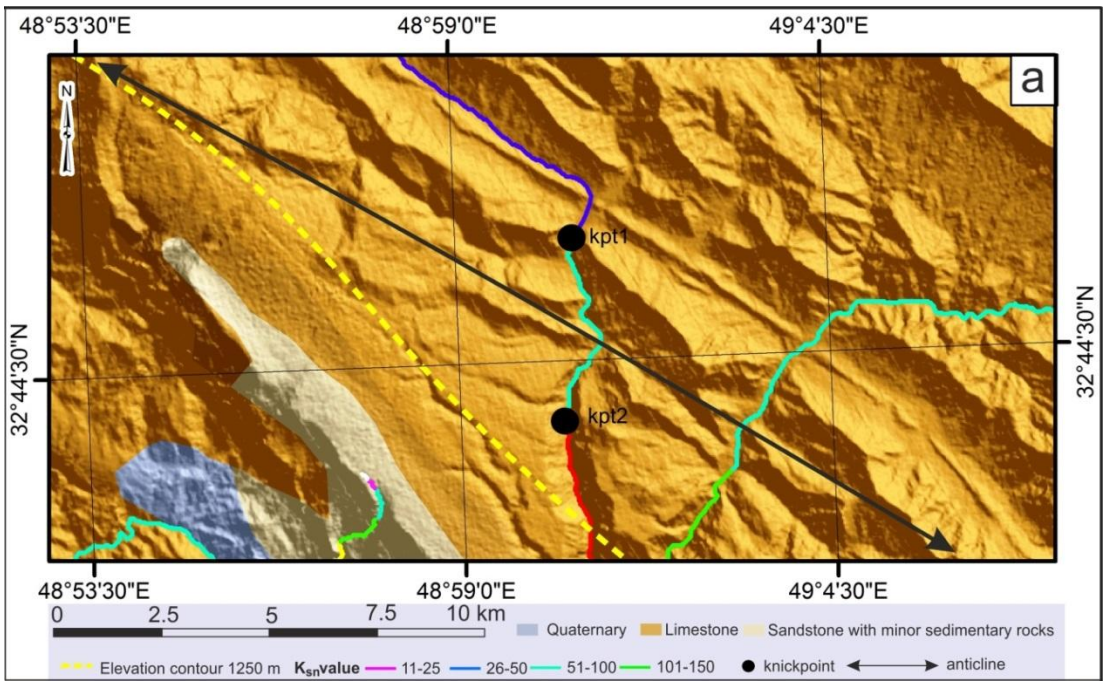

Fig. 2.28a. Knickpoints for river segment within the limestone lithology of the Asmari Limestone Formation (geology from sources in Fig. 2.1B). These knickpoints occur in limestone lithology of the uplifted structure referring to the tectonic control rather than lithology.

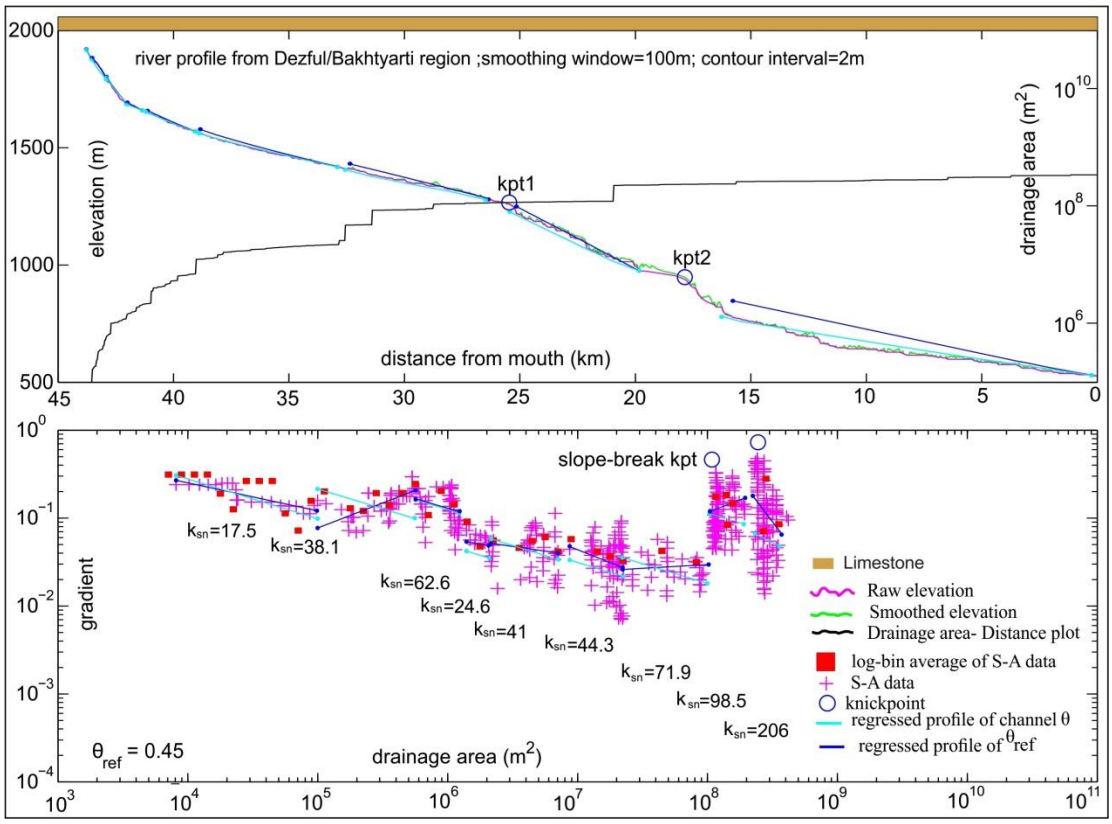

Fig. 2.28b. River profile analysis of the river segment in Fig. 2.28a shows two knickpoints along the profile within the limestone lithology. Kpt 1 refers to break in slope. kpt=knickpoint.

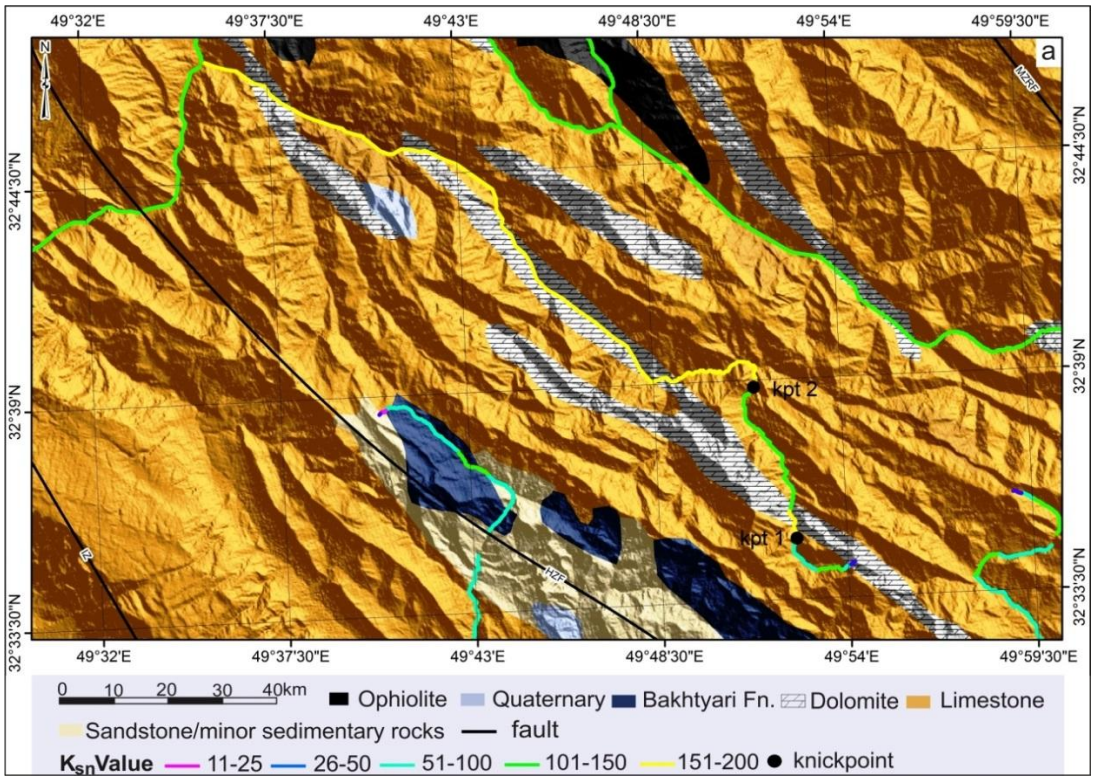

Fig. 2.29a. Two knickpoints for river segment within limestone and dolomite lithologies of the Dalan Formation for the kpt1 and massive thin bedded limestone of the Khami Group (geology from sources in Fig. 2.1B). Knickpoint 2 occurs in limestone and shale of the Bangestan Group. These knickpoints occur in limestone lithology of uplifted structure referring to the tectonic control rather than lithology.

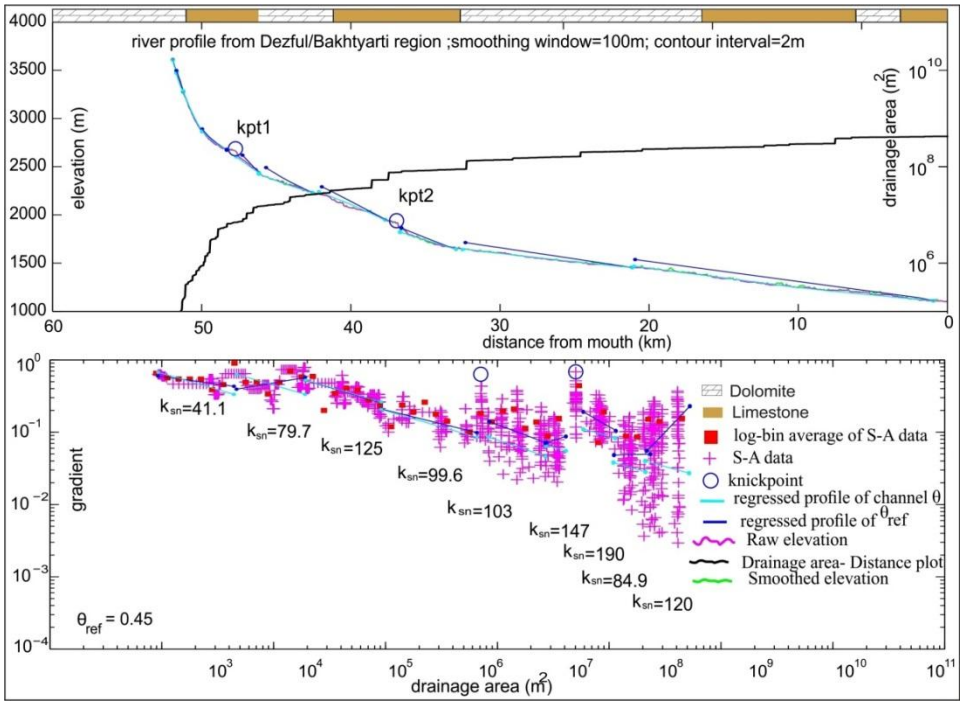

Fig. 2.29b. River profile analysis of the river in Fig. 2.29a shows that the first knickpoint (kpt1) may reflect a combination of the uplift and minor differences in rock strength between limestone and dolomite of the Dalan Formation while kpt2 is break-slope knickpoint.

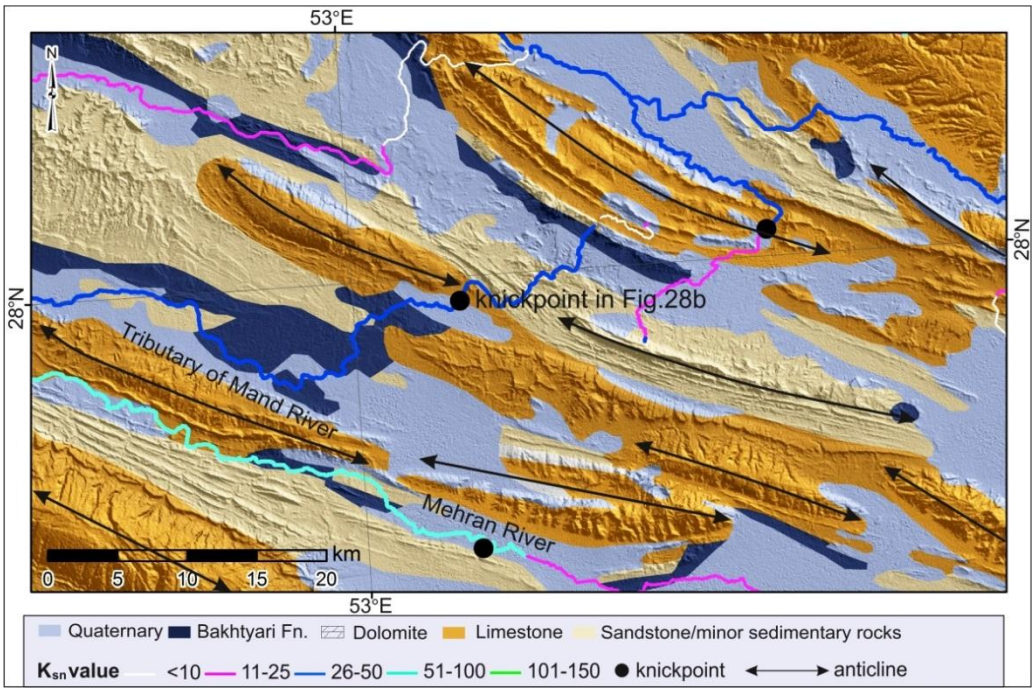

Fig.2.30a. knickpoint relation with the bedrock geology in the western Fars Region. Location of Knickpoint at lithological change (geology from sources in Fig. 2.1B) but it is also on the tip of anticline.

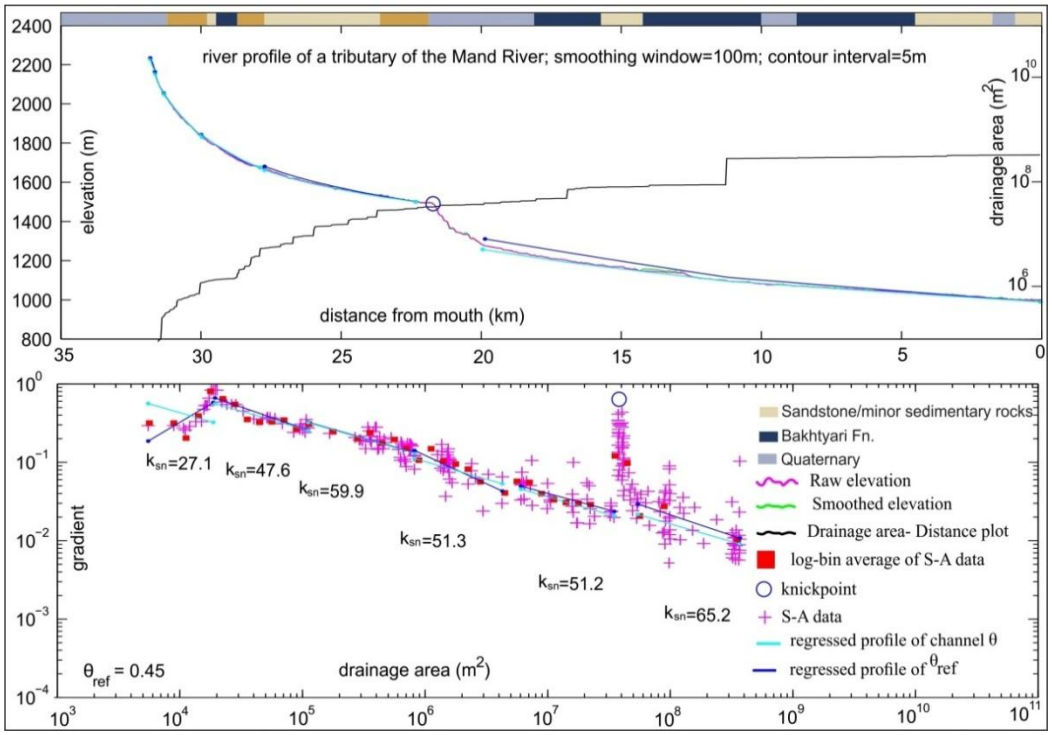

Fig. 2.30b. River profile analysis of a tributary of the Mand River in Fig. 2.30a shows a suspicion of break in slope and contribution of rock strength differences between the limestone lithology and Bakhtyari Formation lithology. The knickpoint might be mostly tectonic in origin as it falls in the zone of anticline uplift; also there is a moderate change in (k_{sn}) above and below knickpoints.

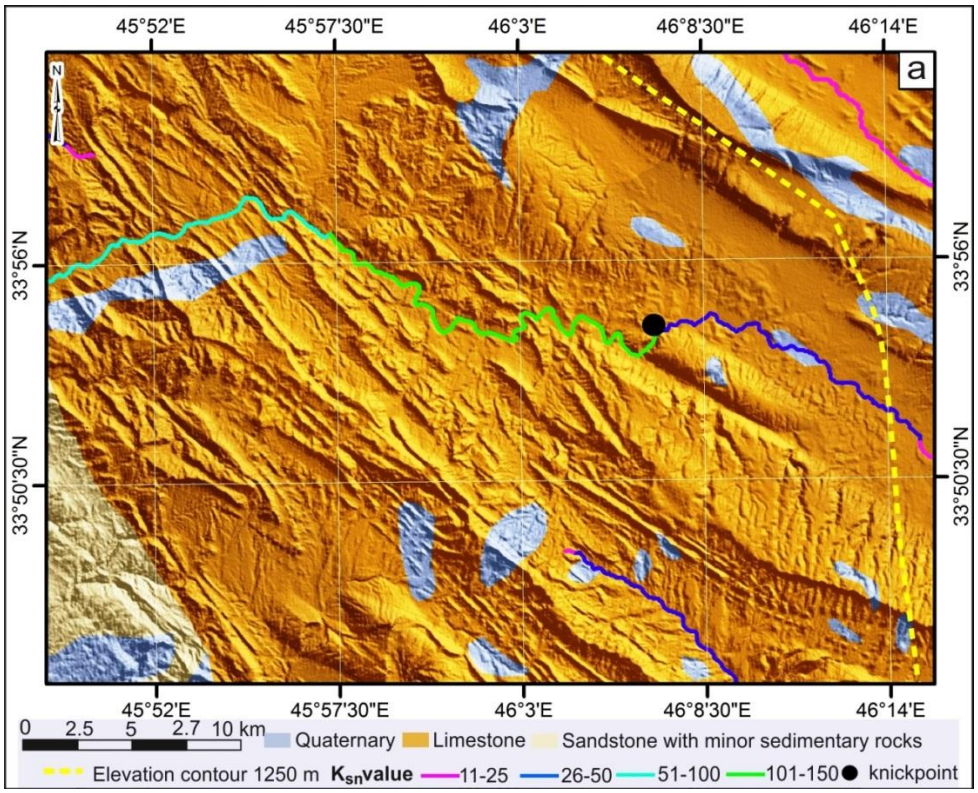

Fig. 2.31a. Knickpoint relations with bedrock lithology (geology from sources in Fig. 2.1B) in the NW Zagros specifically the Lurestan region (see Fig. 2.20 for location).

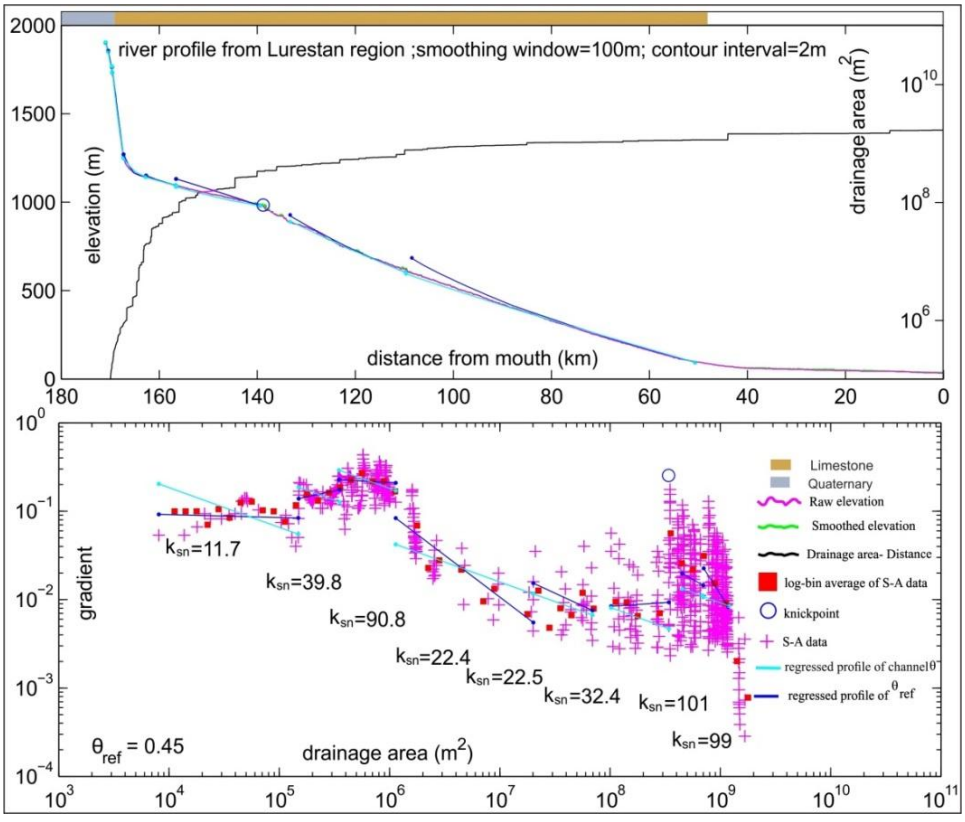

Fig. 2.31b. River profile analysis for the river in Fig. 2.31a shows the location of knickpoints within the limestone lithology and at the tip of anticline.

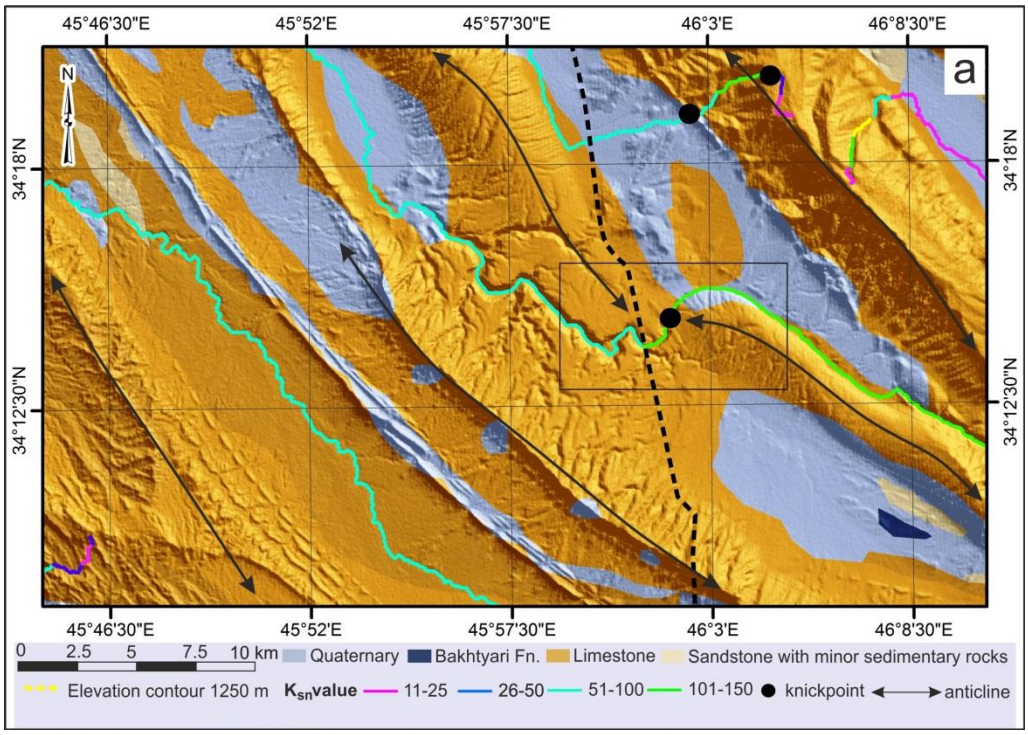

Fig. 2.32a. Knickpoint located on the connection point between two linked anticlines (see Fig. 2.27 for knickpoint location) within the lithology of the Kazhdumi limestone (geology from sources in Fig. 2.1B).

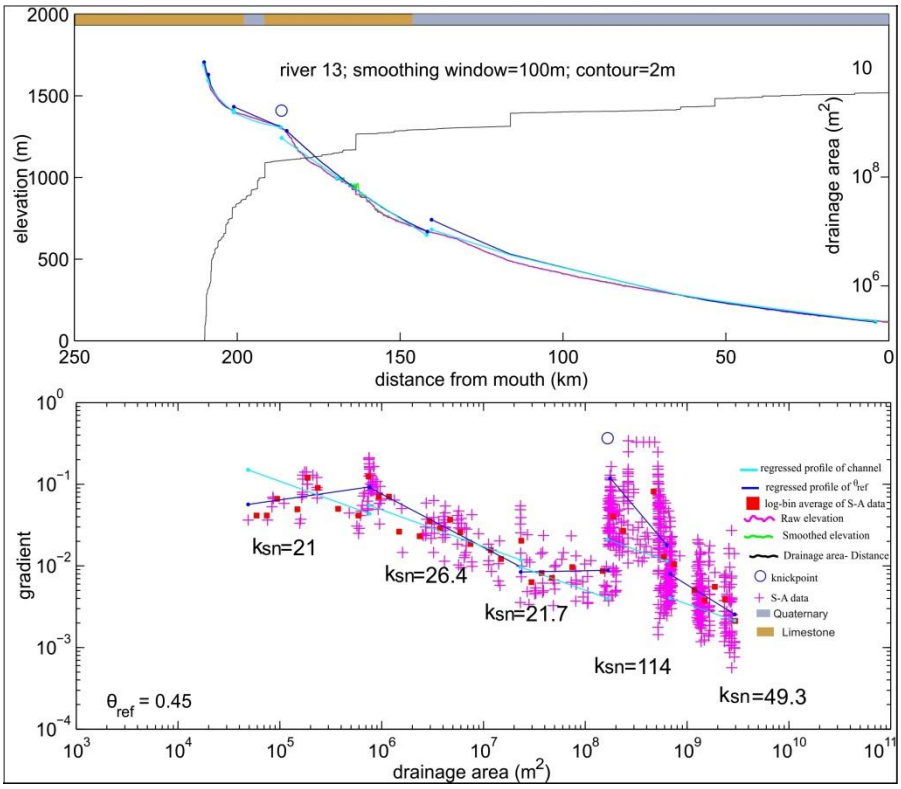

Fig. 2.32b. River profile analysis for the river in Fig. 2.32a (black rectangle) shows the location of knickpoint within the limestone lithology and at the tip of anticline.

2.3.6 Hypsometric Index (HI)

Results from 17380 third order river basins across the Zagros reflect two major groups of low HI values (HI <0.3) (Fig. 2.33). The first group of low HI values represents the Turkish-Iranian Plateau where topographic gradients are very low (Allen et al., 2013). The second group of low HI region occurs across the foreland and Mesopotamian plain. Intermediate and relatively high HI values (>0.3) occur across the mountainous areas of the Zagros which are characterized by high relief and gradient (Fig. 2.33).

Along much of the Zagros there is a coincidence between the transition limit from HI values of <0.3 to >0.3 and the 1250 m contour line, which itself is the approximate upper elevation limit of seismogenic thrusting (Fig. 2.33). This pattern is seen northeast of the Kirkuk Embayment, along the Pusht-e Kuh Arc and in the region of the Kazerun Fault (western Fars). Different patterns occur in the Bakhtyari Culmination and in the southeast of the Zagros (Fars region). In the Bakhtyari Culmination youthful topography and relatively high HI values persist northeast of (above) the 1250 m elevation contour and the limit of seismogenic thrusting. In the Fars region seismogenic thrusting continues north of the transition from high to low HI values (taken as HI = 0.3).

Swath profiles form raster data of the HI value across the Zagros (Fig. 2.34) show the HI value raising in areas of high relief but not the high elevations. Differences in lithology have been examined, and show limited effects on HI values (Figs. 2.35).

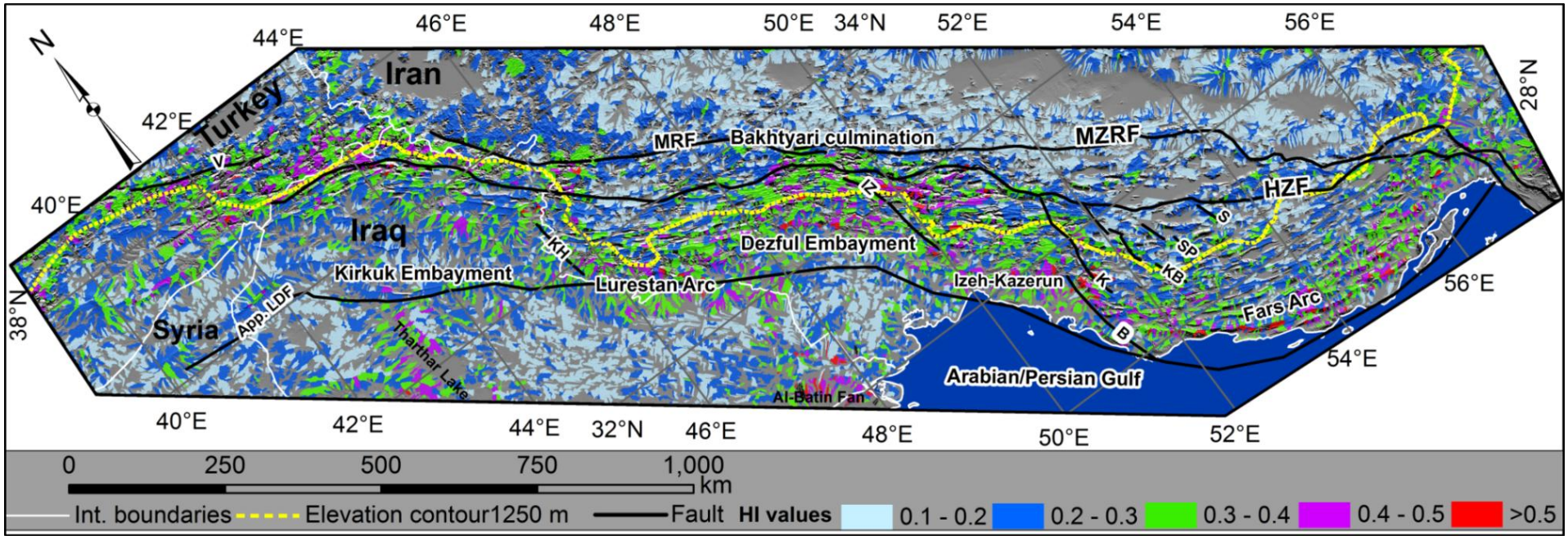

Fig. 2.33. HI values for 3rd order drainage basins across the Zagros. Note the cut-off of thrust seismicity at ~1250 m (Nissen et al., 2011). There is a broad region of high HI (>0.3; green-amethyst colours) along the Zagros, between the Iranian Plateau and the foreland. Specific regions show variations in this broad trend. In the Bakhtyari Culmination, the high/low HI transition lies above the thrust seismicity cut-off while in the Fars region, the high/low HI transition takes place below this cut-off.

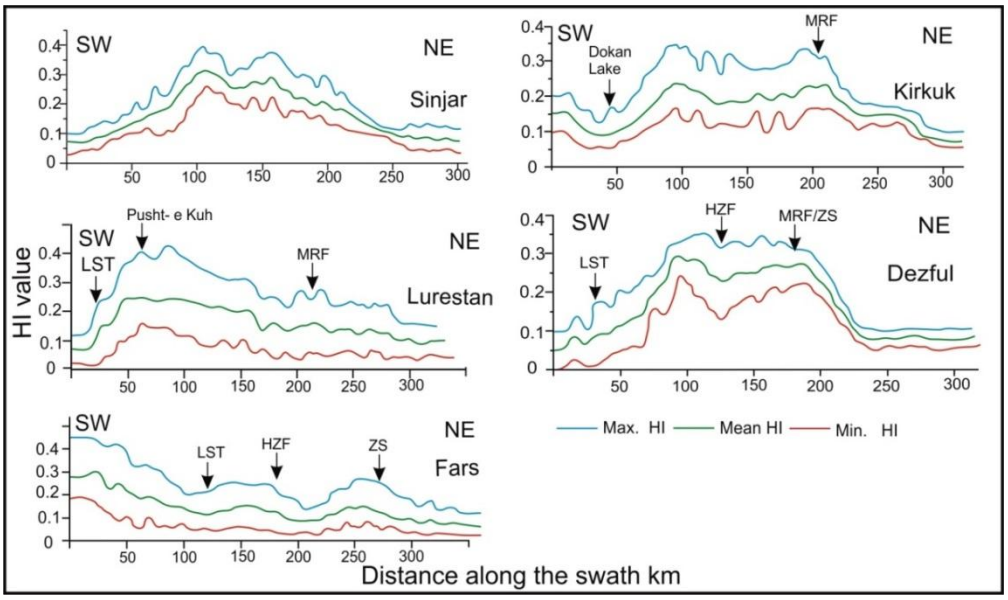

Fig. 2.34. profiles extracted from HI raster data show the distribution of the HI value along swaths in Fig. 2.7a across the Zagros range. LST = Limit of seismogenic thrusting; ZS = Zagros Suture; HZF = High Zagros Fault; MRF = Main Recent Fault. Note the similarities of the HI value distribution between the Kirkuk and Dezful embayments where the imbricate thrust sheets and high strain deformation respectively occurred. Also, the Arc of Fars produces high HI southwest of the LST in opposite sense to the Dezful where the high HI occurs northeast of LST.

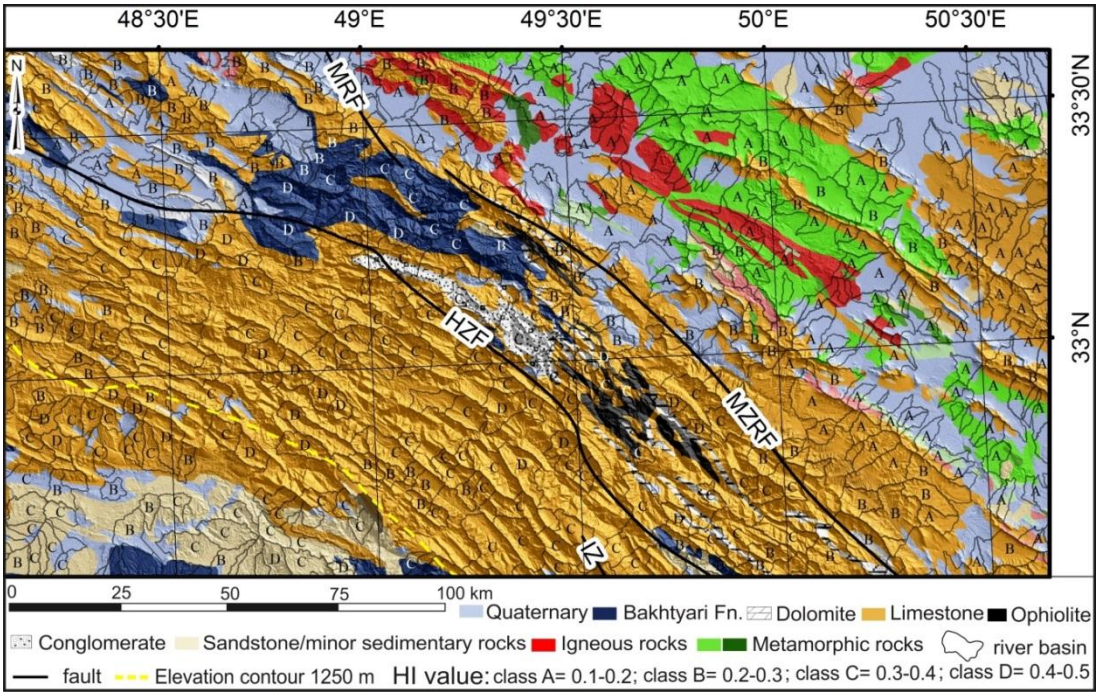

Fig. 2.35. HI values in the Bakhtyari Culmination underlain by exposed lithology (geology from sources in Fig. 2.1B), which show similar HI value across different lithologies and different HI value across same lithology.

2.3.7 Sensitivity analysis

SRTM data have inherent errors (Boulton and Stokes, 2018) which result in voids that affect the flow-routing algorithm. Therefore, for the accuracy of river profile extraction, the QaraChwalan River profile was extracted manually from the SRTM 30 m data using Global Mapper GIS, and compared with the automatic extracted profile (Fig. 2.36). No difference has found between the two profiles, which indicates the reliability of the automatic drainage network extraction technique.

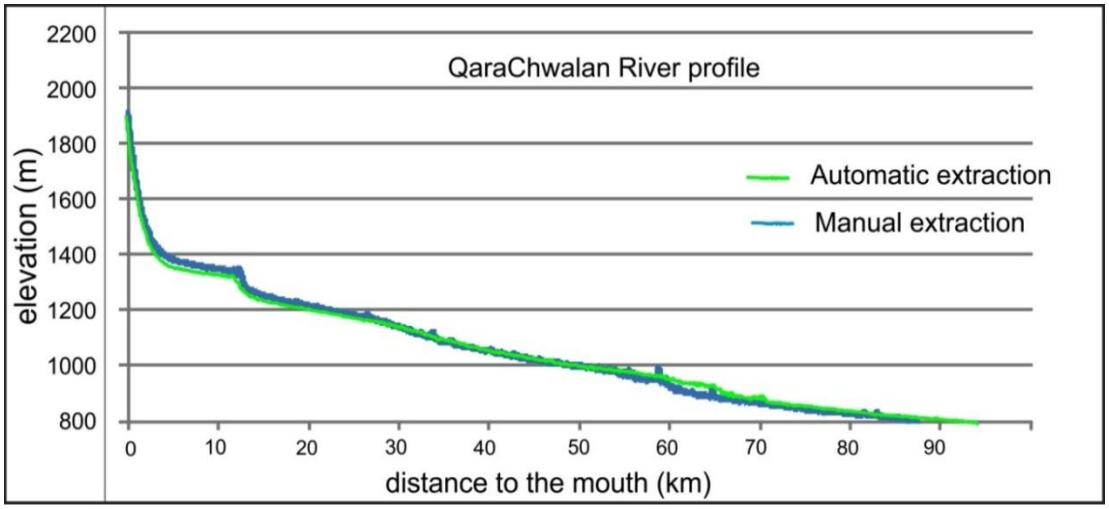

Fig. 2.36. Matching between manual and automatic extractions of QaraChwalan River profile (Fig. 2.5a).

HI values for the 4th, 5th and 6th order river basins have been tested for a comparative analysis of HI values at different scales of drainage (Fig. 2.37). The distribution of HI classes across the Zagros is similar for all orders of river basins, but the large area basins (i.e. 6th order) lack enough resolution to distinguish changes in HI values and hence potential changes in tectonic style. Thus, the use of the third order river basin is preferred as it gives more detailed results about landscape response to tectonics. Using second or first order basins introduced problems because of the extra processing time required, and artefacts introduced by the resolution of the DEM data and the ability of the software to define drainage basins accurately.

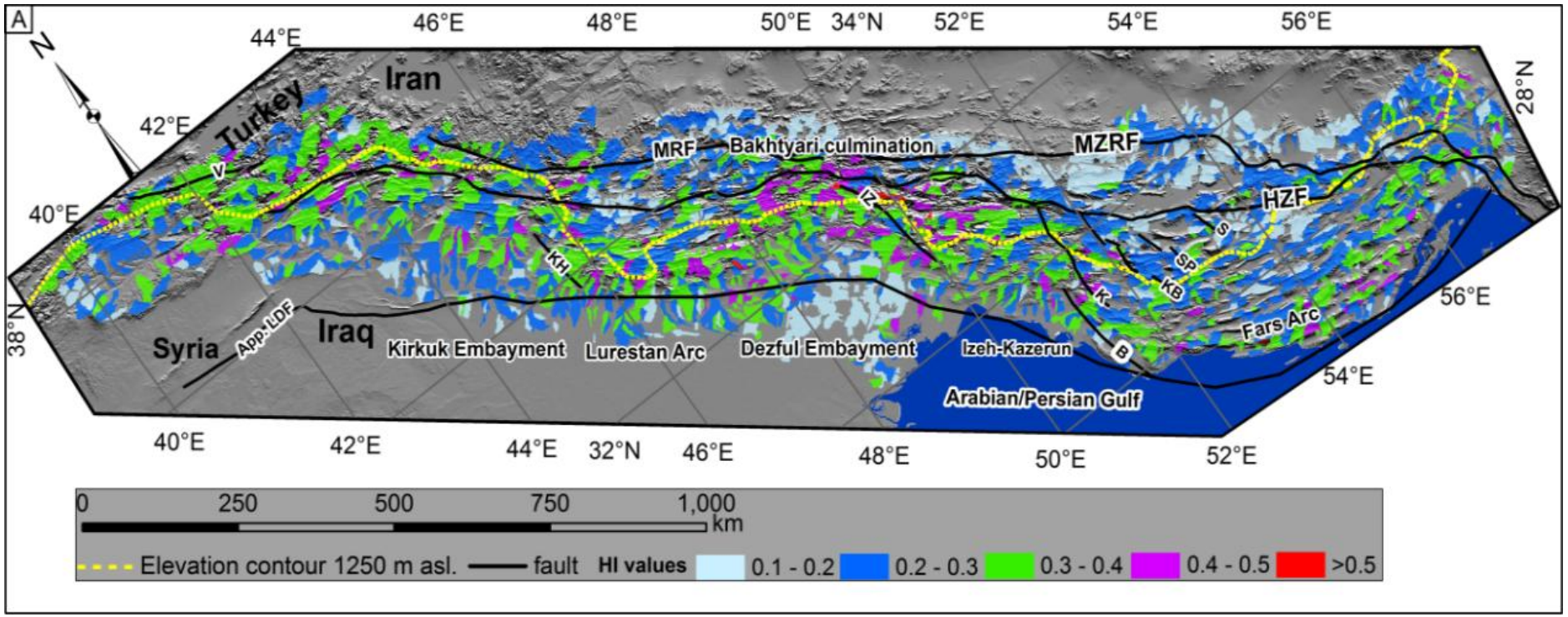

Fig. 2.37 (Continued with caption on next page)

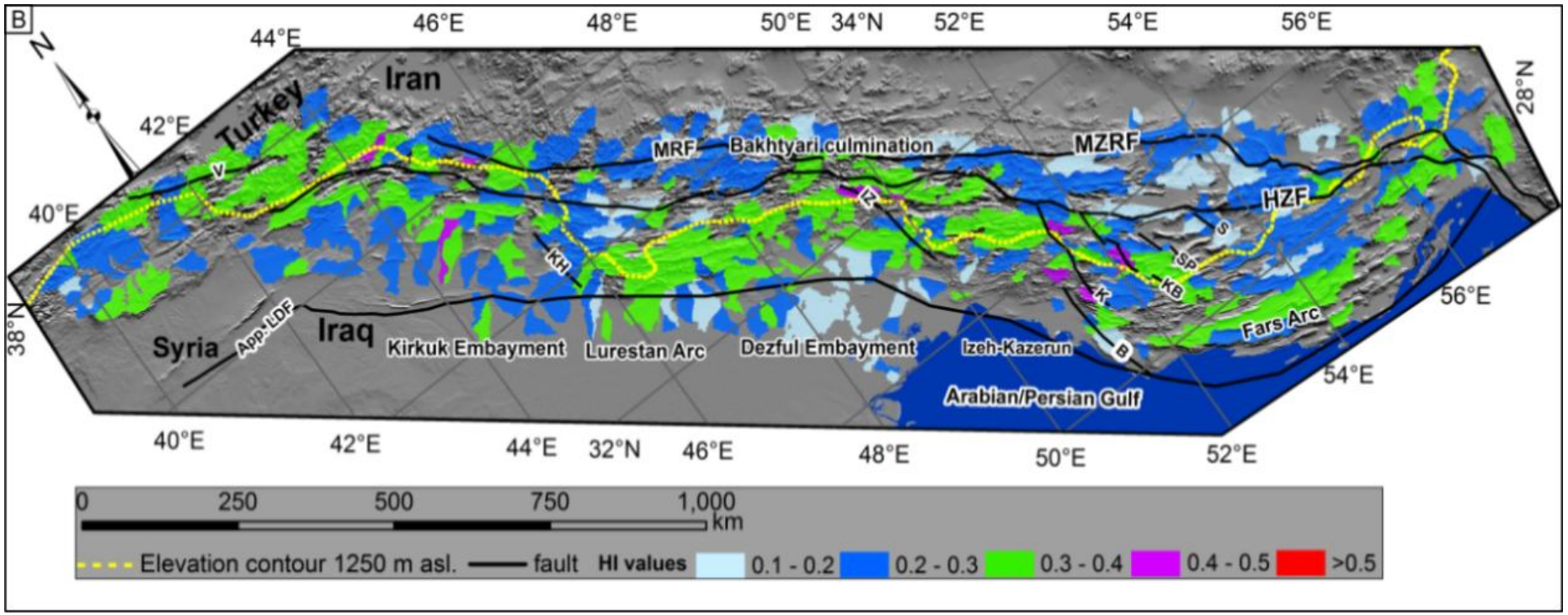

Fig. 2.37 (Continued with caption on next page)

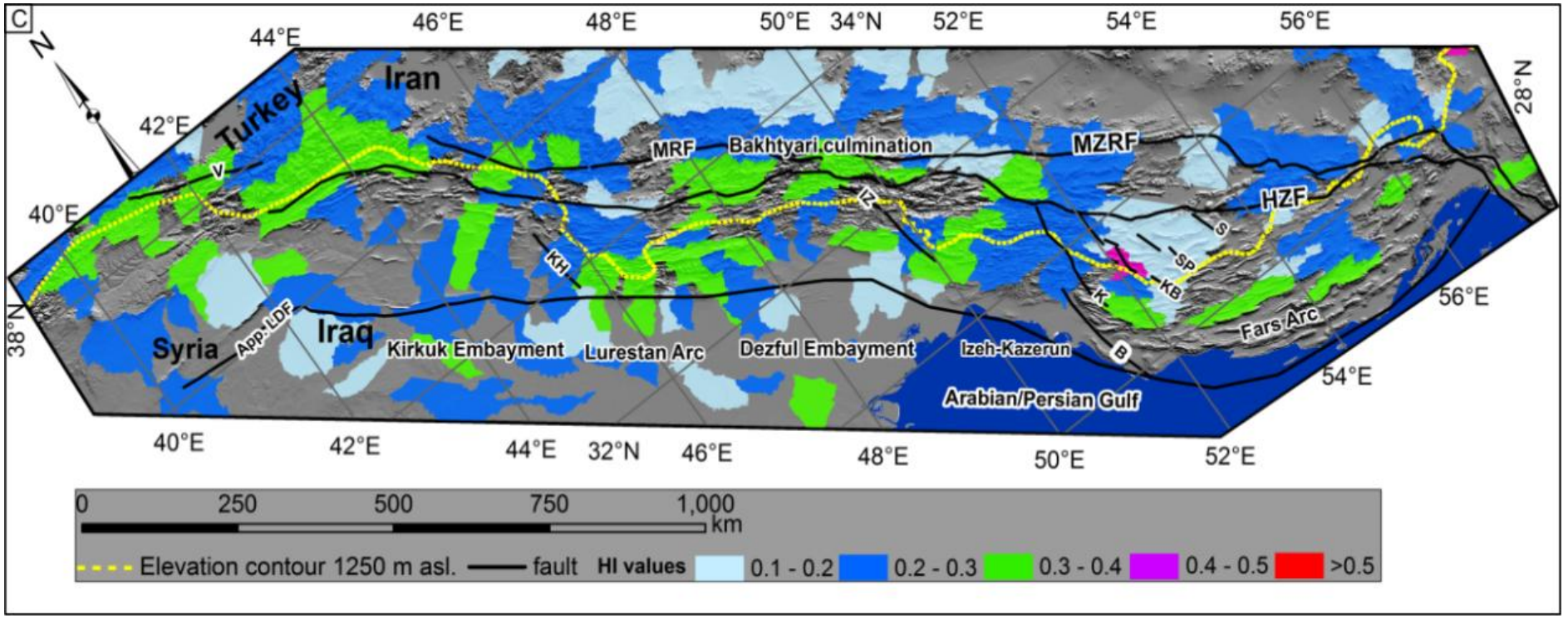

Fig. 2.37. HI values for the 4th (a), 5th (b) and 6th (c) orders drainage basins across the Zagros. In the higher order, some HI values of features of interest are not resolved, but they are represented well using the lower order basin (3rd), presumably because of the smaller area involved. The effect is similar to varying the pixel size in a digital photographic image.

2.4. Discussion

2.4.1 Swath profiles

The statistical parameters of swath profiles describe clearly the topography within the range of the swath. The Sinjar, Kirkuk and Fras sections show steady increases in elevation toward the hinterland for the first ~200 km of the profiles (Fig. 2.7b), which is well-established by previous work (see McQuarrie, 2004; Mouthereau et al., 2012; Allen et al., 2013 and references therein). It is a new approach to integrate the relief along each profile (Fig. 2.7b), which yields the interesting result that the values for each profile are within ~20% of each other, at 2.2 – 2.8 x 10^8 km^2. This suggests that the integrated relief of the mountain range may be less controlled by the parameters which vary along the Zagros, such as the width of the seismogenic belt, or maximum topographic gradient, and more by parameters which are similar across strike, such as strain rate (Masson et al., 2005), overall shortening (McQuarrie, 2004; Vergés et al., 2011; Allen et al., 2013), or the elevation difference between the hinterland plateau and the undeformed foreland. It is therefore an interesting idea to test another example of a fold-and-thrust belt in the future, especially where one of more of these parameters varies more strongly along the range. The Andes might be a suitable case study, or the Tian Shan or Greater Caucasus.

2.4.2 River profiles

There is a general pattern that higher k_{sn} values occur where the rivers cross the 1250 m contour (Fig. 2.16), and so from the interior, aseismic region into the seismogenic part of the Zagros, but this is a broad distinction, without a sharp change. k_{sn} values are lower in the Fars region (Fig. 2.19) than elsewhere in the Zagros. Kirby and Whipple (2012) noted the correlation between the linear physiographic transition of lesser/Greater Himalaya and the northward increase in k_{sn} values. The zone of high k_{sn} is on the hanging wall of the Main Central Thrust (MCT), interpreted as relating to the long-lived uplift in the vicinity of this fault (but see also the analysis of Himalayan geomorphology presented as Chapter 4 in this thesis). The Longmenshan in SE Tibet is another example of a sharp boundary, between the high and low k_{sn} in the zone of the active Yingxiu-Beichuan (YBF) and Pengguan faults (PF). This pattern has not found in the Zagros, perhaps due to the tectonic difference between the multiple, segmented, blind thrusts of the Zagros, and the laterally continuous and large scale thrusts of the Himalaya (i.e. the MCT) and SE Tibet (i.e. the YBF).

Knickpoints occur in the limestone lithology of the Asmari Formation (e.g. Fig. 2.28a), but show no overall correlation with zones of lithological change, and can be attributed more to tectonic factors, i.e. active uplift along anticlines. In the Fars Region, knickpoints also occur in limestone; these limestones (largely from the Cretaceous Bangestan Group and its equivalents) crop out along anticlines or at relay zones between anticlines. The lithology control is also tectonic in origin: knickpoints are located at points where the rivers cross the anticlines (Figs. 2.30, 2.31 and 2.32). The example of Fig. 2.30a shows a knickpoint between limestone lithology and sandstone and conglomerate of the Bakhtiari beneath the Quaternary; however this knickpoint is located on the tip of the anticline. This might refer to a combination of uplift and lithological change, which has not been studied before.

Rivers in the Fars region commonly divert around the tips of anticlines or cross relay zones between them. This is because of low discharge of rivers including the internally drained basins in the region. The climate changes across the Zagros (Fig. 2.6); the relatively dry climate has led to limited and ephemeral discharge of rivers which is not enough to overcome the growth of anticlines. Therefore Fars region rivers commonly divert around anticlines (Ramsey et al., 2008).

Knickpoints are aligned along or close to fault zones in two regions (Fig. 2.20). Within the Lesser Zab River Basin (LZR), knickpoints between elevations 1000-1400 m, but commonly at ~1350 m, are aligned along the Main Recent Fault (MRF). Not many studies have addressed the occurrence of knickpoints in the zone of strike-slip faults (e.g. Nicholson et al., 2013). Talebian and Jackson (2002) studied river offsets in the zone of the MRF of the Zagros but not knickpoint analysis. The main stream of the LZR flows parallel to the knickpoints band for >40 km (Fig. 2.21). Drainage networks show that a few knickpoints occur at the confluence point between tributaries (Fig. 2.21), which might be an additional cause of knickpoint occurrence. However the majority of these knickpoints connect low order rivers with the main or higher order river. These low order rivers are less in discharge and sediment load and therefore, unable to produce knickpoints according to their hydrological condition. It has been reported that within the same catchment, a drop of local base level will generate nearly similar elevation knickpoints (Neimann et al., 2001; Whipple and Tucker, 1999). The Lesser Zab River basin which is bordered from the northeast by the MRF, exhibits knickpoints located on the ~1350 m contour

elevation (Fig. 2.22) which might refer to the drop of local base level of the LZR basin due to the uplift activity in the zone of the MRF – however, such recent uplift has not been proved, and is speculative. Also there is no correlation between the lithology and the occurrence of knickpoint (Fig. 2.21) as they are mostly occur within one class of rock type. From the bottom of Fig. 2.23, the 1st, 2nd and 3rd knickpoints lie within the limestone of the Kuhe-e-Bistoon Formation, Penjween intrusion, and Giom metamorphic group respectively. The rest of knickpoints lie within sandstone and minor argillaceous shale. Thus the lithological effect on the occurrence of knickpoint is less than other factors.

Two more aligned zones of knickpoints lie in the region of the Khanaqin Fault (Fig. 2.20). This structure has not been studied in detail, but is in the vicinity of the causal fault for the 12 November 2017 *M* 7.3 earthquake near the Iran-Iraq border. It also forms the boundary between the lowlands of the Kirkuk Embayment to the northwest, and the higher ground of the Lurestan (Pusht-e Kuh) Arc to the southeast (e.g. Blanc et al., 2003). There is one aligned zone of knickpoints, roughly along the 1250 m elevation contour to the east of the 2017 earthquake (Figs. 2.20 and 2.27). These knickpoints are not collectively located along any single emergent structure, but it is possible they relate to the hypocentral region of the blind thrust associated with the 2017 earthquake at depth ca. 20 km (Tavani et al., 2018). This oblique thrust (strike 351°, dip 16°) was associated with a north-south band of aftershocks. The hypocentral depth and dip angle imply a low angle basement fault, possibly the explanation for the interpretation of the Mountain Front Fault (MFF) as a N-S feature in this region, and responsible for the elevation of the Lurestan Arc (Vergés et al., 2011). The second zone of knickpoints occurs to the west, close to the commonly-drawn location of the MFF in this region (Fig. 2.20), and in the region of the tip of the 2017 earthquake, which moved on a blind structure.

If so, it would be unusual for the Zagros that a zone of knickpoints correlates with a specific, identifiable thrust. It is also distinctive that there is not one aligned zone of knickpoints, but two, above both the tip of the (blind) thrust and above the hypocentral region. I also tested the sensitivity of these knickpoints to lithology, and conclude they are independent of lithology (Fig. 2.27).

A vertical distribution relation between knickpoints has previously been identified in the High Atlas (e.g. Boulton et al., 2014), but does not occur in the Zagros, probably because of the differences in the tectonics of the Zagros and High Atlas. In the High Atlas, the South Atlas Fault (SAF) accommodates a high proportion of Cenozoic shortening of the area. The first phase of surface uplift occurred >25 Ma followed by <5Ma further uplift in the Plio-Quaternary (El Harfi et al, 2001, 2006). No obvious vertical distribution of knickpoints has been found (Fig.2.24) nor there was a correlation between the area above knickpoint and the distance of river segment below knickpoint to be considers for knickpoint migration (Fig. 2.25). This might be relate to the ongoing deformation of the Zagros expressed by numerous fault related folds across the range, at least below the 1250 m regional elevation contour (Nissen et al., 2011). Thus the knickpoints do not exhibit elevation bands which may refer to fault reactivation during geological time, and this produces a non-systematic distribution of knickpoints elevations across the Zagros, except in the zones of the MRF and the KH, which are discussed above in detail.

Also the relation between steepness and concavity indices above and below knickpoints has been used by Boulton et al. (2014) and Kirby and Whipple (2012) where the tectonic conditions are nearly constant along strike. In other words their work specifically dealt with one emergent structure such as the SAF in Morocco and the Bhimgoda thrust in the Siwalik Hills of the Himalaya, and thus the comparison gave meaningful results. In the case of the Zagros, there are variations in tectonics along strike and within the width of range (Allen and Talebian, 2011; McQuarrie, 2004; Talbot and Alavi, 1996), therefore the relation between steepness and concavity will not show meaningful results, because of tectonic variation across the Zagros.

2.4.3 Hypsometric Index (HI)

In the Bakhtyari Culmination (Fig. 2.35) I examine changes in bedrock lithologies and their effects on the HI value. The Culmination consists mainly of limestones, limestones alternating with marls and conglomerates, patches of ophiolitic lithologies (e.g. serpentinite, basalt), and sandstones and conglomerates of the Bakhtyari Formation. To the northeast of the Culmination there is a series of igneous and metamorphic rocks. For the same lithology there are significant differences in the HI value. In contrast, there are areas where different lithologies, such as the ophiolitic

assemblages and limestones, show similar HI values (0.3-0.4) (Fig. 2.35). This result implies that differences in lithology have limited effects on the HI value.

The relatively wet climate in the Dezful/Bakhtyari regions (Fig. 2.6) enables the river system to erode the landscape in an area where the deformation taking place in narrow zone of high strain and steep slopes. This high HI region continues to the northeast of the seismogenic limit of thrusting (Fig. 2.38). From the tectonic perspective, this region has become part of the Turkish-Iranian Plateau, in that it is not experiencing active (seismogenic) shortening; from a geomorphic perspective, it has not yet become a plateau, because of the high relief created and maintained by the drainage network (Figs. 2.33 and 2.34).

In the Fars region, the major exposed lithology is limestone, which represents the main erosional surfaces in the region (Fig. 2.1B). The relatively dry climate in Fars (Fig. 2.6) reduces the stream power of rivers, and thus erosion rates, and consequently the low HI zone occurs south of the limit of seismogenic thrusting (Fig. 2.33). This part of the Fars region behaves in the opposite sense to the Dezful/Bakhtyari region, in that it is still experiencing thrust seismicity, even in a low relief area that resembles the plateau interior to the north (Fig. 2.38). I attribute the differences in the location of the low/high HI transition to differences in the basement tectonic of the Dezful/Bakhtyari and Fars regions. Deformation in the Bakhtyari Culmination is spatially restricted by the adjacent, strong strain of the Dezful Embayment. No such constraint operates in the Fars region (Allen et al., 2013; Talebian and Jackson, 2004). These tectonic differences have a climatic positive feedback result in the relatively wet climate in the Dezful/Bakhtyari, where there is a higher topographic barrier, while in contrast, a relatively dry climate and low topography occur in the Fars (Figs. 2.1A, 2.33 and 2.6).

Unusually high HI values occur locally within the low HI area of the Mesopotamian foreland (Fig. 2.33), in two areas. At Tharthar Lake local base level has dropped due to water scarcity, leading to an increase in local slope and local erosion. Consequently, drainage basins around the border of the lake have relatively high HI values. The distal part of the foreland (i.e. the Al-Batin fan) also has relatively high HI for drainage basins located on the fan, due to local increases in slope (Figs. 2.33). The local increase of the HI in both areas reflects nontectonic effects (climatic).

Regional analysis of HI values on a drainage basin scale does not show sharp changes across individual structures, which would be expected if active deformation was controlled by a small number of major thrusts in the Zagros. This pattern contrasts with the east of the Tibetan Plateau (Longmenshan), where such abrupt jumps in HI have been observed (Gao et al., 2016).

The next chapter propose the application of moving window technique in mapping the hypsometric index in small scale area (Kirkuk Embayment) and the reasons of applying different techniques for the regional and local scales will describes in the discussion chapter.

2.5. Summary

The chapter uses geomorphic indices including k_{sn}, relief and HI to investigate how landscape responds to tectonic and climatic drivers in the Zagros fold-and-thrust belt, and shows how geomorphology can be a sensitive indicator of tectonic processes. Variations in k_{sn} and knickpoint distributions are not sensitive indicators of active tectonics in the whole range of the Zagros. Knickpoint locations in the Fars region (eastern Zagros) preferentially occur where rivers cross anticlines, commonly at relay zones. There is a broad association of higher k_{sn} values (>50 $m^{0.9}$) with the upper elevation limit for seismogenic thrusting, roughly at the 1250 m topographic contour. High k_{sn} values occur beyond this seismicity cut-off in the Bakhtyari Culmination, but are rare in the Fars region. These results are in agreement with the HI distribution for 17380 third order river basins; in many parts of the Zagros the low/high HI transition (0.3) is approximately at the elevation limit of seismogenic thrusting. In the Dezful Embayment/Bakhtyari Culmination the low/high HI transition lies northeast of, and at higher elevations than the thrust seismicity cut-off. In the Fars region, the HI transition lies south of the seismicity cut-off.

I explain these differences by the different climates of the two areas: wetter conditions and vigorous drainage systems in the Dezful/Bakhtyari region retard plateau growth; drier climate and low power rivers in the Fars region promote plateau growth. Orographic precipitation may itself have a tectonic control; regional basement strength variations have caused intense thrusting and steep relief in the Bakhtyari Culmination (Allen and Talebian, 2011). Integrated relief along different Zagros swath profiles is in the range 2.2 – 2.8 10^8 m^2. I argue that this consistency

relates to the comparable strain rates across different sectors of the Zagros (Masson et al., 2005), regardless of local structural, drainage network or climatic variations.

Drainage patterns of the Zagros have entirely been affected by the climatic and tectonic differences. It can provide information of past deformation (Jones, 2002). Transverse rivers commonly occur in the Dezful/Bakhtyari as a result of relative high precipitation and intense thrusting in the Bakhtyari which enable rivers to incise transversely through numerous growing anticlinal structures. Although there were many anticlinal structures and active seismicity in the Fars, but dry climate has an important effect in the occurrence of axial rivers which might be established transversely before the deformation (Ramsey, 2008). These geomorphic differences show retreat and growth of geomorphic plateau in the Fars and the Dezful/Bakhtyari regions respectively (Fig.38).

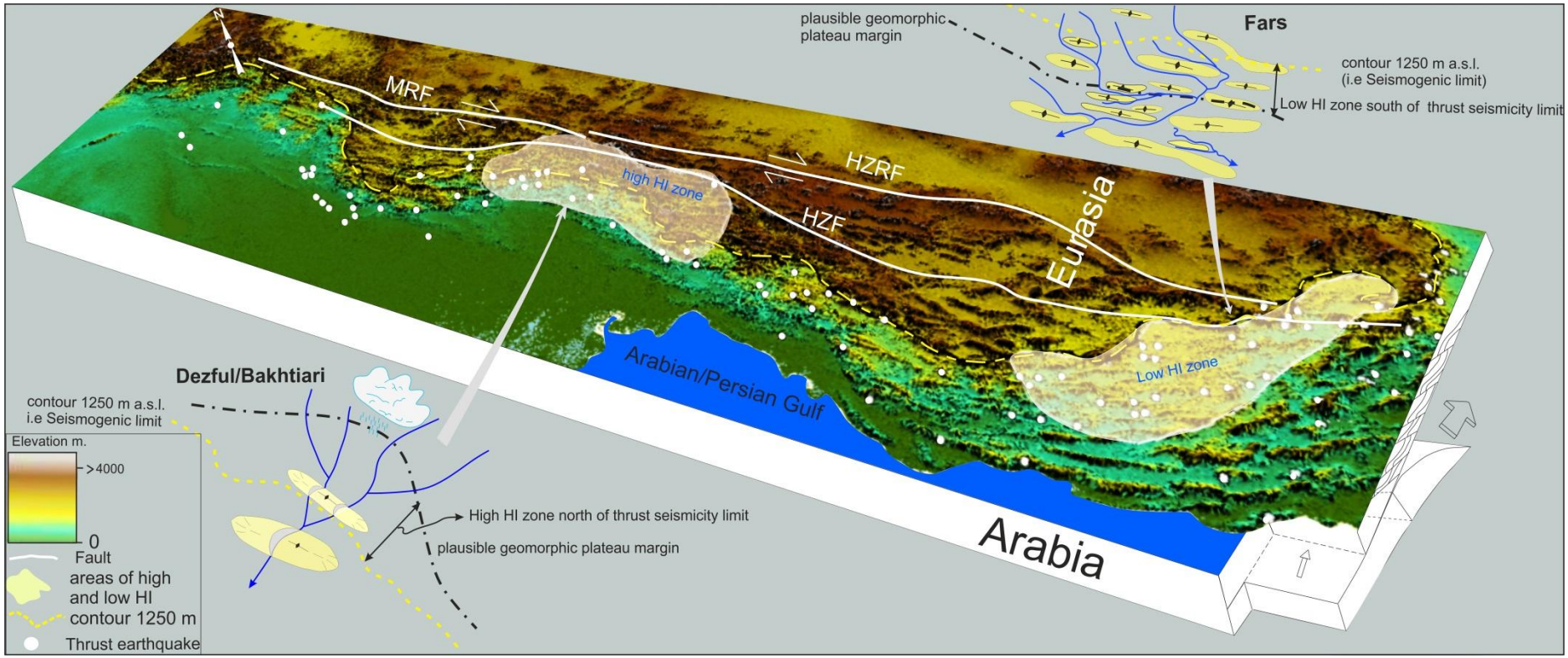

Fig. 2.38. Model shows how the topography of the Zagros responds to tectonism in term of change in the HI value. Note the high and low HI groups and the relation with thrust seismicity (contour 1250 m elevation). Geomorphologically, the plateau margin retreats NE in the Dezful/Bakhtyari and advances SW in the Fars region in consistent pattern with the high HI value.

3. Landscape Maturity Index analysis of the Kirkuk Embayment, Iraqi Zagros

3.1Introduction

This chapter was published as Obaid and Allen (2017), and is presented here with minor edits, including expanded descriptions of the stratigraphy and the methodology.

The Kirkuk Embayment (Fig. 3.1) is of special importance within Zagros as it contains the southwestern limit of deformation in the Zagros fold-and-thrust belt, and a large proportion of the hydrocarbon reserves in Iraq. The region includes the transition between the stable and unstable shelf of the northern part of the Arabian Plate (Jassim and Goff, 2006). It is a key question whether Cenozoic deformation started from the northeast at the continental suture and moved towards the southwest, either in quasi-continuous progression or in a series of pulses (Allen et al. 2013; Farahpour and Hessami 2012; Hessami et al. 2001; Karim et al. 2011; Lawa et al. 2013; Vergés et al. 2011). Koshnaw et al (2017), used patterns of syn-tectonic sedimentation to interpret "out-of-sequence" fold growth, towards the northeast, but as a late, localized exception to a northeast-southwest fold propagation sequence.

Digital elevation models (DEM) and satellite images have proven to be effective datasets for use in morphotectonic studies (Font et al. 2010; Singh and Jain 2009). With the aid of digital data, morphometric indices have therefore been widely used in active tectonic studies (e.g. Alipoor et al. 2011; Andreani et al. 2014; Bagha et al. 2014; Bahrami 2012; Bahrami 2013; Dehbozorgi et al. 2010; Ehsani and Arian 2015; Fard et al. 2015; Keller and Pinter 2002; Mosavi et al. 2015; El Hamdouni et al. 2008). Recently, researchers have used quantitative geomorphic indices maps to assess tectonic activity in many regions in the world. These indices include: surface roughness, hypsometric index, and surface indices (Andreani at al., 2014; González et al. 2015; Grohmann 2004; Mahmood and Gloaguen 2012; Shahzad and Gloaguen 2011b; Siddiqui 2014). Such approaches are especially useful where there is a lack of subsurface data and/or difficulty with access, which is the current situation in the Iraqi Zagros.

Geomorphic indices are used in this chapter to study landscape maturity, with a view to understanding the relative time of fold growth in the Kirkuk Embayment and therefore the sequence of deformation propagation. I also show the capacity of this kind of analysis to identify previously unrecognized folds, which may have hydrocarbon potential.

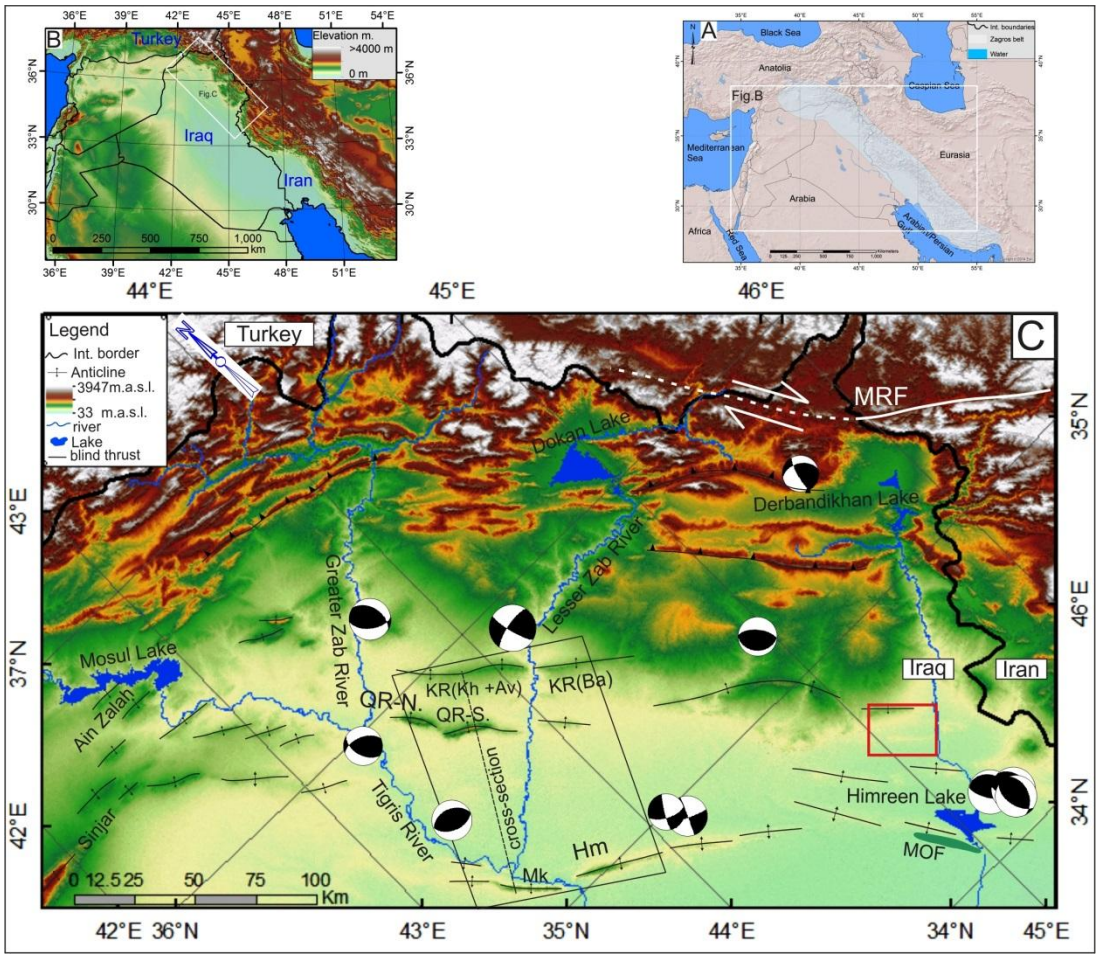

Fig. 3.1. A) World Shaded Relief map from Esri showing the location of the Zagros Fold-and Thrust Belt. B) Map shows Iraq and neighboring countries. C) Structural map of the northwest part of the Zagros fold and thrust belt shows the Kirkuk Embayment. QR-N, QaraChauq North; QR-S, QaraChauq South; KR (Kh.+Av.), Kirkuk (Khurmala and Avanah); KR (Ba), Kirkuk (Baba); Mk, Makhool; Hm, Himreen; MOF, Mansuriya Oil Field. Focal mechanisms are adapted from the Global CMT catalogue, and show the widespread distribution of thrust faulting. The black box shows the location of Figs. 3.2, 3.4, 3.5, 3.6 and 3.10. The red box shows the location of the field photographs in appendix 1.

3.2 Stratigraphy

Many formations are exposed in the Kirkuk Embayment (Fig. 3.2), and many wells have been drilled which help in understanding the depositional environments and ages of geological formations. The Eocene to Pliocene units can be summarized as follows (Jassim and Goff 2006), with outcrop photographs in (Appendix 1) from recent fieldwork near the eastern margin of the Embayment.

The Avanah Formation (Middle-Late Eocene) described first in well Kirkuk 116 by McGinty in 1953 in the southeastern segment of the Kirkuk Anticline, which is called the Avanah done (Bellen et al., 1959). This unit crops out locally on the southwest flank of the south QaraChauq Anticline. It is unconformable with the underlying lagoonal facies of the Khurmala Formation and also overlain unconformably by the Middle Miocene deposits. The thickness of the formation is ~200 m, which consists primarily of dolomitized and recrystallized limestone (shoal facies). As the formation was deposited on the border between the High Folded and Foothill zones the thickness varies from one well to another, but the maximum thickness can be found in the Foothill Zone area (e.g. Kirkuk Embayment).

The Jaddala Formation (Middle-Late Eocene) comprises 350 m of argillaceous and chalky limestone as it was described first by Henson 1940 in the Sinjar structure (Bellen et al., 1959). The maximum thickness of the formation is 1131 m in well Chemchemal-2 to the NE of the Kirkuk Anticline. The formation appears in Syria to the west and the Hibr Formation in Saudi Arabia to the south is very similar to the Jaddala Formation while in Iran the middle Pebdeh Formation is the equivalent formation to the Jaddala Formation (Jassim and Goff, 2006).

Kirkuk Group: This unit consists of several formations divided into a lower group. The Palani Formation (Early Oligocene) which is unconformably overlain by and underlain by the Jaddala and Sheikh Alas and /or Tarjil formations respectively. It comprises outer shelf basinal deposits of dolomitized globigerinal limestone (Majid and Vizer, 1986 in Jassim and Goff, 2006). The Tarjil Formation (Early Oligocene) overlies the Palani Formation unconformably, and consists of globigerinal marly limestone, which is slightly dolomitized. The rich fauna indicates that the age of the formation is Early Oligocene and it was deposited in an outer shelf environment for

its lower part and an open marine environment in its upper part (Hamid and Vizer, 1986 in Jassim and Goff, 2006).

The Sheikh Alas (Early Oligocene) is represented by porous and recrystallized limestone, which reaches a maximum thickness of 50 m in the Kirkuk area. The available fossils refer to a change from foreslope to lagoonal environment from the lower part to the upper part respectively, which changes into reefal environment of the overlying Shurau Formation (Majid and Vizer, 1986 in Jassim and Goff, 2006). The 18 m thickness represents the Shurau Formation (Early Oligocene) which passing form coralline limestone into grey and dense limestone from the lower part to the upper part of the formation respectively, referring to a change from reefal to tidal flat environment (Majid and Vizer, 1986 in Jassim and Goff, 2006).

The upper part of the Kirkuk Group consists of the following:

The Ibrahim Formation (Late Oligocene): It was deposited in a basinal environment as it first described in the Sheikh Ibrahim structure, NW Mosul by Bellen in 1957. Its thickness is 56 m, and it comprises globigerinal marly limestone, containing planktonic foraminifera which recorded the Late Oligocene age (Jassim et al., 1984 in Jassim and Goff, 2006).

The Baba Formation: it takes the name of Baba village near Kirkuk city as it first described in well Kirkuk 109 by Bellen in 1957 (Jassim and Goff, 2006), and it is represents 20 m thickness of porous, dolomitized limestone, rich in fossils, which indicate the Middle Oligocene age of the formation. A forereef depositional environment in interpreted of the Baba Formation and it is overlain unconformably by the Bajawan Formation. The Bajawan Formation (late Oligocene) was deposited in a reef environment, then the depositional basin changed into mud flats (Hamid and Vizer, 1986 in Jassim and Goff, 2006). The available fauna refer to the Late Oligocene age and it comprises 40 m of miliolid limestone. The Bajawan Formation is unconformably overlain by the Baba Formation and trangressively oversteps the older formations.

The Azkand Formation (Late Oligocene) comprises a thick massive recrystallized and dolomitized limestone with a thickness of 100 m. It overlies the Baba Formation

unconformably in the type area in QaraChauq, and is conformably and gradationally overlain by the Anah Formation.

The Anah Formation (Late Oligocene) comprises the last upper formation of the Kirkuk Group. The formation consists of 40-60 m of dolomitic and recrystallized limestone in the locality of QaraChauq. The formation in all localities is unconformable with overlying strata. The unit represents a reefal environment, alternating with back reef.

The Euphrates Formation (Aquitanian): It consists mainly of oolitic to chalky and well bedded limestone. This unit is equivalent to part of the Asmari Limestone in Iran and passes laterally into the Hadrukh Formation in Saudi Arabia.

The Jeribe Formation (Langhian): This formation consists mainly of marly recrystallized and dolomitized limestone. It is equivalent to the Kalhur limestone and part of Asmari limestone in SW Iran. In many hydrocarbon fields, the whole of the Kirkuk Group, together with the Euphrates and Jeribe formations, represents the main reservoir unit.

The Fat`ha Formation (Middle Miocene): The formation is equivalent to the Gachsaran Formation in Iran. It forms the regional topseal for Cenozoic hydrocarbon reservoirs in the Arabia. The lithology is mainly anhydrite, alternating with marl and limestone, with halite northeast of the Kirkuk Embayment (Aqrawi et al. 2010). The formation regionally divided into two members; the Lower member, which lacks the red mudstone, and the Upper member, which is characterized by a cyclic succession of mudstone and gypsum (Fig. 3.2 and appendix 1). The anhydrite, gypsum and halite in the lower member are very important as they facilitate thrusting of most of the anticlines in the Kirkuk Embayment (Jassim et al., 1981 in Jassim and Goff, 2006).

Injana Formation (Early Late Miocene): This unit is the equivalent to the Aghajari (Upper Fars) strata in Iran. South of the Himreen Anticline which is the subsidiary type section, the formation consists of 600 m thin-bedded calcareous sandstones, marls, red mudstone, and siltstone. In the Khanooqa area there is rare fresh water limestone containing ostracods (Al-Naquib, 1960 in Aqrawi et al., 2013). The layers

of sandstone thicken upward and the whole formation gets coarser upward (Fig. 3.2 and Appendix 1).

The Mukdadiyah Formation is equivalent to the lower part of the Bakhtiari Formation in Iran (Late Miocene-Early Pliocene). It consists of sandstones, pebbly sandstone and red mudstones and siltstone. The formation reaches its maximum thickness in the Kirkuk Embayment, at ~2000 m. The formation was deposited during anticline growth (Dunnington 1958). This formation is not reported in the northeast of the Zagros, which may mean that it is represented by the Bai Hassan Formation (see below) with the implication that both the Mukdadiyah and Bai Hassan formations are strongly diachronous. The formation comprises stacked fining-upward depositional cycles (Basi and Jassim, 1973 in Jassim and Goff, 2006) which might refer to tectonic quiescence represented by fine grained deposits and the absence of gravelly sandstone layers (Fig. 3.2 and Appendix1).

The Pliocene Bai Hassan Formation (Upper Bakhtiari) consists of mudstone, conglomerate with siltstone and sandstone, and is generally coarser than the Mukdadiyah Formation. The conglomerate layers increase in thickness and frequency towards the northeast (Fig. 3.2 and Appendix 1). The Mukdadiyah and Bai Hassan formations are debated as to their provenance and significance, as there is no specific geochronological study to differentiate between the two formations. It is very hard to differentiate between the Mukdadiyah and Bai Hassan units (Al-Naquib, 1960 in Aqrawi et al., 2013), and the provenance of the Late Miocene-Pliocene deposits across the Zagros is not yet proven. This implication is of importance in understanding the neotectonics of the Zagros.

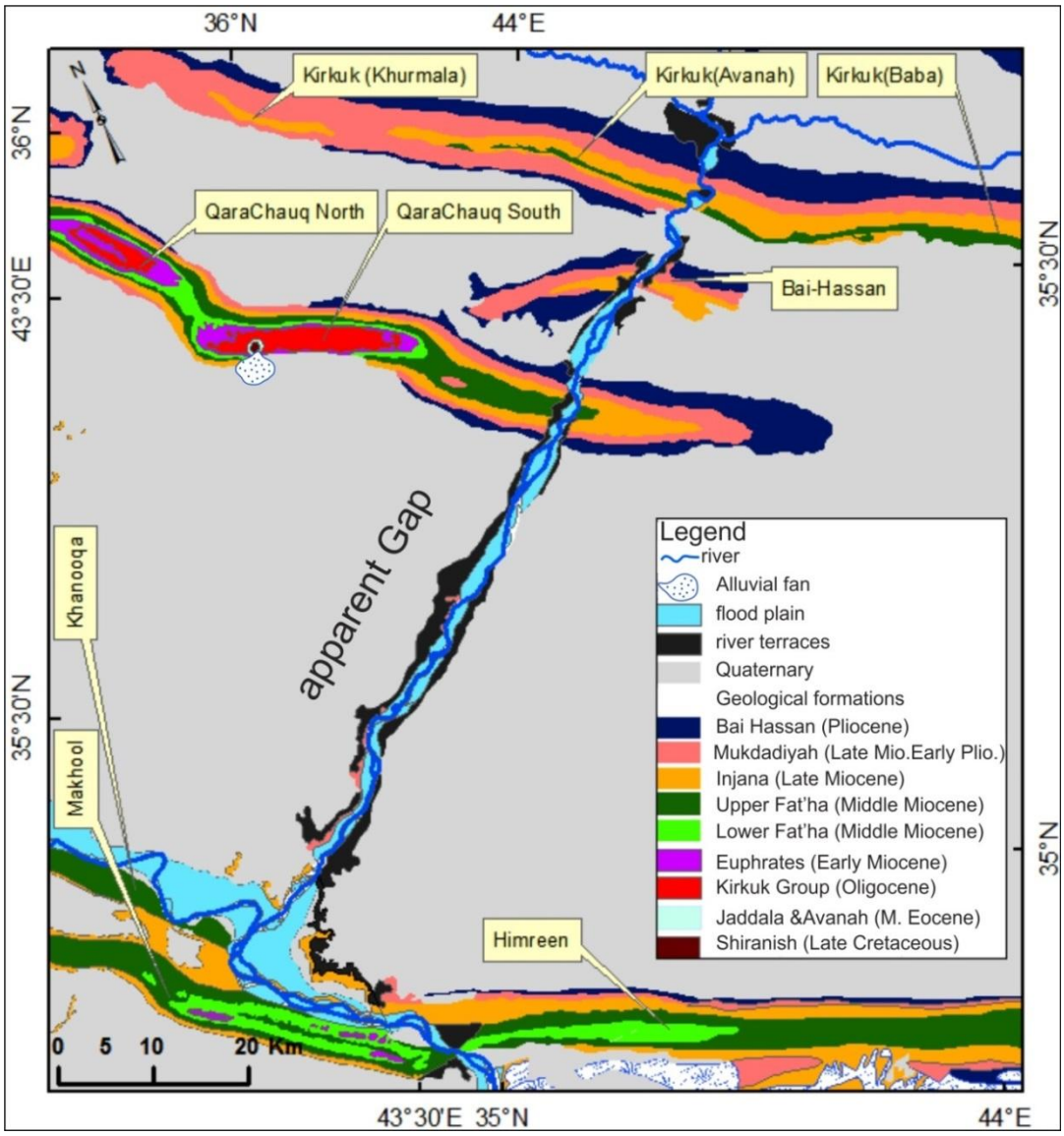

Fig. 3.2 Geological map of the NW part of the Kirkuk Embayment (Sissakian 1993; Sissakian 1995; Zwaid 1993). The Kirkuk Group is the main hydrocarbon reservoir in the region, which is mostly limestone. The Fat'ha Formation is mainly anhydrite, with prominent marls and clay layers in its upper part. The Injana Formation consists of a variety of non-marine clastic sediments. The Mukdadiyah Formation consists dominantly of sandstone. The Bai Hassan Formation consists of very coarse–grained conglomerate, with sandstone and clays dominantly in the lower part of the formation.

3.3 Seismotectonics

I have compiled the focal mechanisms available from the instrumental seismicity record (Fig. 3.1). These data are from the Global CMT catalogue (http://www.globalcmt.org); body-wave modelling studies for the Zagros have not included events from the Iraqi sector of the range (Talebian and Jackson, 2004; Nissen et al., 2011). The earthquake dataset shows that active deformation occurs

across the width of the Kirkuk Embayment, similar to the rest of the Zagros, with the caveat that major thrust seismicity is located in the lower elevation portions of the range, below the regional 1250 m elevation contour (Nissen et al. 2011). Kirkuk Embayment earthquakes are a combination of thrusts and strike-slip faults. Thrust earthquake depths, where constrained, are in the upper 20 km of the crust in the rest of the Zagros range to the southeast (Talebian and Jackson 2004). There is a typical uncertainty of 5 km in the depths of events, even where well-constrained. There is no reason to suppose the depth distribution is markedly different for the Iraqi sector of the range, despite the lack of accurate estimates for individual earthquakes. There are two implications of this regional depth distribution. First, seismogenic thrusting is an upper crustal phenomenon, and does not indicate any subduction of the Arabian Plate. Second, crystalline basement must be involved in at least some of the deformation, as the deeper hypocentres are too deep to be nucleated within the sedimentary cover, even allowing for the depth uncertainties noted above.

None of these earthquakes is associated with surface ruptures, so that the identification of the correct nodal plane cannot be done directly. Uncertainties in teleseismically-located epicentres are up to 20 km, making it impractical to link individual events to specific faults in the sub-surface. Either choice of nodal plane in the thrust events is steep ($>30^{o}$). I assume that northwest-southeast striking plane represents the real fault orientation of a strike-slip event near the Kirkuk anticline (Fig. 3.1), as the event would be the right-lateral component of partitioned strain, acting with the thrusts to achieve the overall north-south plate convergence (Talebian and Jackson 2002).

A similar event occurred just to the southeast of Figure 3.1. It is notable that strike-slip faulting occurs across the Kirkuk Embayment, and is not restricted to the Main Recent Fault at the northeast margin of the Zagros, which is the case in the northwestern Iranian sector of the range. Two strike-slip focal mechanisms near the Himreen Anticline (Fig. 3.1) are not consistent with such right-lateral faulting, parallel to the fold trace. These earthquakes could relate to oblique cross faults on the anticline, not exposed at surface levels, as depicted by Kent (2010) for the Kirkuk Anticline.

The southwestern margin of the Kirkuk Embayment (Fig. 3.1) is the southwestern limit of the active deformation in the Zagros fold-and-thrust belt, which seems to be located at the transition between the pre-collisional stable and unstable shelf of the northern part of the Arabian Plate (Jassim and Goff 2006). It seems that the pre-collisional structure of the Arabian Plate exerts an influence on the extent of collisional deformation. In the Zagros fold-and-thrust belt several studies have interpreted unconformities as an indication of tectonic pulses (Farahpour and Hessami 2012; Hessami et al. 2001; Karim et al. 2011; Lawa et al. 2013) resulting in the step-wise progression of deformation towards the foreland. Given the diachronous nature of Cenozoic sedimentation in the region (e.g. Fakhari et al., 2008), and the possibility of unconformities being a response to base-level change and/or drainage re-organization, I consider that it is timely to re-evaluate these models for the Zagros tectonic evolution.

3.4 Methods and Data

3.4.1 Data

The 90 m DEM of Shuttle Radar Topography Mission (SRTM) is used in this study; the data have a specified vertical absolute accuracy of ≤16 m, and a vertical relative accuracy quoted as ≤10 m (Rodriguez et al. 2006 and references therein). These DEM data have been used in conjunction with satellite imagery, in particular Quickbird images. Geological maps (Sissakian 1993; Sissakian 1995; Zwaid 1993) were used for comparison with the exposed geology in each region. The MATLAB-based TecDEM software (Shahzad and Gloaguen 2011a,b) was used in combination with ArcGIS10.3.1 for data processing and the extraction of geomorphic indices. Part of the analysis is a simple qualitative investigation of the patterns of topography and drainage across the study area, including longitudinal river profile analysis. This inspection was performed to identify anomalous patterns, including topographic highs that might correspond to previously-unidentified folds and drainage diversion patterns and knickpoints that might correspond to zones of active deformation.

The SRTM data were prepared to have a UTM projection in tiff format to be compatible with the inputs of the TecDEM 2.2 MATLAB-based toolkit. All voids and depressions in the original data needed to be filled using the depression fill function within the interface window of the software. Drainage network for the area

was be constructed by using flow grid function and applying the D8 algorithm (Fig. 3.3 A). Minimum contributing area was assigned to 1km^2 using the contributing area function to consider all streams and basins of lowest orders in the area, which depend upon in the next step. By this stage the data were ready for drainage network and basin automatic extraction using drainage network extraction and basin extraction functions respectively.

For the purpose of constructing raster mode maps for the analysed geomorphic indices (in here the Hypsometric Index, surface roughness and surface Index), I applied the spatial statistics function which has many sub functions (Fig. 3.3B). Each function has specific setting depending on the resolution of the SRTM data and the purpose of analysis and I discuss that in the sensitivity section (3.4.2) within this chapter. All produced maps must be exported in a tiff format to the ENVI software and saved in its environment as .hdr format to be readable in the ArcGIS, and then classified easily into intervals of classes.

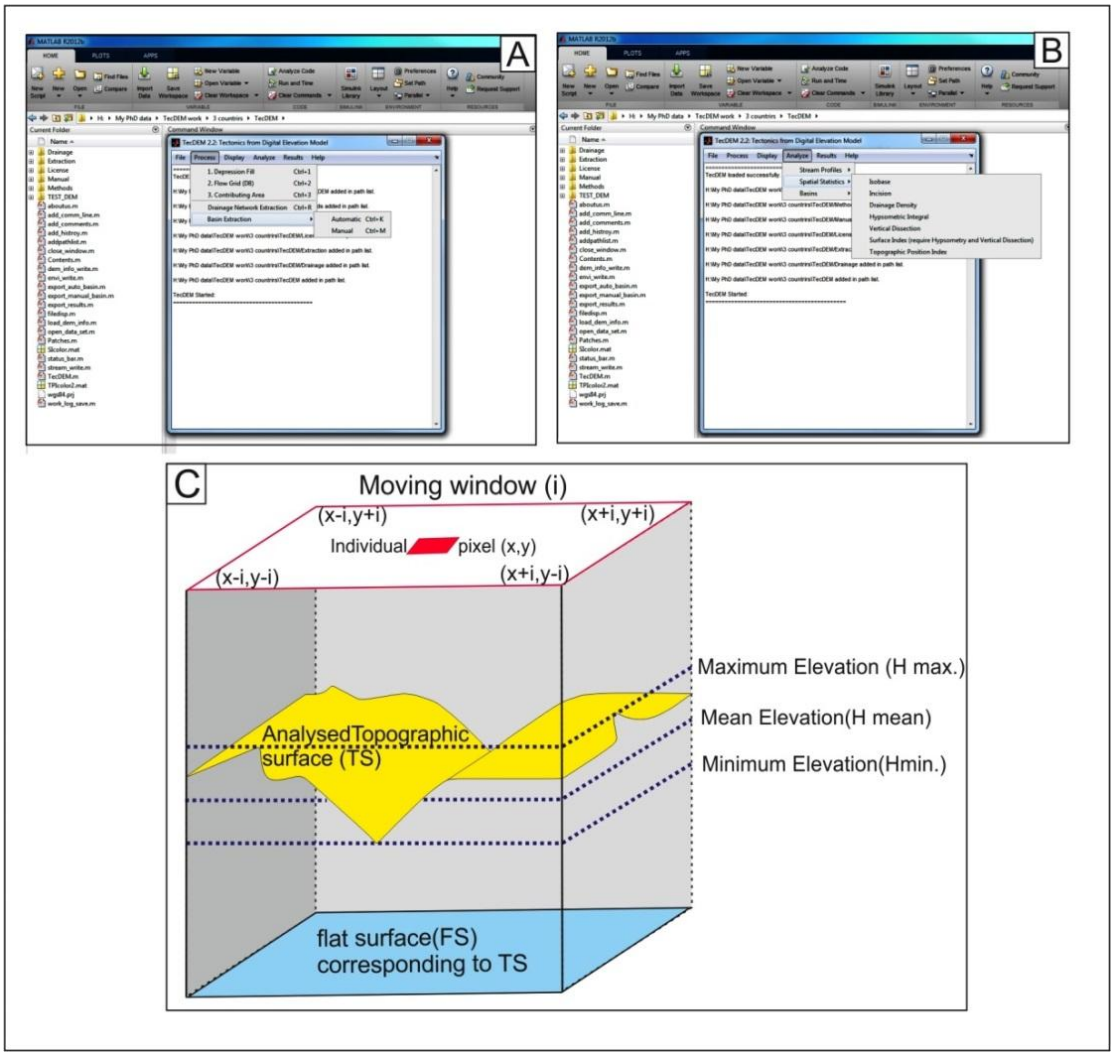

Fig. 3.3. A) Drainage network extraction, B) functions that use to produce geomorphic indices maps and C) Sketch diagram shows the basic of HI and SR calculation (modified after Andreani et al. 2014).

3.4.2 Geomorphic indices

This section describes the geomorphic indices used in the landscape analysis in this study (Fig. 3.3C). The numerical ranges presented in Figures 3.4-6 are relative values, rather than absolute values that could be directly compared with other areas. The Hypsometric Index (HI) refers to the amount of surface above a given area and it highlights the elevated surfaces. When the HI is linked with the degree of dissection, it is considered to be a suitable parameter for detecting landscape evolution stages in the erosion cycle (Keller and Pinter 2002; Ohmori 1993; Strahler 1952). Low HI values are associated with dissected or more mature areas, while high values represent relatively youthful topography and less eroded areas (Keller and Pinter

2002; Pérez-Peña et al. 2009). For a given area, HI can be calculated using Equation 3.1 (Pike and Wilson 1971).

$$HI = \frac{H_{mean} - H_{min}}{H_{max} - H_{min}} \quad (3.1)$$

Where $H_{max,}$ H_{min} , and H_{mean} are the maximum, minimum, and mean elevations respectively (Fig. 3.3C).

An important difference between the approach of this chapter and Chapter 2 is that HI, and the other indices, are used in a moving window format, rather than by drainage basin. The moving window approach is appropriate for a smaller area, where high resolution of subtle features is important. The drainage basin approach is more appropriate for orogen-scale studies such as Chapter 2 (and Chapter 4).

The surface roughness (SR), also known as vertical dissection, has been defined as the ratio between the analyzed topographic surface of an area and the area of flat topography, when the analyses are performed to the same geographic extent and constant elevation (Berti et al. 2013; Grohmann 2004; Hani et al. 2012). SR can be calculated using Equation 3.2. SR values close to 1.0 represent flat areas and the value increases as the surface becomes irregular.

$$SR = \frac{TS}{FS} \quad (3.2)$$

Where SR is the surface roughness, TS is the analyzed topographic surface area, and FS is the corresponding horizontal area (Fig. 3.3C).

Surface Index (SI) is the combination of both HI and SR characteristics which enables SI to be used to consider tectonic and erosion evolution, thereby determining the relative age of the landforms and the degree of dissection associated with them (Andreani et al. 2014; González et al. 2015). Uplifted surfaces become more irregular because of erosion as a result of rivers progressing toward their equilibrium state (Keller and Pinter 2002). Less mature landforms are therefore associated with high HI values and low SR values, and consequently, positive SI value. While more mature or more irregular surfaces associated with high SR values and low HI values and, therefore, negative SI values (Andreani et al. 2014; González et al. 2015). SI has been calculated as in Equation 3.3 (Andreani et al. 2014).

$$SI = \left(\frac{HI - HI_{min}}{HI_{max} - HI_{min}}\right) * \left(\frac{H - H_{min}}{H_{max} - H_{min}}\right) - \left(\frac{SR - SR_{min}}{SR_{max} - SR_{min}}\right) \quad (3.3)$$

Where HI, H, and, SR are the hypsometric index, elevation, and surface roughness respectively. These parameters are converted automatically to a ratio using the minimum and maximum values for each raster datum (Andreani et al. 2014). SI has also been used in rock differentiation, by exploiting different erosion characteristics of different rocks (Othman and Gloaguen 2014). These indices are used in this paper to investigate landscape maturity and to explore whether the deformation has simply propagated from the northeast to the southwest, which would result in a consistent progression in the value of indices between anticlines in this direction if other factors are equivalent (e.g. climate, lithology), or if the situation is more complex.

For meaningful results of geomorphic indices the moving window should cover the whole width of the feature under study. The approximate width (half wavelength) of the anticlines in the Kirkuk Embayment is ~ 4000-5000 m. To address these features, I selected a 50 by 50 pixel moving window for the SRTM 90 m dataset, and a 150 by 150 pixel moving window for the SRTM 30 m dataset as optimal. These configurations are equally effective in picking out variations between the major structures in the study area (compare Fig. 3.6 and Appendix 3.2I for example). A sensitivity analysis has been conducted, to investigate the robustness of the DEM analysis, and is presented in section 3.5.2.

River profile analysis (the method is described in Chapter two) has been conducted for an ephemeral river in the Kirkuk Embayment. Also, the ratio of channel length over valley length (sinuosity index, Appendix 3.1) for each 5 km segment along the Lesser Zab River in the Kirkuk Embayment has been calculated (Schumm, 1963) to indicate subsurface anticlines growth in the Kirkuk Embayment (section 3.5.4).

3.5 Results

3.5.1 Morphotectonic Indices

Figure 3.4 and Appendix1C show the change in the HI value across the major structures in the Kirkuk Embayment using the SRTM 90 m resolution and the SRTM 30 m resolution datasets respectively. Low HI values are distributed across the

QaraChauq anticline: in the range 0.14-0.17 for the SRTM 90 m dataset and 0.11-0.25 for the SRTM 30 m dataset.

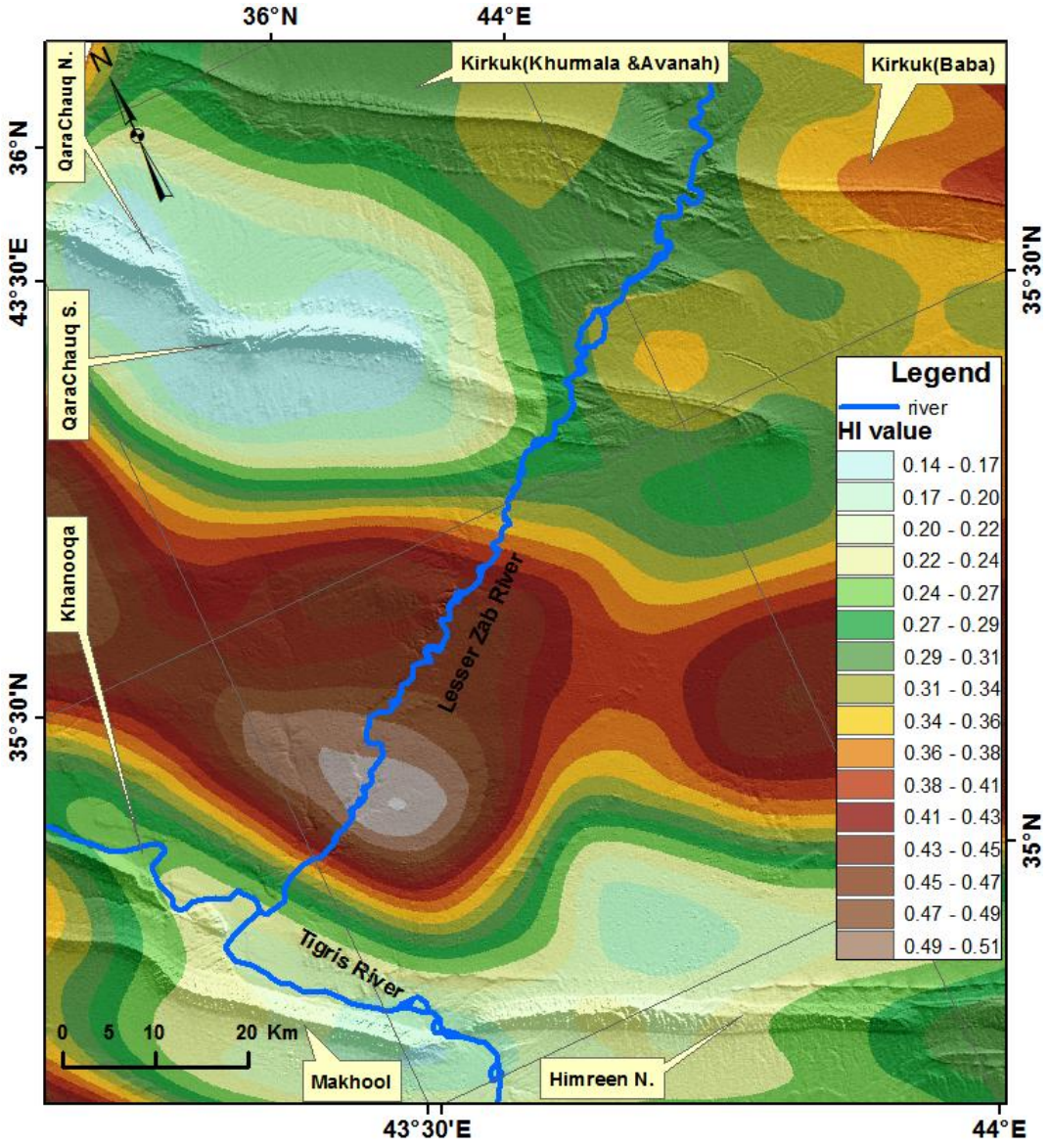

Fig. 3.4. Hypsometric Index (HI) map for the study area in the Kirkuk Embayment.

The HI values increase towards the south (0.35-0.5 for the SRTM 90 m and 0.34-0.55 for the SRTM 30 m), across an undulating area between the QaraChauq and Makhool anticlines. Further south, the HI value begins to decrease again (0.18-0.27 for the SRTM 90 m and 0.2-0.3 for the SRTM 30 m) along the Khanooqa, Makhool, and Himreen anticlines. To the north of QaraChauq Anticline, the HI values increase (0.29-0.41 for the SRTM 90 m and 0.3-0.41 for the SRTM 30 m) along the crest of the Kirkuk Anticline. As the HI values of the QaraChauq Anticline represent a relative low in the mapped area, it can be therefore identified as an area of higher

landscape maturity if not an area of earlier uplift. In contrast, the HI values of the Kirkuk Anticline represent a relative high, identifying it as a less mature area. There is also a variation in the SR values between the different folds (Fig.3.5 and Appendix 3.2F). The QaraChauq Anticline shows the highest SR values (1.032-1.059 for the SRTM 90 m and 1.033-1.059 for the SRTM 30 m), and the Kirkuk Anticline shows the lowest values (1.0026-1.009 for the SRTM 90 m and 1.005-1.018 for the SRTM 30 m).

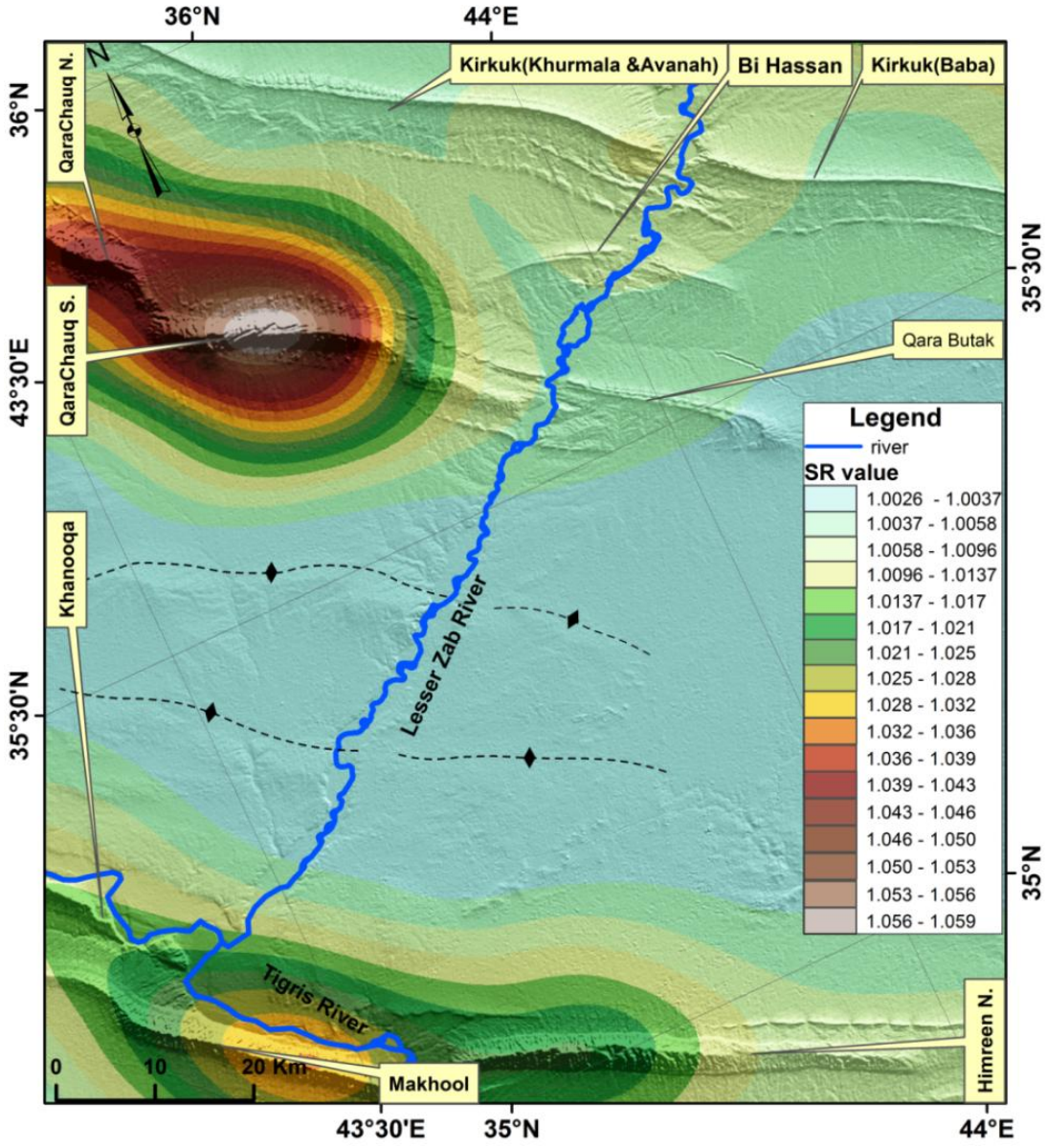

Fig. 3.5. Surface Roughness (SR) map, showing different degree of dissection.

Building on these HI, and SR values, the SI index reveals different levels of landscape maturity and probably different times and /or rates of surface uplift (Fig. 3.6 and Appendix 3.2I). Negative SI values (-0.08 to -0.17 for the SRTM 90 m and -0.07 to -0.17 for the SRTM 30 m) occur across the QaraChauq Anticline, representing more mature and relatively highly dissected areas. Positive SI values (0.05-0.16 for the SRTM 90 m and 0.04 to 0.14 for the SRTM 30 m) are distributed across the surface of the Kirkuk Anticline representing relatively less mature and less dissected areas (Fig. 3.6 and Appendix 3.2I).

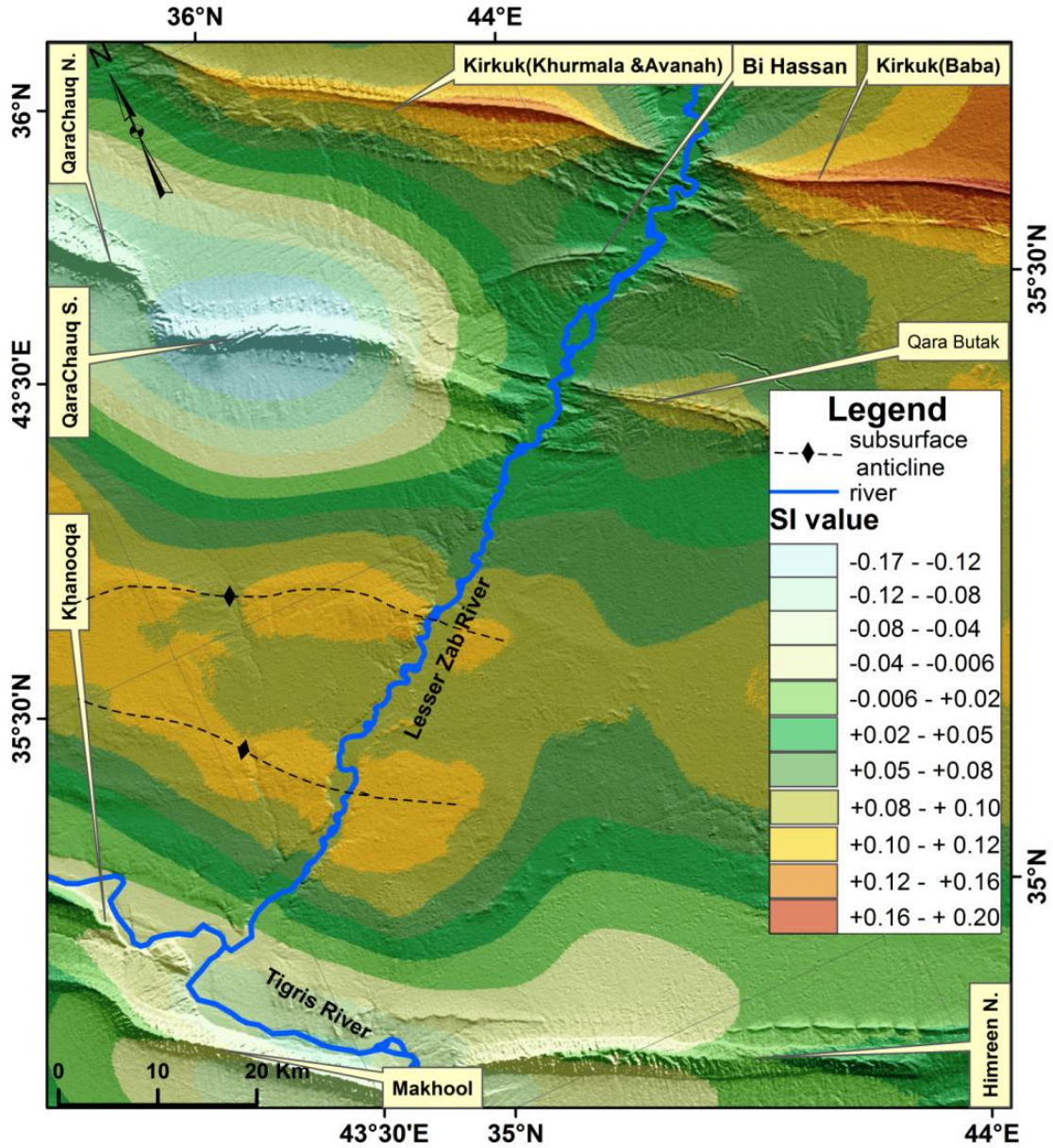

Fig. 3.6. Surface Index (SI) map shows different stage of landscape maturity in the Kirkuk Embayment. The positive values represent relatively less mature areas and the negative values represent relatively more mature areas. See text for details.

An important question may be raised as to what differences across the study area lead to differences in the landscape maturity indices. To answer this question, three parameters need to be taken into consideration: climate, tectonic activity, and the variation in rock type (Burbank and Anderson 2002). First, it can be argued that the effect of the climate can be neglected as no noticeable regional climate variation is present on the scale of the study area in figures 3.4-6. Nor is it expected that differences in elevation between the anticlines could be the reason for the differences in the indices used: the differences in elevation do not exceed a few tens of meters between the studied anticlines (Fig. 3.1). Second, closer scrutiny of the geology of the anticlines shows that their outcrops consist of the same sequences of rock units (Kirkuk Group, Fat`ha, Injana, Mukdadiyah, and Bai Hassan formations). Whilst there are likely to be differences between the lithologies of these units, e.g. between resistant limestone of the Kirkuk Group and erodible siltstones of the Injana Formation, it is not recorded that any individual unit is highly variable on the scale of the study area. According to the independent study of Bretis et al (2011) these formations all have a similar resistance to erosion, except for the resistant limestones of the Kirkuk Group, which is only locally exposed on the crest of the QaraChauq Anticline (Fig. 3.2). If I exclude the exposures of the Kirkuk Group from this analysis it does not affect the overall results, as the area involved is <1% of the total study area.

Figure 3.2 shows the major exposure of the Injana Formation (Late Miocene) and minor exposure of the Fat`ha Formation (Middle Miocene) on the crest of the Kirkuk Anticline, while the majority of these formations have been removed from the crest of the QaraChauq Anticline and are exposed only on the flanks of the south and north QaraChauq and in the saddle between them. Kirkuk Group strata (Oligocene) are exposed on the south and north QaraChauq crests. In addition to the Kirkuk Group, the Euphrates Formation (Early Miocene) appears on the north QaraChauq crest, but is not found on the Kirkuk Anticline crest. The Fat`ha Formation is the major formation to be exposed on the Makhool and Himreen anticline crests. The Fat'ha Formation is older than the units exposed on the Kirkuk Anticline and younger than the formations exposed on the QaraChauq Anticline.

From the above discussion it can be inferred that the climate and rock type have no effect on the variation in the calculated geomorphic indices across the area of Fig.

3.2 as a whole. Tectonic effects should therefore be the controlling factor on the geomorphic indices, but this includes both the age of the structures and their rock uplift rates.

Using the variation in SI values (Fig. 3.6), and the age of the exposed geology on the crests of anticlines in the Kirkuk Embayment, it can be concluded that the main anticlines formed in the order of S. QaraChauq, N. QaraChauq, Makhool, Himreen, and lastly Kirkuk, which is the order of increasing SI value. According to the thinning over anticline crests recorded in the Mukdadiyah Formation, which reflects syn-tectonic deposition, folding in the Kirkuk Embayment started in a short period in the Late Miocene (Fig. 15b in Kent 2010). This means that the deformation of the prominent structures in the Kirkuk Embayment is a late Cenozoic phenomenon.

3.5.2 Sensitivity analysis

Errors and uncertainties related to the original DEM quality and resolution are inevitable, and analytical methods attempt to reduce these errors (Kirby and Whipple 2012). In this section I explore the effects of using different moving windows for the three indices, using both the 90 m and 30 m SRTM data.

If the moving window covers too small an area, it highlights local features related to drainage patterns, which obscure the signals from the main anticlines. If the moving window is too large, the anticlines themselves are not successfully resolved. Appendix 3.2 A-O gives examples of both of these phenomena.

The extra processing time required for the SRTM 30 m data is a reason not to use this dataset. Again, I stress that the intention of this study is to investigate variations in landscape maturity on the scale of the major anticlines. In this context, the extra resolution of the 30 m data is of no advantage.

For all the three indices (HI, SR and SI) the 90 m and the 30 m SRTM datasets have ranges which are different from each other by a maximum of <0.08, across the major anticlines in the Kirkuk Embayment. The subtlest variations in the studied landscape which seem to have a real tectonic significance are on the order of 0.02 units in the SI diagram (Fig. 3.6); see section 3.5.4.

3.5.3 Lesser Zab River interactions with folds

The Lesser Zab is the main river in the study area (Figs. 3.1 and 3.2). It runs northeast-southwest across the anticlines discussed above. The river maintains a distinctly straight course across the Kirkuk, Bai Hassan and QaraButak anticlines (Fig. 3.2) without showing clear knickpoints (Fig. 3.7).

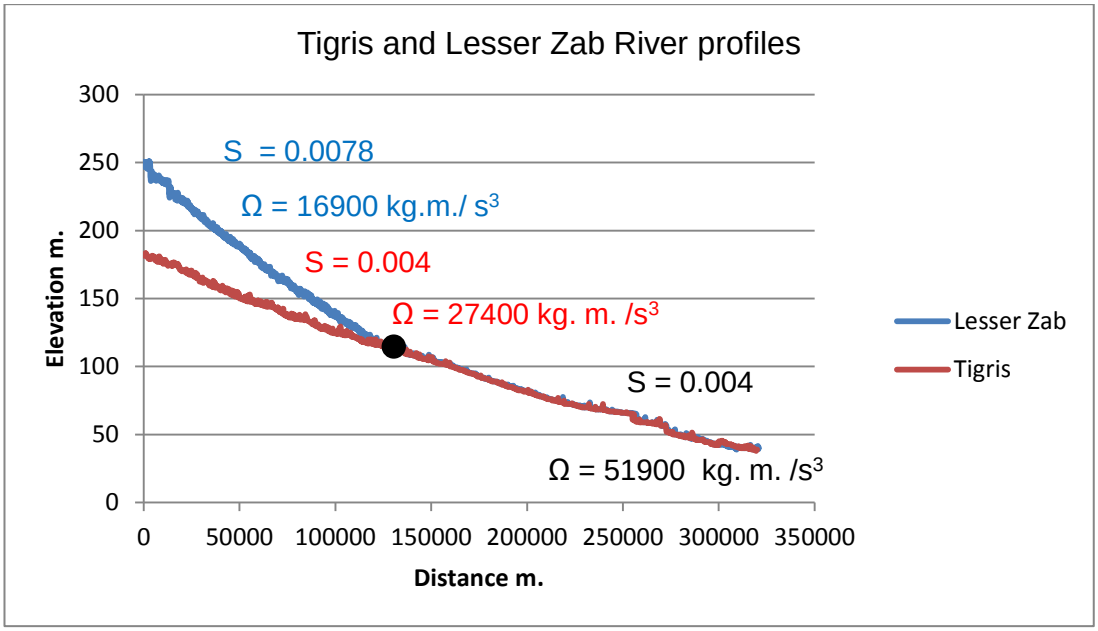

Fig. 3.7. Longitudinal profile of the Lesser Zab River and Tigris River showing the gradient (S) and stream power (Ω) of the two rivers. Also there is no change in the base level of the river as knickpoints. The solid black circle represents the confluence point between Lesser Zab River and Tigris River.

Nor is there a knickpoint associated with either of the newly-identified folds which are described in the next section. None of these anticlines is appreciably offset in either horizontal or vertical dimensions; there is no evidence that a reactivated basement structure runs along the length of the Lesser Zab, as has been indicated in some previous tectonic maps of the region (e.g. Burberry, 2015), cross-cutting anticlines such as Kirkuk. The Lesser Zab joins the Tigris, ~10 km north of the Makhool Anticline, and the combined river flows another ~20 km to the SE before crossing the Makhool Anticline at its termination, which is also the relay zone with the tip of the Himreen Anticline. The junction of the Makhool and Himreen anticlines is an example of the kind of en echelon fold linkage described by Bretis et al (2011) northeast of the Kirkuk Embayment in the Iraqi Zagros, in this case exploited by the Tigris River. Figure 3.8 shows that the Tharthar trough, south of the

Makhool Anticline, could be the original continuation of the course of the Tigris River, if the Makhool Anticline had not developed. As rivers tend in nature to gravitate towards the zones of subsidence when there is no topographic barrier (Holbrook and Schumm, 1999), the Tharthar trough would represent a pathway for the Tigris, rather than diverting eastwards across the nose of Makhool Anticline as it does now. The modern drainage in the Tharthar trough seems distinctly misfit, as though at an earlier time the trough was occupied by a much larger river (see the cross-valley profiles in Figure 3.8).

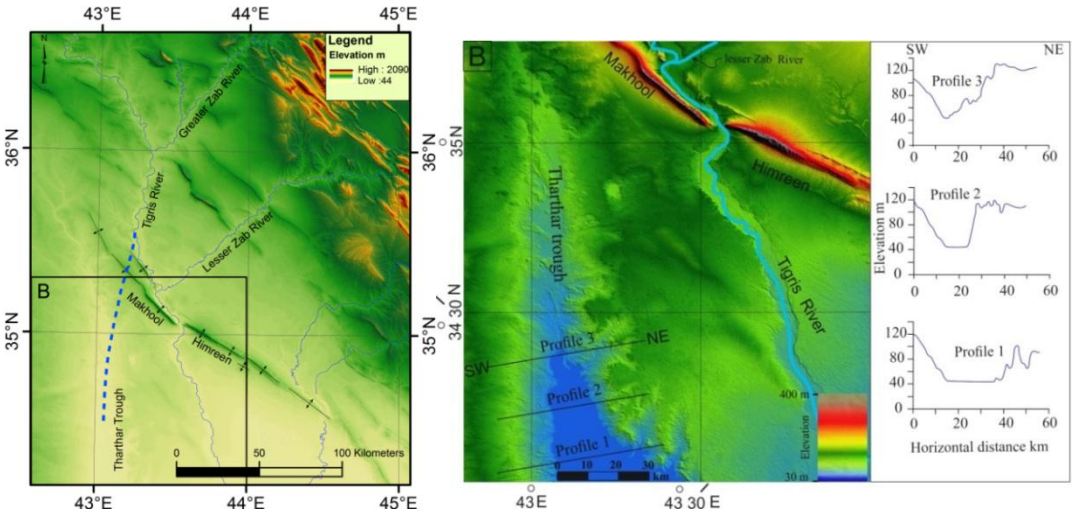

Fig. 3.8. Map showing the location of the Tharthar trough, and the possibility for it being a paleo-channel of Tigris River (inset B). The dashed blue line is the plausible pathway for the Tigris River.

According to the discharge data (Saleh, 2010) the stream power of the Tigris River (Fig. 3.7) before approaching the Makhool anticline is 27,400 kg.m/s^3 (and a near-constant gradient of 0.004). The Lesser Zab River crosses the Kirkuk, Bai-Hassan, and QaraButak anticlines with a straight flow path, near-constant gradient (0.007) and stream power of 16,900 kg. m/s^3. The two rivers combine north of the Makhool Anticline, but, unlike the behaviour of the Lesser Zab to the north, even the combined rivers are diverted eastwards by the growth of the Makhool Anticline, before flowing across the nose of the fold.

The cross-cutting relationships between the Lesser Zab River and the anticlines in the Kirkuk Embayment can be interpreted to give a scenario about the sequence of anticlinal growth in this area. The Lesser Zab River crosses the Kirkuk and Bai Hassan anticlines (which are relatively less mature according to the surface index), while it diverts around the nose of the Makhool anticline (which is relatively more

mature). There is no noticeable change in gradient along Lesser Zab River profile (Fig. 3.7). Thus, the Lesser Zab River overcomes the growth of the Kirkuk and Bai Hassan anticlines, and the river crosses these anticlines without deflections, wind gaps or knickpoints. However, it appears that the Makhool Anticline exceeded the ability of the combined Lesser Zab and Tigris River to cut through the growing fold, and consequently the river was diverted by the fold; this relationship could mean faster growth of Makhool than the folds to the north, but may mean that the paleo-gradient was lower before the uplift of structures to the north. Note that Koshnaw et al. (2017) put the initiation of the Kirkuk Anticline during the deposition of the Mukdadiyah Formation in the Late Miocene, based on syn-fold strata of this age on the south side of the anticline; their data come from an area ~100 km southeast of the area of this study, so there is the potential for different sectors of the same fold to be of different ages due to lateral fold growth.

3.5.4 Identification of incipient folding

The broad synclinal area between the Kirkuk and Himreen anticlines is covered by Holocene sediments (Jassim and Goff 2006). Published structural maps typically show a gap between the QaraChauq Anticline and the Himreen Anticline with no fold structures in this region (e.g. Fouad 2015; Burberry et al. 2015; Koshnaw et al., 2017; Figs. 3.1 and 3.2). Figure 3.9 shows two subdued topographic rises within this area, both trending northwest-southeast, in parallel with the regional fold trend. The spacing between these rises is ~20 km, which is similar to the spacing between at least some of the well-developed folds in the Iraqi Zagros, such as QaraChauq and Kirkuk (Fig. 3.2). Four topographic profiles have been drawn perpendicular to the hinge lines of the Khderat Anticline (on the flank of the adjacent Makhool Anticline), and the two newly-identified rises. These profiles show the similarity in half wavelength and amplitude of the three structures (Fig. 3.9). It can be seen that the northeastern rise is similar in relative elevation to the Khderat Anticline (Fig. 3.9).

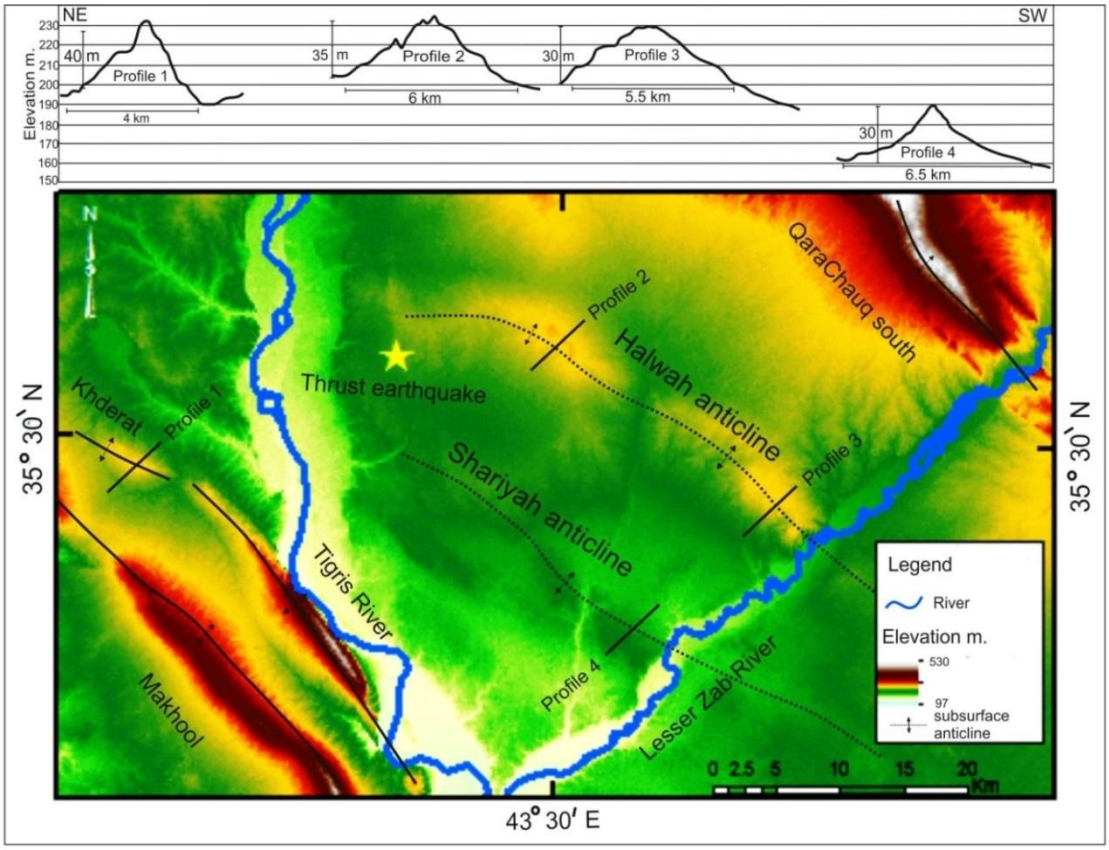

Fig. 3.9. Topographic analysis of SRTM 90 m resolution data shows the subdued expressions of the new anticlines between QaraChauq and Makhool/ Himreen.

The SI values show isolated areas of positive values that could represent youthful topography and uplifted surfaces, with a difference of ~ 0.02 in the SI value between the rises and adjacent areas. These areas between the QaraChauq and Makhool anticlines are represented by the orange color in the SI map (Fig. 3.6).

Drainage patterns were also analyzed as an indication of uplift, and show a radial pattern that reflects a dome-shaped topography (Fig. 3.10). Tracing the drainage network configuration shows clearly the occurrence of elongated and low relief structures in a consistent pattern with the youthful topography highlighted by SI contours (Fig. 3.6). The notable advantage of the drainage network analysis is that it shows both crests to the east of the Lesser Zab River, with a clarity that is not present in the morphotectonic indices or the raw topographic data. These features are similar in their linkage and orientation with QaraChauq/QaraButak anticlines. In addition, seismicity data shows a thrust earthquake (Fig. 3.1 and Fig. 3.9) with a depth of ~20 km occurred in 2013 in the vicinity of this uplifted topography.

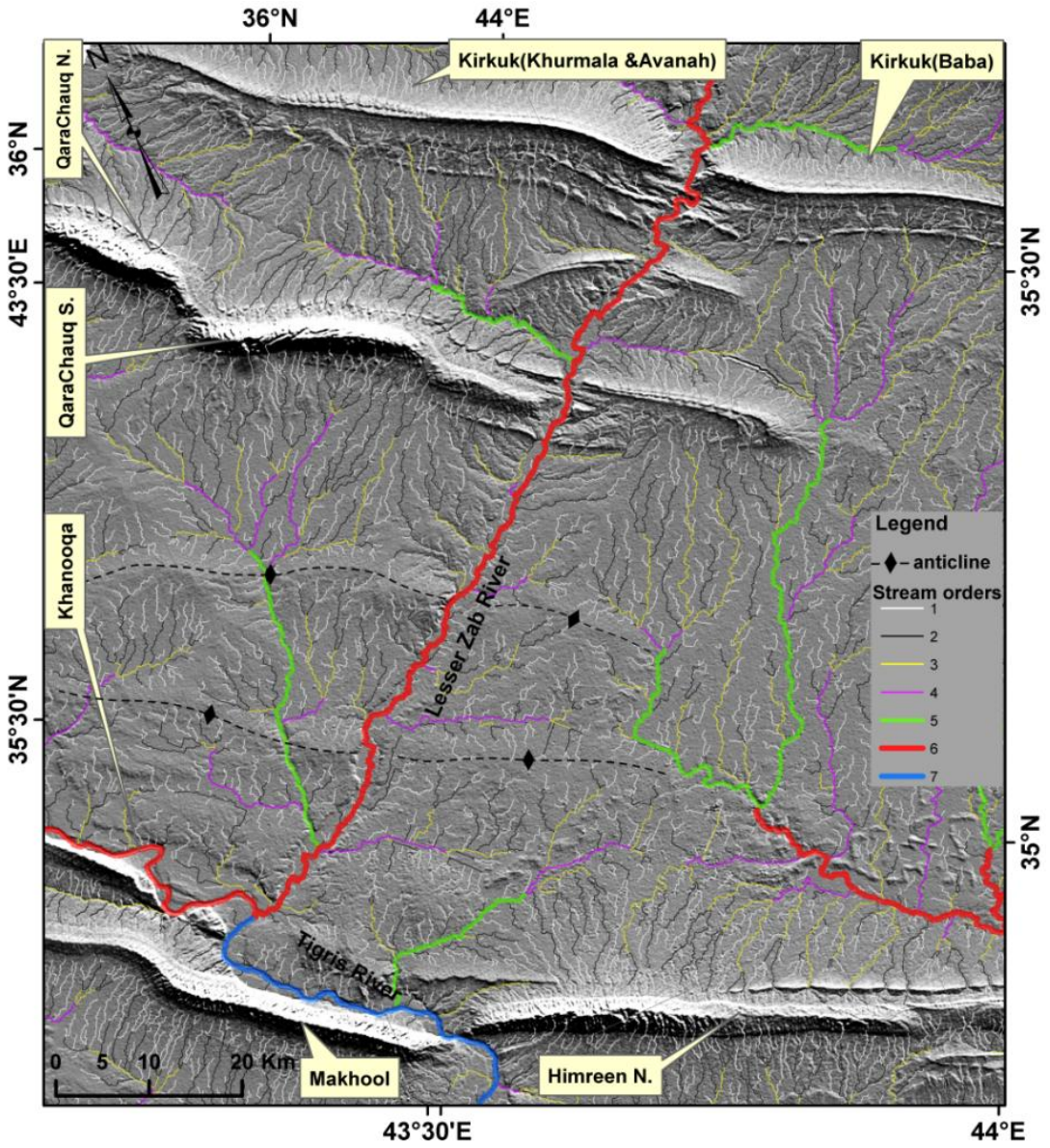

Fig. 3.10. Drainage network of the Kirkuk-Himreen area extracted from SRTM 90m according to the hierarchical order of Strahler using MATLAB-based TecDEM software. Note the radial pattern that reflects the subsurface uplift around the new anticlines.

River profile analysis for the 5th order stream which crosses the two rises shows a change to higher k_{sn} value and occurrence of knickpoints, consistent with the location of these two rises (Fig 3.11). Also, the sinuosity of the Lesser Zab River shows a low value consistent with the zones of uplift of the Kirkuk, Bai Hassan, QaraButak anticlines (Fig. 3.12 A) and the two rises (Fig. 3.12 B).

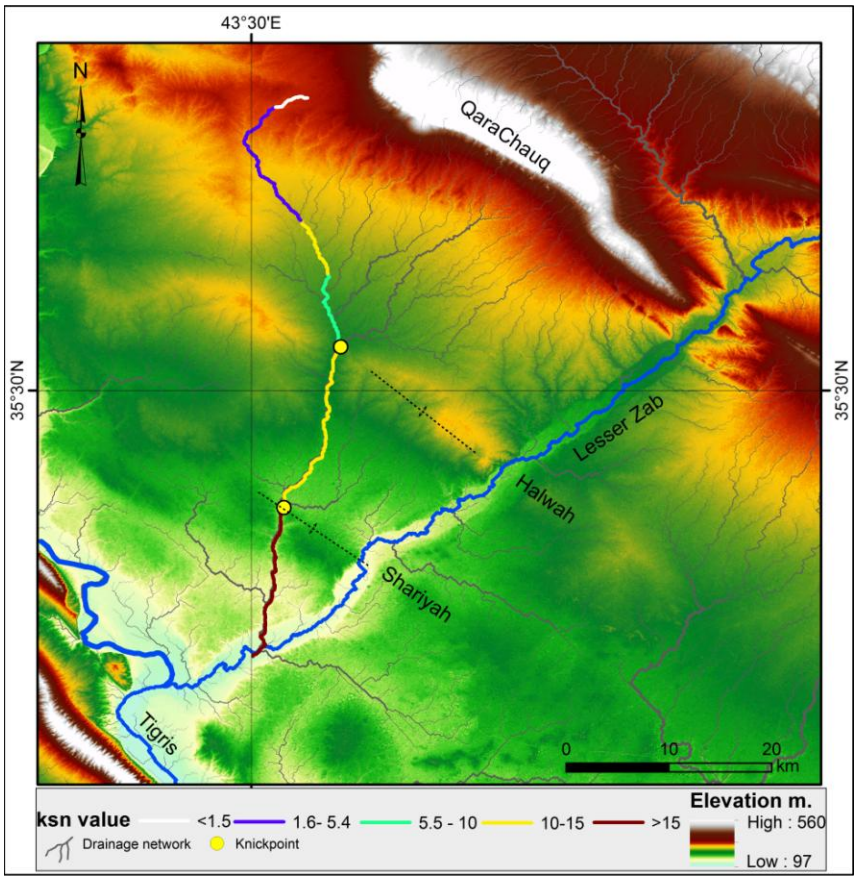

Fig. 3.11. Map shows the topography for the two new rises mentioned in section 3.4.4 and river profile analysis. Note the change of the Ksn value and knickpoint occurrence when approaching the area of the two rises.

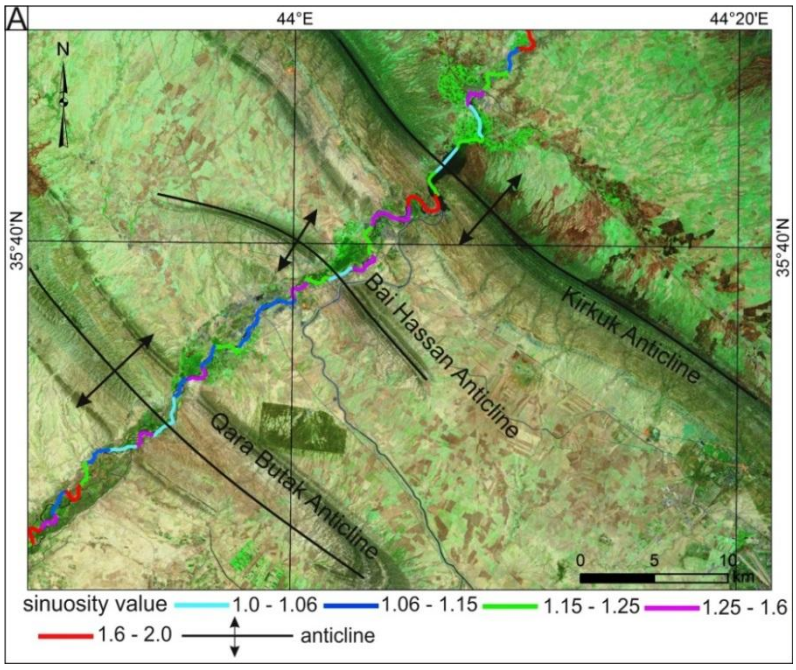

Fig. 3.12a. Sinuosity value of the Lesser Zab River. Note that the low value occurs when river crosses the anticlines in the area.

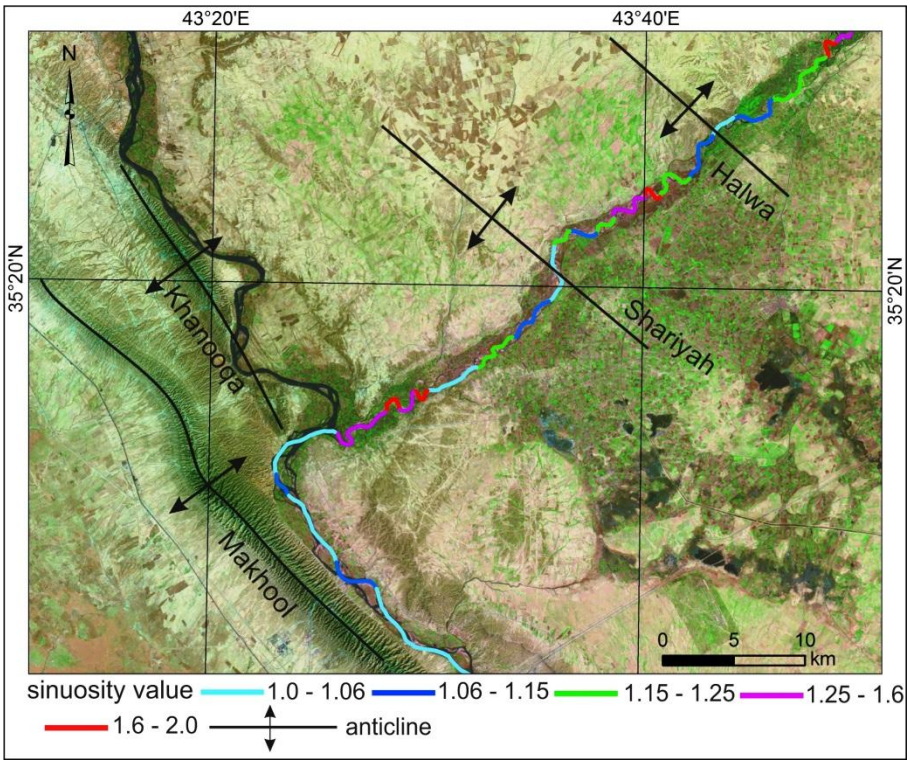

Fig. 3.12b. sinuosity value of the Lesser Zab River. Note that the low value occurs when river crosses the area of new identified anticlines.

Based on the topography, drainage patterns, river sinuosity, steepness, HI and SI values, these two rises between the QaraChauq and Himreen anticlines are interpreted to represent low relief anticlines that are growing due to the activity of thrust faults at depth, evidenced by the seismicity in the region. I informally named the two rises according to the names of the nearest villages as i) Halwah, which the northern rise towards QaraChauq (Fig. 3.13), and ii) Shariyah, which is the southern rise, closer to Makhool. These structures have not previously been mapped in the Iraqi geological survey publications (e.g. Fouad 2015; Sissakian 2000). The Halwah and Shariyah structures might be of importance as 4-way closure anticlines that trap oil and/or gas, like the existing oil and gas fields distributed in the area.

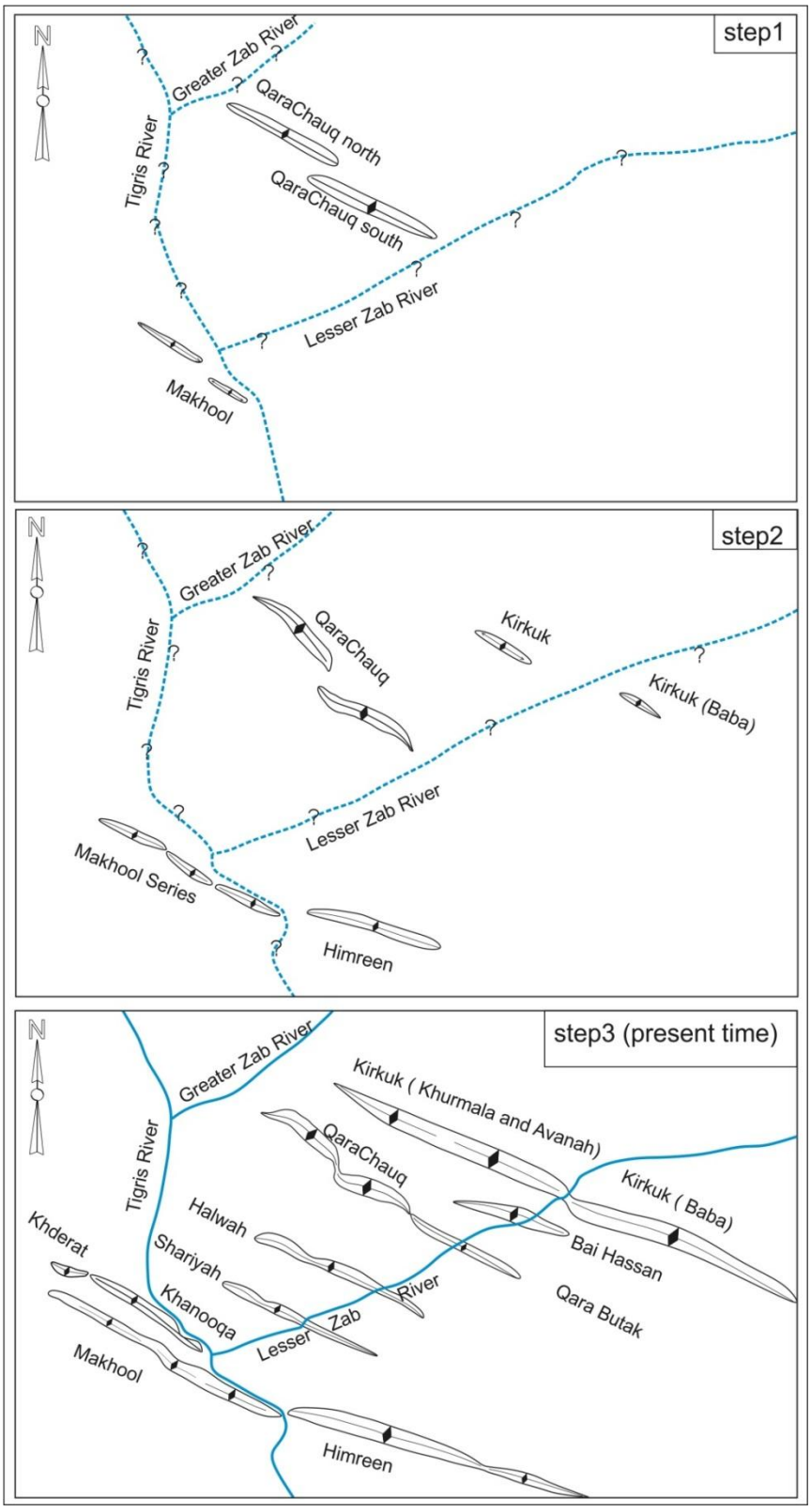

Fig. 3.13. Conceptual model of anticline growth in the Kirkuk Embayment

Further southwest of the Zagros belt, in the Baghdad Oil Field (central Iraq), seismic interpretation has demonstrated the presence of subsurface large scale block-faulted structures with lengths over 120 km and 20-30 km width. These are present from Baghdad (central Iraq), Balad, Samarra, and Tikrit towards the northwest **(**Aqrawi et al. 2010 and reference therein**)**. These structures were deformed by wrench faulting in Late Cretaceous (Cenomanian) and they have internal horst and graben and flower structures, as described by Kent (2010) for the Makhool/Khanooqa, Kirkuk/Bai Hassan, and Mansuriya structures. This Cretaceous deformation took place in the foreland to the present Zagros, i.e. the deformation front related to the continental collision has not reached as far southwest as the deformation related to the Cretaceous obduction of ophiolites onto the Arabian margin. In addition, Aqrawi et al. (2010) i.e. their Figs. 5 and 6, and Mohammed (2006) i.e. his Fig. 8, show that steeply dipping basement faults control the deformation of Paleozoic, Mesozoic, and Cenozoic sequences for the whole area of the northwestern Zagros. It is probable that differential rates of movement of these basement faults might control the uplift of anticlines towards the foreland, but the onset of late Cenozoic activity did not occur in sequence towards the foreland.

3.5.5 Balanced cross-section

I have used previously published data for the region in conjunction with my own analysis to construct a new cross-section across the Kirkuk Embayment (Fig. 3.14). Outcrop constraints, including dip and strike data, are extrapolated from fieldwork observations at the east of the Kirkuk Embayment, which will be reported in detail elsewhere. In particular, this section utilizes the detailed sub-surface data shown by Kent (2010) in a cross-section for the Mansuriya Anticline, which is located to the southeast of our study area, along strike from the Himreen Anticline (Fig. 3.1). Relevant aspects of the Mansuriya Anticline structure include: localized detachment within the Fat'ha Formation (consistent with the small-scale deformation features seen in field photographs in appendix 2; underlying thrust faults that penetrate below the Mesozoic section towards the basement (consistent with seismicity evidence for the Zagros, Nissen et al., 2011); stratigraphic evidence for Cretaceous extensional faulting and subsequent inversion; divergent thrust faults underlying fold crests and possible flower structure geometries.

I used the regional seismicity record as a further guide to the general structural style, without over-reliance on any single event. In particular, the nodal planes for the earthquakes in the Iraqi Zagros are relatively steep (>30^{o}), regardless of which is the real and which is the auxiliary plane; this observation is consistent across the great majority of *M* >5 earthquakes in the Zagros (Nissen et al., 2011). I depict the thrust faults on Figure 3.14 in keeping with this observation. If there is a low-angle detachment thrust beneath the Zagros, it is aseismic. Alternatively, no such thrust exists.

This section in essence repeats these structural styles across the Kirkuk Embayment anticlines (for which there are limited subsurface data), and furthermore incorporates the Halwah and Shariyah structures between the QaraChauq and Makhool/Himreen anticlines. These folds, albeit modest in size, occupy what would otherwise be a gap in the Embayment, and mean that the typical spacing between folds (and their underlying thrusts) is ~20 km (Fig. 3.14).

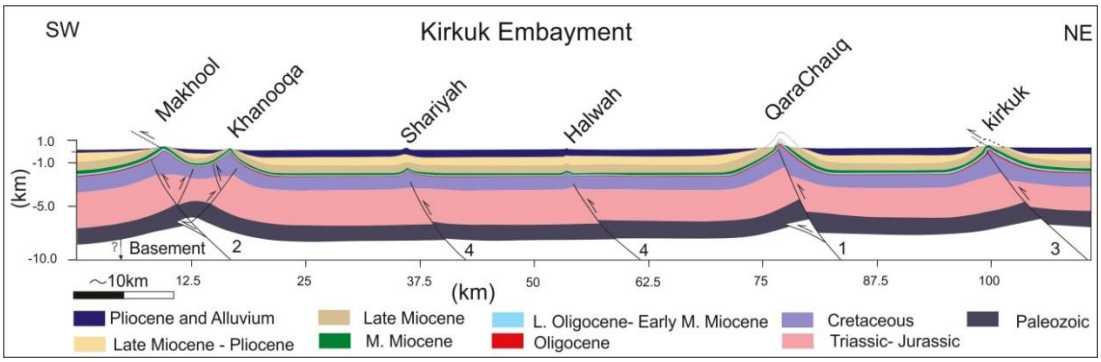

Fig. 3.14 Balanced cross-section of the Kirkuk Embayment developed using landscape maturity, unpublished surface data (Othman et al. 2004) and published subsurface data (Kent 2010), earthquake data (Fig. 3.1), and field observations from the eastern margin of the Kirkuk Embayment. This model shows the local detachment in the Fat'ha Formation and the involvement of basement faults in the deformation. Numbers refer to order of faulting: see text.

3.6 Discussion

Three possible hypotheses might be envisaged in relation to fold growth, based on the variation in SI values and other geomorphic indices (Figs. 3.4-6). First, it may be that the folds grew out of sequence (in the order of initiation: QaraChauq, Makhool, Himreen, Kirkuk, and finally Halwah and Shariyah), and at different times (Fig. 3.13). Second, the folds grew all at the same time, but with different rates of exhumation. Both of these scenarios mean that the progression of deformation was

not simply from the northeast to the southwest. Third, the folds grew in sequence towards the foreland, but with different rates of exhumation, to produce the observed variation in geomorphic indices. This seems the most complicated arrangement, and therefore the least likely. On the basis of all the above-discussed evidence, I conclude that the deformation in the Kirkuk Embayment does not follow simple foreland progression of deformation from the northeast to the southwest. Possibly, the arrangement and the apparent order of activity (Fig. 3.13) might be attributed to the activity of basement faults, available for reactivation during the late Cenozoic compressional deformation.

Koshnaw et al (2017) also interpreted out-of-sequence thrusting and fold growth in another area of the Iraqi Zagros, northeast of our study area, based on the different ages of syn-fold growth strata within the fold-and-thrust belt; their conclusion is entirely consistent with our independent observations of the same phenomenon, based on the landscape maturity indices. Where I differ from the interpretation of Koshnaw et al. (2017) is that I do not regard the later structures as the only ones to be basement-involved, but interpret all of the main thrusts to be thick-skinned.

Flower structures are present in the Mansuriya oil field (MOF) to the east of the Kirkuk Embayment (Fig. 3.1), and the Jebissa/Sinjar anticlines and Butmah/Ain Zalah anticlines to the northwest of the Kirkuk Embayment. These structures were interpreted as reactivated graben structures which is also a good interpretation for the occurrence of pairs of folds such as Kirkuk/Bai Hassan, and Makhool/Khanooqa (Kent 2010). It can be inferred that Halwah and Shariyah anticlines are other examples of flower structures in the region. The distributed strike-slip earthquakes across the Kirkuk Embayment (Fig. 3.1) are another suggestion of flower structure development across the region, i.e. many of the folds expressed at the surface as linear anticlinal ridges may have a strike-slip component, not obvious in the shallow geology. An implication of this result is that the strain partitioning of north-south Arabia-Eurasia plate convergence does not occur via a single strike-slip fault, as is the case further to the southeast (Talebian and Jackson, 2004), but is instead partly distributed across a family of structures within the Kirkuk Embayment.

The spacing between anticline crests is ~20 km (Fig. 3.14), identified through the discovery of the Halwah and Shariyah anticlines by analysis of the drainage patterns

and geomorphic indices. The length of many fold segments is similar (Fig. 3.2), although there are also long, linear sections of folds such as the Kirkuk Anticline where no such segmentation has yet been identified; see Koshnaw et al (2017), Figure 3.2. This 20 km figure is notable for being similar to the length and separation of Zagros fold segments identified to the southeast, in the Iranian sector of the range (Ramsey et al. 2008). Both the length and across-strike spacing of the folds (and inferred underlying faults) may relate to the distribution of pre-Cenozoic normal faults within the Arabian Plate, reactivated as thrusts by the Cenozoic collision (Ramsey et al. 2008).

The amount of late Cenozoic shortening across the new cross-section is relatively small, in the order of 5%, which is roughly 5 km across the 100 km section line (Fig. 3.14). It is consistent with the pattern of narrow anticlines, separated by wide regions of essentially undeformed strata and levels of exhumation typically no deeper than the Neogene. This result is therefore no surprise, but emphasizes the likelihood that strain is not evenly distributed across the Zagros, in the embayments and the adjacent regions to their northeast. In this respect, the pattern of deformation in the Kirkuk Embayment is similar to the Dezful Embayment to the southeast. It is very important to use high resolution seismic data to investigate the distribution of basement faults and to understand the deformation in the Cenozoic strata. This will serve the oil exploration and also help in understanding the structural evolution of the northwest Zagros.

3.7 Summary

The Kirkuk Embayment is located in the southwest of the Zagros fold-and-thrust belt of Iraq. Like fold-and-thrust belts worldwide, the Zagros is conventionally understood to have grown sequentially towards the foreland. I use landscape maturity analysis to understand anticline growth in the Embayment. Digital Elevation Model (DEM)-based geomorphic indices Hypsometric Index (HI), Surface Roughness (SR) and their combination Surface Index (SI) have been applied to quantify landscape maturity. The results inform new ideas for the sequence of anticline growth. Maturity indices are highest for the QaraChauq Anticline in the center of the Embayment, then Makhool/Himreen to the south and lastly, the Kirkuk Anticline to the north. The pattern suggests the growth sequence is not classical

‘piggy back’ thrusting. This result fits the exhumation record, which is loosely constrained by the stratigraphic exposure level. Favored hypotheses for fold growth order are either i) the folds have grown at different times and out of sequence (QaraChauq first, then Makhool/Himreen, and Kirkuk last), or, ii) the growth occurred with different rates of exhumation but at broadly the same time. There are few constraints from available data on syn-tectonic sedimentation patterns. Fold growth across much of the Embayment might have begun within a limited timeframe in the late Miocene–Pliocene, during the deposition of the Mukdadiyah Formation. Another hypothesis is that folds grew in sequence towards the foreland with different rates of exhumation, but I consider this less likely. I also construct a new cross-section for the Embayment, which indicates limited Cenozoic strain: ~5% shortening. Analysis of topography and drainage patterns shows two previously-undescribed anticlines with hydrocarbon trap potential, between the Makhool and QaraChauq anticlines.

4. Landscape memory and tectonic legacy: geomorphic expressions of the Himalayan fold-and-thrust belt

4.1 Introduction and geological setting

The purpose of this chapter is to use geomorphic indices and Hypsometric Index (HI) in particular, to provide insights into the active deformation pattern across the Himalayas, which has been the subject of a vigorous debate for several decades. The chapter builds on Chapter 2, where HI was analysed across the Zagros fold-and-thrust belt at the drainage basin scale, utilizing the approach applied by Gao et al (2016) to the Longmenshan region at the eastern side of the Tibetan Plateau. The main part of this chapter applies a similar analysis to the Himalayas, backed up by other geomorphic observations. The rationale is to examine the Earth surface response to subsurface deformation, governed by major fault activity, through variations in basin scale HI.

Due to continent-continent collision of India and Eurasia, the Himalayan fold-and-thrust belt and the Tibetan Plateau (Fig. 4.1) have been built up since the Eocene (Dupont-Nivet et al., 2010). The southward vergent structures of the Himalayas extend laterally over ~2500 km and comprise three geographic segments, which are from the west to east: Western Himalaya, Central Himalaya and Eastern Himalaya. The maximum elevation is >8000 m a.s.l., which decreases to the south where the Indo-Ganga plain is ~200 m above sea level and increases northwards to the Tibetan Plateau to ~5000 m above sea level. Three physiographic breaks have been identified (Hodges et al., 2001), labelled PT_1, PT_2 and PT_3 from north to south. Their relationship to the structures is described below. The main Himalayan faults get younger to the south, with differences in the time of activity. The South Tibetan Detachment (STD) was active in the Early-Middle Miocene (Searle and Godin, 2003), the Main Central Thrust (MCT) was active over a similar time interval (Elliott et al., 2016). The quality of exposure of the MCT in the east is not good as to the west because it crops out in cultivated and forested areas (Hodges, 2000; Searle and Godin, 2003). The outcrop pattern of the MCT is very sinuous (Fig. 4.2), which is a consequence of its low dip angle in regions of high relief (Yin, 2006).

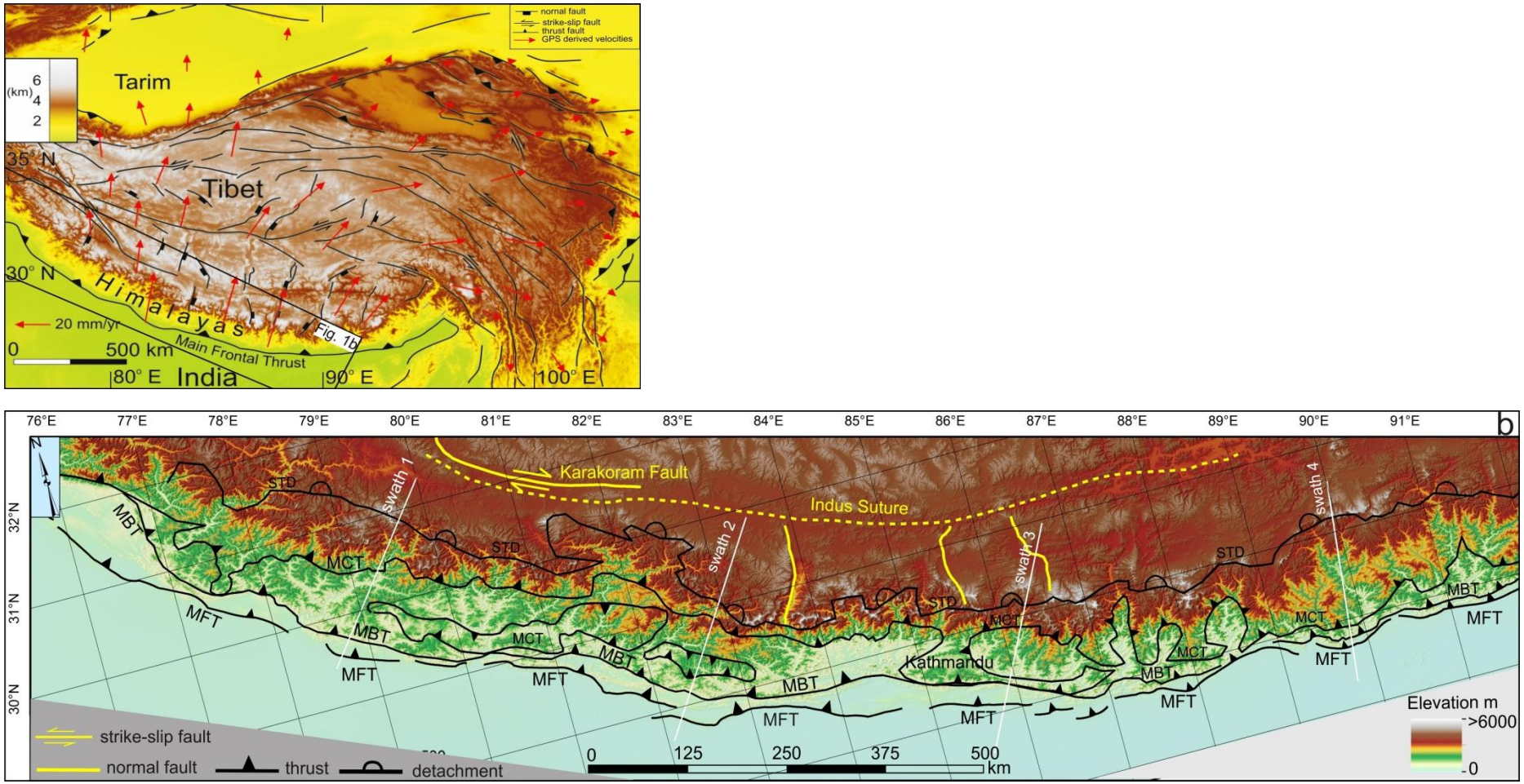

Fig. 4.1. Location map of the Himalayan orogen and Tibetan Plateau (after Allen et al., 2017), b) topographic map shows the main structures in the Himalayas (redrawn after Yin, 2006, and references therein). MFT = Main Frontal Thrust; MBT = Main Boundary Thrust; MCT = Main Central Thrust; STD = South Tibetan Detachment

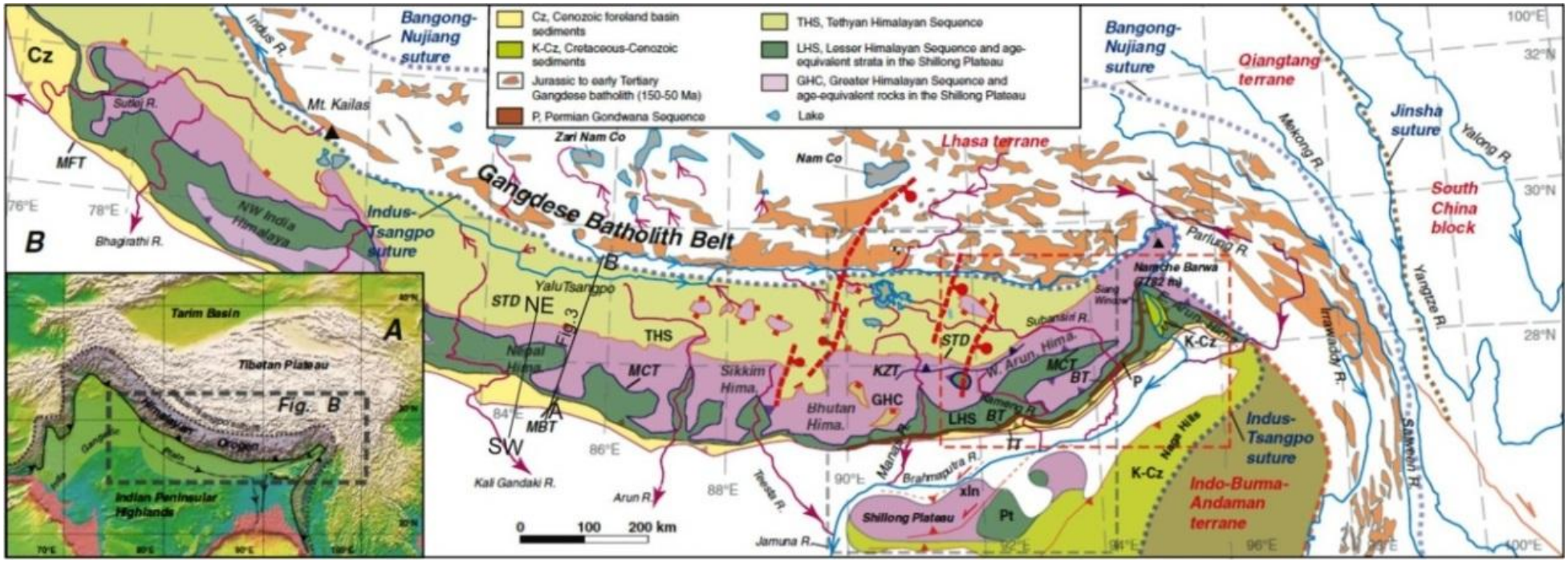

Fig. 4.2. A) Geographic location of the Himalayas and Tibetan Plateau. B) Regional geological map of the Himalayan orogen (after Yin, 2006). Abbreviations: MFT = Main Frontal Thrust; MBT = Main Boundary Thrust; MCT = Main Central Thrust; STD = South Tibetan Detachment; BT = Bome Thrust; TT = Tipi Thrust.

The Main Boundary Thrust (MBT) was initially active between 10-12 Myr Late Serravallian-Early Tortonian (Meigs et al., 1995), but the cessation of activity is uncertain (it is not active now). Lastly, and at the southern margin of the Himalayas, the Main Frontal Thrust (MFT) has been active since Plio-Pleistocene times (Lavé and Avouac, 2000). Actual exposure of the MFT is very rare, except where the thrust cuts alluvial fans and river terraces (Nakata, 1989).

These faults separate the main geological units of the Himalayas (Fig. 4.2) as follows from south to north: 1) the Main Frontal Thrust (MFT) separates the Indo-Gangetic plain from the northern Cenozoic foreland sequences; 2) the Main Boundary Thrust (MBT) is the boundary between the Cenozoic foreland strata and the Lesser Himalaya; 3) the Main Central Thrust (MCT) separates the Lesser Himalaya to the south from the Higher (Greater) Himalaya to the north, and, 4) the South Tibetan Detachment (STD) separates the northern Tethyan Himalayan Sequences from the Higher Himalaya. In terms of lithology, the Lesser Himalaya consists of schists, phyllites and related rock types, commonly at greenschist facies metamorphism. These contrast with resistant gneisses of the High Himalaya. The Tethyan Himalayan Sequences are deformed but not metamorphosed. Other structural units of the northern Indian Plate, exposed to the north of the STD, are not considered in this chapter.

Physiographic transition PT_1 roughly correlates with the position of the STD, on the northern side of the Himalayas, and is the change, from south to north, from mountainous Himalayan topography to the plains of the Tibetan Plateau. PT_3 is equivalent to the position of the MFT, at the south side of the range, and so represents the southernmost structure of the Himalayas. PT_2 is somewhat more enigmatic, lying within the range, typically 10-20 km to the south of the trace of the MCT (Hodges et al., 2001).

Although the Himalayan structure is remarkably consistent along the ~2000 km length of the range, there are variations in the relative positions of the main faults and the structural units they juxtapose. The main trace of the MCT lies much closer to the front of the range east of ~ 84.5^{o} E than it is in the west (Fig. 2). Regions west of ~84.5^{o} E include large klippen of the MCT and the High Himalaya rocks above it.

Bollinger et al. (2006) and Lavé and Avouac (2000) suggested that all the main faults are connected to the Main Himalaya basement Thrust (MHT) which acts as an active detachment thrust, above which nappes of the Indian Plate are stacked southwards towards the continental interior (Fig. 4.3). Thus the MFT and MHT are not really separate structures, but the MFT is the term used for the emergent thrust front at the south side of the Himalayas, while the MHT is used to identify the range-scale underlying thrust.

The ongoing collision of India with the Eurasian Plate causes very active tectonics in the Himalayas (Lavé and Avouac, 2001) with horizontal shortening in the range of 15-20 mm/yr and up to several mm/yr of surface uplift (Bilham et al., 1997; Hurtrez et al., 1999; Lavé and Avouac, 2000, 2001; Bettinelli et al., 2006; Bollinger et al., 2006; Blythe et al., 2007; Stevens and Avouac, 2015). Lavé and Avouac (2001) showed that Holocene convergence across the MFT is ~20 mm/yr, i.e. close to the total geodetic strain rate across the entire Himalayas.

Recent seismic, geodetic and geomorphic studies suggest alternative structural models of active Himalayan tectonics. These are: 1) deformation focussed on an underlying thrust, the MHT (Stevens and Avouac, 2015; Elliot et al., 2016), possibly with a mid-crustal ramp; 2) as for #1, but with additional, out-of-sequence deformation on an active fault near the location of the MCT/PT_2 (Wobus et al., 2003; 2005; 2006; Whipple et al., 2016); and 3) a combination of underplating underneath the Higher Himalaya and slip on a duplex of thrust slices (Morell et al., 2017). Models 2) and 3) are similar, in that they propose active out-of-sequence deformation at high crustal levels in the vicinity of the MCT/PT_2. In model #1, rapid uplift and high values for geomorphic indices (e.g. k_{sn}) north of PT_2 are interpreted to result from passive uplift across a ramp in the underlying MHT.

The basis for models 2) and 3) are combinations of geomorphic and geochronological/thermochronological data, which have been used to interpret active internal deformation in the region of the MCT/PT_2. Seeber and Gornitz (1983) produced one of the pioneering works in this respect; they reported a zone of high river gradients, consistent with the location of the MCT between the Lesser and Higher Himalaya. The interpretation of this hypothesis is that the MCT is a major

and active tectonic boundary, which controls the topography and consequently controls change in river profile gradients.

More recent work has refined the Seeber and Gornitz (1983) study, utilising k_{sn} analysis (e.g. Morell et al., 2017; Cannon et al., 2018). These works show that k_{sn} increases in general further north and at higher elevations in the Himalayas, interpreted to mean active deformation and uplift across PT_2, rather than the original, Miocene, MCT structure. Geomorphic results have been reinforced by exhumation data from a variety of techniques and over different timescales, including cosmogenic exposure ages (Wobus et al., 2005), detrital $^{40}Ar/^{39}Ar$ thermochronology (Wobus et al., 2003, 2006) and apatite fission track analyses (Thiede et al., 2004). These studies and others confirm faster exhumation rates north of PT_2 than to its south, and like the geomorphic studies, have been used to interpret active deformation across the foot of the Higher Himalaya.

There are other explanations possible for these results, including passive uplift above a mid-crustal ramp in the MHT (Lavé and Avouac, 2001; Godard et al., 2014). These studies note that there has been very little evidence produced in support of an active structure along or close to PT_2, which is defined solely on grounds of an abrupt increase in elevation and gradient (Hodges et al., 2001). Data from the 2015 Gorkha earthquake have not resolved the issue. Elliott et al (2016) modelled the geodetic expression of the earthquake using the mid-crustal ramp (Fig. 4.3), but Whipple et al (2016) modelled the same data without a ramp, and argued that if the ramp is not present, internal out-of-sequence deformation of the Higher Himalayas must be required to explain high exhumation rates and the geomorphic signatures of the region.

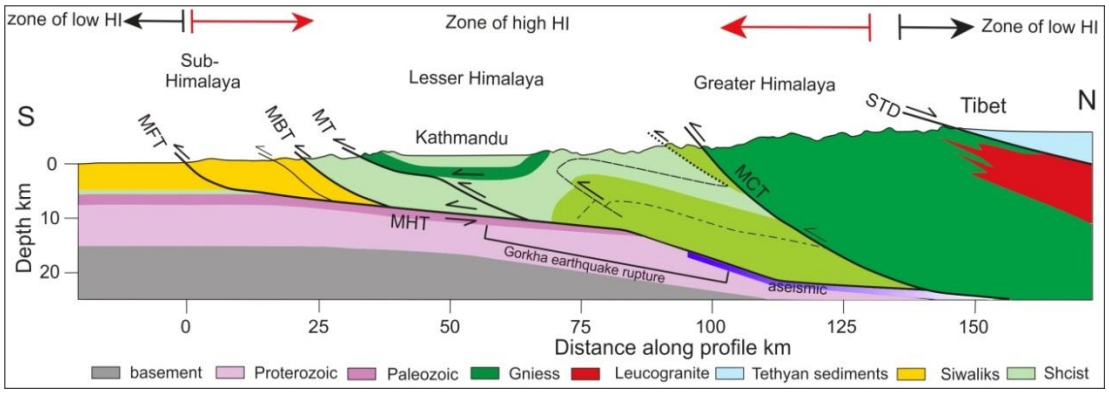

Fig. 4.3. Geological cross-section of the Himalaya oriented S-N across the Kathmandu (modified after Lavé and Avouac, 2001; Elliot et al., 2016) shows the zone of high HI (see later) which correlates with the seismicity of the MHT during and after the 2015 earthquake. The sharp boundary of the low/high HI transition in consistent with the emergent MFT and the correlation between the high HI and the seismicity possibly refer to the MFT controls on the topography of the Himalaya. Abbreviations: MFT = Main Frontal Thrust; MBT = Main Boundary Thrust; MT = Munsiari Thrust; MCT = Main Central Thrust; STD = South Tibetan Detachment; MHT = Main Himalayan Thrust.

4.2 Data and methods

The SRTM 30 m resolution dataset (http://www2.jpl.nasa.gov/srtm/) was used, and processed using ArcGIS 10.3.1 and MATLAB-based TecDEM software for the purpose of extracting hypsometric index values (HI) for the third order river basins. More details of the methods and data are described in Chapter 2.

Basin scale HI analysis has been conducted for the main tectonic units of the Himalayas, namely the southern side of the Tibetan Plateau, the Greater Himalaya, the Lesser Himalaya, Sub-Himalaya and the Indo-Gangetic foreland.

The basin scale HI shapefiles were converted into raster mode using the polygon-to-raster function within the ArcGIS 10.3.1. This process allows a swath profile analysis of the raster HI data. Four selected swath profiles in a width of 100 km and length of 300 km across strike of the western, central and eastern Himalayas were analysed to show the HI value distribution across strike of the Himalayas.

The normalized steepness index k_{sn} analysis has been performed by Cannon et al. (2018) for the whole Himalayan range; therefore, 23 main rivers were selected randomly and analysed for comparison using the stream profiler MATLAB-based software (Wobus et al., 2006). John Cannon kindly provided the data files for his k_{sn} analysis for comparison with this study. Climatic data are taken from the TRMM-

based datasets of Bookhagen and Burbank (2006). Victoria Stevens kindly provided the data files for her uplift results, derived from the geodetic patterns of interseismic strain (Stevens and Avouac, 2015). These data enable the geomorphic analysis of this study to be compared to an orogen-wide picture of climate, and active surface uplift.

4.3 Results

Fig. 4.4 shows changes in the HI value across the Himalayan range, with enlargements for the western Himalayas, central Himalayas and eastern Himalayas respectively.

On the broadest scale, the Himalayas show low values of HI (<0.3) across the Tibetan Plateau and Indo-Gangetic Plain and high HI (>0.3) across intervening areas of high relief and highest elevation (Fig. 4.4). HI values rise up (>0.3) sharply northward from the foreland across the trace of the MFT, and continue to rise until the trace of the STD, at which point they decline towards the Tibetan Plateau interior, where the HI has similar values to the Gangetic foreland (< 0.2).

Within the broad zone of high HI values there are small areas of lower HI values, at least some of which, including Kathmandu (at ~ 85.3^{o} E), represent intermontane basins which have low relief. The trace of the MCT does not correspond to a consistent signal in the data. It roughly coincides with HI ≥0.3 where the MCT is very close to the MFT in eastern Nepal (east of ~ 84.5^{o} E). In contrast, western Nepal shows high HI values in the footwall of the MCT, which in turn is the hanging wall of the MFT (Fig. 4.4).

Using the threshold of HI = 0.35 for both HI vector data (Figs. 4.4a, 4.4a1, 4.4a2 and 4.4a3) and HI raster data (Fig. 4.4b), the physiographic boundary PT_2 can be traced laterally.

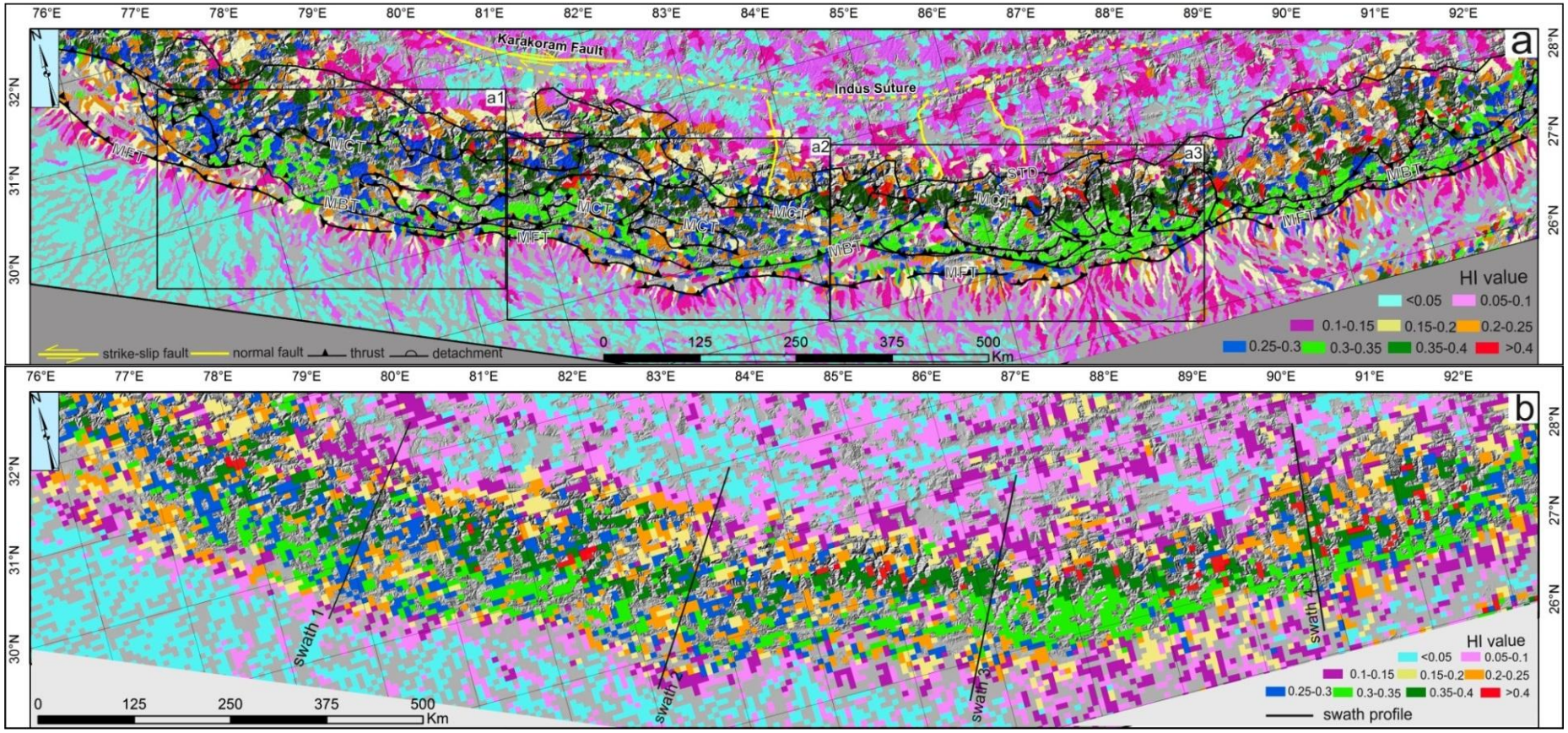

Fig. 4.4. a) Distribution of HI value for the 3rd order drainage basins of the Himalayas shows a sharp boundary between higher and lower HI values along the Mountain Front Thrust (MFT). b) HI raster map shows the location of swath profiles in Fig. 4.6. Note the overall high HI values within the Himalayas, bounded by the MFT from the south and the South Tibetan Detachment (STD) from the north.

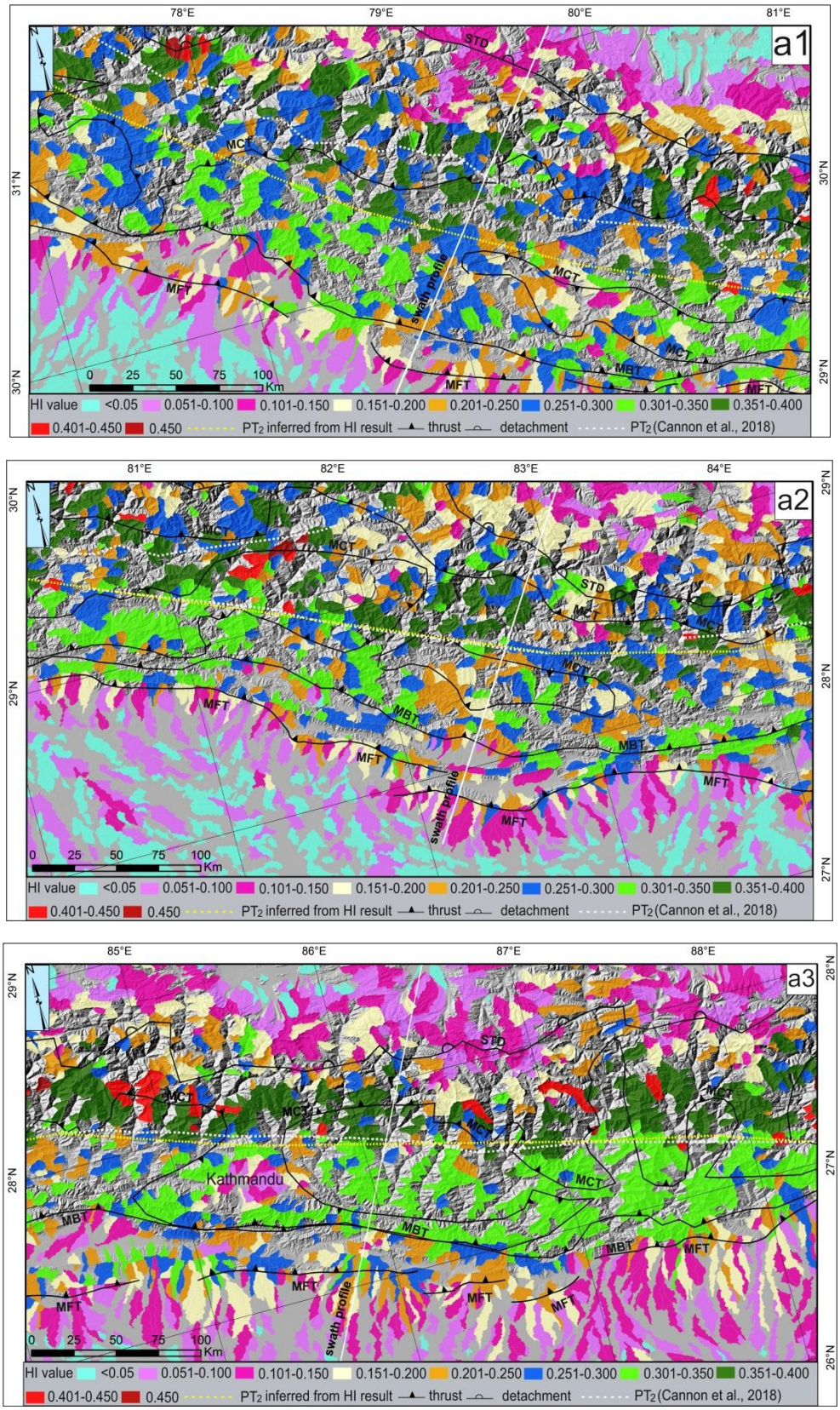

Fig. 4.4a1, a2 and a3. Enlarged figures from Fig. 4.4a show distribution of HI value for the 3rd order drainage basins of the Himalayas. Note the approximate similarity and difference between the PT2 inferred from HI result and the on proposed by Cannon et al 2018.

The normalized steepness k_{sn} from the current study shows similar values and patterns to the k_{sn} results of Cannon et al., (2018). Also, k_{sn} results show a correlation with the location of PT_2 for long regions of the range (Fig. 4.5), which is not surprising: k_{sn} has been used to pick out the location of PT_2 in several studies (e.g Harvey et al., 2015; Morell et al., 2017; Cannon et al., 2018). The MFT and STD do not show up in either this study of k_{sn}, or the Cannon et al (2018) study. There is a small shift in the western Himalayas between the PT_2 trace inferred from the HI >0.35 threshold, and the trace of PT_2 suggested by Cannon et al. (2018) (Fig. 4.4a1)

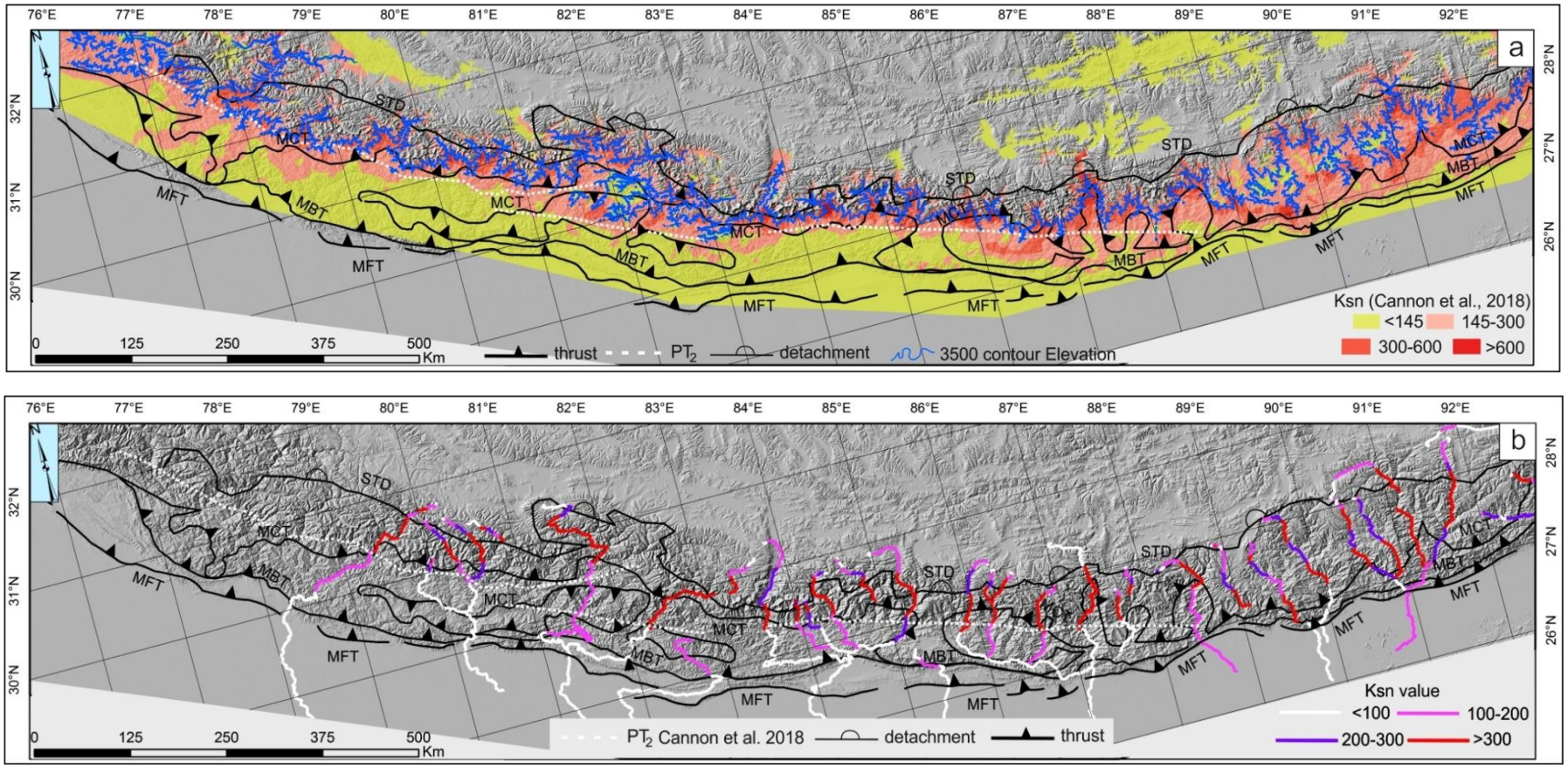

Fig. 4.5. Distribution of k_{sn} values from a) Cannon et al., 2018 and b) current study shows the similarity between the two studies in regard to the PT_2. In both maps, the white dashed line is the PT_2 digitized from Cannon et al (2018).

A swath analysis for the HI values across the strike of the Himalayas shows similar behaviour for each of the swaths (Fig. 4.6). Elevation derived from the same SRTM data is shown alongside each swath profile. A first rising step in each profile refers to the trace of the MFT. PT_2 is harder to pick out in each profile. A sharp decline in HI value can be seen from the Higher Himalaya towards the Tibetan Plateau for all HI swath profiles. This decline is roughly coincident with the location of the STD within each profile (Fig. 4.4). In all the profiles HI values reach their maximum south of the highest mean or absolute elevations. Swath 4 (easternmost profile) is somewhat different to the other three, in that the elevation profiles are less concave-up, and the highest HI values are more to the south of the maximum elevation values.

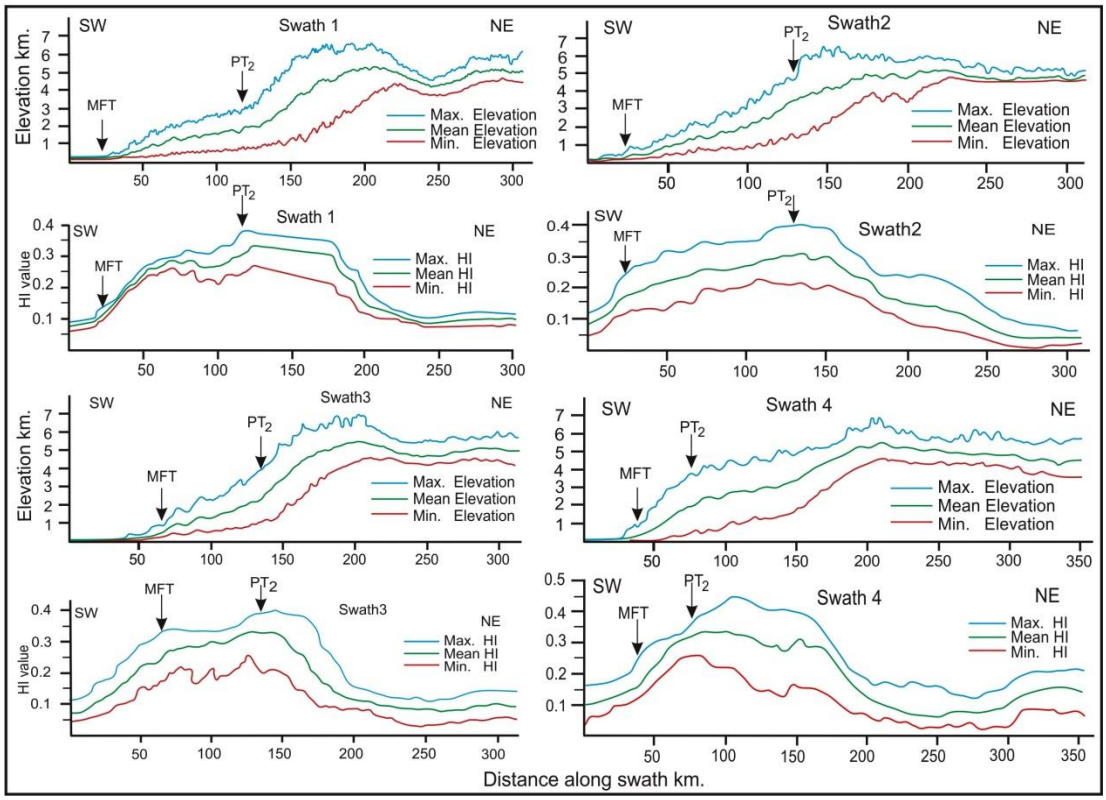

Fig. 4.6. HI and elevation graphs for the swaths in Fig. 4.4b across the Himalayan range show the variation in the HI value with respect to the location of PT_2 and the MFT.

4.4 Discussion

The Himalayan HI data show that the MFT sharply separates areas with higher HI north of the fault and lower HI south of the fault (Fig. 4.4), which is different to the case in the Zagros (Chapter Two). The Zagros displays gradual change in the value of HI along short segments of numerous, blind, thrust faults but not abrupt change across the strike of major, emergent, faults in the style of the Himalayas. Therefore

the first order differences in HI distribution are consistent with the different tectonics of each range.

Within the Himalayas, a comparison between the bedrock geology (Fig. 4.2) and the HI values (Fig. 4.4) shows that lithological differences have no precise correlation with changes in HI value. There is a suggestion of different patterns of HI in eastern and western parts of the range, with the changeover at roughly 84.5^{o} E. East of this longitude, the HI seems more consistent, and high (>0.3) values occur close to the MFT. The locations of the main thrust traces are notably condensed in this part of the Himalayas. West of 84.5^{o} E, there is greater dispersion in the HI values, and they are not concentrated in such well-ordered bands, increasing in value northwards. In this part of the Himalayas the structure involves klippen of the MCT and Higher Himalayan rocks sitting over the Lesser Himalaya, and a greater distance (commonly ~ 100 km) between the main trace of the MCT and the MFT.

From the climatic aspect, the mountain range represents high and intermediate precipitation areas. The Tibetan Plateau is a zone of very low precipitation while the Ganges plain represents an intermediate to low precipitation area (Bookhagen and Burbank, 2006). So, there are two different areas bordering the Himalayas with different lithologies and tectonic settings (i.e. Tibetan Plateau and Ganges Plain), and different climate, which both have low HI values (Fig. 4.4). The rainfall map (Bookhagen and Burbank, 2006) shows the eastern Himalayas is wetter than the western Himalayas (Fig. 4.7), and that there are two parallel bands of high rainfall along much of the Himalayas, which merge in the east and in the west.

High HI values are distributed across the Lesser and the Higher Himalayas, but highest k_{sn} values occur in the Higher Himalaya, and have been used to define the location of PT_2 (e.g. Morell et al., 2017; Cannon et al., 2018). This could mean a relationship between wet climate and high k_{sn} values and hence the origin and location of PT_2 (Wobus et al., 2003). But, the more widespread occurrence of high HI values in areas of different climatic conditions implies that the climatic variations have no overall control on the changes in the HI values. Even the rainfall/k_{sn} relationship is only moderately robust (Cannon et al., 2018).

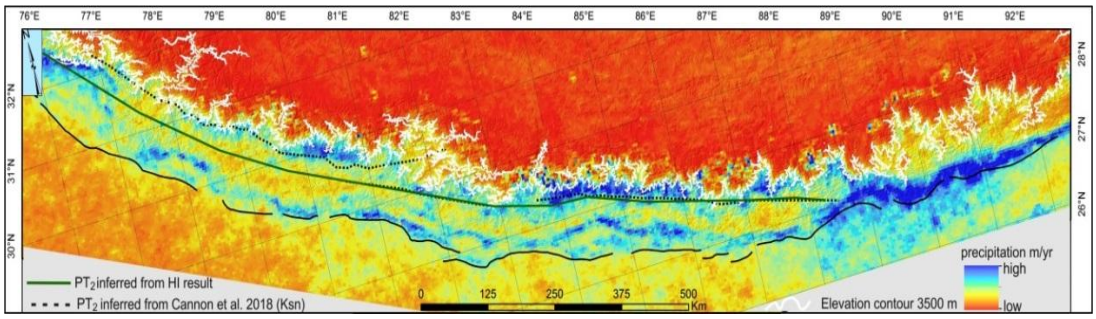

Fig. 4.7. TRMM precipitation map for the period from 1998-2005 (after Bookhagen and Burbank, 2006) shows the wetter climate of the eastern Himalayas and Lesser Himalayas.

The HI results of this study can be compared with geodetic and seismicity data (Ader et al., 2012; Elliot et al., 2016), and estimates for the Holocene strain across the MFT based on deformed river terraces (Lavé and Avouac, 2001). The geodetic, seismicity and Holocene deformation data suggest that the MFT is the only active, emergent thrust across the Himalaya, and that the MHT controls the overall topography of the range. This can be compared to the marked rise in HI across the trace of the MFT (Figs. 4.4 and 4.6).

The HI analysis is relevant to the debate about the physiographic transition from the Lesser to Higher Himalaya (Seeber and Gornitz; 1983; Hodges et al., 2001; Wobus et al., 2003, 2006; Kirby and Whipple, 2012; Whipple et al., 2016). To recap, these papers and others suggest active out-of-sequence deformation in the vicinity of PT_2, using the existence of PT_2 as evidence, alongside data for more rapid exhumation to its north. Kirby et al. (2012) suggested that the most likely structure is an out-of-sequence duplex (Fig. 4.8) beneath the rising Higher Himalaya in the vicinity of the MCT.

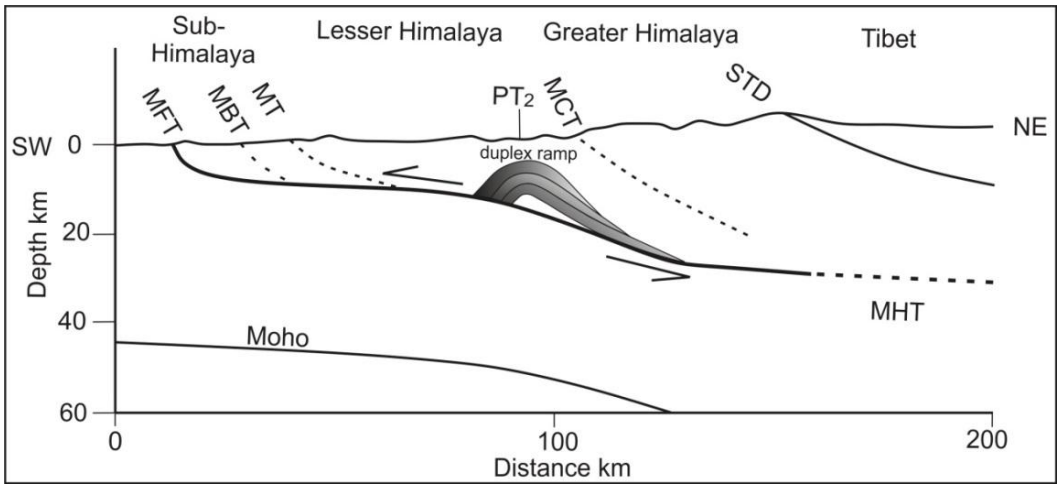

Fig. 4.8. Conceptual model of the Himalayan tectonics, invoking a sub-surface duplex model to explain the physiographic and exhumation patterns seen in the region of PT_2 (after Wobus et al., 2003; Kirby et al., 2012).

The distribution of high (> 0.3) HI values partly correlates with PT_2 and the locus of the duplex suggested by Wobus et al. (2006), but is also distributed across both the footwall and the hangingwall of the MCT and extends south as far as the MFT trace, especially west of 84.5^{o} E (Fig. 4.4). Therefore the HI data provide partial support for the existence of PT_2, but do not prove it is a zone of active shortening, either by a sub-surface duplex (Fig. 4.8) or an emergent fault.

It has been suggested that rapid exhumation and uplift in the vicinity of PT_2 relates to behaviour of the underlying MHT, either on a ramp (Elliott et al., 2016) (Fig. 4.3), and/or at the transition from coupled to uncoupled (locked to creeping) behaviour on this thrust (Stevens and Avouac, 2015) (Figs 4.9 and 4.10). The locations of MHT decoupling, rapid exhumation, rapid surface uplift, high k_{sn}, high HI (> 0.35) and PT_2 are all coincident to a first order (Figs. 4.4, 4.5, 4.9 and 4.10).

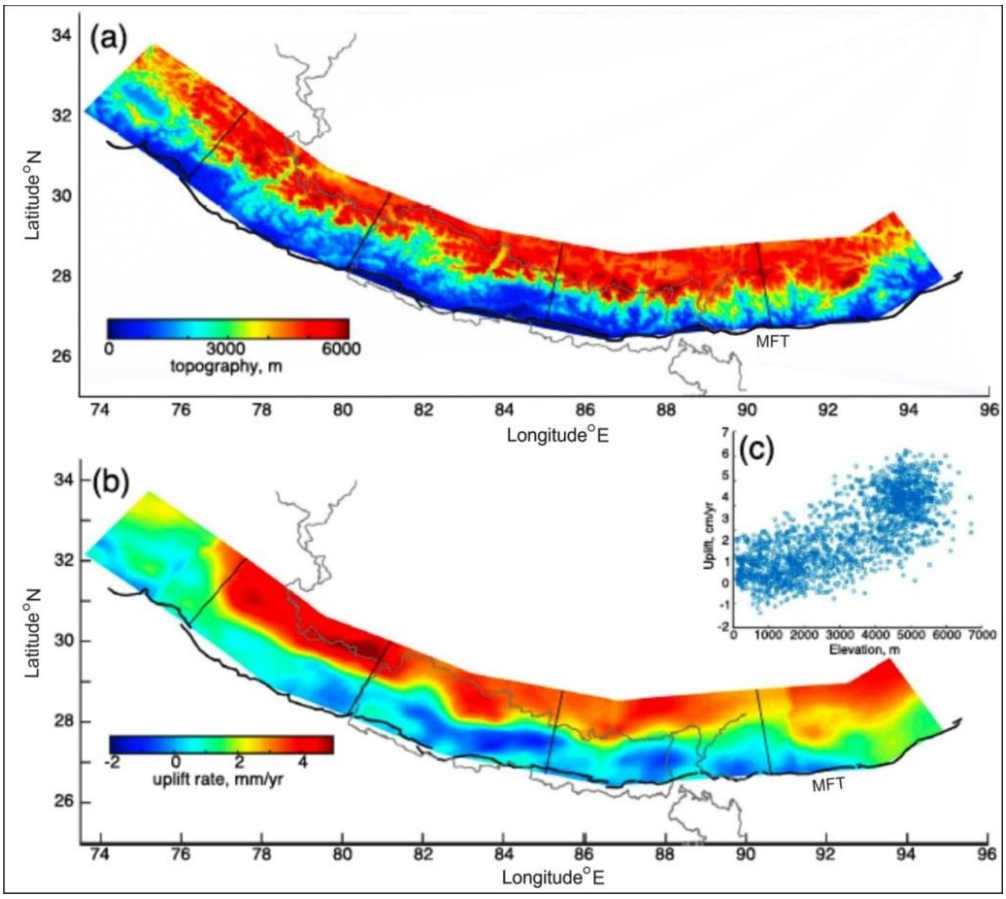

Fig. 4.9. Comparison between topography (a) and rate of uplift (b) of the Himalaya and their correlation (Stevens and Avouac, 2015).

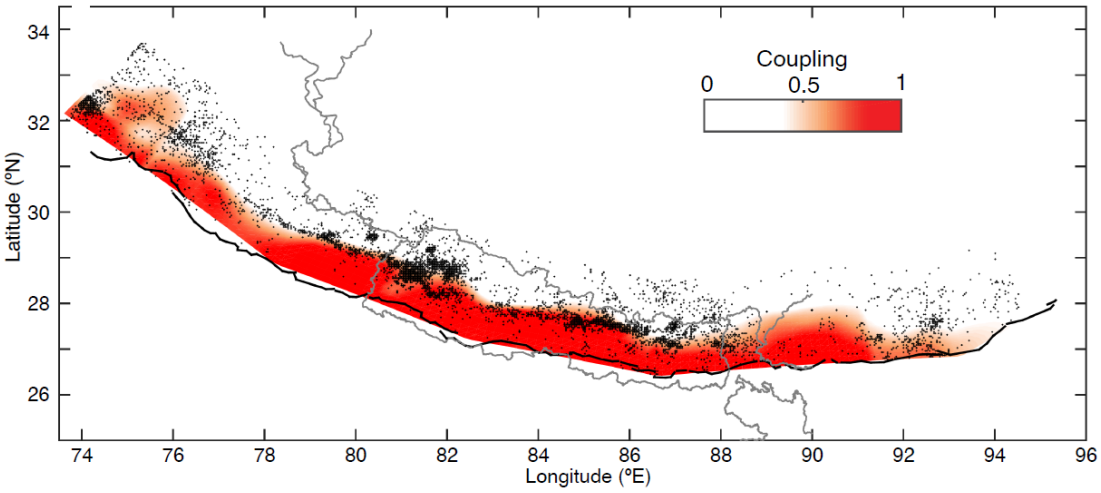

Fig. 4.10. Coupling model of the MHT (Stevens and Avouac, 2015).

Regions in the north with low degrees of coupling (i.e. creeping behavior) correspond to more surface uplift, with a sharp transition into the high uplift zone corresponding to the relatively abrupt change from coupled to non-coupled behavior.

This transition zone is consistent with the onset of high topography (i.e. the regional 3500 contour of elevation).

The HI data do indicate a difference in the geomorphology of the western and eastern Himalayas, with the transition at about 84.5^{o} E. The east-west difference in HI might relate to climate, as the eastern Himalayas are wetter than the west (Bookhagen and Burbank, 2006; Fig. 4.7). There are other possibilities to explain this east-west difference in HI values and patterns. The bedrock geology of the range differs along strike, with crystalline basement of the Higher Himalaya located closer to the MFT in the east than the west (Fig. 4.2), in a continuous nappe rather than an isolated klippe. This might promote the more continuous bands of HI in the east compared with the variable values of HI in the west (Fig. 4.4). Alternatively, the western Himalayas is a region of strain partitioning (Murphy et al., 2014), with overall convergence achieved by a combination of Himalayan thrusting and strike-slip on the Karakoram Fault at its continuation in western Nepal. It is not clear why this particular difference in tectonics should cause the variation in HI, however. It may be lower convergence rates across the MFT in the west than the east (Ader et al., 2012) translate into lower HI values in the landscape, but this is unproven.

It is notable that the modern landscape of the northern side of the Himalayas, and the sharp northwards drop in HI (Figs. 4.4 and 4.6) seems to reflect the time when the STD was last active in the Miocene. In the Early Miocene the combined effect of the MCT and STD rapidly exhumed the High Himalayan crystalline basement at rates up to 10 mm/yr (White et al., 2002). In this example, the modern landscape seems to record a tectonic signal from >10 Myr ago, possibly helped by the relatively low rainfall on the northern side of the range.

It is worth considering why k_{sn} analysis does not pick out either activity of the MFT, or the presence of the STD in the landscape. This might be due to the limitation of the stream profile analysis in areas of transport limited rivers or areas of low relief. Because slopes are low in the region of the MFT, at the tip of the Himalayan wedge, it is not picked out by k_{sn} analysis. Highest k_{sn} occurs at elevations of ~ 3500 m (Fig. 4.5), which is roughly the boundary of the Tibetan Plateau in all of its margins, not just the southern, Himalayan front (Saville, 2012). Rivers have high convexity at this elevation so that the k_{sn} is high. Expressed another way, rivers draining the Tibetan

Plateau and flowing across the Himalayas have considerable lengths before they reach high gradient sections at 3500 m elevation, corresponding to the edge of the plateau. These issues with k_{sn} analysis suggest that the HI analysis is more representative and useful than k_{sn} to express the topographic response to tectonics in areas of different elevations and relief patterns.

4.5 Summary

In this study SRTM 30 m datasets were used to extract basin scale value (HI) for the 3rd order river basins of Himalayan range and southern Tibetan Plateau using ArcGIS 10.3.1 and MATLAB-based TecDEM software. Results show sharp boundary of the high/low HI transition along the trace of the MFT. North of this boundary the area has high values of HI (>0.3) including the zones of the mapped MBT and the MCT, which means that the MHT and MFT has the major control on the topography of the Himalayas.

There is debate in Himalayan tectonics over the style of deformation and distribution of strain across the fold-and-thrust belt. This debate has implications for the operation of fold-and-thrust belts in general. One model proposes that deformation is localized along the Main Himalayan Thrust (MHT), underlying the entire range and becoming emergent at the Main Frontal Thrust (MFT). In part this model is based on the similarity between overall geodetic rates for shortening across the Himalayas and Holocene slip rates along the MFT (both ~ 20 mm/yr) (Lavé and Avouac, 2001). An alternative model focusses on the significance of a physiographic boundary known as PT_2, which occurs south of the Main Central Thrust (MCT), which itself separates the Lesser Himalayan and Higher Himalayan zones. k_{sn} values have previously been shown to be higher north of this line, reflecting steeper profiles and more rapid uplift (Kirby and Whipple, 2012). Published geochronological data also indicate that more rapid exhumation takes place to its north (Wobus et al., 2006). This evidence has been used to propose that PT_2 marks the position of an active, out-of-sequence thrust in the Himalayas, which is distinct from the underlying MHT. This study shows that the biggest changes in HI occur at the northern side of the Himalayas (roughly coincident with the location of the South Tibetan Detachment, STD) and the MFT. There is an increase in HI across PT_2, but of smaller magnitude. Therefore there is limited evidence from HI distributions for active tectonics along PT_2 or the MCT.

The difference between results of k_{sn} and HI analyses comes from their different sensitivities: k_{sn} is dependent on slope and is sensitive to relative uplift rates, but these may be climatically and/or lithologically controlled, and do not necessarily mean active shortening across an area. Also, many of the Higher Himalayan rivers rise in southern Tibet, and flow southwards past the highest peaks in the range, so that they have long reaches at the locations where they achieve steepest gradients. This configuration leads to high k_{sn} values. The sharp change in HI values across the MFT is consistent with slip along the MHT raising the entire crustal wedge above it. This HI analysis does not conclusively resolve the debate about the style of Himalayan tectonics, but offers no strong support for the out-of-sequence model.

A pronounced drop in HI on the northern side of the Himalayas seems to be a legacy of the Miocene tectonic regime and activity on the STD, showing that landscape can have a clear "memory" of tectonics on timescales >10 Myr. HI results show effectively the MHT activity, and how it controls the topography of the Himalayas in terms of the consistency between the high HI zone and the slip of the MHT.

5. River sand petrology of the Zagros Suture Zone and the Late Miocene formations northern Iraq

5.1 Introduction

This chapter presents a study of the petrology of samples of modern river sediment and Cenozoic sandstones, mainly from the Lesser Zab and Diyala drainage basins, northern Iraq (Fig. 5.1). The work is effectively a reconnaissance study, based on a short fieldtrip and sample collection completed by the author. The aim of the work is to begin to set up a dataset for the petrology of the sedimentary rocks and modern rivers of the Iraqi sector of the Zagros fold-and-thrust belt, which have received little attention in the international literature. Through such a database, it is hoped that it will be possible to reconstruct changes in the provenance of sedimentary suites from different areas, and relate these shifts to changes in tectonics and drainage routes through the Zagros.

Some samples from the fieldwork were analysed and used in the regional study by Garzanti et al. (2016). The samples were analysed by conventional petrographic techniques, and the results have been used to validate analyses conducted for this thesis. Additionally, the regional study by Garzanti et al (2016) provides a context for this study, in that it has shown the variation in petrology within the Tigris drainage basin, part of which is analysed in this study.

The Zagros foreland (Fig. 5.1) is the result of the Late Cretaceous ophiolite obduction (Alavi, 2004; Okay, 2010), closure of the Neo-Tethys Ocean and the Cenozoic collision of the Arabia-Eurasia (Alavi 2007; Blanc et al. 2003; Ghasemi and Talbot 2006; McQuarrie 2004; Vera and Gines 2009). Within the width of this tectonic domain ≤ 1000 km (Yılmaz et al., 1998; Allen et al., 2013) a series of sedimentary, volcanic and ophiolite rocks are exposed with rare crystalline basement and high-pressure metamorphic rock (Şengör et al., 2003).

Studies of the modern interactions of sedimentation and tectonics in the Zagros are relatively rare. Sedimentation and tectonism north of the Zagros fold-and-thrust belt has been studied by Jones et al. (2014) in order to address whether the sedimentary signature of the Late Pleistocene-Holocene alluvial fans of the Kohrud Mountain belt in the central Iran is controlled by tectonism, or if the fans are climatically

controlled. The outcomes of Jones et al. (2014) study show the fans sequences are mostly affected by climatic variations although the tectonism can motivate fan growth. Zhang et al. (2017) conducted provenance analysis in the Lurestan province, southwest of the Zagros using U-Pb and Hf isotope analyses of detrital zircon from a Cenozoic sedimentary sequence. The Zhang et al (2017) study suggested that Late Miocene strata were sourced from Eurasia only and there was no involvement from Arabia; while the Early Pliocene strata originated from Arabia and Eurasia suggesting the commencement of collision in the Late Miocene. Another recent study conducted by Koshnaw et al. (2017) utilised sandstone petrography, conglomerate composition and geochronological analysis for strata close to two major faults (Kirkuk Fault and Main Frontal Fault) and two small scale faults (Qamar and Shakal), in addition to Neogene sandstones. Results from Zhang et al. (2017) and Koshnaw et al. (2017) are in agreement in relation to the source of the Late Miocene-Pliocene formation being partly Arabia; while there is disagreement about the source of the Late Miocene formation of the Injana (Aghajari) Formation. This study focusses on modern river sands and the Late Miocene-Pliocene sandstone petrology, to shed light on similarities and differences of sediment source and their tectonic implications.

The Zagros Suture Zone (ZSZ) comprises the result of a complex geodynamic evolution of the northern Arabia and southern Tethyan margin, which is debated due to the lack of detailed studies and data (Jassim and Goff, 2006; Sissakian, 2013). This zone crops out along the Iraq-Turkey-Iran border and comprises three tectonic subzones from the southwest to the northeast: the Qulqula-Khwakurk, the Penjween-Walash, and the Shalair subzone (Sanandaj-Sirjan). The subduction of Arabia beneath Eurasia, followed by ophiolite obduction and lastly the Oligo-Miocene-Recent collision of Arabia-Eurasia controlled the Mesozoic-Cenozoic stratigraphy of this region of the Zagros. The exposed geology consists of autochthonous and allochthonous units (Figs. 5.1 and 5.2), which are describe briefly as follows, to give context for the petrography data and analysis. The account is taken largely from Jassim and Goff (2006) and Sissakian (2013).

5.1.1 The Balambo-Tanjero Zone and Qulqula-Khwakurk Zone Sequences

The marine and continental Suwais Red Beds (Late Maastrichtian-Paleogene) belong to both the Balambo-Tanjero and Qulqula-Khwakurk tectonic subzones (Figs. 5.2 and 5.3) and is composed of four units, Suwais-1 to Suwais-4. The Suwais Group passes laterally into the Naopurdan Group of the Penjween-Walash Zone, which corresponds with it in age. It is composed of flysch and molasse clastics, alternating with limestone. Probably due to thrusting by the Naopurdan Group, the Suwais Group crops out in a narrow zone along the base of the Qandil range with a thickness of ~1000 m. The basal conglomerate of Suwais-1 overlies the Aqra Limestone, while the upper part of Suwais-4 underlies unconformably (angular unconformity) the Govenda Limestone. The Govenda Limestone is composed of ~110 m of polygenic basal conglomerates, pebbly sandstone, siltstone, detrital limestone and major constituents of reef and fore-reef limestone. The remainder of the Red Beds is the intermontane molasse of Mirga-1, which comprises calcareous silty shale interbedded with sandstone, and Mirga-2, which consists of massive conglomerates of igneous and metamorphic clasts.

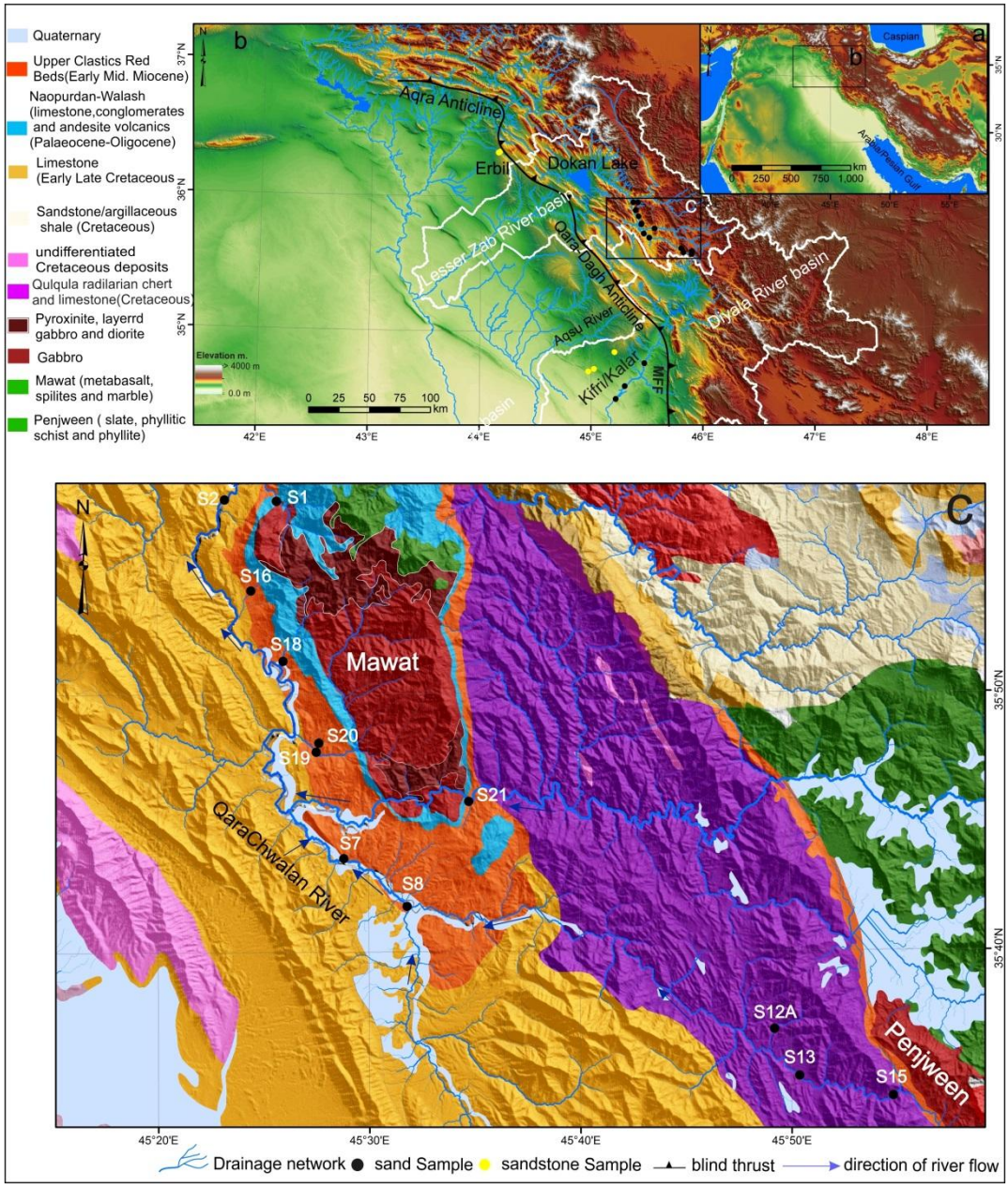

Fig. 5.1. a) Geographical location of the study area, b) Topographic map shows the collected river sand samples from the QaraChwalan (inset c) and Diyala River basin in addition to the sandstone samples from the Neogene formation in the Zagros foreland basin. c) Bedrock geology of the upstream area of the Lesser Zab shows the location of sediment samples in respect to the lithology and drainage network of the area.

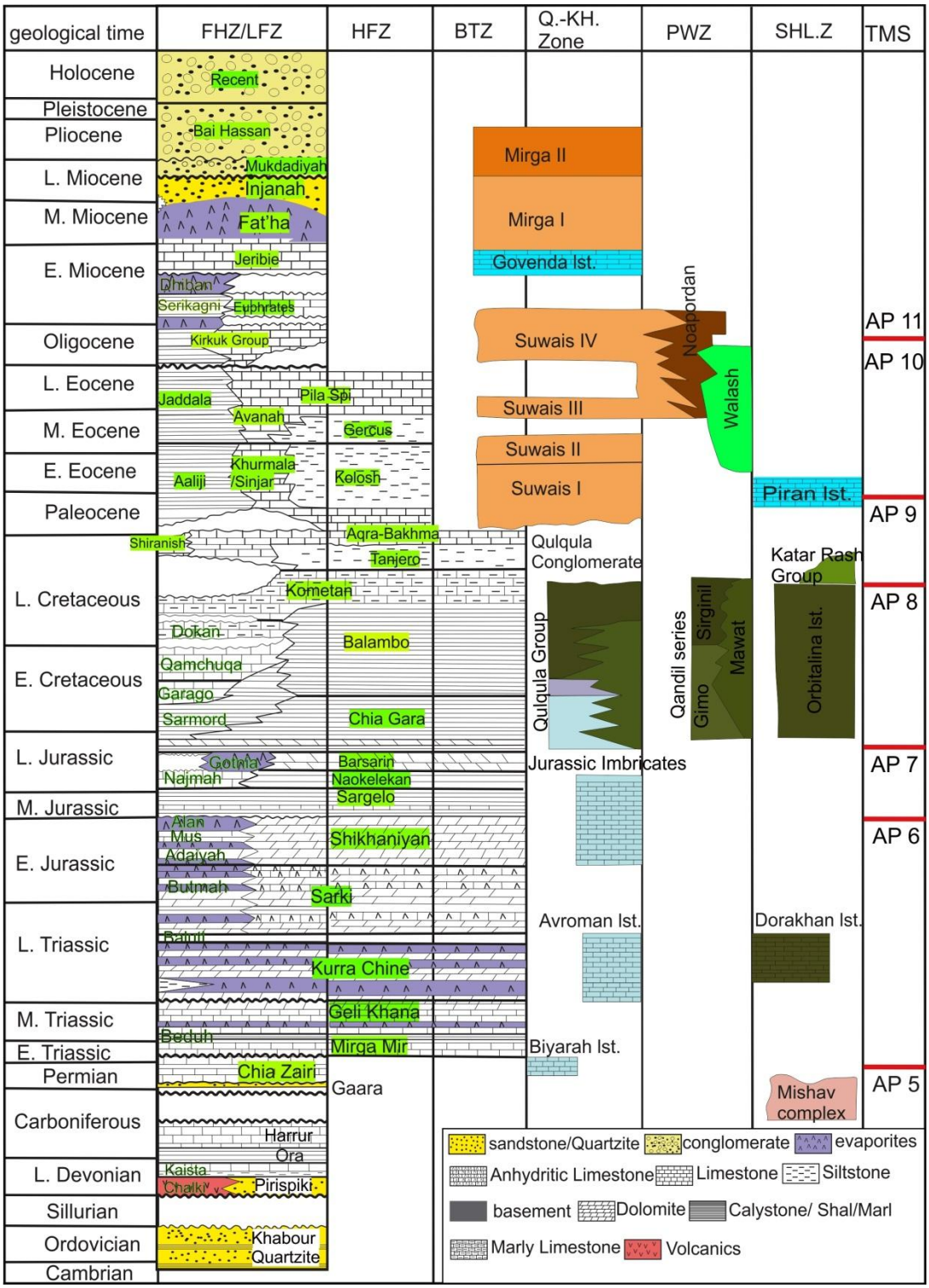

Fig. 5.2 Stratigraphic column across the Suture Zone, northern Iraq (redrawn after English et al., 2015; Jassim and Goff, 2006; Sissakian, 2013). FHZ = Foot Hill Zone; LFZ = Low Folded Zone; HFZ = High Folded Zone; BTZ = Balambo-Tangero Zone; Q-KHZ = Qulqula-Khwakurk Zone; PWZ = Penjween - Walash Zone and TMS = Tectonic Mega -Sequences.

A marine limestone of Biyarah is known only in the Qulqula-Khwakurk zone (Fig. 5.3) east of Halabja and comprises muddy, micritic and fossiliferous limestone. It is probably equivalent to Permian limestones of Khuzestan, SW Iran and deep water limestone of Ba'id in Oman, as they contain the same fauna.

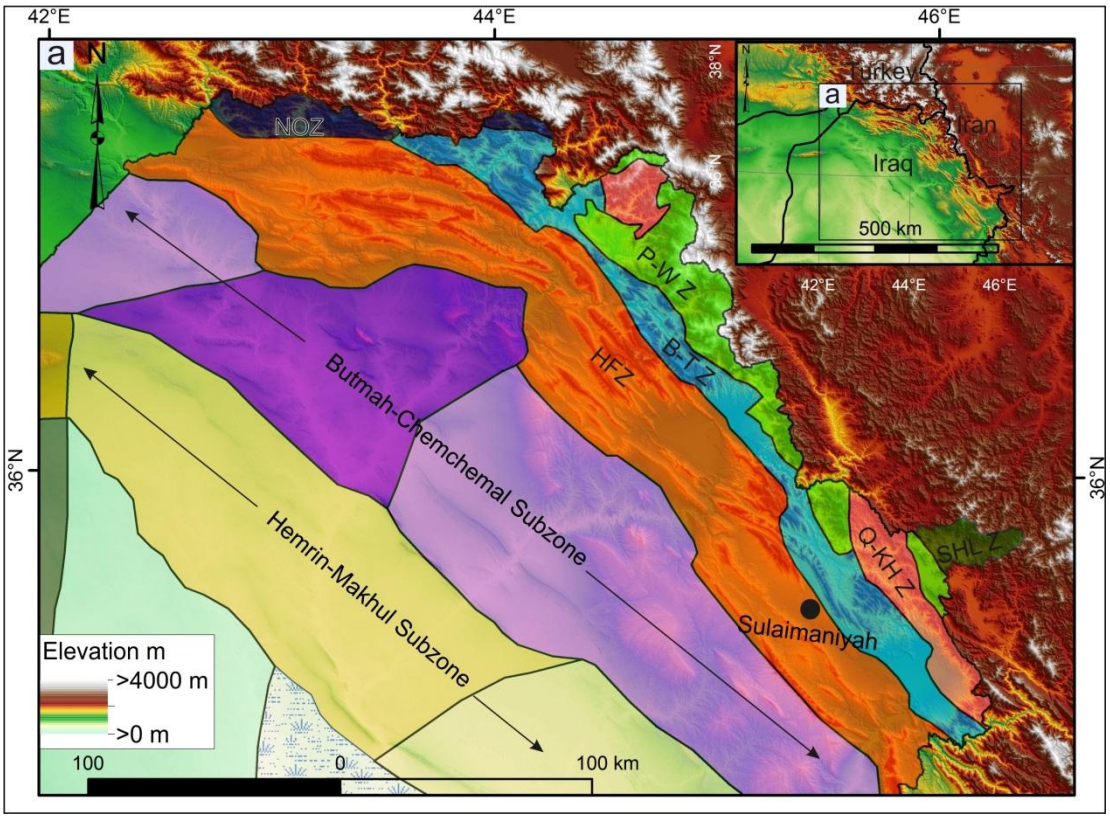

Fig. 5.3 Tectonic subdivision of the Zagros Suture Zone (after Jassim and Goff, 2006) overlays shaded relief map of SRTM 30 m. HFZ = High Folded Zone; BTZ = Balambo-Tangero Zone; Q - KHZ = Qulqula-Khwakurk Zone; PWZ = Penjween - Walash Zone; NOR = Northern Ora Zone.

The Avroman Limestone comprises 800 m thick bedded to massive limestone of a shallow carbonate platform. Limestone purity suggests the deposition is far from the influence of continental clastics. The formation is rich in fauna and equivalent to the lower part of the Bisitoun Limestone southwest of Iran.

The Jurassic imbricates consist of the Shikhaniyan, Sargelu and Naokelekan carbonates and possibly the Barsarin Formation. They form the substrate platform beneath the Qulqula-Khwakurk zone. The Jurassic imbricates are common southeast of Sulaimaniyah city in the Naorbad area, which is part of the Qulqula-Khwakurk zone.

Jurassic rocks were imbricated in the Qulqula-Khwakurk zone probably during the Miocene. Three parts of limestone, limestone with chert and radiolarian limestone comprise the Qulqula radiolarian Formation and these lithologies collectively with the Qulqula conglomerates form the Qulqula group (Late Jurassic-Late Cretaceous).

5.1.2 The Penjween-Walash Zone Sequences

Across the Iraq-Iran-Turkey border, lavas of acidic and basic composition occur and are associated with agglomerate, jasper, slate and minor limestone, and comprise the Khwakurk Series (Late Jurassic-Early Late Cretaceous). Pillow basalt, keratophyres and volcanics of the Mawat Group (the oldest part of the Qandil Series), interfinger with marble, calc-schist and metavolcanics of the Gimo Group and metapelite, calc-schist, marble and metavolcanics of the Sirginil Group, all collectively forming the Qandil Metamorphic Series (Late Jurassic-Late Cretaceous). Volcanosedimentary and non-metamorphosed Tertiary units consist of 1) the Walash Series (Eocene-Oligocene), which consists of two units of volcanics; the lower basic and acidic lavas and pillow lava and the upper basalt, andesite flows and pyroclastics; 2) the Naopurdan Series (Eocene-Oligocene), which consists of andesite volcanics, and argillaceous conglomerate composed of basic volcanic rocks. Limestones and shales altered by sills and basic volcanics, greywacke, coralline limestone and red shale also occur.

5.1.3 The Shalair Zone Sequences

The oldest exposed rocks are the granite and metamorphic of the Mishav Complex in the Shalair Valley. It is intruded within the continental basement of the Sanandaj-Sirjan Zone (Shalair, Fig. 5.3) and exposed widely in Iran. The granite body formed in the Carboniferous (Jassim and Goff, 2006 and reference therein). The Dorakhan Limestone comprises massive and slightly recrystallised and metamorphose limestone, intercalated occasionally with phyllite. It is deposited probably in an outer shelf on the Sanandaj-Sirjan Zone and separated from the phyllite Shalair Group by tectonic contact. The included fossils indicate the Late Triassic age.

Exposed only in Shalair Valley, the Shalair Group (Late Jurassic-Late Cretaceous) consists of multi-composition schist, such as quartz-schist, silty-clayey schist, tuffaceous slate, relatively recrystallised and slightly metamorphose limestone. There is an unclear original stratigraphic relationship with other adjacent units and the

Shalair may gradationally pass into the overlaying Qatar Rash volcanic Group, which is predominated by calc-alkaline volcanics of the andesite. The grade of metamorphism of the Qatar Rash group is similar to the Shalair. The Piran limestone (Late Cretaceous-Paleocene) of the carbonate shelf of the Sanandaj-Sirjan Zone comprises massive, argillaceous and fossiliferous limestone. The unit is believed to have been thrusted and overturned according to the available fossils in the upper and lower parts of the unit.

The Anatolia-Zagros Orogen is expected to be the source of sediments of the Mesopotamian foreland (Garzanti et al., 2016). The arid climate conditions helped in the preservation of the detrital component due to the reduced effect of chemical weathering. This chapter focuses on the petrology of modern river sediment of rivers draining the Zagros Suture Zone and Imbricate Zone, which also comprises the upstream area of the Lesser Zab River, specifically the QaraChwalan River basin (Fig. 5.1). The remainders of the sediment samples were collected from downstream of the Diyala River basin, in addition to the Neogene formations in the eastern and part of the Kirkuk Embayment and the Erbil area. The provenance fingerprint of sediments may shed light on tectonic events of the NW part of the Zagros.

5.2 Data and Methods

The late 19th century was the beginning of modern sedimentary petrology studies when H.C. Sorby invented thin section petrography. It grew by the enhancements of P.D. Krynine in the first half of the 20th century. The evolution of this field of study transferred to the classification scheme of sands using three elements (quartz, feldspar and rock fragments) projected onto a triangular diagram (Dott, 1964; Folk, 1980; Krynine, 1948; McBride, 1963; Pettijohn, 1954). Dickinson and Suczek (1979) formulated the use of the sandstone detrital mode in paleogeodynamic scenarios.

The classic provenance technique simply depends on the percentages of three main parameters. First is quartz (Q) in its monocrystalline, cryptocrystalline and polycrystalline forms, or even if quartz occurs within aphanitic and microphaneritic lithic fragments. Second is feldspar (F) as an individual monocrystalline grain or included with lithic fragments as a feldspar or microphenocryst feldspar within microphanerite lithic and aphanite lithic fragments respectively. Third is the total amount of polycrystalline aphanite lithic fragments (L) with minor occurrence of

microphenocryst and quartzes, chalcedonic and opaline aphanite lithic fragments (Dickinson, 1970). Irrespective of the other constituents of the sediments such as cement materials, the variety of heavy minerals and the type of matrix, the three parameters (Q, L and F) are calculated to 100 percent.

The Iraqi part of the Zagros has been a conflict area since the Second World War. It became relatively stable from 1974 to the mid-1980s, and then it experienced a long conflict period during the war between Iraq and Iran and its consequences in the distribution of a large number of mines. Since 2003, the Iraqi Zagros has been governed by local government and it is very hard to do any research. In April 2016, with a legal agreement from the Department of Geology, Sulaimaniyah University in northern Iraq, I conducted the fieldwork and collected samples wherever possible during a very short period of time, and with big security limitations. The rest of the area was under control of the Islamic State in Iraq and Syria (ISIS), which made it impossible to be accessed.

Fifteen representative samples were chosen from modern river sediments: 12 samples from the Lesser Zab River upstream area, three samples from the Diyala River sediments (Fig. 5.1). In addition, two samples were collected from the Kifri-Kalar area from the Late Miocene formations (Mukdadiyah and Bai Hassan). An additional two samples belong to Mukdadiyah and Bai Hassan formations from the Erbil area, collected for the purpose of identifying the variation of this formation along the front of deformation, which might be affected by different drainage systems. Unfortunately, I could only collect small amounts of samples because of the difficulties mentioned above and also because of limitations at the Iraqi airports. The small amounts were not enough for performing detrital zircon analysis, which at least require 5 kg to collect enough zircon grains for age constrains and determining the source of sedimentation.

At least 340 grains per sample have been counted following the Gazzi-Dickinson method (Dickinson and Suczek, 1979; Dickinson et al., 1983; Dickinson, 1985; Gazzi, 1966; Ingersoll et al., 1984) to identify the three main constituents (Q, F and L) for the purpose of sand composition and provenance identification. Point counting result was plotted on a triangular diagram according to Folk (1980) and Dickinson et al. (1983) for the purpose of identifying sample compositions.

Conventional thin section analysis was complemented by Scanning Electron Microscopy study (SEM), performed on the Durham University Hitachi SU-70 FEG system. Details of operating parameters are at:

https://www.dur.ac.uk/electron.microscopy/facilities/sem/

SEM analysis allows a resolution of sediment textures not possible using conventional techniques. A small amount of spectral analysis was performed, to confirm mineral identifications made on the optical microscope.

This chapter deals with a basic classification of river sand and sandstone, which contrasts with and complements the results of the previous chapters. It does not attempt detailed reconstructions because they are not justified by the size of the datasets, but it is hoped that the results will provide a resource for future provenance studies to build on. In particular, it is hoped that the geomorphic studies of chapters 2 and 3 can be combined with more extended provenance studies of this type, to reconstruct the evolution of the Zagros topography and drainage systems over time.

5.3 Results

5.3.1 Modern river sediment petrology

Petrological analyses of 12 samples of modern river sediment of the QaraChwalan River and three samples of downstream sediment of the Diyala River, showing the minerology (Table 5.1) and grain size of the samples. The fragments are mostly angular to sub-angular, with a few sub-rounded grains. The diameters of grains are mostly in the order of 0.1-0.5 mm, with a secondary group with diameter of 1.0 mm and a few grains in the size range of 0.05-0.1 mm. The main compositions of the sand grains are lithic fragments, little quartz and feldspar grains (Fig. 5.4). The sand grains show relatively good sorting, but poor rounding. According to the sand composition (Table 5.1), the quartz grains represent ~ 2 % to 7 %, feldspar ~ 1% to 2 %, and lithic fragments ~ 89 % to ~ 95 %. The sedimentary fragments are the major constituents; the lowest content of the fragments are metamorphic grains while the volcanic fragments are intermediate. The metamorphic fragments dominate the sand composition of the samples S1, S18 and S20, where tributaries drain metamorphic rock outcrops. The sedimentary fragments are mainly microcrystal-cryptocrystal limestone, and some limestone fragments contain quartz grains (Figs. 5.5, 5.6 and Appendix 4A). The percentage of lithic fragments reflects the exposed geology of the area where the samples were collected (Fig. 5.1C).

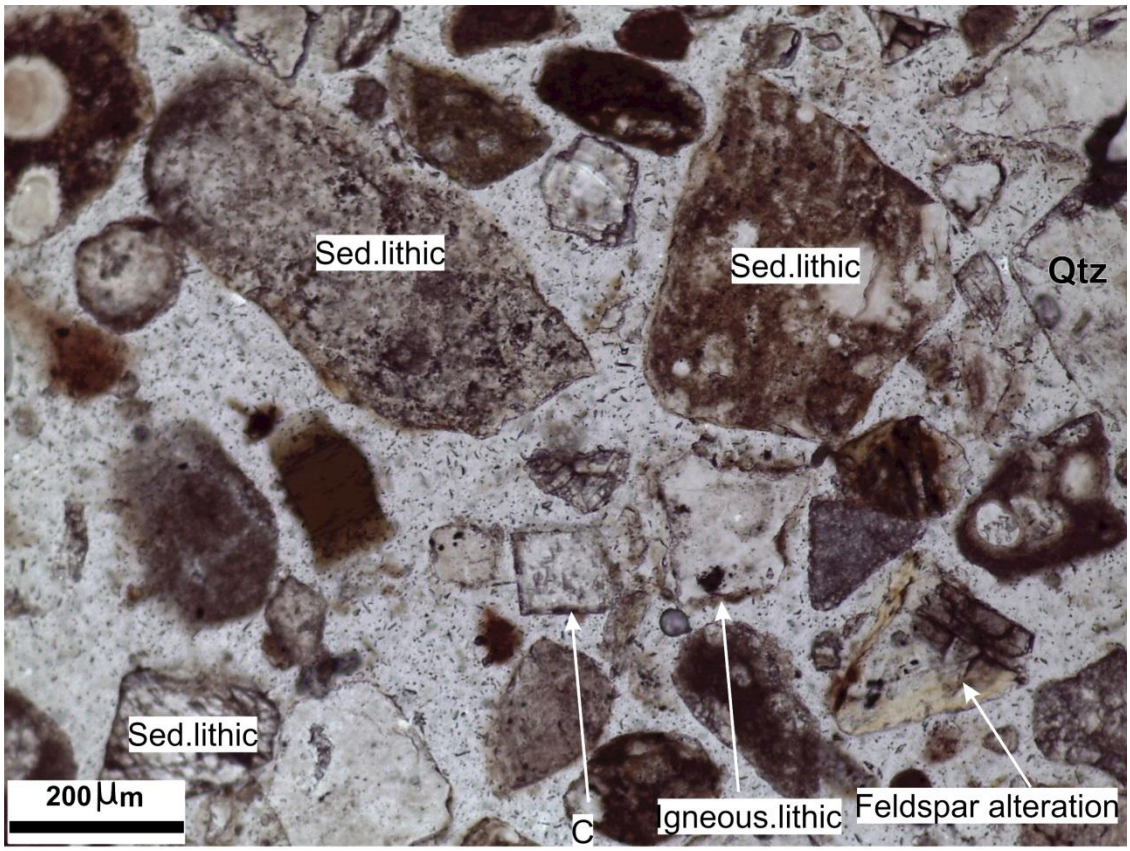

Fig. 5.4. 10x_ppl micrograph shows the mineralogy and grain size of sediment from the Diyala River (S24, NE Kirkuk Embayment. Qtz = monocrystalline quartz, C= Carbonate, Sed. = sedimentary..

Table 5.1: Quartz-feldspar-lithic (QFL) analysis of modern river sediment from the QaraChwalan and Diyala River basins; in addition to the Late Miocene formations. Q = quartz, F = Feldspar, L = Lithic fragments, Qm = monocrystalline quartz, Qp = Polycrystalline quartz, Lv = volcanic fragments, Ls = sedimentary fragments, Lm = metamorphic fragments. Note: samples S1, S8, S12A, S13, S15, S16, S18, S19 and S20 are analysed in the University of Milano as a cooperation work with Professor Edwardo Garzanti.

Site's name	Sample No. %	Qp%	Qm%	Q%	F%	L%	Lm%	Lv%	Ls%
Gulea	S1	1	2	3	3	94	56	12	32
Khazena	S2	1	4	5	13	82	41	9	50
Wazha	S7	1	2	3	6	91	22	10	68
QaraChwalan	S8	3	6	9	6	84	18	16	66
Galoz	S12A	0	0	0.0	0	100	3	0	97
Harzala	S13	0	8	8	7	83	35	11	54
Kani Sard	S15	2	7	9	9	81	43	10	47
Mawat	S16	1	2	3	23	74	34	19	47
Perdapan	S18	1	3	4	10	86	84	8	8
Kougerien	S19	1	3	4	5	90	14	12	75
Sakal	S20	1	3	4	25	70	89	8	3
Tazadea	S21	1	1	2	7	92	10	25	65
Gerdagozina	S24	1	3	4	10	86	1	26	73
BawaNur	S25	1	3	4	2	94	1	16	83
Zhallanaw	S26	0	2	2	3	95	2	16	82

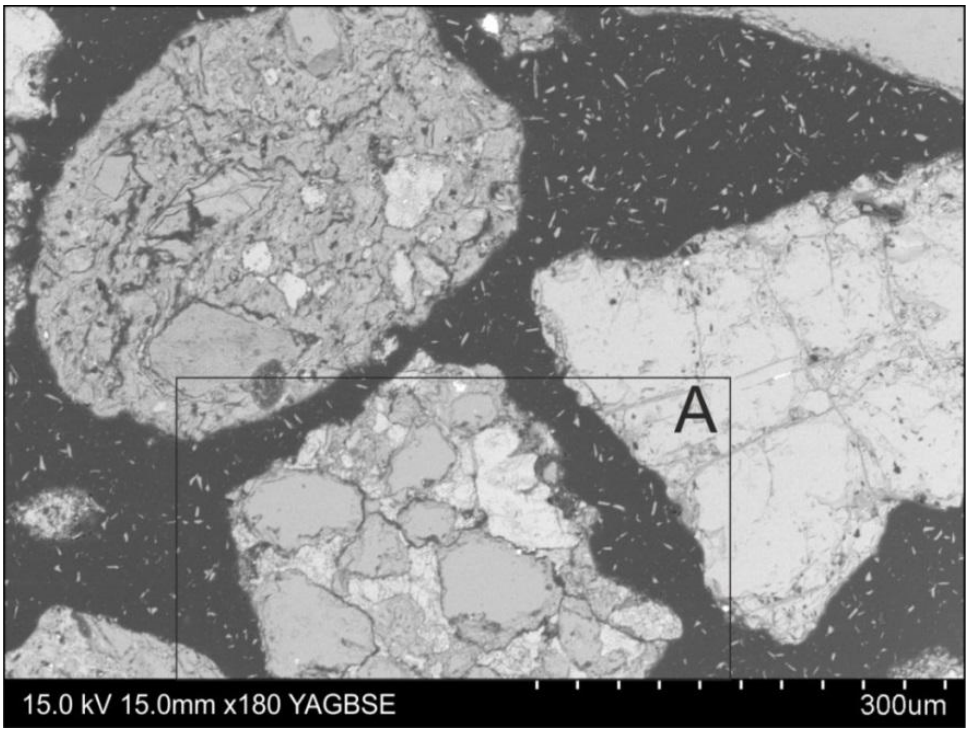

Fig. 5.5. SEM image of sample S7 shows the abundance of sedimentary fragments in river sand. The fragments in places contain polycrystalline quartz (inset A).

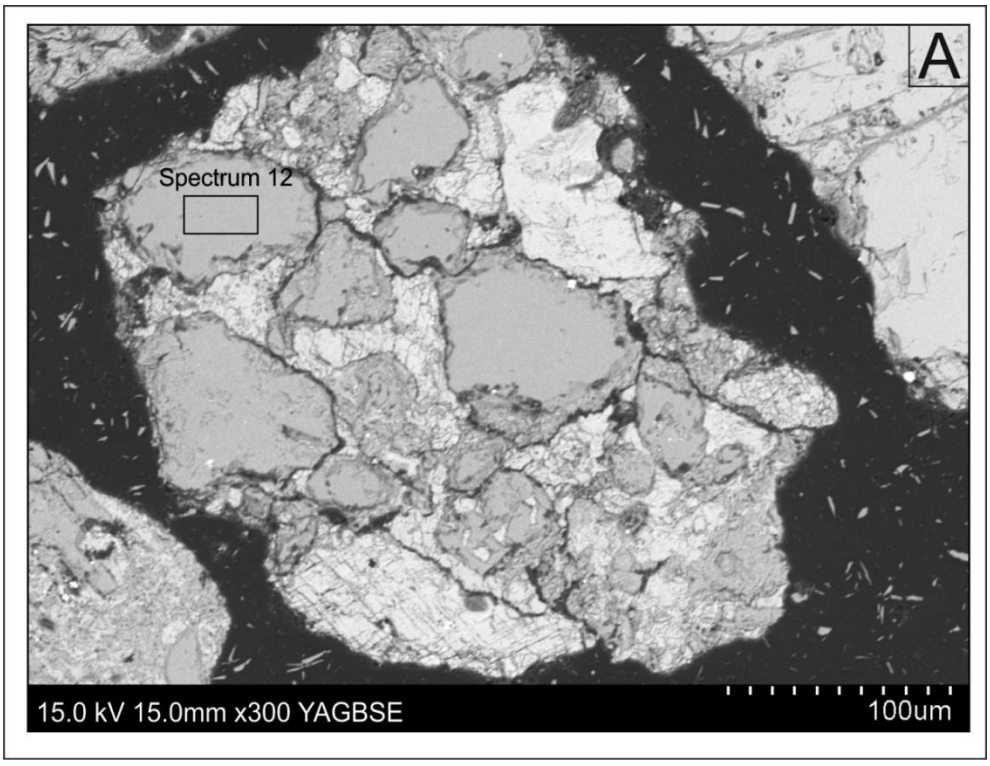

Fig. 5.6. SEM image shows polycrystalline quartz contained in lithic fragments (inset A in Fig. 5.4).

Following Folk (1980) and Dickinson et al. (1983), point counting results are plotted in a triangular diagram; results show a litharenite composition for all samples as the lithic fragments are the main constituents (Fig.5.7-A). Recycled orogen sedimentation dominance (Lithic recycled) can be recognised from the prominence of sedimentary lithics and the scarcity of igneous and metamorphic lithics (Fig. 5.7-B).

Sand from headwaters of the Lesser Zab River (LZR) is classified as quartzo-lithic clastic sediment, with a minority of schist and serpentinite fragments and a majority of limestone, shale and chert (Fig. 5.7). Igneous and metamorphic fragments increase in the samples (15 and 18) where tributaries drain the Penjween and Mawat complexes (table 5.1 and Figs. 5.8 and 5.9). This is unsurprising, given the varied and commonly ophiolitic nature of these complexes. The downstream area of the LZR carries lithic to quartzo-lithic fragments (Garzanti et al. 2016) probably due to accumulation of most of the upstream sediments in the Dokan reservoir. Tributaries beyond the Dokan reservoir (i.e. Aqsu River) are draining the Cenozoic sedimentary strata and show recycled sedimentation from the older foreland (Garzanti, 2017). There is a change in the sedimentation signature of the Diyala River sand, which is characterised by lithic clastic sediment sand dominated by chert, limestone and shale, accompanied with volcanic/metavolcanic fragments.

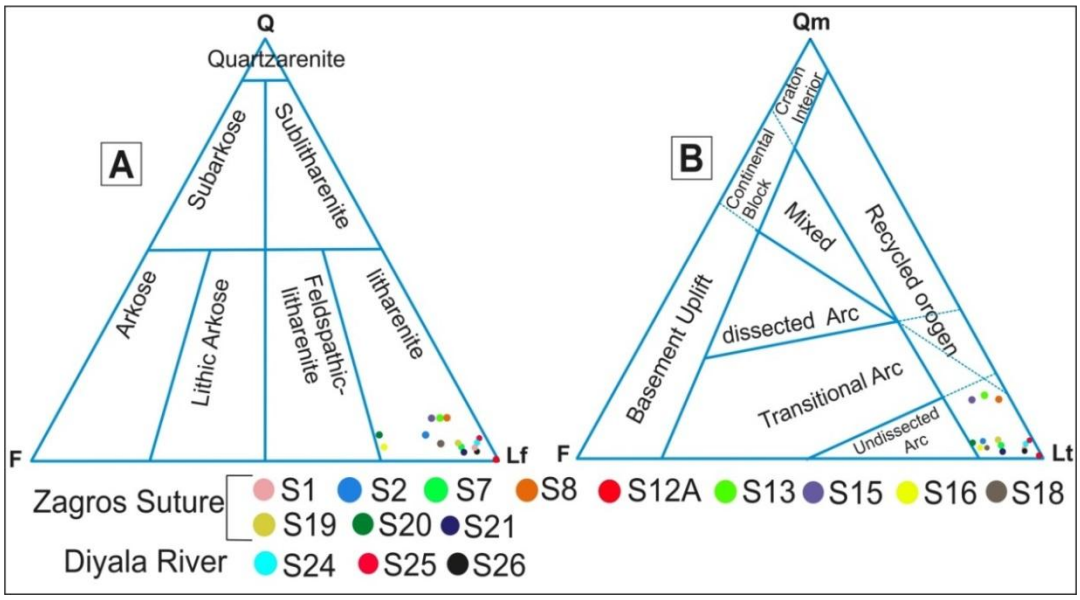

Fig. 5.7. Ternary diagram for the 15 samples of the Lesser Zab River and the Diyala River shows sand composition. A: Quartz-Feldspar-Lithic (QFL) (after Folk, 1980). B: QFL (after Dickinson et al., 1983). Q = Total quartz (Folk: Qm + Qp); F = total feldspar (K + P); Lf = total lithic fragments (Folk: L + C + S); Qt = total quartz (Qm + Qp + C + S); Lt = total non-quartzose lithic grains (Lv + Lm + Lc + Lsh).

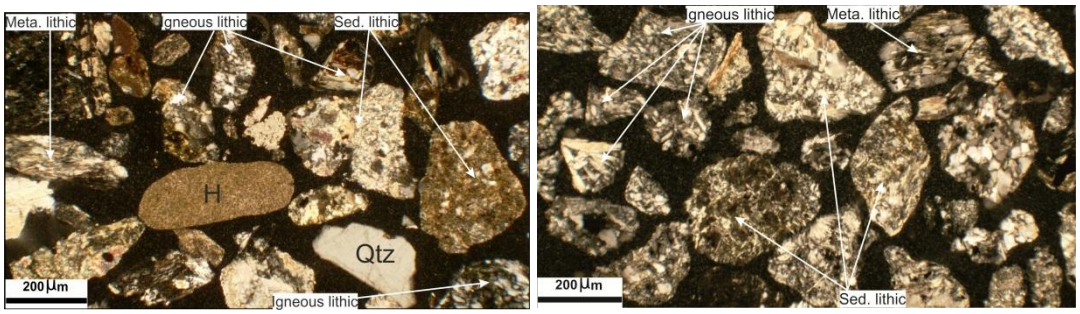

Fig. 5.8. River Sand composition, the left is 10x_xpl micrograph belong to sample S15 and the right is 10x_xpl micrograph belong to sample 18 from upstream area of the Lesser Zab River (see Fig.1C for samples location). H = chert; Qtz = Quartz, Meta= metamorphic, Sed.= sedimentary.

The Lm-Lv-Ls diagram (Ingersoll and Suczek, 1979) shows suture belt recycled sand (Fig. 5.9). Table 5.2 shows the heavy mineral composition of river sand collected from the right bank of QaraChwalan River, NE Iraqi Kurdistan Region, which occupies part of the Zagros suture zone. The river carries lithic sand dominated mainly by sedimentary fragments and locally by metavolcanic fragments derived from the Penjween and Mawat complexes (Fig. 5.9). Heavy mineral assemblages were analysed by E. Garzanti, as part of the study published as Garzanti et al (2016),

and show epidote, hornblende and amphibole dominance, and zircon, tourmaline and garnet scarcity (Table 5.2).

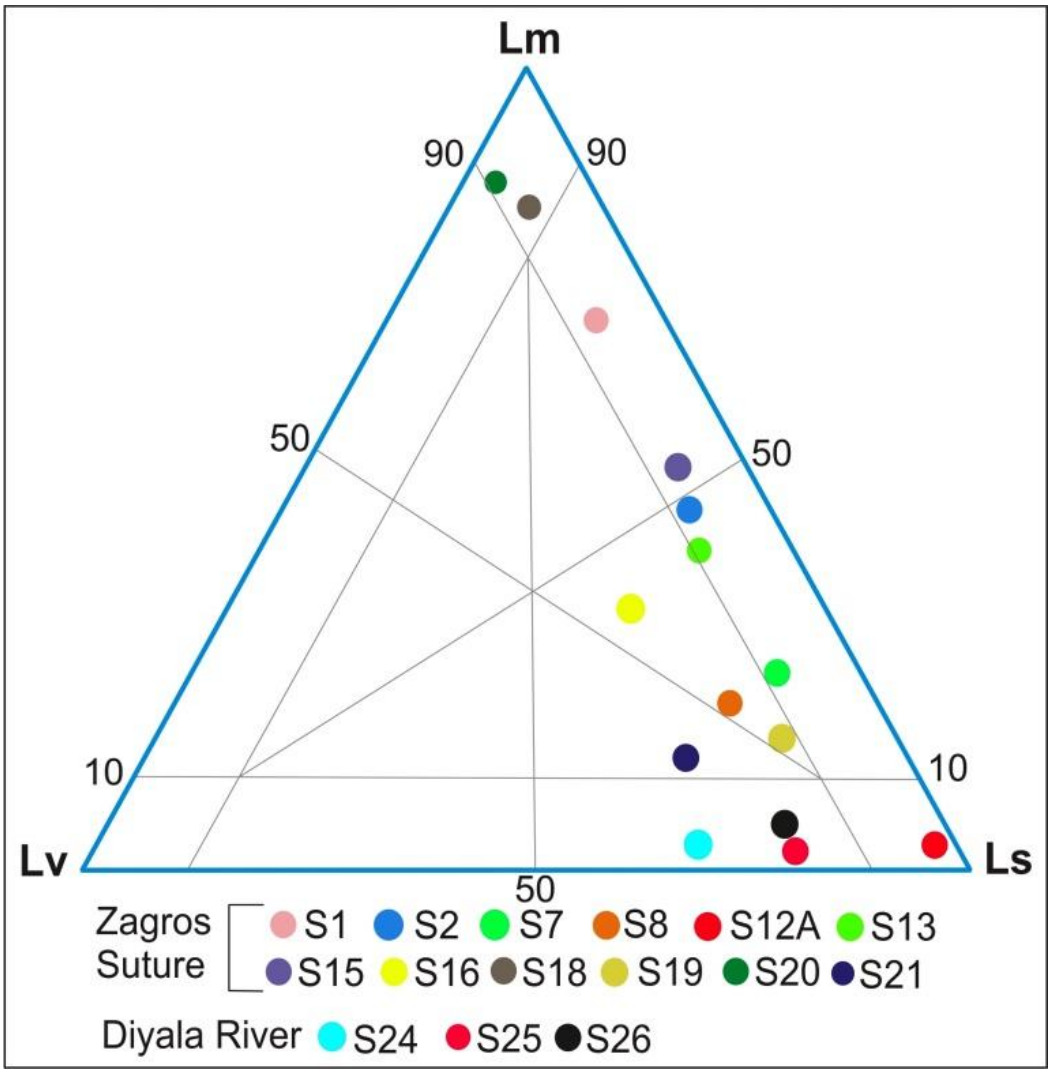

Fig. 5.9. Lm-Lv-Ls diagram (after Ingersoll and Suczek, 1979) for the 15 samples of the Lesser Zab river network and the Diyala River shows lithic composition. Lv = volcanic fragments, Lm = metamorphic fragments, Ls = sedimentary fragments. Note the relative high metamorphic grains content of the samples from rivers draining the Mawat complex (S1, S18 and S20) and the Penjween complex (S15).

Table 5.2. Heavy mineral contents of sands collected from the QaraChwalan River (From Garzanti et al., 2016).

Site's Name	Sample's No.	Zircon %	Tourmaline %	Garnet %	Apatite %	Epidote %	Hornblende%	Amphibole%	Pyroxene%
Gulea	S1	0	0	1	0	29	40	14	8
Khazena	S2	0	0	0	0	30	47	11	5
Wazha	S7	0	1	0	0	25	24	38	3
QaraChwalan	S8	0.7	0	0.7	0.3	34	36	17	0.7
Galoz	S12A	0	0.5	3	0.5	36	33	15	2
Harzala	S13	0	0.5	1	0	19	34	37	0
Kani Sard	S15	0	0.5	0	0.5	23	39	33	0
Mawat	S16	0	0	0	0	26	20	13	41
Perdapan	S18	0	0	0	0	22	18	59	0
Kougerien	S19	0.5	0	0.5	5	64	18	6	3
Sakal	S20	0	0	0	0	19	55	23	2
Tazadea	S21	0	1.5	0	1	30	41	21	3

5.3.2 Late Miocene and Pliocene-Pleistocene petrology

Four samples from Late Miocene and Pliocene-Pleistocene formations were collected for the purpose of sandstone composition and provenance analysis. Two samples from the Kifri-Kalar area southeast of the Kirkuk Embayment are from the Mukdadiyah (Late Miocene) and Bai Hassan (Pliocene-Pleistocene) formations (Fig. 5.1). An additional two samples from the Erbil area, NW of the Kirkuk Embayment (Fig. 5.1), also belonging to the Mukdadiyah and Bai Hassan formations were collected for comparison with formations in the southeast of the Kirkuk Embayment. This is a small sample collection, but a considerable enhancement to the datasets in the literature, which are very limited. The four samples are described on an individual basis, before the regional implications are discussed.

5.3.2.1 Bai Hassam Formation

The Bai Hassan sandstone in the Kifri area, southeast part of the Kirkuk Embayment (Fig. 5.1) is represented by the sample St15 in table 5.3. The rock has a medium to fine grained texture. The grains occupy about 80% of the rock; most grains are angular to subangular, with a few subrounded grains (Fig. 5.10). The diameters of grains are mostly ~ 0.2 mm and very few grains are more than 0.5 mm. The sand grains show relative good sorting and poor roundness. The main compositions of the sand grains are lithic fragments and few quartz and feldspar grains. The proportion of quartz grains is 4%, feldspar 3%, and lithic fragments 93% (Table 5.3). The sedimentary fragments are mainly microcrystalline to cryptocrystalline limestone, with few argillaceous fragments.

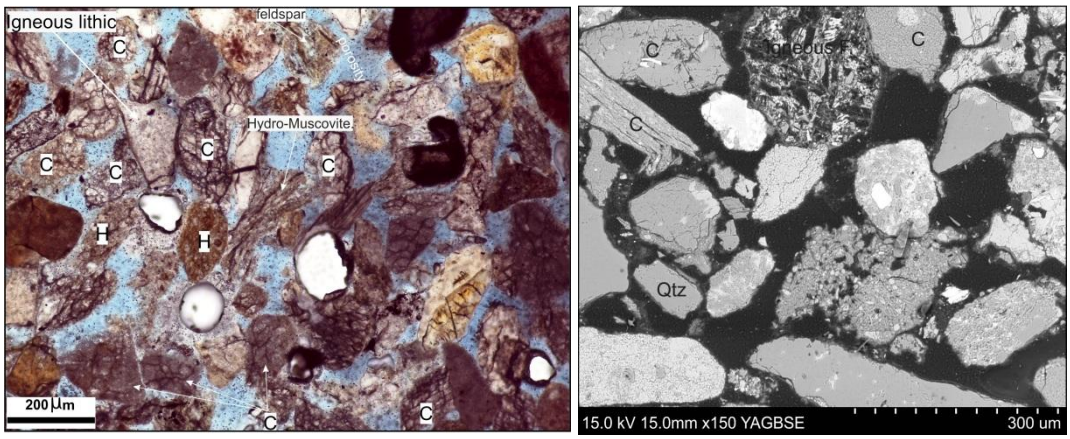

Fig.5.10. Left plate shows the mineralogy and grain sizes of the Bai Hassan Formation in the Kifri area (magnification 10x_ppl). Right plate is SEM image shows grain size distribution and friable matrix. Qm = monocrystalline quartz, Lv = volcanic fragments, Ls = sedimentary fragments, lst = limestone.

Table: 5.3. Petrological analysis of the Mukdadiyah and Bai Hassan formations: Q = quartz, F = Feldspar, L = Lithic fragments, Qm = monocrystalline quartz, Qp = Polycrystalline quartz, Lv = volcanic fragments, Ls = sedimentary fragments, Lm = metamorphic fragments.

Site name	Sample No.	Formation	Qp%	Qm%	Q%	F%	L%	Lm%	Lv%	Ls%
Kifri	St15	Bai Hassan	1	3	4	3	93	1	7	85
Erbil	St70	Bai Hassan	3	19	22	5	73	3	16	57
Kifri	St7	Mukdadiyah	2	5	7	4	89	2	8	79
Erbil	St71	Mukdadiyah	3	17	20	4	76	4	11	61

St70 represents the Bai Hassan Formation in the Erbil area, which is composed of 73% lithic, 22% quartz and 5% feldspar. This sample shows a noticeable increase in the number of quartz grains, which is much higher than the same formation in the SE of the Kirkuk Embayment (Fig. 5.11). Also, the grains have higher roundness and better sorting than the same formation in Kifri (St15). Some fragments hold high content of quartz grains (Fig. 5.11), which refer to the maturity of the source area of the fragment.

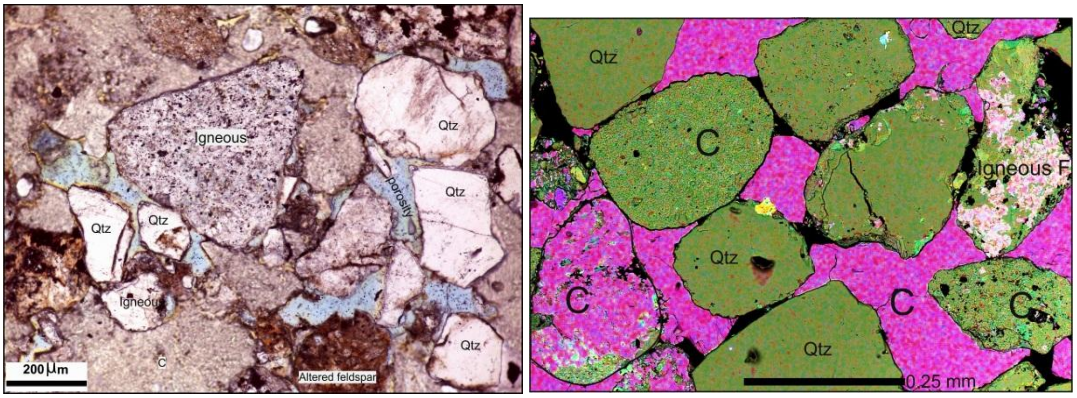

Fig.5.11. Left plate shows the mineralogy and grain size of the Bai Hassan Formation in the Erbil area (magnification 10x_ppl). Right plate shows SEM phase map: C = carbonate, Qtz = quartz. Note, the increase in the number of quartz grains compare with the Kifri sample.

5.3.2.2 Mukdadiyah Formation

The Mukdadiyah sandstone (St7) in the Kifri area, southeast part of the Kirkuk Embayment, Fig. 5.1) comprises a medium to fine grained texture, which is can be classified as medium-fine litharenite. The grains occupy about > 85% of the rock; most of the grains are angular to subangular, with a few subrounded grains. The diameters of grains mostly are ~ 0.1- 0.4 mm, and a few reach 0.5 mm. Lithic fragments are the main constituents, which comprise 89%, complemented by a few quartz grains in a proportion of 7% and 4% feldspar. The sand grains show relative good sorting and medium roundness (Fig. 5.12). The sedimentary fragments are mainly microcrystal to cryptocrystal limestone with a few argillaceous fragments.

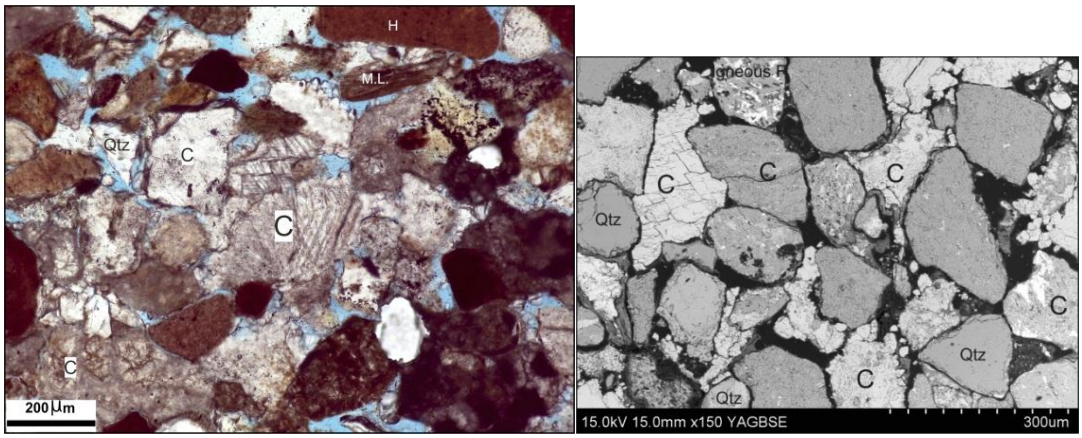

Fig. 5.12. Left plate shows the mineralogy and grain size of the Mukdadiyah Formation in the Kifri area (St7), SE of the Kirkuk Embayment (magnification 10x_ppl). Right plate is SEM image shows the friable calcite matrix and other constituents of the rock sample. Qtz = quartz. C= carbonate, M.L.= metamorphic lithic, H= chert.

The Mukdadiyah sandstone St71 from the Erbil area, NW of the Kirkuk Embayment (Fig. 5.1) exhibits a fine grained texture, and is classified as fine grained litharenite similar to the Kifri sample. Most of the grains are subrounded to subangular, with a few angular and rounded grains. The diameters of grains mostly are less than 0.25 mm, and a few 0.3-1 mm; sometimes pebbles can found in a diameter of 2.5-2.7 mm and the grains show relative good sorting and medium roundness (Fig. 5.13). Quartz grains comprise 20% of the total, (which is higher than the sample of the Kifri area), feldspar 4%, and lithic fragments 76%. The main lithic fragments are sedimentary with minor metamorphic and volcanic fragments. The sedimentary fragments are mainly microcrystalline to cryptocrystalline limestone, with a few argillaceous

fragments. The interstitial minerals are mainly calcite, occupying about 25% of the total rock.

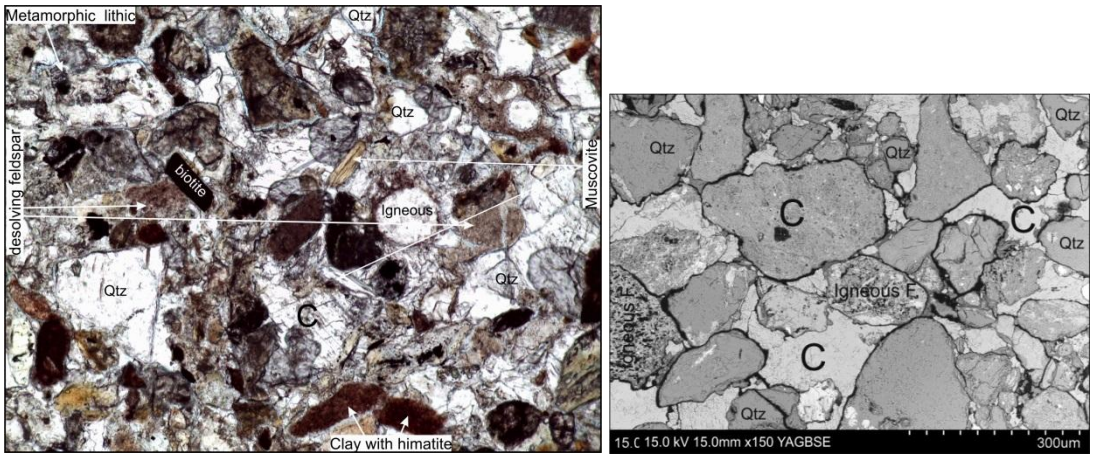

Fig. 5.13. Left plate shows the mineralogy and grain size of the Mukdadiyah Formation (St71) in the Erbil area (magnification 10x_ppl). Right plate is SEM image, showing more consolidated matrix and higher content of quartz compare with the Kifri sample. Qtz=quartz, C= carbonate, M.L.= metamorphic lithic.

The point counting results were plotted on a triangular diagram following the classification of Folk (1980) and Dickinson et al. (1983). The results show a litharenite composition for all samples, as lithic fragments are by far the main constituents (Fig. 5.14 A). A recycled orogen setting (Fig. 5.14 B) can be recognised from the prominence of sedimentary lithics and the lower content of igneous and metamorphic lithics.

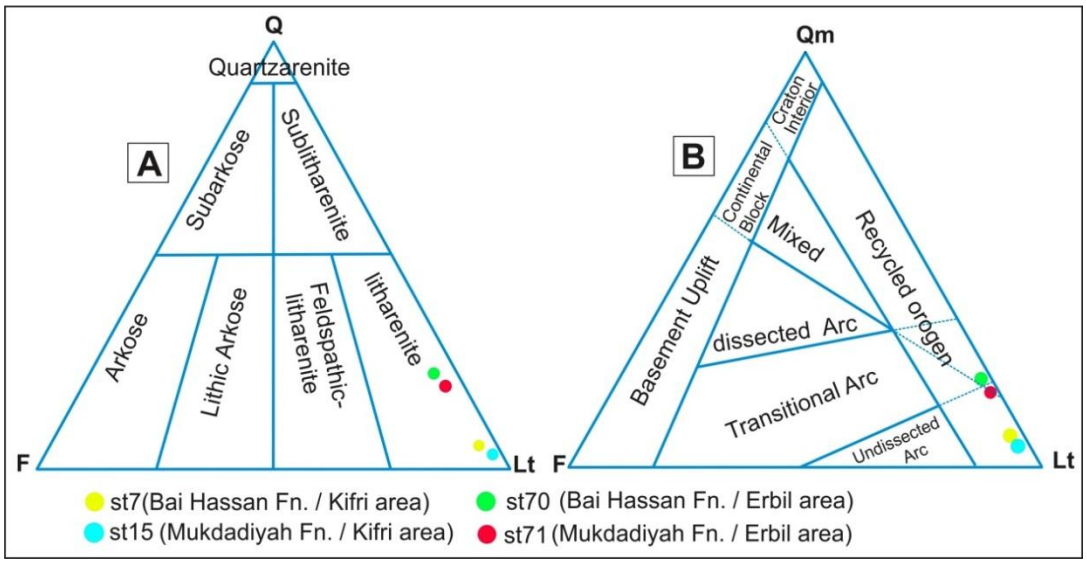

Fig. 5.14. Ternary diagram of the four sandstone samples shows sand composition: A: quartz-feldspar-lithic (after Folk, 1980). B: QFL (after Dickinson et al., 1983) for tectonic provenance. St7 and St71 are from the (older) Mukdadiyah Formation; St 15 and St70 are from the (younger) Bai Hassan Formation (Table 5.3). St 7 and St15 are from Kifri area, and St70 and St71 are from Erbil area (Fig.5.1). Therefore the compositional trend is more spatial than temporal, with more quartz-rich compositions in the NW (Erbil region).

5.4 Discussion

The occurrence of metamorphic, metavolcanic and volcanic fragments in the QaraChwalan River sand (Table 5.1) is consistent with sediment source from the Penjween-Mawat ophiolite. Also, the occurrence of sedimentary fragments dominated by limestones refers to the derivation from the Qulqula-Khwakurk Zone and Balambo-Tanjero subzone (Fig. 5.3). The heavy mineral assemblage of the QaraChwalan River sand (Table 5.2) shows enrichment in the amphibole associated with epidote, which is possibly sourced from the Penjween-Mawat ophiolite. This result is not surprising as it reflects the exposed lithology across the QaraChwalan River basin where the samples were collected. Changes in the sediment sources across this area between the Late Miocene formations and modern river sands might be related to fault activity (i.e. uplift and exhumation) and/or drainage reorganisation. Such studies could provide evidence to help in solving the evolution of the Zagros Suture Zone.

The Mountain Front Fault (MFF) is a pre-existing basement fault marking the topographic boundary between the Zagros foreland and the Zagros Simply Folded Belt along the Qara-Dagh and Aqra Anticline (Fig. 5.1, inset b) north of the Kirkuk

Embayment (Jassim and Goff, 2006). Published Apatite-Helium (AHe) ages indicated the Late Miocene-Pliocene emergence of the Qara-Dagh Anticline as a result of out-of-sequence basement fault reactivation of the MFF (Koshnaw et al., 2017). Since the emergence of the Qara-Dagh Anticline, the sedimentation of the Zagros foreland has been dominated by coarse conglomerates of the Bai Hassan and coarse sediments of the Quaternary, which is the result of recycling from the older foreland (Fig. 5.15). Therefore, a comparison between modern river sand and the latest deposits in the Zagros foreland could help in understanding the tectonics of this region.

Fig. 5.15. Field photograph shows the similarities in sediment grain size and overall appearance between the Bai Hassan Formation and Quaternary sediments in Kifri/Kalar area SE of the Kirkuk Embayment/northern Iraq.

The river sediment data in this study plot close to the lithic apex of the QFL diagram, and indicate litharenite compositions, consistent with a recycled orogeny provenance (Fig. 5.7). These results are consistent with an end member of the Tigris system defined by Garzanti et al (2016), which is not surprising as samples from this study were used in that work. The Tigris trend plots from the lithic end-member of the QFL plot towards the quartz apex. Therefore there is a spatial distribution in the composition of sands within the Tigris drainage system; more lithic compositions appear to be sands derived from metamorphic rocks exposed in the Iraqi Zagros, such as the Penjween and Mawat ophiolite complexes, while the more quartz-rich compositions reflect partial derivation from Palaeozoic and Mesozoic sedimentary successions of the Arabian Plate, which are exposed in the far north of Iraq and neighbouring parts of Syria and Turkey.

The four sandstone samples analysed show a similar story (Fig. 5.14), where compositions are more quartz-rich in the NW sample site (Erbil area), than to the SE (Kifri/Kalar area).

These results are different to the conclusion made by Koshnaw et al (2017), who interpreted a temporal change in composition from the Mid-Miocene to the Pliocene-Pleistocene, towards a more lithic end-member. It is possible that both trends are real, and that a spatial trend of increased maturity to the NW of the Zagros foreland (this study and Garzanti et al., 2016) co-exists with a temporal trend to more lithic compositions (Koshnaw et al., 2017), which reflects increased uplift and exhumation of the metamorphic complexes in the structurally-higher units of the Iraqi Zagros. Part of this increase in exhumation may result from the out-of-sequence deformation recently recognised in the Iraqi Zagros, both by this study (Chapter 3 and Obaid and Allen, 2017), and Koshnaw et al (2017) (Fig. 5.16): instead of sequential deformation propagating towards the foreland, uplift along the Qara-Dagh Anticline and the MFF has increased the erosion of metamorphic rocks in the Zagros hinterland.

Part of this evolution has involved the separation of the Aqsu River drainage basin (which in the present is a seasonal river draining internal basin) from the drainage on the northern side of the Qara-Dagh Anticline (Fig. 5.1), such that modern river sediments of the Aqsu River and its tributaries are derived from Neogene sedimentary rocks, and not directly from the basement to the northeast (Fig. 5.16). As Garzanti (2017) noted, this isolation has not increased the maturity of the modern Aqsu River sands, which look essentially the same as the ones in this study.

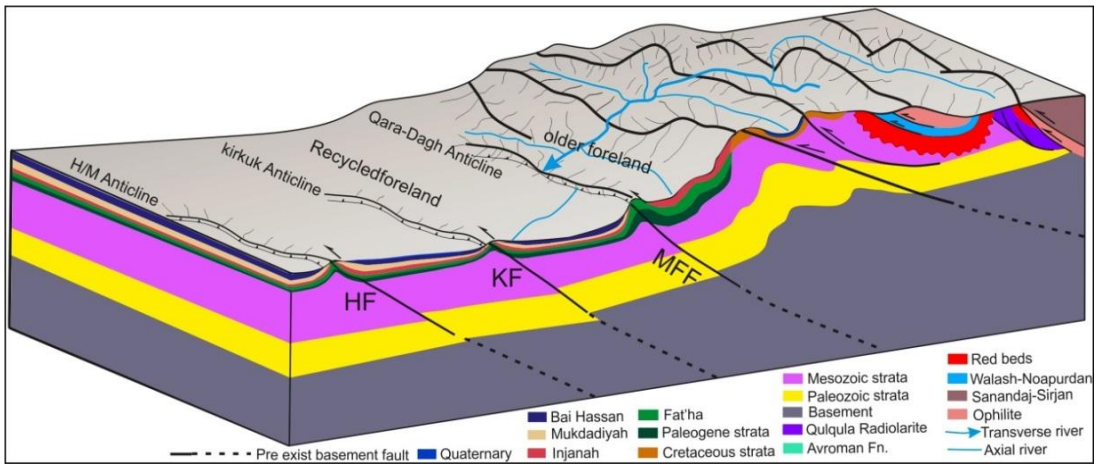

Fig. 5.16. Conceptual model based on the information from Koshnaw et al., (2017), Obaid and Allen (2017), Jassim and Goff, (2006) and data from the sediment analysis result of the current study. The model shows the evolution of the NW Zagros and the emergence of the Qara-Dagh Anticline as a result of the MFF re-activation, which has led to a change in the sedimentation system south of the MFF to be recycled from the older foreland to the north. HF = Himreen Fault, KF = Kirkuk Fault, MFF = Main Frontal Fault, H/M = Himreen/Makhool.

5.5 Summary

The Zagros foreland sedimentary rocks are believed to be derived from Sanandaj-Sirjan, the Zagros Suture and the Turkish-Iranian Plateau. However the dynamic evolution of northern Arabia is debated due to the complex configuration of the Zagros Suture Zone (ZSZ), which is located at the northern margin of the Arabian Plate. The sediment source of the Zagros foreland contains many clues about the ZSZ tectonics. Thus, sediment of the QaraChwalan River draining the ZSZ and sandstone of the Bai Hassan Formation (Pliocene-Pleistocene) and the Mukdadiyah Formation (Late Miocene) have been collected for petrological analysis.

A petrological analysis was conducted for 15 samples from the QaraChwalan and Diyala rivers sediment and four samples from the Late Cenozoic sandstones of the Mukdadiyah and Bai Hassan formations in the Zagros foreland. The results show a litharenite composition and a recycled orogen source for the modern river sediment and Late Cenozoic formations. Results from this study and equivalent studies show changes of the sediment composition from the SE (Kifri) to NW (Erbil) localities, for both the Mukdadiyah and Bai Hassan formations: there is an increase in quartz content to the NW (Fig. 5.14). The fifteen modern river sand samples are all from the Lesser Zab and Diyala drainage basins, and show a more lithic composition (Fig.

5.7). This lithic signature refers to the ongoing uplift of the Zagros suture and partly affected by out-of sequence backward deformation studied in chapter 3 and by Koshnaw et al (2017). What is missing from this study, because of access constraints, are modern river sand samples from the Greater Zab drainage basin further NW, for comparison with the two pre-Holocene sandstones with the more quartz-rich composition (Fig. 5.14).

A geochronological investigation of the sandstones and sand lenses included in conglomerate layers is required for the sequences exposed in deep gorges along the Zagros orogen; with special attention to the Bai Hassan and Mukdadiyah formations along the Zagros to constrain their ages and minerology.

6. Discussion, conclusions and future work

6.1 Discussion

Chapters two, three, four and five contain discussions of the results from the work within each chapter. This chapter is a collective discussion of results of individual chapters included in the thesis. There is also a discussion of the limitation of the methods and approaches used in the thesis chapters.

6.1.1 Tectonic and climatic records in landscapes

In order to test whether tectonic and climatic records in landscapes can be useful tools to investigate regional deformation of fold-and-thrust belts; geomorphic analysis of topographic swath profiles, normalized steepness index (k_{sn}) of river profiles, and basin-scale hypsometric index (HI) has been conducted for the Zagros fold-and-thrust belt (Chapter 2). Results show contrasting patterns of HI and k_{sn} across two distinct areas: the Dezful Embayment/Bakhtyari Culmination of the northwest Iranian Zagros, and the Fars region in the east of the range. The Dezful/Bakhtyari region exhibits low relief and elevation across the Embayment, but shows a sharp increase in elevation at the edge of the Embayment and within the Culmination; this zone includes the upper cut-off limit of major thrust seismicity (roughly at the elevation contour 1250 m; Nissen et al., 2011). A group of high k_{sn} values occurs in high relief areas of the Bakhtyari Culmination and in the northwest of the Zagros, also around the 1250 m elevation contour, but k_{sn} does not show a distinct signal or pattern that can be used to explain tectonic processes.

Hypsometric index results are more useful. In general across the Zagros there is a switch from low HI within the plateau, to higher HI within the main part of the fold-and thrust belt, declining to low values in the foreland plains. The edge of the plateau, defined tectonically as the limit of thrust seismicity at the 1250 m elevation contour, coincides well with the transition from low to high HI values – i.e. the tectonic and geomorphic expressions of the Turkish-Iranian Plateau are approximately in the same position. But, the Bakhtyari region shows the extension of high HI values northeast of seismicity cut-off, towards the interior of the Turkish-

Iranian Plateau. This phenomenon may be interpreted as the geomorphic plateau being inhibited from advancing as far south as the seismicity cut-off as a result of the vigorous drainage in the Bakhtyari Culmination: several rivers converge towards the Karun River to the southeast in a centripetal drainage pattern. This region has the wettest climate in the Zagros. The climatic and drainage patterns inhibit the formation of a geomorphic plateau, but the tectonics still follows the pattern that there are no major thrust earthquakes above the 1250 m regional elevation.

For the Fars region there is an inverse story. The elevation swath profiles rise gently to the northeast with no prominent step. The k_{sn} of the Fars region has an approximate similarity with Turkish-Iranian Plateau and the Zagros foreland: it is hard to distinguish a separate band of high values. HI values for the Fars region remain high south of the upper elevation limit for thrust seismicity. Expressed another way, the geomorphic limit of the plateau is further south than the seismic (tectonic) limit: regions which have subdued landscapes are still tectonically active, and presumably will remain so until the crust has thickened to the extent that, by isostasy, the 1250 m elevation contour is reached. Again, there seems to be a major climatic factor: the dry climate of the Fars region inhibits stream power and erosion, and the rivers take sinuous courses before reaching the Gulf. In both regions (Dezful/Bakhtyari and Fars), climate appears to play a decisive role in the geomorphology, but, climate cannot be decoupled from tectonics. Arguably the sharp division of strain between the Dezful Embayment and the Bakhtyari Culmination is what causes the abrupt topographic step into the latter region, accompanied by orographic precipitation. Conversely, the uniform structure across the Fars region (Allen et al., 2013) means that there is no such topographic step and no such orographic precipitation. In the case of the Bakhtyari Culmination, the zone of high HI beyond the seismicity threshold may reflect that this region has a vigorous drainage network and youthful topography – with a climatic driver – but it is not undergoing active uplift on a scale that makes an impact on k_{sn} values.

These differences in geomorphic indices across two specific areas in the Zagros can be explained by the different climate of the two areas: wetter conditions and vigorous drainage systems in the Dezful/Bakhtyari region retard plateau growth; drier climate leads to low power of rivers in the Fars region and promote plateau growth.

Orographic precipitation may itself have a tectonic control; regional basement strength variations are another plausible cause (Allen and Talebian, 2011). Strong basement in the Dezful Embayment keeps the amount of strain in this region low, but produces intense thrusting and steep relief in the Bakhtyari Culmination to its northeast, so that the overall stain across this part of the Zagros is similar to adjacent regions (Allen and Talebian, 2011). It is possible that the Kirkuk Embayment has a similar origin to the Dezful Embayment, with the same consequence, that high strain is concentrated in the imbricate zone to its northeast where high k_{sn}, HI and high relief occur. Possibly beyond the 1250 m elevation the crust stop its thickening and shortening as a result of bouncy forces. In other words, to reach equilibrium state there is no much differential stress to continue crust thickening.

Although there is a difference in elevation patterns, and also k_{sn} and HI across the Zagros, there is similarity in the integrated relief between the different areas of the Zagros. This new approach shows a maximum difference of 20% between the different swath profiles, which most likely relates to the similar strain rates across the Zagros (Masson et al., 2005). There is not an obvious correlation with other factors, where there are differences across the range: such as climate, drainage networks and tectonic structures (Talebian and Jackson, 2004). This simple approach could be extended to other fold-and-thrust belts, such as the Himalayas and Andes.

Knickpoints didn't show notable consistency in location with thrusts in the Zagros. This is likely to be because they are blind, and so the effect on the overlying geomorphology is diffused within the folded but unfaulted sedimentary cover above each fault tip. There are two areas where knickpoints do seem to be aligned. One is the area around the active Main Recent Fault, which is a right-lateral strike-slip fault. The other is around the area of the *M* 7.3 2017 earthquake, in the vicinity of the Khanaqin Fault. Although this structure appears to be a thrust, based on the 2017 earthquake, it is unusual because of the high magnitude of the 2017, and the orientation, which gives the appearance of being a lateral ramp. With these exceptions in mind, it is unusual to find group of knickpoint near fault zone in the Zagros, and further detailed study is recommended.

Similar geomorphic analysis of the Zagros was conducted for the Himalayan range, in order to compare and contrast the two great Eurasian continental collision zones that are active on Earth. One specific issue for the Himalayas is the significance of the physiographic transition known as PT_2, and especially its relation with the Main Central Thrust (MCT); this has been taken in consideration when applying the basin scale HI and k_{sn} analysis to the Himalayan range (Chapter 4). PT_2 has previously been interpreted to be a step-change in the topography of the Himalayas, and roughly separates the Lesser Himalaya and the Greater Himalaya, is in the vicinity of the MCT. It has been interpreted to mean active, out-of-sequence deformation in the Himalayas, probably uplift as a result of a growing duplex in the sub-surface.

Himalayan topography shows that the biggest changes in the HI occur at the northern side of the Himalayas (roughly coincident with the location of the South Tibetan Detachment, STD) and the MFT in the south. There is an increase in HI across PT_2, but of smaller magnitude representing limited evidence from HI distributions for active tectonics along PT_2 or the MCT. The sharp change in HI values across the MFT is consistent with the locked portion along the MHT raising the entire crustal wedge above it.

Though the analysis of HI didn't solve the debate of the Himalayan tectonics in regard to PT_2, the consistency of the high HI values with the locked portion of the MFT (Stevens and Avouac, 2015) implies the control of the MFT on Himalayan topography, rather than the MCT or duplexing underneath PT_2 which is not necessary to initiate the high topography of the Himalayas (Elliot et al., 2016).

The Himalaya is a complicated tectonic story and there might be many interpretations in regard to fold-and-thrust belt. HI shows incredible cut-off in the front and back of the Himalaya which is not found in the Zagros. Differences in the HI result between the Himalayan and Zagros are possibly related to the differences in tectonics such as the low angle, emergent and elongated thrusts of the Himalaya, that cause different landscape signatures than the numerous non-emergent thrust faults go up to seismogenic limit of the Zagros.

It is interesting that the basin scale HI analysis is more successful in showing lateral variations in tectonics and geomorphology than analysis of individual river profiles (k_{sn}); perhaps this indicates the higher sensitivity of the HI, in the form of landscape

responses to combined tectonic and climatic drivers. Also, it could be because analysing HI by drainage basin produces a three dimensional dataset for the whole area, rather than the two-dimensional data recorded by river profiles. Moreover, HI is a regional measure across an entire landscape, and is understood to reflect the maturity of a landscape but not necessarily uplift rates, while k_{sn} is a linear measurement along river profiles, and is understood to reflect uplift along the river profile. Above that, errors of extracting river profile due to DEM resolution can be overcome in the basin-by-basin approach to HI analysis. It can be concluded from the above discussion that geomorphic indices are useful tools to pick up tectonic signals and able to differentiate between different landscape responses to tectonics of different orogenic belts (i.e. the Himalaya and the Zagros)

6.1.2 Quantify relative time of fold growth using remote sensing data

Relative time of fold growth exploiting landscape maturity in the Kirkuk Embayment (KE) of northern Iraq has been investigated (Chapter 3) using SRTM remote sensing data. The outcomes of this implementation show that the Kirkuk Anticline to the northeast, towards the hinterland, is relatively the youngest anticline; while the Himreen/Makhool Anticline to the southwest is relatively the oldest anticline (Fig 3.2). This result is based on the maturity indices extracted from remote sensing data and suggests out-of-sequence deformation towards the hinterland but not the classical ‘piggy back’ thrusting model of thrust belt propagation. This phenomenon may be because structural inversion as the thrusts below anticlines are reactivating pre-existing normal faults, rather than being entirely new structures generated during the late Cenozoic deformation. This deformation constrained by a new structural cross-section and shows limited shortening in the range of ~5%. Surface maturity index recognized previously-undescribed subsurface anticlines, which are of importance for the gas and oil industry.

Three sizes of moving windows have been tested and two kinds of datasets (SRTM 30 m and SRTM 90 m) have been used to show the importance of using suitable data, and using a moving window which is not too big or too small compared with the dimensions of major features in the studied area. Both datasets give approximate similar results, but the SRTM 90 m dataset (which is preferable) overcomes the limitations of computer efficiency and time of processing.

It is important to mention the use of the moving window approach in chapter three for mapping the HI, SR and SI indices within a relatively small area, for which a moving window approach is appropriate (i.e. Kirkuk Embayment) to pick out lateral variations in landscape. For larger areas (i.e. the whole Zagros range) the difference in the size of geological features dimensions is much higher and more variable, which lead to difficulties in finding a single suitable moving window to differentiate between different sizes of geological features and give meaningful results. The approach of automatic change of moving window according to changes in geological features dimensions requires high performance computer and high programming skills which would be a future work plan. Thus using a basin-by-basin approach is computationally easier than using a moving window. Conversely, the basin-by-basin application for a small area does not gives enough resolution as a geological feature might covered by one basin from the third order and lead to misidentification of geomorphological variations across the features under study. In turn, going into smaller basin scales such as second or first order basins will be curbed by the limitations of DEM resolution.

6.1.3 Modern river sands and tectonics

River sand petrology has not been investigated previously in the Zagros Suture zone, which exhibits very complex tectonics; the arrangement of its tectonic units is still debated. Petrological analysis of sand from rivers that drain the region of the Zagros Suture, in addition to the Neogene sandstones shows litharenite composition and recycled orogeny source for both river sand and the Neogene sandstone. River sand petrology reflects an ophiolitic signature as a result of the derivation from the Zagros Suture which in its essence is not surprising. Both river sand and Neogene sandstone exhibit a spatial distribution from lithic towards the quartz-rich end member of the QFL diagram, which probably could be temporal as interpreted by Koshnaw et al., 2017. The NW quartz-rich spatial trend could be the result of uplift and/ or changes in drainage system which requires further investigation.

Sand maturity of this study is similar to the Aqsu River sand (Fig. 5.1b), which is not directly derived from the northern suture but from the Neogene molasse (Garzanti, 2017). This suggests the northeast uplift which is maybe partially due to out-of-sequence fault re-activation of the MFF beneath Qara-Dagh Anticline (Koshnaw et

al., 2017) and the Kirkuk Fault beneath the Kirkuk Anticline (Obaid and Allen, 2017) stops sediment supply from the Suture Zone of the Zagros towards the Kirkuk Embayment (Fig. 5.16). This study and Garzanti et al. (2016) noted the trend of quartz-rich sand increasing towards the NW where the continuation of the MFF along the Agra Anticline occurs (Fig. 5.1 inset b)

Maturity indices (Chapter 3) and modern river sand petrology (Chapter 5) indicated the out-of-sequence deformation at least in the Zagros foreland (Kirkuk Embayment) which is not 'Piggyback thrusting' as commonly believed. Though the basin scale HI shows differences in landscape response to tectonics across the Zagros, the progression of deformation ("piggyback" or out-of-sequence) haven't been expressed by this analysis. This absence of a signal might be due to the occurrence of numerous and non-emergent fault segments, or it might simply be that the range of HI values is not sensitive enough to detect the fault propagation sequence. The front of deformation is defined nicely in the Himalaya by HI analysis, across the active, long-distance and emergent MFT.

6.2 Conclusions

This thesis has shown how the geomorphic indices *k*sn, HI and the topographic swath profiles vary across the Zagros fold-and-thrust belt, and suggests how these differences relate to both the structure across the range (transition from the Turkish-Iranian Plateau across the fold-and-thrust belt into the foreland), the segmented nature of the range along its length, with tectonic "salients" (Fars, Pusht-e Kuh arc) and "embayments" (Dezful, Kirkuk). Some specific conclusions are:

- The positive feedback of tectonics and climate might lead to the wetter climate in the Bakhtyari Culmination, and cause rivers to cut efficiently through landscapes and thus, high values of geomorphic indices occur, in contrast with the drier climate of the Fars region. Topographic plateau growth is inhibited in the Bakhtyari Culmination, with the transition from high to low HI occurring north of and at higher elevations than the regional 1250 m elevation contour (higher limit of thrust seismicity; Nissen et al., 2011). The drier Fars climate promotes southward plateau growth, south of the 1250 m elevation contour. The positive feedback of tectonic and climate might led to

wetter climate in the Bakhtyari Culmination and motivate rivers to cut through landscapes and thus, high value of geomorphic indices occurs, in contrast with drier climate of the Fars region which is promote southward plateau growth.

- The integrated relief across different sections of the Zagros is similar for different cross-section profiles (within ~20%), which is possibly attributed to the similar strain across the Zagros (Masson et al., 2005), regardless of the local structural fluctuations, and climatic and drainage network differences.
- Landscape maturity indices are used to examine relative timing of fold growth in the Kirkuk Embayment, and suggest out-of-sequence (retreating) deformation to the northeast, but not the classical 'piggy back' thrusting model of thrust belt propagation. This phenomenon may be because the thrusts below the anticlines are reactivating pre-existing normal faults (structural inversion), rather than being entirely new structures generated during the late Cenozoic deformation.
- The shortening in the Kirkuk Embayment is a late Cenozoic phenomenon, limited in the range of ~5% (constrained by a new structural cross-section).
- Surface Index (SI) has been proven effectively in the discovery of subdued anticlines in the Kirkuk Embayment. Two previously undescribed anticlines have been identified; potentially they can be traps of oil and gas in the region.
- The differences in the geomorphic indices *k*sn, HI and the topographic swath profiles across different areas of the Zagros (i.e. Bakhtyari Culmination and Fars) possibly relate to differences in the regional basement strength. Strong basement in the Dezful Embayment keeps the amount of strain in this region low, but produces intense thrusting and steep relief in the Bakhtyari Culmination to its northeast, so that the overall stain across this part of the Zagros is similar to adjacent regions (Allen and Talebian, 2011). It is possible that the Kirkuk Embayment has a similar origin to the Dezful Embayment, with the same consequence, that high strain is concentrated in the imbricate zone to its northeast.

The thesis has applied the geomorphic indices to examine the tectonics of the Himalayan fold-and-thrust belt, thus giving a comparative study to the Zagros work. Main conclusions are as follows:

- HI values lie in three main bands: low in the Tibetan Plateau, high across the interior of the fold-and-thrust belt, and low in the Gangetic foreland.
- The consistency between the location of the south-to-north increase of HI values and the emergent trace of the Main Frontal Thrust (MFT) suggests the efficiency of HI in showing the MFT's activity, and the major control by this structure on the Himalayan topography.
- HI results show the Miocene tectonic legacy in the Himalayas on a time scale of >10 Myr, by determining a pronounced drop in HI in the north of the range across the South Tibetan Detachment (STD).
- The debate on the role of active deformation within the Himalayan wedge has not been solved by the HI analysis, however this index offers no 'strong proof' for the out-of-sequence thrusting model of the Himalayas.
- Results from this study suggest that the *k*sn is dependent on slope and is sensitive to relative uplift rates, but this sensitivity doesn't necessarily reflect active shortening, as it may be climatically and/or lithologically controlled. In areas of different elevations and relief patterns, HI analysis by drainage basin is more representative and useful than *k*sn to detect tectonic signals in the landscape.
- Differences in the HI result between the Himalayan and Zagros are possibly related to the differences in tectonics such as the low angle, emergent and elongated thrusts of the Himalaya, that cause different landscape signatures than the numerous non-emergent thrust segments of the Zagros.

The third strand to the PhD is the analysis of modern and pre-Quaternary river sediments, based on fieldwork and sampling in part of the Iraqi Zagros. Main conclusions are:

- River sand composition of rivers north and south of Qara-Dagh Anticline characterised the out-of-sequence thrusting of the Zagros.
- Quartz contents of the Bai-Hassan and Mukdadiyah formations in the Kifri and Erbil areas might suggest different sediment sources and /or drainage reorganization.

- The relative similarity in a (modest) quartz-rich trend between the Neogene sandstone and modern river sand of the Zagros Suture region probably could be due to the latest stage of fault re-activation and uplift in the Zagros.

6.3 Implications

For those who study and are interested in the tectonic geomorphology of fold-and-thrust belts, results of this study provide good information about the application of the geomorphic indices in the investigation of landscape responses to tectonism. Relative landscape maturity will open up a possibility to understand sub-surface deformation from remote sensing data and DEMs. One example is the implementation of this method by a PhD student (Mjahid Zebari) from the University of Jena, Germany, who presented his work in the EGU 2018 Annual Meeting under the title 'Assessing Relative Landscape Maturity of Anticlines along the NW segment of Zagros Mountain Flexure, Kurdistan Region of Iraq'.

He adapted the method presented in Chapter Three and published as a paper in Tectonophysics (2017) **717,** 27–40. He is trying to develop the work using numerical modelling to a create landscape evolution model. Basin scale HI could be a suitable metric for assessing tectonic activity and gives initial impression about fault geometry and behaviour (i.e. Chapter Four). Knickpoint distribution in the zone of strike-slip faulting such as the case of the MRF (Chapter Two) would be very interesting to be study in more detail.

6.4 Suggestions for future work

Though this study proposed broad and significant results about the tectonic geomorphology of the Zagros, there are numerous unknowns that need to be investigated.

Results of this study lead to the idea of conducting further studies in the Zagros, similar to the Kirkuk Embayment study of Chapter Three, using high resolution DEMs to investigate the applicability of this technique on the different tectonic regions of the range.

For the Kirkuk Embayment, it is important to conduct Optically Stimulated Luminescence analysis for the river terraces of the Lesser Zab River in the KE. This analysis allows the determination of exhumation level across anticlines crosses by the LZR to be compared with the results of relative anticline growth calculated by SI.

Also, detailed geochronological and sedimentological studies for sandstones from many deep gorges along the Zagros will constrain the certain age, composition and sediment source of these sandstone sequences, which will help to deliver clearer images of the tectonics of the Zagros.

Terrestrial cosmogenic nuclide ^{10}Be will be a useful technique to apply to modern river sands of trunk rivers and tributaries draining the Zagros orogeny, for the purpose of constraining the exhumation and surface uplift history, which has not been investigated in this region before. It is also useful to compare the rate of uplift with the knickpoint occurrence and assess the relation between river profiles and tectonics for a specific drainage basin.

Additionally, the basin-scale HI analysis would useful to be applied to other fold-and-thrust belts such as the Andes, Atlas and Alps to understand tectonic process differences preserved in landscapes. A comparison between landscapes of active orogens such as the Himalayas and non-active orogens such as the Alps (which is thought to be presently exhumed due to ice sheet removal) will shed light on different landscape responses. Moreover, the application of the proposed geomorphic indices in this study to active rift zones would plausibly give interesting results. It might help identify regions of active deformation (and high seismic risk) from inactive fault segments.

Furthermore, climatic signals need to be tested for different fold-and-thrust belt to understand the interplay between tectonic and climate in different tectonic regions.

References

Ader, T., Avouac, J-P, Liu-Zeng, J., Lyon-Caen, H, Bollinger, L., Galetzka, J., Genrich, J., Thomas, M., Chanard, K., Sapkota, S. N., Rajaure, S., Shrestha, P., Ding, L., Flouzat, M., 2012. Convergence rate across the Nepal Himalaya and interseismic coupling on the Main Himalayan Thrust: Implications for seismic hazard, Journal of Geophysical Research, 117, B04403, doi: 10.1029/2011JB009071.

Afaghi, A, Salek, M. M., 1975. Geological map of Iran, sheet No., 5 North-west Iran, National Iranian Oil Company, Tehran, Iran, scale 1:1,000,000.

Afaghi, A, Salek, M. M., 1977. Geological map of Iran, sheet No., 2 North-Central Iran, National Iranian Oil Company, Tehran, Iran, scale 1:1,000,000.

Afaghi, A, Salek, M. M., 1977. Geological map of Iran, sheet No., 3 North-East Iran, National Iranian Oil Company, Tehran, Iran, scale 1:1,000,000.

Afaghi, A, Salek, M. M., Moazami, J., 1978. Geological map of Iran, sheet No., 1 North-west Iran, National Iranian Oil Company, Tehran, Iran, scale 1:1,000,000.

Afaghi, A, Salek, M. M., 1977. Geological map of Iran, sheet No., 6 South-East Iran, National Iranian Oil Company, Tehran, Iran, scale 1:1,000,000.

Afaghi, A, Salek, M. M., 1975. Geological map of Iran, sheet No., 4 South-West Iran, National Iranian Oil Company, Tehran, Iran, scale 1:1,000,000.

Alavi, M., 2007. Structures of the Zagros fold-thrust belt in Iran. American Journal of Science 307, 1064–1095.

Alavi, M., 2004. Regional stratigraphy of the Zagros fold-thrust belt of Iran and its proforland evolution. American Journal of Science 304, 1-20.

Alipoor, R., Pourkermani, M., Zare, Mm., El Hamdouni, R., 2011. Active tectonic assessmentaround Rudbar Lorestan dam site, High Zagros Belt (SW of Iran). Geomorphology 128, 1–14.

Allen, M. B., Saville, C., Blanc, E. J-P, Talebian, M., Nissen, E., 2013. Orogenic plateau growth:Expansion of the Turkish-Iranian Plateau across the Zagros fold-and-thrust belt. Tectonics 32, 171–190.

Allen, M. B., Armstrong, H. A., 2008. Arabia-Eurasia collision and the forcing of mid-Cenozoic global cooling. Palaeogeography, Palaeoclimatology, Palaeoecology 265, 52-58.

Allen, M. B., Talebian, M., 2011. Structural variation along the Zagros and the nature of the Dezful Embayment. Geological Magazine 148, 911–924.

Allen, M.B., Walters, R.J., Song, S.G., Saville, C., De Paola, N., Ford, J, Hu, Z.X. & Sun, W.L. (2017) Partitioning of oblique convergence coupled to the fault locking behavior of fold-and-thrust belts: Evidence from the Qilian Shan, northeastern Tibetan Plateau. Tectonics 36, 1679-1698, doi:10.1002/2017TC004476.

Al-Husseini, M. I., 2000. Origin of the Arabian Plate structures: Amar collision and Najd rift. GeoArabia, 5, 527-542.

Al-Hajri,S. A., Filatoff, J.,Wender,L. E. and Norton, A.K., 1999. Stratigraphy and operational palynology of the Devonian System in the Saudi Arabia, GeoArabia, 4, 53-68.

Ameen, M. S., 1992. Effect of basement tectonics on hydrocarbon generation, migration, and accumulation in Northern Iraq. American Association of Petroleum Geologists Bulletin 76, 356–370.

Andreani, L., Stanek, P. K., Gloaguen, R.,Krentz, Ottomar, Dominquez-Gonzalez, L., 2014.DEM-Based Analysis of Interactions between Tectonics and Landscapes in the OrMountains and Eger Rift (East Germany and NW Czech Republic). Remote Sensing 6, 7971–8001.

Aqrawi,A. M., Goff, J.C., Horbury, A.D., Sadooni, F.N., 2010. The Petroleum Geology of Iraq, First ed. Scientific Press Ltd, Aberystwyth.

Aswad, K.J., 1999. Arc-continent collision in Northeastern Iraq as evidenced byMawat and Penjwin Ophiolite Complexes. Raffidain J. Sci. 10, 51–61.

Bagha, N., Arian, M., Ghorashi, M., Pourkermani, M., El-Hamdouni,.R., Solgi, A., 2014. Evaluation of relative tectonic activity in the Tehran basin, central Alborz, northern Iran. Geomorphology 213, 66–87.

Bahrami, S., 2012. Morphotectonic evolution of triangular facets and wine-glass valleys in the Noakoh anticline, Zagros, Iran: Implications for active tectonics. Geomorphology 159–160, 37– 49.

Bahrami, S., 2013. Analyzing the drainage system anomaly of zagros basins: Implications for active tectonics. Tectonophysics 608, 914–928.

Bellen, V.R.C., Dunnington, H.V., Wetzel, R., Morton, D.M., 1959. Lexique Stratigraphique International. 3. Asie, fasc. 10a, Iraq. CNRS (Cent. Natl. Rech. Sci.), Paris.

Berberian, M., 1995. Master "blind" thrust faults hidden under the Zagros folds: active basement tectonics and surface morphotectonics. Tectonophysics 241, 193–224.

Berti, M., 2013. Copmarative analysis of surface roughness algorithms for the identification of active landslides. Geomorphology 182, 1–18.

Bettinelli, P., J.-P. Avouac, M. Flouzat, F. Jouanne, L. Bollinger, P.Willis, and G. R. Chitrakar, 2006. Plate Motion of India and Interseismic Strain in the Nepal Himalaya from GPS and DORIS Measurements. Journal of Geodesy 80, 567–589, doi: 10.1007/s00190-006-0030-3.

Bilham, R., K. Larson, J. Freymueller, and P. I. Members, 1997. GPS measurements of present-day convergence across the Nepal Himalaya. Nature 386, 61–63.

Blanc, E. J.-P., Allen, M. B., Inger, S., Hassani, H., 2003. Structural styles in the Zagros Simple Folded Zone, Iran. Journal of the Geological Society 160, 401–412.

Blythe, A. E., D. W. Burbank, A. Carter, K. Schmidt, and J. Putkonen, 2007. Plio-Quaternary exhumation history of the central Nepalese Himalaya: 1. Apatite and zircon fission track and apatite [U-Th]/He analyses. Tectonics 26, 1–16, doi: 10.1029/2006TC001990.

Bookhagen, B., and D. W. Burbank 2006. Topography, relief, and TRMM-derived rainfall variations along the Himalaya, Geophysical Research Letters, 33(8), L08,405–, doi:10.1029/2006GL026037.

Bollinger, L., P. Henry, and J. Avouac, 2006. Mountain building in the Nepal Himalaya: Thermal and kinematic model. Earth and Planetary Science Letters 244, 58–71, doi:10.1016/j.epsl.2006.01.045.

Boulton, S.J., Stokes, M. and Mather, A.E., 2014. Transient fluvial incision as an indicator of active faulting and Plio-Quaternary uplift of the Moroccan High Atlas. Tectonophysics 633, 16-33.

Boulton, S.J. and Whittaker, A.C., 2009. Quantifying the slip rates, spatial distribution and evolution of active normal faults from geomorphic analysis: Field examples from an oblique-extensional graben, southern Turkey. Geomorphology 104, 299-316.

Boulton, S.J. and Stokes, M., 2018. Which DEM is best for analyzing fluvial landscape development in mountainous terrains?. Geomorphology 310, 168-187.

Boroujerdy, P., Nasrollahi, N., Hsu, K., Sorooshian, S., 2013. Evaluation of satellite-based precipitation estimation over Iran. Journal od Arid Environments 97, 205–219.

Bowman, D., Shachnovich-Firtel, Y., Devora, S., 2007. Stream channel convexity induced by continuous base level lowering, the Dead Sea, Israel. Geomorphology 92, 60–75. doi:10.1016/j.geomorph.2007.02.009.

Bretis, B., Bartl, N., Grasemann, B., 2011. Lateral fold growth and linkage in the Zagros fold and thrust belt (Kurdistan, NE Iraq). Basin Research 23, 615–630.

Burbank, D. W., Anderson, R. S. 2002. Tectonic geomorphology, second ed. Wiley-Blackwell, USA.

Burberry, C.M., Cosgrove, J.W. and Liu, J.G., 2008. Spatial arrangement of fold types in the Zagros Simply Folded Belt, Iran, indicated by landform morphology and drainage pattern characteristics. Journal of Maps 4, 417-430.

Burberry, C. M., Cosgrove, J. W. Liu, J.-G., 2010. A study of fold characteristics and deformation style using the evolution of the land surface: Zagros Simply Folded Belt, Iran. Geological Society, London, Special Publications 330,139-154.

Burberry, C. M. 2015. The effect of basement faults reactivation on the Triassic-

Recent geology of Kurdistan , North Iraq. Journal of Petroleum Geology 38, 37–58.

Cannon, J.M., Murphy, M.A., Taylor, M., 2018. Segmented strain accumulation in the High Himalaya expressed in river channel steepness. Geosphere 14, 1131-1149.

Crosby, B.T., Whipple, K.X., 2006. Knickpoint initiation and distribution within fluvial networks, 236 waterfalls in the Waipaoa River, North Island, New Zealand. Geomorphology 82, 16–38.

Casciello, E., Vergés, J., Saura, E., Casini, G., Fernandez, N., Blanc, E., Homke, S., Hunt, D.W., 2009. Fold patterns and multilayer rheology of the Lurestan Province, Zagros Simply Folded Belt (Iran). Journal of the Geological Society 166, 947–959.

Davoudzadeh, M., Lensch, G.,Weber-Dierenbach, K., 1986. Contribution to the paleogeography, stratigraphy and tectonics of the Infracambrian and Lower Paleozoic of Iran. Neues Jahrbuch für Geologie und Paläontologie Abhandlungen 172, 245–269.

Dehbozorgi, M., Pourkermani, M., Arian, M., Matkan, A. A., Motamedi, H., Hosseiniasl, A., 2010. Quantitative analysis of relative tectonic activity in the Sarvestan area, central Zagros, Iran. Geomorphology 121, 329–341.

Dickinson, W.R., 1970. Interpreting detrital modes of graywacke and arkose. Journal of Sedimentary Research, 40, 695-707.

Dickinson, W.R., Suczek, C.A., 1979. Plate tectonics and sandstone compositions. American Association of Petroleum Geologists Bulletin 63 , 2164–2182.

Dickinson, W.R., 1985. Interpreting provenance relations from detrital modes of sandstones. In: Zuffa, G.G. (Ed.), Provenance of Arenites. D. Reidel, Dordrecht, 333–361.

Dickinson, W.R., Beard, L.S., Brakenridge, G.R., Erjavec, J.L., Ferguson, R.C., Inman, K.F., Knepp, R.A., Lindberg, F.A., Ryberg, P.T., 1983. Provenance of North American Phanerozoic sandstones in relation to tectonic setting. Geological Society of America Bulletin 94, 222–235.

Dietrich, W.E., Bellugi, D.G., Heimsath, A.M., Roering, J.J., Sklar, L.S., Stock, J.D.,

2003. Geomorphic Transport Laws for Predicting Landscape Form and Dynamics. Geophys. Monogr. 135, 1–30.

Domínguez-González, L., Andreani, L., Stanek, K. P., Gloaguen, R.,, 2015. Geomorpho-tectonicevolution of the Jamaican restraining bend. Geomorphology 228, 320–334.

Dott, R.H., 1964. Wacke, greywacke, and matrix –what approach to immature sandstone classification? Journal of Sedimentary Petrology 34, 625-632.

Dunnington, H. V. 1958. Generation, migration, accumulation and dissipation of oil in Northern Iraq. Journal of Petroleum Geology (special publications), 1192–1251.

Dupont-Nivet, G., P. C. Lippert, D. J. Van Hinsbergen, M. J. Meijers, and P. Kapp , 2010. Palaeolatitude and age of the Indo-Asia collision: palaeomagnetic constraints. Geophysical Journal International 182, 1189–1198.

Ehsani, J., Arian, M., 2015. Quantitative analysis of relative tectonic activity in the Jarahi-Hindujan basin area, Zagros, Iran. Geosciences Journal. DOI:10.1007/s12303-015- 0016–3

El Hamdouni, R., Irigaray, C., Fernandez, T., Chacon, J., Keller, E. A., 2008. Assessment ofrelative active tectonics, southwest border of the Sierra Nevada (southern Spain). Geomorphology 96, 150 –173.

El Harfi, A., Lang, J., Salomon, J., Chellai, E.H., 2001. Cenozoic sedimentary dynamics of the Ouarzazate foreland basin (central High Atlas Mountains, Morocco). International Journal of Earth Sciences 90, 393–411.

El Harfi, A., Guiraud, M., Lang, J., 2006. Deep-rooted “thick skinned” model for the High Atlas Mountains (Morocco). Implications for the structural inheritance of the southern Tethys passive margin. Journal of Structural Geology 28, 1958–1976.

Elliott, J. R., Jolivet, R., González, P. J., Avouac, J.-P., Hollingsworth, J., Searle, M. P., Stevens, V. L., 2016. Himalayan megathrust geometry and relation to topography revealed by the Gorkha earthquake. Nature Geoscience 9, 174-180.

English, J.M., Lunn, G.A., Ferreira, L., Yacu, G., 2015. Geologic evolution of the Iraqi Zagros, and its influence on the distribution of hydrocarbons in the Kurdistan region. American Association of Petroleum Geologists Bulletin 99, 231–272.

Fakhari, M.D., Axen, G. J., Horton, B.K., Hassanzadeh, J., Amini, A. , 2008. Revised age of proximal deposits in the Zagros foreland basin and implication for Cenozoic evolution of the High Zagros. Tectonophysics, 451, 170–185.

Farahpour, M. M., Hessami, K., 2012. Cretaceous sequence of deformation in the SE Zagrosfold-thrust belt. Journal of the Geological Society 169, 733–743.

Fard, N. G., Sorbi, A., Arian, M., 2015. Active Tectonics of Kangavar Area. Open Journal of Geology 5, 422–441.

Flint, J.J., 1974. Stream gradient as a function of order, magnitude, and discharge. Water Resources Research 10, 969–973.

Folk, R.L., 1980. Petrology of Sedimentary Rocks. Hemphill Publication Company, Austin,Texas (182 pp).

Font, M., Amorese, D., Lagarde, J. L., 2010. DEM and GIS analysis of the stream gradient index to evaluate effects of tectonics: The Normandy intraplate area (NW France). Geomorphology 119, 172–180.

Fouad, S., 2015. Tectonic map of Iraq, scale 1:1000,000. Iraqi Bulletin of Geology and Mining 11, 1–7.

Gao, M., Zeilinger, G., Xu, X., Tan, X. Wang, Q., Hao, M., 2016. Active tectonics evaluation from geomorphic indices for the central and the southern Longmenshan range on the Eastern Tibetan Plateau, China. Tectonics 35, 1812–1826,

Ghasemi, A., Talbot, C., 2006. A new tectonic scenario for the Sanandaj-Sirjan Zone (Iran). Journal of Asian Earth Sciences 26, 683–693.

Garzanti, E., Al-juboury, A.I., Zoliekhaei, Y., Vermeesch, P., Jothgeri, J., Akkoca, D.B., Obaid, A. K., Allen, M., And`o, S., Limonta, M., Padoan, M., Resentini, A., Rittner, M., Vezzoli, G., 2016, The Euphrates–Tigris–Karun river system:

provenance, recycling and dispersal of quartz-poor foreland-basin sediments in arid climate: Earth-Science Reviews 162, 107–128.

Garzanti, E., 2017. The sedimentary myth in sedimentology and provenance analysis. Journal of Sedimentary Research 87, 353-365.

Gazzi, P., 1966. Le arenarie del flysch sopracretaceo dell'Appennino modenese: Correlazioni con il flysch di Monghidoro. Mineral. Petrogr. Acta 12, 69–97.

Godard, V., Bourles, D.L., Spinabella, F., Burbank, D.W., Bookhagen, B., Fisher, G.B., Moulin, A., Leanni, L., 2014. Dominance of tectonics over climate in Himalayan denudation. Geology 42, 243-246.

Goldrick, G., Bishop, P., 2007. Regional analysis of bedrock stream long profiles: evaluation of Hack's SL form, and formulation and assessment of an alternative (the DS form). Earth SurfaceProcesses and Landforms 32, 649–6714. doi:10.1002/esp.

Grohmann, C. H., 2004. Morphometric analysis in geographic information systems: Applications of free software GRASS and R. Computers and Geosciences 30, 1055–1067.

Guest, B., Stockli, D.F., Grove, M., Axen, G.j., Lam, P.S., Hassanzadeh, j., 2006. Thermal histories from the central Alborz Mountains, northern Iran: Implications for the spatial and temporal distribution of deformation in northern Iran. Geological Society of America Bulletin 118, 1507–1521.

Habba, Y.A., Samarrai,A., Al/Jubouri, F, Georgis, N. N. and Ahmed I. M., 1994. Exploration of the Palaeozoic prospects in western Iraq, part 1: Exploratin of the Palaeozoic system in western Iraq. Proceedings of the second siminar on hydrocarbon potential of deep formations in the Arab countries (OAPEC), Cairo 10-13October (in Arabic).

Hack, J.T., 1957. Studies of Longitudinal Stream Profiles in Virginia and Maryland. United State Geological Survey Professional Paper 294-B, 97.

Hani, A. F., Sathyamoorthy, D., Asirvadam, V. S., 2012. Computing surface roughness of individual cells of digital elevation models via multi scale analysis.

Computers & Geosciences 43, 13–146.

Harkins, N., Kirby, E., Heimsath, A., Robinson, R., Reiser, U., 2007. Transient fluvial incision in the headwaters of the Yellow River, northeastern Tibet, China. Journal of Geophysical Research Earth Surface 112, F03S04.

Harmar, O.P., Clifford, N.J., 2007. Geomorphological explanation of the long profile of the Lower Mississippi River. Geomorphology 84, 222–240.

Harvey, J.E., Burbank, D.W., Bookhagen, B., 2015. Along-strike changes in Himalayan thrust geometry: Topographic and tectonic discontinuities in western Nepal. Lithosphere 7, 511-518.

Hessami, K., Koyi, H. A., Talbot, C. J., Tabasi, H., Shabanian, E., 2001. Progressive unconformities within an evolving foreland fold-thrust belt, Zagros Mountains. Journal of theGeological Society 158, 969–981.

Hodges, K.V., Hurtado, J.M., Whipple, K.X., 2001. Southward extrusion of Tibetan crust and its effect on Himalayan tectonics. Tectonics 20, 799-809.

Hodges, K.V., Hurtado, J.M., Whipple, K.X., 2001. Southward extrusion of Tibetan crust and its effect on Himalayan tectonics. Tectonics 20, 799-809.

Hoke, G.D., Isacks, B.L., Jordan, T.E., Blanco, N., Tomlinson, A.J., Ramezani, J., 2007. Geomorphic evidence for post-10 Ma uplift of the western flank of the central Andes 18°30′– 22°S. Tectonics 26, TC5021.

Holbrook, J., Schumm, S. A., 1999. Geomorphic and sedimentary response of rivers to tectonic deformation: a brief review and critique of a tool for recognizing subtle epeirogenic deformation in modern and ancient settings. Tectonophysics 305, 287–306.

Hurtrez, J.-E., F. Lucazeau, J. Lavé, and J.-P. Avouac, 1999. Investigation of the relationships between basin morphology, tectonic uplift, and denudation from the study of an active fold belt in the Siwalik Hills, central Nepal. Journal of Geophysical Research: Solid Earth 104, 12779–12796.

Ingersoll, R.V., Bullard, T.F., Ford, R.F., Grimm, J.P., Pickle, J.D., Sares, S.W., 1984. The effect of grain size on detrital modes: a test of the Gazzi-Dickinson point-counting method. Journal of Sedimentary Petrology 54, 103–116.

Jackson, J., van Dissen, R. and Berryman, K., 1998. Tilting of active folds and faults in the Manawatu region, New Zealand: evidence from surface drainage patterns. New Zealand Journal of Geology and Geophysics 41 , 377-385.

Jassim, S. Z., Goff, J.C., 2006. Geology of Iraq, first ed. Dolin Prague and Moravian Museum, Prague (341pp).

Jones, R., 2002. Algorithms for using a DEM for mapping catchment areas of stream sediment samples. Computers & Geosciences 28, 1051–1060.

Jones, S.J., 2004. Tectonic controls on drainage evolution and development of terminal alluvial fans, southern Pyrenees, Spain. Terra Nova 16, 121-127.

Jones, S.J., Arzani, N. and Allen, M.B., 2014. Tectonic and climatic controls on fan systems: the Kohrud mountain belt, Central Iran. Sedimentary Geology 302, 29-43.

Karim, K. H. Koyi, H., Baziani, M. M., Hessami, K., 2011. Significance of angular unconformities between Cretaceous and Tertiary strata in the northwestern segment of the Zagros fold–thrust belt, Kurdistan Region, NE Iraq. Geological Magazine 148, 925–939.

Keller, E. , Pinter, N., 2002. Active Tectonics: Earthquakes,Uplift, and Landscape. PrenticeHall, New Jersey.

Kent, W. N., 2010. Structures of the Kirkuk Embayment, northern Iraq: Foreland structures or Zagros Fold Belt structures? GeoArabia 15, 147–188.

Kirby, E., Whipple, K., 2001. Quantifying differential rock-uplift rates via stream profile analysis. Geology 29, 415–418.

Kirby, E., Whipple, K.X., Tang, W., Chen, Z.,2003. Distribution of active rock uplift along the eastern margin of the Tibetan plateau:inferences from bedrock river profiles. Journal of Geophysical Research 108, 2217.

Kirby, E., Johnson, C., Furlong, K., Heimsath, A., 2007. Transient channel incision along Bolinas Ridge, California: evidence for differential rock uplift adjacent to the San Andreas Fault. J. Geophys. Res. 112, F03S07.

Kirby, E., Whipple, K. X., 2012. Expression of active tectonics in erosional landscapes. Journal of Structural Geology 44, 54–75.

Koshnaw, R.I., Horton, B.K., Stockli, D.F., Barber, D.E., Tamar-Agha, M.Y., Kendall, J.J.,2017. Neogene shortening and exhumation of the Zagros fold-thrust belt and foreland basin in the Kurdistan region of northern Iraq. Tectonophysics 694, 332–355.

Kottek, M., Grieser, j., Beck, C., Rudolf, B.,Rubel, F., 2006. World Map of the Koppen-Geiger climate classification updated. Meteorologische Zeitschrift 15, 259–263.

Krynine P.D., 1948. The megascopic study and field classification of sedimentary rocks. Geology 56, 130-165.

Lacombe, O., Mouthereau, F., Kargar, S. and Meyer, B., 2006. Late Cenozoic and modern stress fields in the western Fars (Iran): implications for the tectonic and kinematic evolution of central Zagros. Tectonics, 25(1).

Langbein, W. B. et al., 1947. Topographic characteristics of drainage basins. United State Geological Survey W.-S. Paper 968-C, 125-157.

Larue, J.P., 2008. Effects of tectonics and lithology on long profiles of 16 rivers of the southern Central Massif border between the Aude and the Orb (France). Geomorphology 93, 343–367.

Lawa, F., Koyi, H., Ibrahim, A., 2013. Tectono-stratigraphic evolution of the NW segment of the Zagros fold-thrust belt, Kurdistan, NE Iraq. Journal of Petroleum Geology 36, 75–96.

Lavé, J., Avouac, J., 2000. Active folding of fluvial terraces across the Siwaliks Hills, Himalayas of central Nepal. Journal of Geophysical Research 105, 5735-5770.

Lavé, J., and J. Avouac, 2001. Fluvial incision and tectonic uplift across the Himalayas of central Nepal. Journal of Geophysical Research 106, 561–26,

Mahmood, S. A., Gloaguen, R., 2012. Appraisal of active tectonics in Hindu Kush:Insights from DEM derived geomorphic indices and drainage analysis. Geoscience Frontiers 3, 407– 428.

Masson, F., Ch´ery, J., Hatzfeld, D., Martinod, J., Vernant, P., Tavakoli, F., Ghafory-Ashtiani, M., 2005. Seismic versus aseismic deformation in Iran inferred from earthquakes and geodetic data. Geophysical Journal International 160, 217-226.

Mazhari, S. A., Bea, F., Amini, S., Ghalamghash, J., Molina, J. F., Montero, P., Scarrow, J.H. and Williams, I.S., 2009. The Eocene bimodal Piranshahr massif of the Sanandaj–Sirjan Zone, NW Iran: a marker of the end of the collision in the Zagros orogen. Journal of the Geological Society 166, 53-69.

McBride, E. F., 1963. A classification of common sandstones. Journal of Sedimentary Petrology 33, 664-669.

McQuarrie, N., Stock, J.M., Verdel,C., Wernicke, B.P., 2003. Cenozoic evolution of the Neotethys and implication for the causes of plate motions. Geophysicsal Research Letters 30, 2036.

McQuarrie, N., 2004. Crustal scale geometry of the Zagros fold-thrust belt, Iran. Journal of Structural Geology. 26, 519–535.

McQuarrie, N., van Hinsbergen, D. J., 2013. Retrodeforming the Arabia-Eurasia collision zone: Age of collision versus magnitude of continental subduction. Geology 41, 315–318.

Meigs, A. J., D. W. Burbank, and R. A. Beck, 1995. Middle – late Miocene (>10 Ma) formation of the Main Boundary thrust in the western Himalaya. Geology 23, 423 – 426.

Miller, S.R., Baldwin, S.L., Fitzgerald, P.G., Al, M.E.T., 2012. Transient fl uvial incision and active surface uplift in the Woodlark Rift of eastern Papua New Guinea.

Mohammed, S., 2006. Megaseismic section across the northeastern slope of the Arabian Plate, Iraq. GeoArabia 11, 77–90.

Molinaro, M., Leturmy, P., Guezou, J.-C., Frizon de Lamotte, D.&Eshraghi, S.A., 2005. The structure and kinematics of the southeastern Zagros foldthrust belt, Iran: from thin-skinned to thick-skinned tectonics, Tectonics, 24, TC3007.

Montgomery, D.R., Foufoula-Georgiou, E., 1994. Channel Network Source Representation Using Digital Elevation Models. Water Resources Research 29, 3925 3934.

Morell, K.D., Kirby, E., Fisher, D.M., Van Soest, M., 2012. Geomorphic and exhumational response of the Central American Volcanic Arc to Cocos Ridge subduction. Journal of Geophys.ical Research: Solid Earth 117.

Morell, K.D., Sandiford, M., Kohn, B., Codilean, A., Fülöp, R.H. and Ahmad, T., 2017. Current strain accumulation in the hinterland of the northwest Himalaya constrained by landscape analyses, basin-wide denudation rates, and low temperature thermochronology. Tectonophysics 721, 70-89.

Mosavi, E. J. Arian, M., Ghorshi,M., Nazemi, M., 2015. Neotectonics of Tabas Area, CentralIran by Index of Active Tectonics (IAT). Open Journal of Geology 5, 209–223.

Mouthereau, F., Lacombe, O., Vergés, J., 2012. Building the Zagros collisional orogen: timing, strain distribution and the dynamics of Arabia/Eurasia plate convergence. Tectonophysics 532, 27–60.

Murphy, M.A., Taylor, M.H., Gosse, J., Silver, C.R.P., Whipp, D.M., Beaumont, C., 2014. Limit of strain partitioning in the Himalaya marked by large earthquakes in western Nepal. Nature Geoscience 7, 38-42.

Nakata, T., 1989. Active faults of the Himalaya of India and Nepal. Geological Society of America Special Paper 232, 243-264.

Neimann, J.D., Gasparini, N.M., Tucker, G.E., Bras, R.L., 2001. A quantitative evaluation of Playfair's law and its use in testing long-term stream erosion models. Earth Surface Processes and Landforms 26, 1317–1332.

Nicholson, U., VanLaningham, S. and Macdonald, D.I., 2013. Quaternary landscape evolution over a strike-slip plate boundary: Drainage network response to incipient orogenesis in Sakhalin, Russian far east. Geosphere 9, 588-601.

Nissen, E. Tatar, M., Jackson, J. A., Aleen, M. B., 2011.New views on earthquake faulting inthe Zagros fold-and-thrust belt of Iran. Geophysical Journal International 186, 928–944.

Numan, N. M. S., 2000. Major Cretaceous tectonic events in Iraq. Journal of Science 11, 32-52.

Obaid, A.K. and Allen, M.B., 2017. Landscape maturity, fold growth sequence and structural style in the Kirkuk Embayment of the Zagros, northern Iraq. Tectonophysics 717, 27-40.

Ohmori, H., 1993. Changes in the hypsometric curve through mountain building resulting fromconcurrent tectonics and denudation. Geomorphology 8, 263–277.

Okay, A. I., Zattin, M., Cavazza, W., 2010. Apatite fission-track data for the Miocene Arabia-Eurasia collision. Geology 38, 35–38.

Olivetti, V., Cyr, A.J., Molin, P., Faccenna, C., Granger, D.E., 2012. Uplift history of the Sila Massif, southern Italy, deciphered from cosmogenic 10Be erosion rates and river longitudinal profile analysis. Tectonics 31, 1–19.

Othman, A.A., Al-Saady, Y.I., Al-Fares, F.J., Al-Maamar, A.F., Al-Rubaiay, A.T., 2004. Geomorphological study of Makhul dam reservoir – Makhmor. GEOSURV, Iraq Internal Report 2924.

Othman, A., Gloaguen, R., 2014.Improving Lithological Mapping by SVM Classification of Spectral and Morphological Features: The Discovery of a New Chromite Body in the MawatOphiolite Complex (Kurdistan, NE Iraq). Remote Sensing 6, 6867– 6896.

Pérez-Peña, J. V. et al., 2009. Differentiating geology and tectonics using a spatial autocorrelation technique for the hypsometric integral. Journal of Geophysical Research: Earth Surface 114, 1–15.

Perotti, C., Chiariotti, L., Bresciani, I, Cattaneo, L., Toscani, G., 2016. Evolution and timing of salt diapirism in the Iranian sector of the Persian Gulf. Tectonophysics 679, 180–198.

Pettijohn, F.T., 1954. Classification of sandstones. Geology 62, 360-365.

Phillips, J.D., Lutz, J.D., 2008. Profile convexities in bedrock and alluvial streams. Geomorphology 102, 554–566.

Pike, R. J., Wilson, S. E., 1971. Elevation-relief ratio, hypsometric integral, and geomorphicarea-altitude analysis. Bulletin of the Geological Society of America 82, 1079–1084.

Ramsey, L. A., Walker, T., Jackson, J., 2008. Fold evolution and drainage development in the Zagros mountains of Fars province , SE Iran. Basin Research 20, 23– 48.

Rodriguez, E., Morris, C., Belz, J., 2006. A global assessment of the SRTM performance.Photogrammetric Engineering and Remote Sensing 72, 249–260.

Saleh, D. K., 2010. Stream gage descriptions and streamflow statistics for sites in the Tigris River and Euphrates River Basins, Iraq. U.S. Geological Survey Data Series 540, 7–108.

Saura, E., Garcia-Castellanos, D., Casciello, E., Parravano, V., Urruela, A., Vergés, J., 2015. Modeling the flexural evolution of the Amiran and Mesopotamian foreland basins of NW Zagros (Iran-Iraq). Tectonics 34:377–395.

Saville, C., 2013. Fluvial and tectonic geomorphology of orogenic plateaux. Unpublished PhD dissertation, Durham University, http://etheses.dur.ac.uk/7718/.

Schildgen, T.F., Cosentino, D., Bookhagen, B., Niedermann, S., Yildirim, C., Echtler, H.,Wittmann, H., Strecker, M.R., 2012. Multi-phased uplift of the southern

margin of the Central Anatolian plateau, Turkey: A record of tectonic and upper mantle processes. Earth Planetary Science Letters 317-318, 85–95.

Schumm, S.A., 1956. Evolution of drainage systems and slopes in badlands at perth amboy, New jersey. Geological Society of America Bulletin. 67, 597–646.

Schumm, S.A., 1963. A tentative classification of alluvial river channels. U.S. Geologica Survey Circular V477.

Searle, M. P., and L. Godin, 2003. The South Tibetan Detachment and the Manaslu Leucogranite: A structural reinterpretation and restoration of the Annapurna-Manaslu Himalaya, Nepal. Journal of Geology 111, 505 – 523.

Seeber, L., Gornitz, V., 1983. River profiles along the Himalayan arc as indicators of active tectonics. Tectonophysics 92, 335-367.

Şengör, A.M.C., Özeren, S., Genç, T., Zor, E., 2003. East Anatolian high plateau as a mantle supported, north-south shortened domal structure: The Turkey seismic experiment: The study of a young continent-continent collision. Geophysical Research Letters 30, TUR 8-1.

Shahzad, F., Gloaguen, R., 2011a. TecDEM: A MATLAB based toolbox for tectonic geomorphology, Part 1: Drainage network preprocessing and stream profile analysis. Computers and Geosciences 37, 250–260.

Shahzad, F., Gloaguen, R., 2011b. TecDEM: A MATLAB based toolbox for tectonic geomorphology, Part 2: Surface dynamics and basin analysis. Computers and Geosciences 37, 261–271.

Sharland, P.R., Archer, R., Casey, D.M., Davies, R.B., Hall, S.H., Heward, A.P., Horbury, A.D., Simmons, M.D., 2001. Arabian Plate Sequence Stratigraphy. Geo Arabia Special Publication, p. 2.

Sherkati, S., Molinaro, M., Frizon de Lamotte, D. & Letouzey, J., 2005. Detachment folding in the Central and Eastern Zagros fold-belt (Iran): salt mobility, multiple detachments and late basement control. Journal of Structural Geology 27, 1680-1696.

Siddiqui, S., 2014. Appraisal of Active Deformation Using DEM-based

Morphometric Indices Analysis in Emilia-Romagna Apennines, northern Italy. Geodynamics Research International Bulletin 1, 34– 42.

Singh, T., Jain, V., 2009. Tectonic constraints on watershed development on frontal ridges: Mohand Ridge, NW Himalaya, India. Geomorphology 106, 231–241.

Sissakian, K. V., 1993. The Geology of Kirkuk Quadrangle sheet No. NI–38–2, Scale 1:250,000. GEOSURV, Baghdad, Iraq.

Sissakian, K. V., 1995. The Geology of AL-Mosul Quadrangle sheet No. NJ–38–13, Scale1:250,000. GEOSURV, Baghdad, Iraq.

Sissakian, V.K., 2000. Geological Map of Iraq, Geological Survey and Mining, Baghdad, Iraq, Scale 1:1,000,000.

Sissakian, V.K., 2013. Geological evolution of the Iraqi Mesopotamia Foredeep, inner platform and near surroundings of the Arabian Plate. Journal of Asian Earth Sciences 72,152-163.

Snyder, N.P., Whipple, K.X., Tucker, G.E., Merritts, D.J., 2000. Stream profiles in the Mendocino triple junction region, northern California. Geological Society of America Bull. 112, 1250–1263.

Stampfli, G.M., Borel , G.D., 2002. A plate tectonic model for the Paleozoic and Mesozoic constrained by dynamic plate boundaries and restored synthetic oceanic isochrons . Earth and Planetary Science Letters 196, 17-33.

Stern, R. J., Johnson, P., 2010. Continental lithosphere of the Arabian Plate: A geologic,petrologic, and geophysical synthesis. Earth-Science Reviews 101, 29–67.

Stevens, V.L. and Avouac, J.P., 2015. Interseismic coupling on the main Himalayan thrust. Geophysical Research Letters 42, 5828-5837.

Strahler, A., 1952. Hypsometric (area-altitude) analysis of erosional topology. Bulletin of the Geological Society of America 63, 1117–1142.

Talbot, C.J. and Alavi, M., 1996. The past of a future syntaxis across the Zagros. Geological Society, London, Special Publications 100, 89-109.

Talebian, M., Jackson, J., 2002. Offset on the Main Recent Fault of NW Iran and

implications for the late Cenozoic tectonics of the Arabia-Eurasia collision zone. Geophysical Journal International 150, 422–439.

Tavani, S., Parente, M., Puzone, F., Corradetti, A., Gharabeigli, G., Valinejad, M.,Morsalnejad, D., Mazzoli, S., 2018. The seismogenic fault system of the 2017 Mw 7.3 Iran–Iraq earthquake: constraints from surface and subsurface data, cross-section balancing, and restoration. Solid Earth 9, 821–831.

Thiede, R.C., Bookhagen, B., Arrowsmith, J.R., Sobel, E.R., Strecker, M.R., 2004. Climatic control on rapid exhumation along the Southern Himalayan Front. Earth and Planetary Science Letters 222, 791-806.

Vera, J., De Gines, J., 2009. Structure of the Zagros fold and thrust belt in the Kurdistan Region, northern Iraq. Trabajos de Geología, Universidad de Oviedo 29, 213–217.

Vergés, J.Saura, E., Casciello, E., Fernandez, M., Villasenor, A., Jimenez-Mount, I., Garcia-Castellanos, D., 2011. Crustal-scale cross-sections across the NW Zagros belt: implications for the Arabian margin reconstruction. Geological Magazine 148, 739–761.

Vernant, P., Nilforoushan, F., Hatzfel, D., Abbassi, M. R., Vigny, C., Masson, F., Nankali, H., Matinod, J., Ashtiani, A., Bayer, R., Tavakoli, F., Chery,J., 2004. Present-day crustal deformation and plate kinematics in the Middle East constrained by GPS measurements in Iran and northern Oman. Geophysical Journal International 157, 381–398.

Walcott, R., Summerfield, M, 2008. Scale dependence of hypsometric integrals: An analysis of southeast African basins. Geomorphology 96, 174–186.

Walker, R. T., Ramsey, L. A., Jackson, J., 2011. Geomorphic evidence for ancestral drainage patterns in the Zagros Simple Folded Zone and growth of the Iranian plateau. Geological Magazine 148, 901-910.

Whipple, K.X. and Tucker, G.E., 1999. Dynamics of the stream-power river incision model: Implications for height limits of mountain ranges, landscape response

timescales, and research needs. Journal of Geophysical Research: Solid Earth 104, 17661-17674.

Whipple, K.X., Tucker, G.E., 2002. Implications of sediment-flux dependent river incision models for landscape evolution. Journal of Geophysical Research: Solid Earth 107 (B2).

Whipple, K.X., 2004. Bedrock Rivers and the Geomorphology of Active Orogens. Annual Review Earth Planetary Science 32, 151–185.

Whipple, K.X., Shirzaei, M., Hodges, K.V., Arrowsmith, J.R., 2016. Active shortening within the Himalayan orogenic wedge implied by the 2015 Gorkha earthquake. Nature Geoscience 9, 711-716.

White, N.M., Pringle, M., Garzanti, E., Bickle, M., Najman, Y., Chapman, H., Friend, P., 2002. Constraints on the exhumation and erosion of the High Himalayan Slab, NW India, from foreland basin deposits. Earth and Planetary Science Letters 195, 29-44.

Whittaker, A.C., Cowie, P. A., Attal, M., Tucker, G. E., Roberts, G. P., 2007. Contrasting transient and steady-state rivers crossing active normal faults: new field observations from the Central Apennines, Italy. Basin Research 19, 529–556.

Whittaker, A.C., Attal, M, Cowie, P. A., Tucker, G. E., Roberts, G., 2008. Decoding temporal and spatial patterns of fault uplift using transient river long profiles. Geomorphology 100, 506–526.

Whittaker, A.C., , S.J., 2012. Tectonic and climatic controls on knickpoint retreat rates and landscape response times. Journal of Geophysical Research: Earth Surface 117, F02024.

Wobus, C.W., Hodges, K. V., Whipple, K.X., 2003. Has focused denudation sustained active thrusting at the Himalayan topographic front? Geology 31, 861–864.

Whol, E. A., Merritt, D. M., 2001. Bedrock channel morphology. Geological Society of America Bulletin 113, 1205–1212.

Yılmaz, Y., Güner, Y., Şaroğlu, F., 1998. Geology of the Quaternary volcanic centres of the East Anatolia. Journal of Volcanology and Geothermal Research 85, 173–210.

Yin, A., 2006. Cenozoic tectonic evolution of the Himalayan orogen as constrained by along-strike variation of structural geometry, exhumation history, and foreland sedimentation. Earth-Science Reviews 76, 1-131.

Zebari, M.M. and Burberry, C.M., 2015. 4-D evolution of anticlines and implications for hydrocarbon exploration within the Zagros Fold-Thrust Belt, Kurdistan Region, Iraq. GeoArabia 20, 161-188.

Zhang, Z., Xiao, W., Majidifard, M.R., Zhu, R., Wan, B., Ao, S., Chen, L., Rezaeian, M. and Esmaeili, R., 2017. Detrital zircon provenance analysis in the Zagros Orogen, SW Iran: implications for the amalgamation history of the Neo-Tethys. International Journal of Earth Sciences 106, 1223-1238.

Zwaid, A. Q., 1993.The Geology of AL-Qaiyara Quadrangle sheet No. NI–38–1, Scale1:250,000. GEOSURV, Baghdad, Iraq.

Appendices

Appendix 1: Stratigraphic columns (after Al-Rawi et al., 1992 in Aqrawi et al., 2010) of the Fat'ha, Injanah, Mukdadiyah, and Bai Hassan formation from their type locality in the Makhool/Himreen Anticline (Fig 3.2 chapter three).

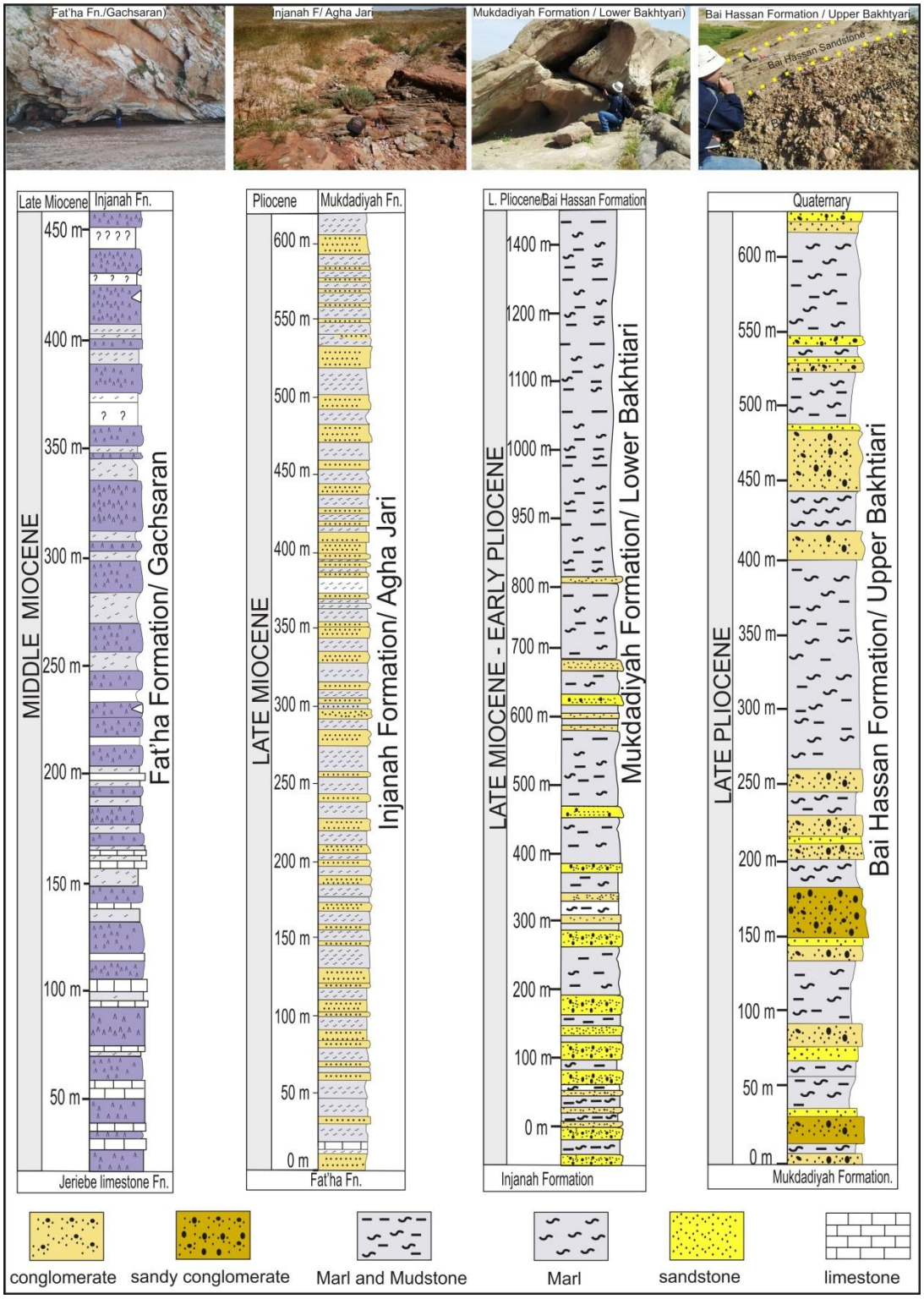

Appendix 2: River profile analysis of rivers in the MRF and KH zones.

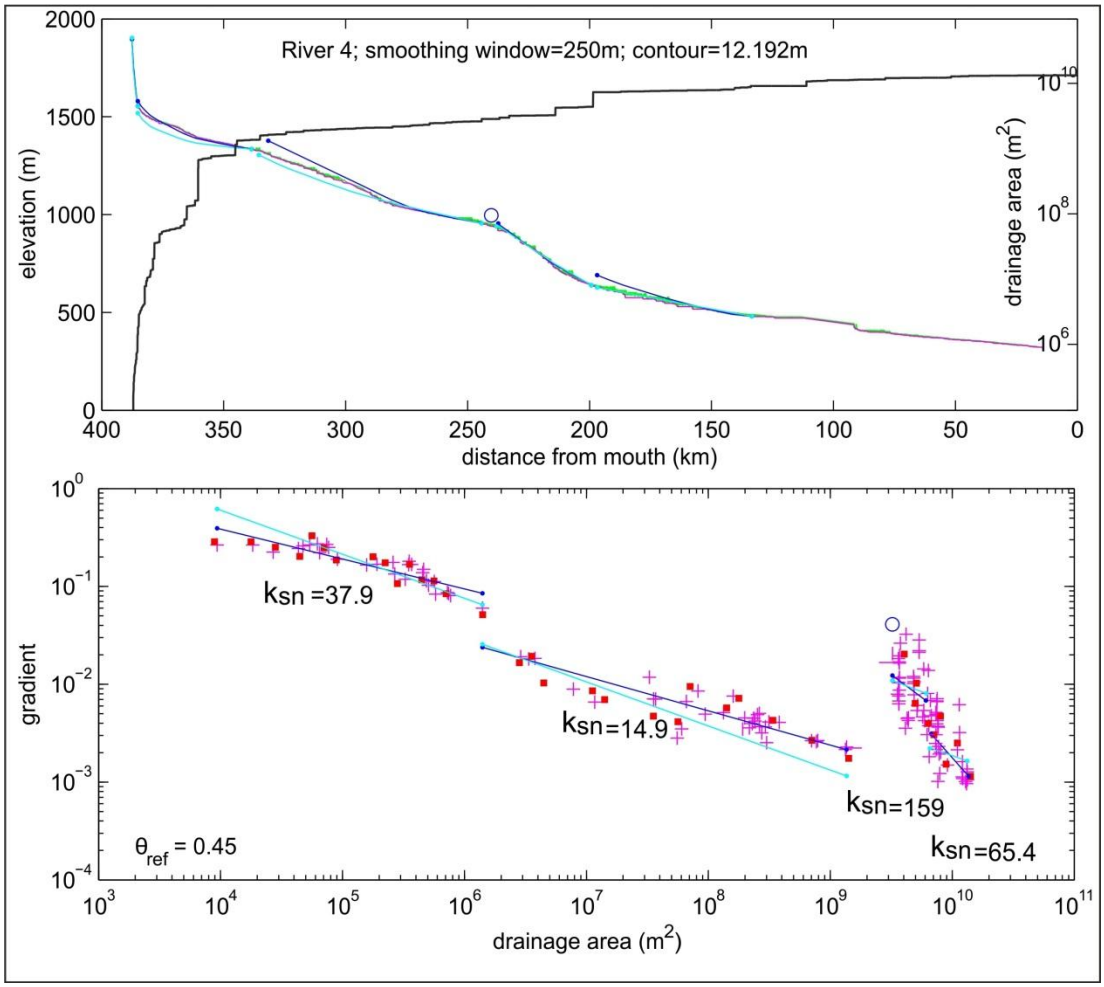

Appendix 2-1. River profile analysis of the river segment in Fig. 2.23 shows slop-break knickpoint in the Main Recent Fault zone.

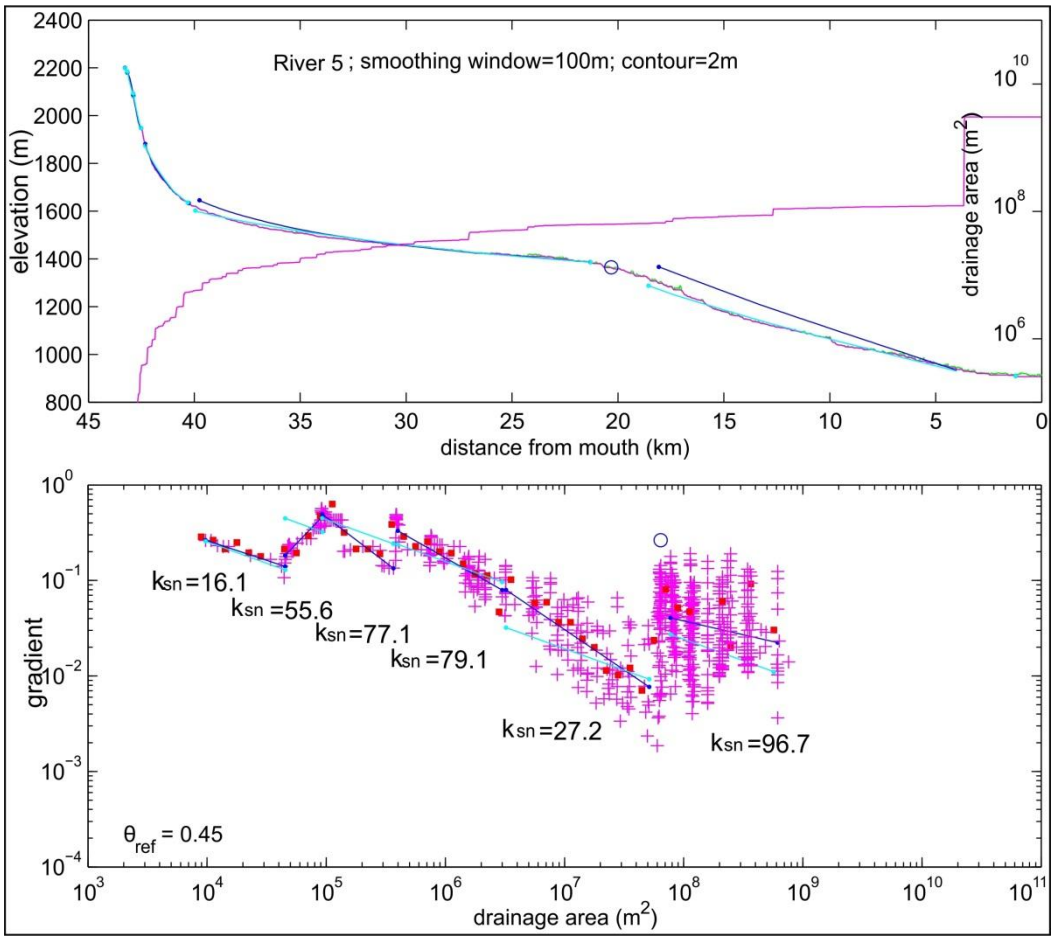

Appendix 2-2. River profile analysis of the river segment in Fig. 2.23 shows knickpoint and high steepness value below knickpoint in the Main Recent Fault zone.

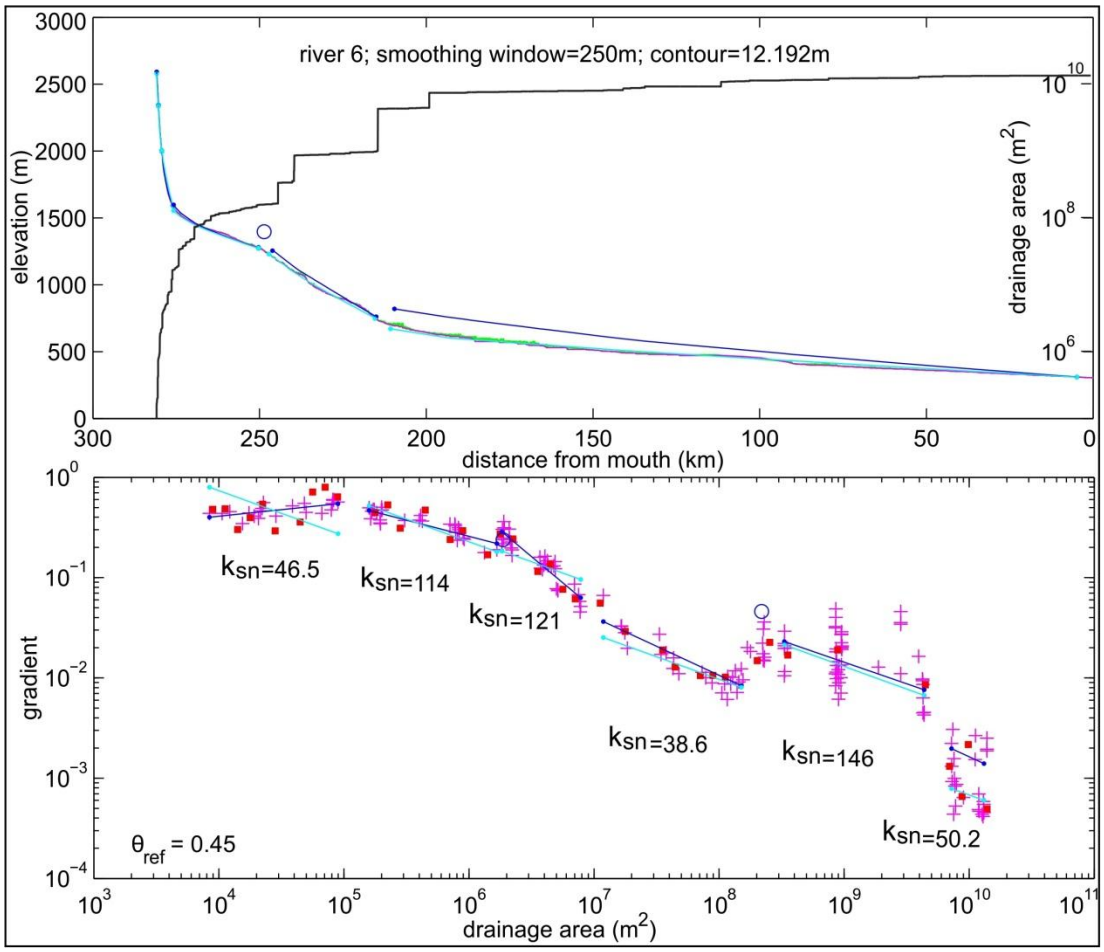

Appendix 2-3. River profile analysis of the river segment in Fig. 2.23 shows knickpoint and rising steepness value below it in the Main Recent Fault zone.

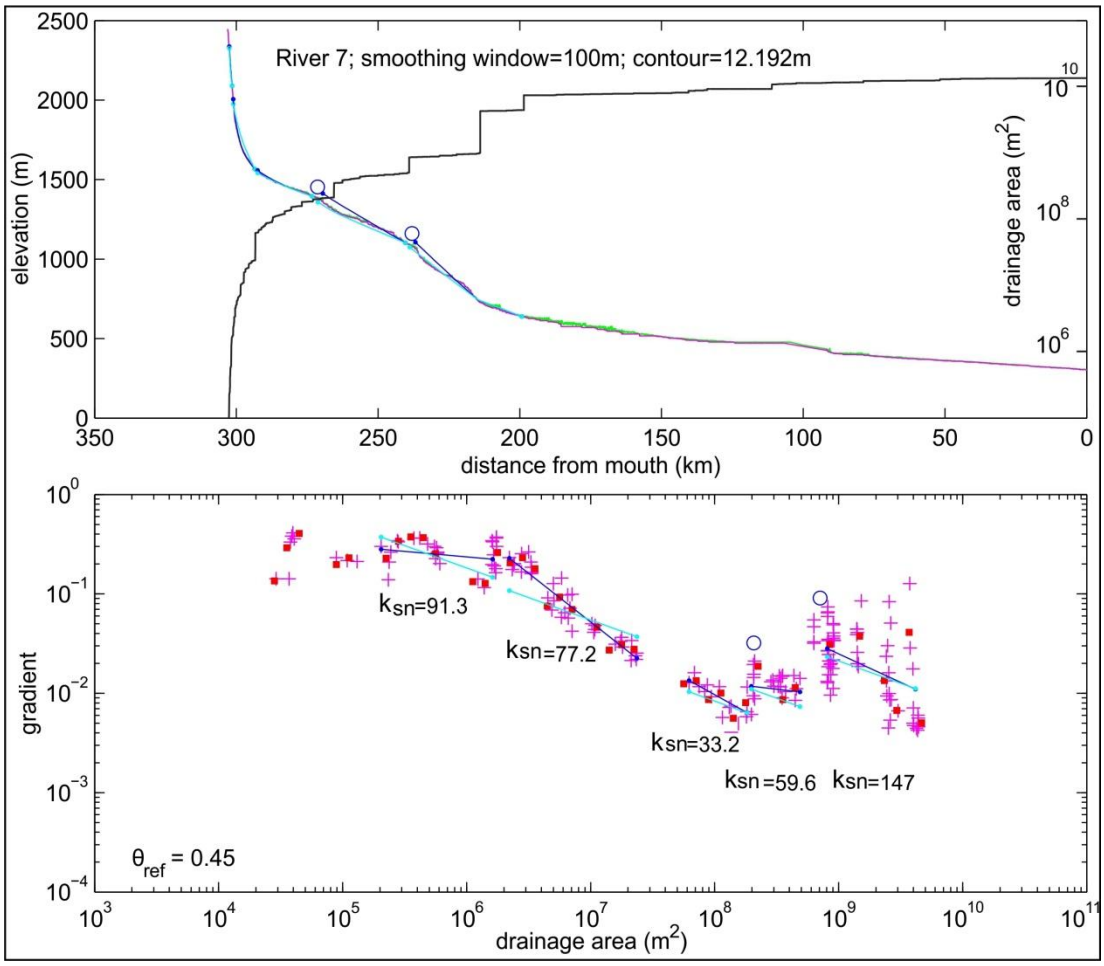

Appendix 2-4. River profile analysis of the river segment in Fig. 2.23 shows two slop-break knickpoint in the Main Recent Fault zone.

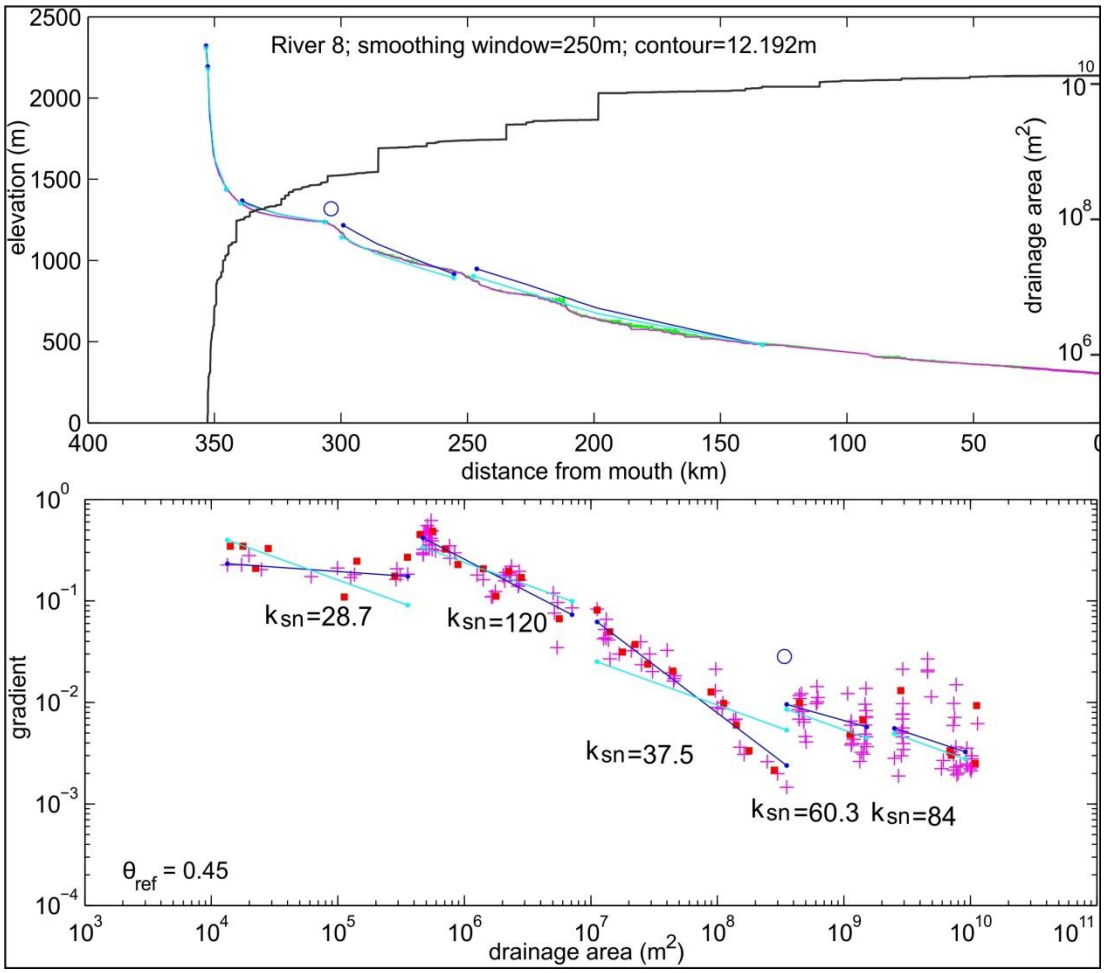

Appendix 2-5. River profile analysis of the river segment in Fig. 2.23 shows clear slop-break knickpoint in the Main Recent Fault zone.

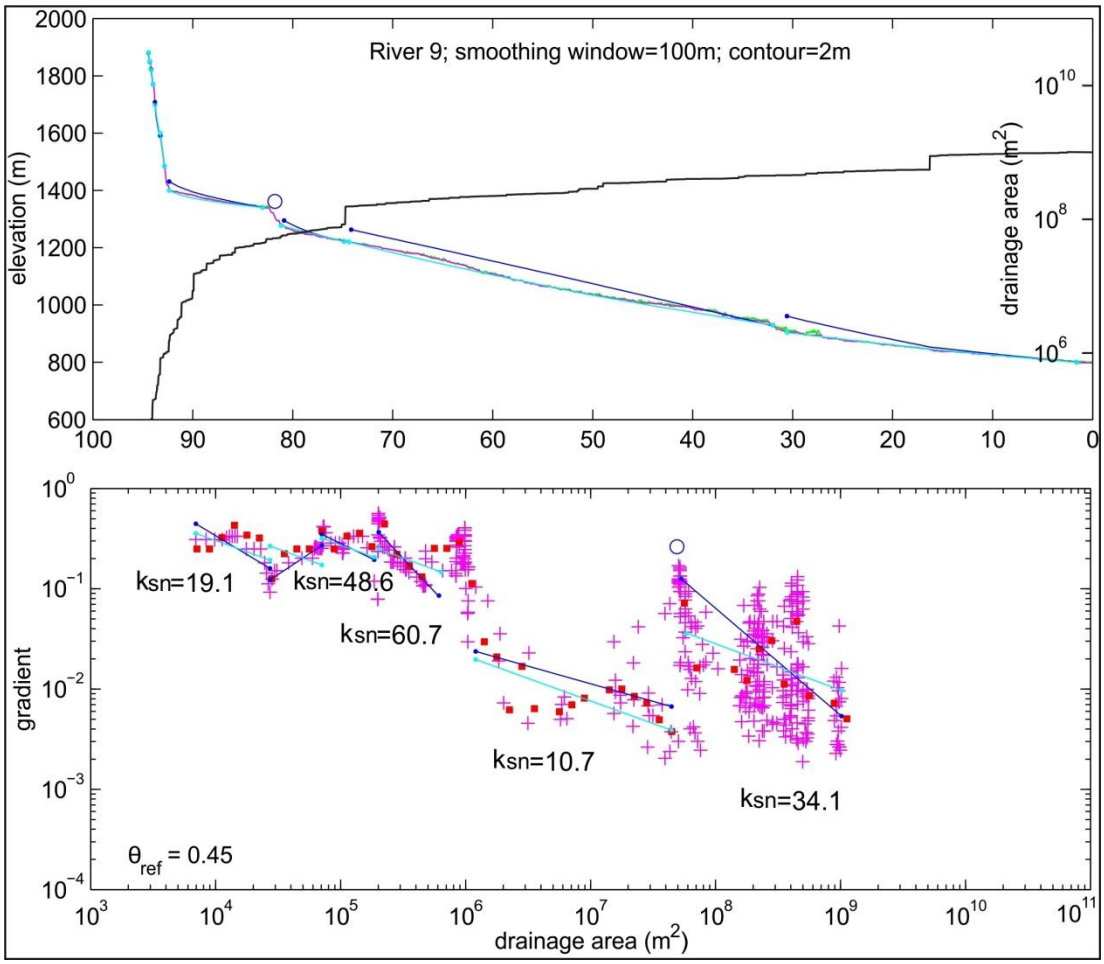

Appendix 2-6. River profile analysis of the river segment in Fig. 2.23 shows typical slop-break knickpoint in the Main Recent Fault zone.

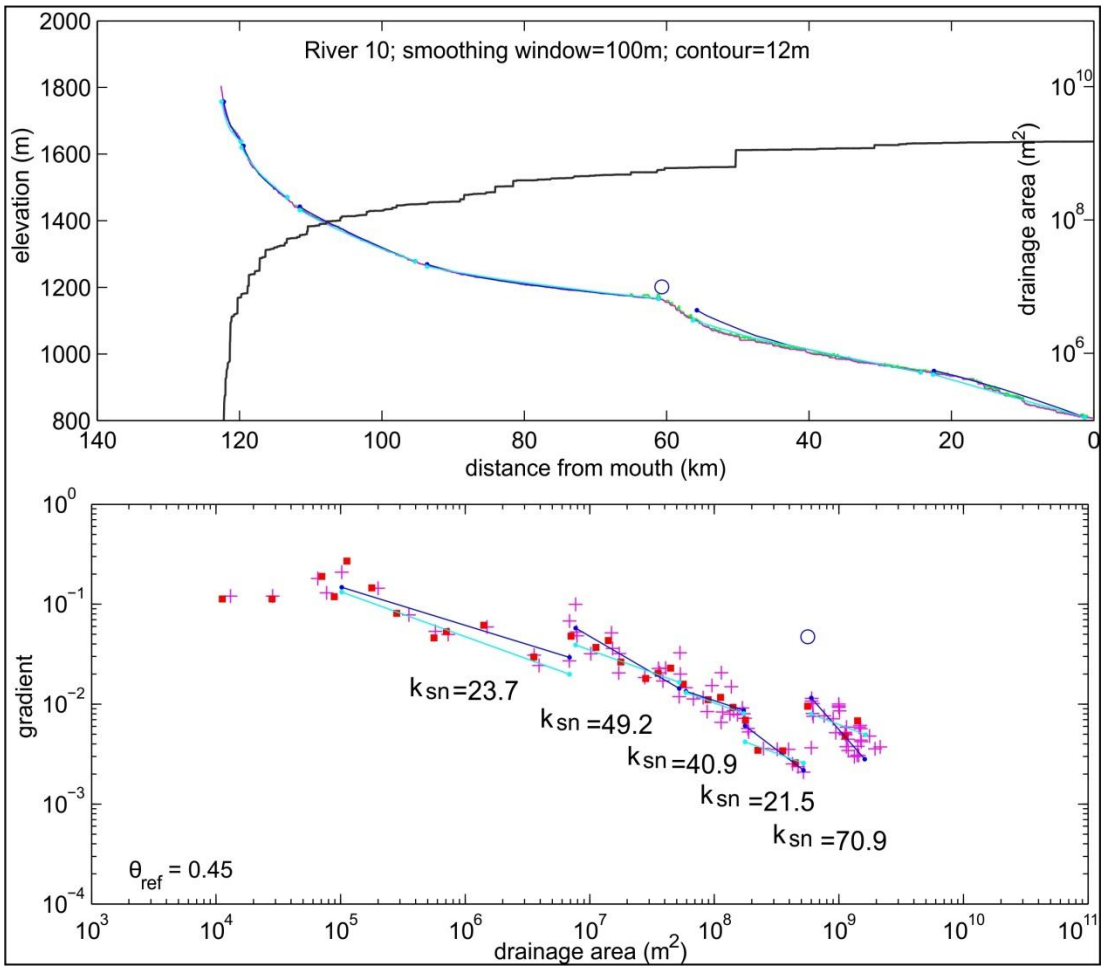

Appendix 2-7. River profile analysis of the river segment in Fig. 2.23 shows slop-break knickpoint in the Main Recent Fault zone.

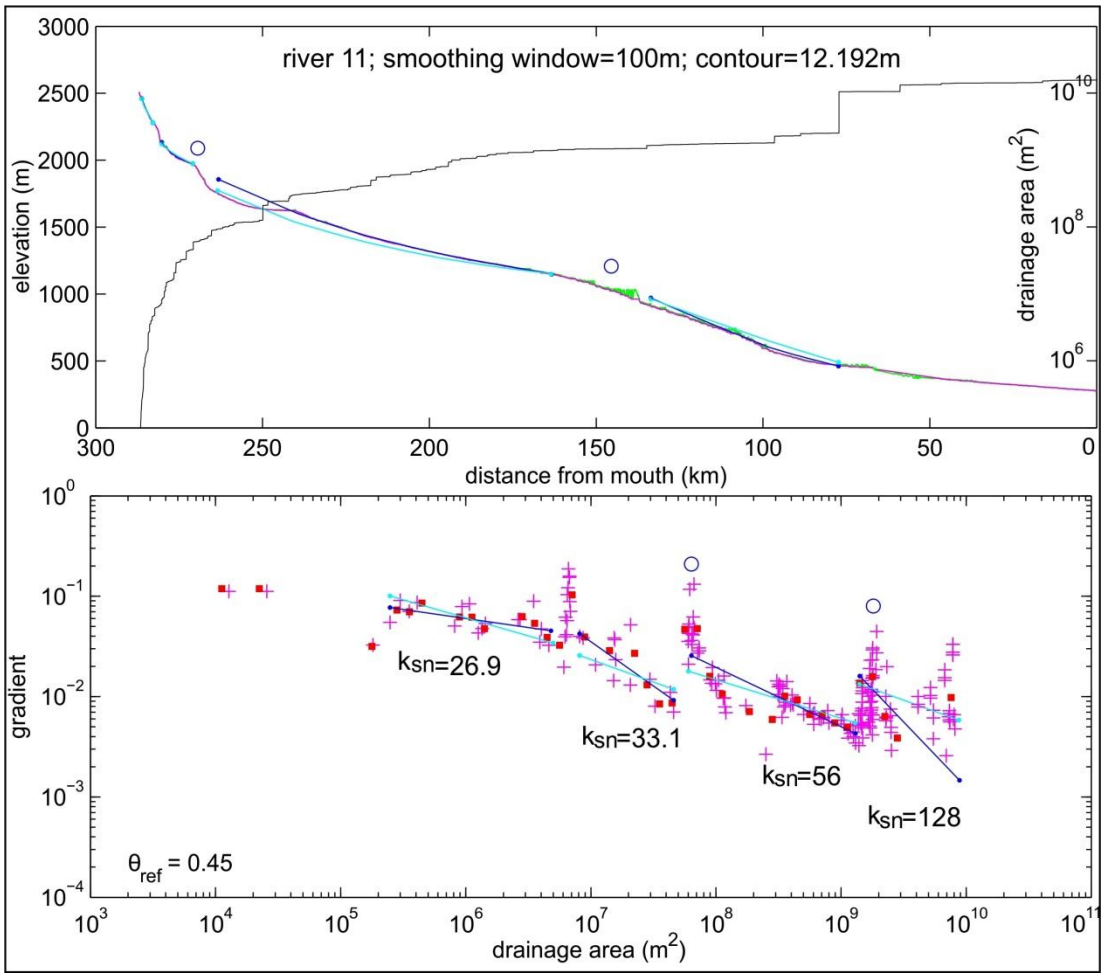

Appendix 2-8. River profile analysis of the river segment in Fig. 2.27 shows slop-break knickpoint in the Khanaqin zone.

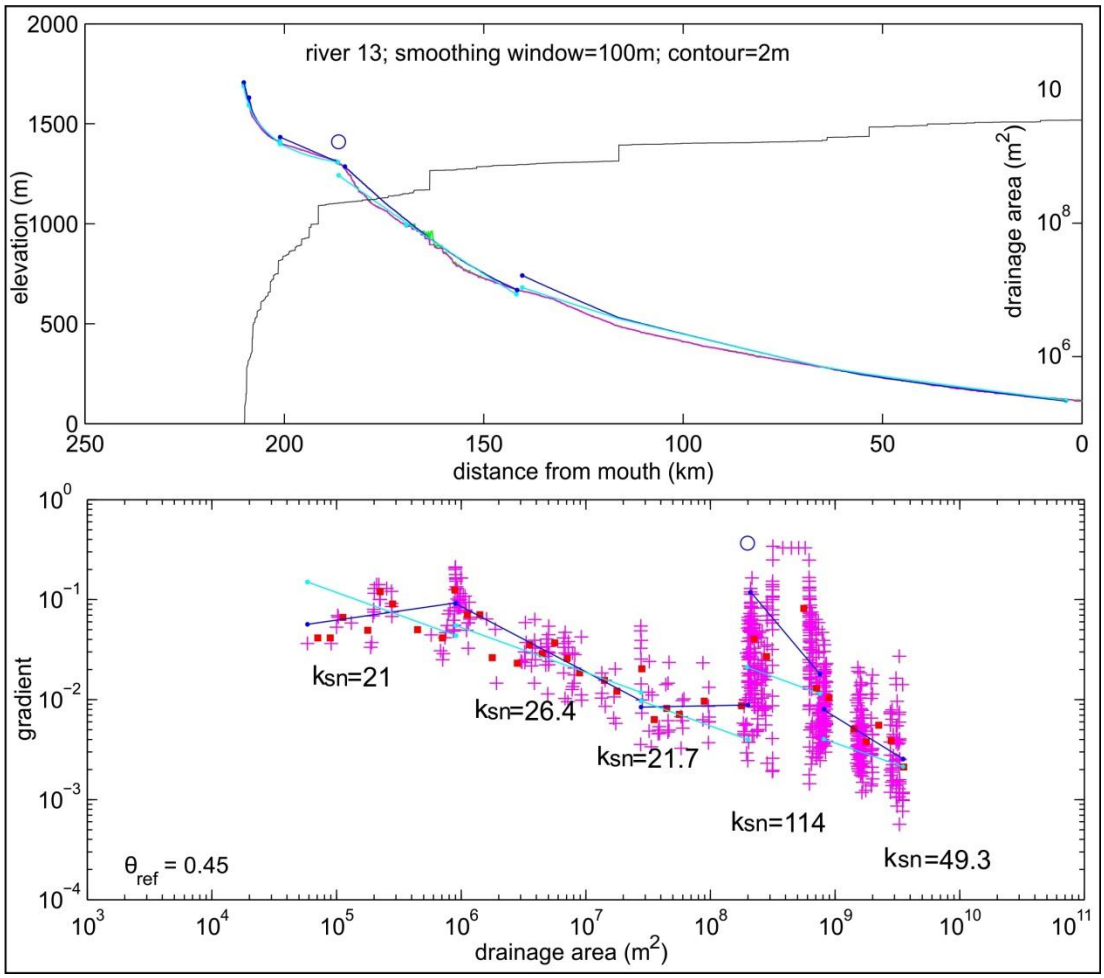

Appendix 2-9. River profile analysis of the river segment in Fig. 2.27 shows slop-break knickpoint in the Khanaqin zone.

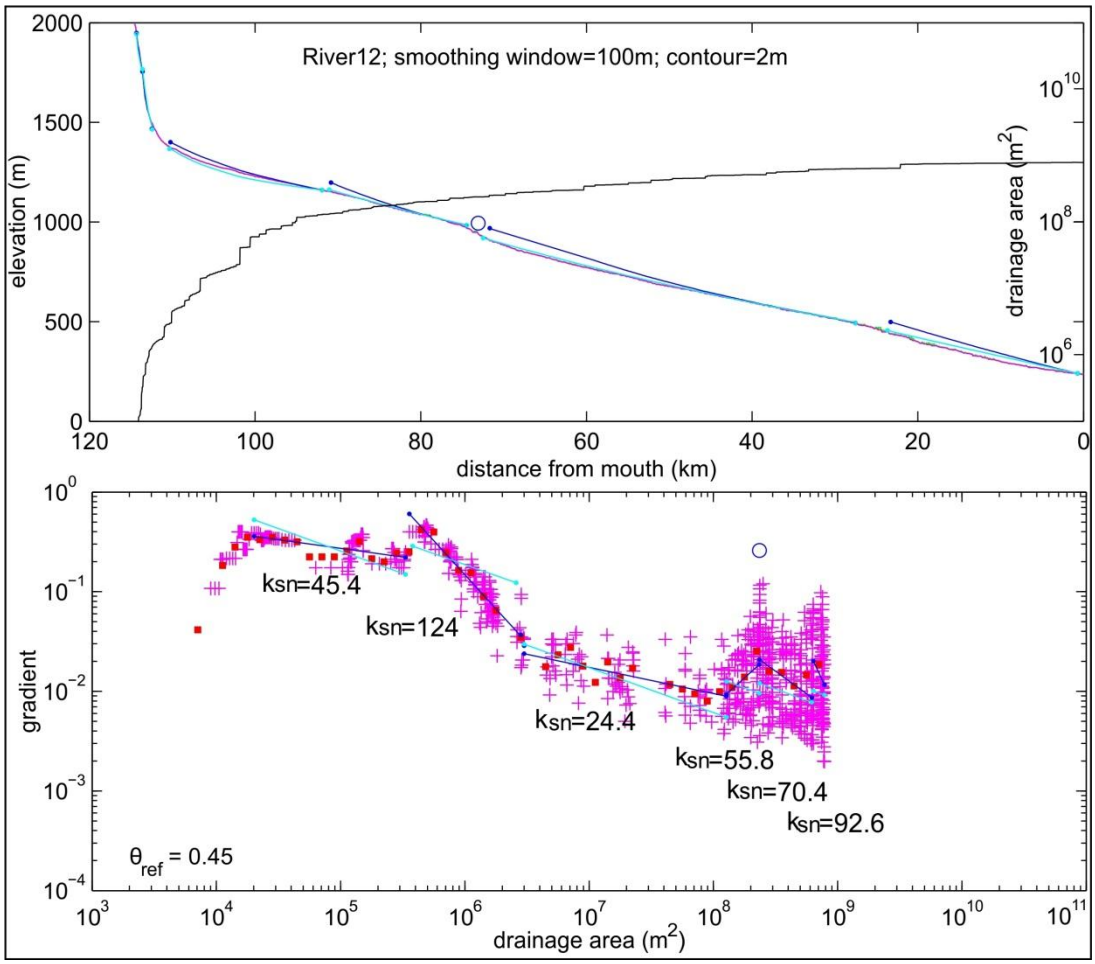

Appendix 2-10. River profile analysis of the river segment in Fig. 2.27 shows slop-break knickpoint in the Khanaqin zone.

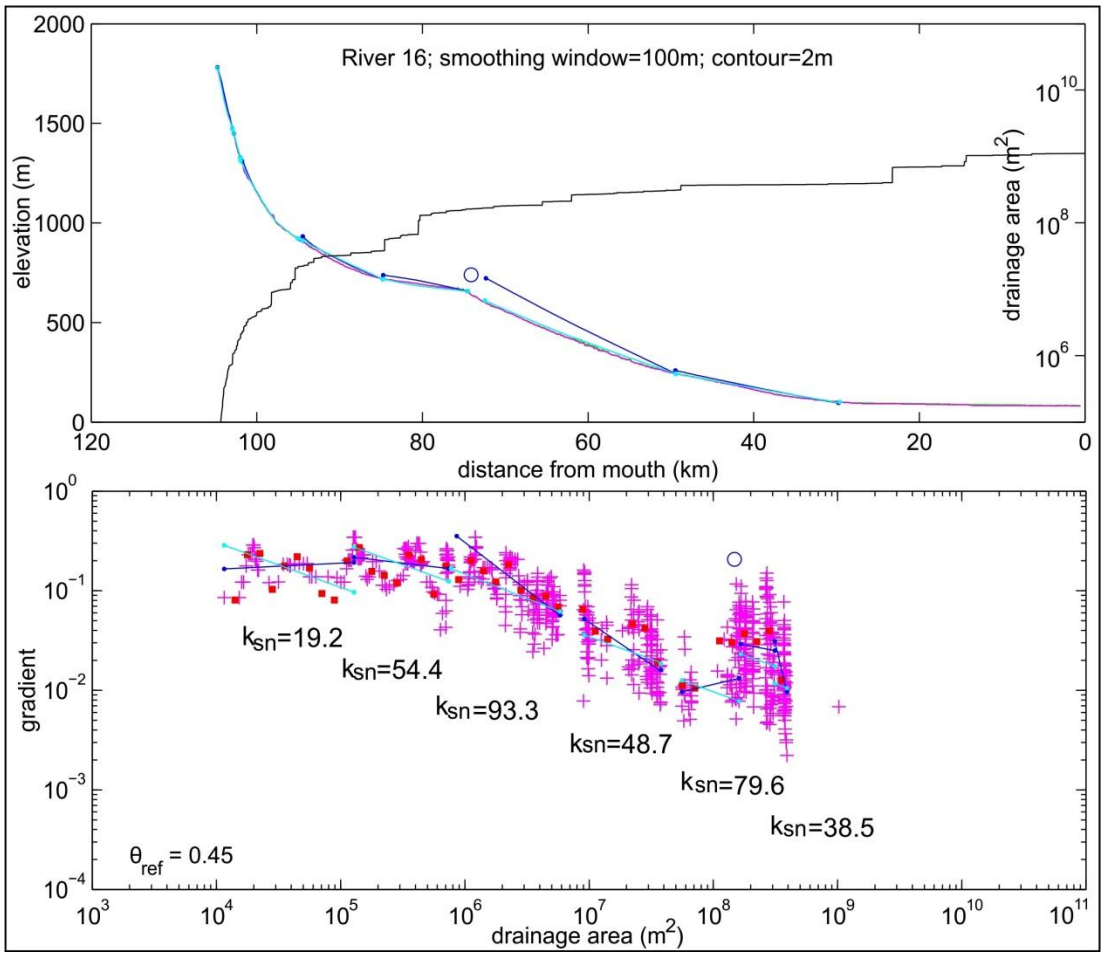

Appendix 2-11. River profile analysis of the river segment in Fig. 2.27 shows slop-break knickpoint in the Khanaqin zone.

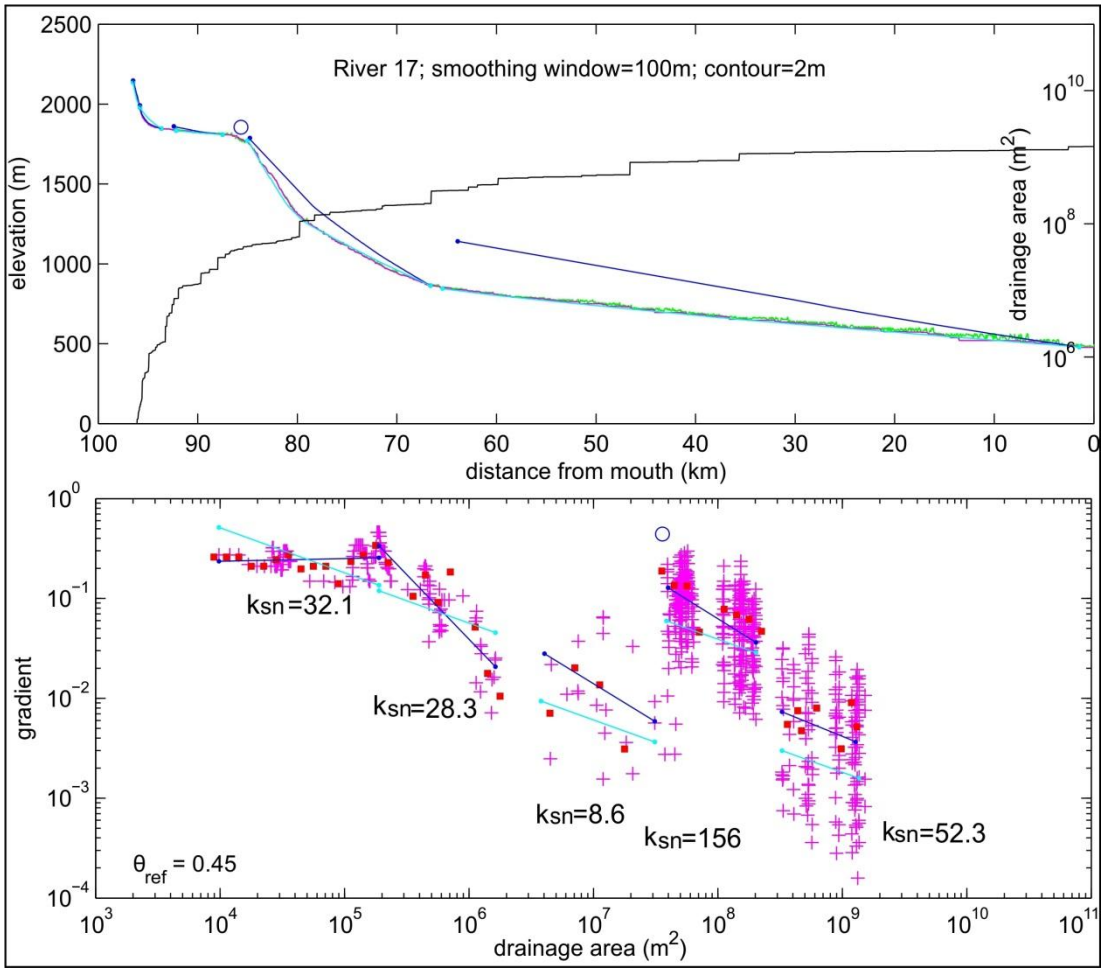

Appendix 2-12. River profile analysis of the river segment in Fig. 2.27 shows slop-break knickpoint in the Khanaqin zone.

Appendix 3-1: method adapted to calculate Sinuosity index.

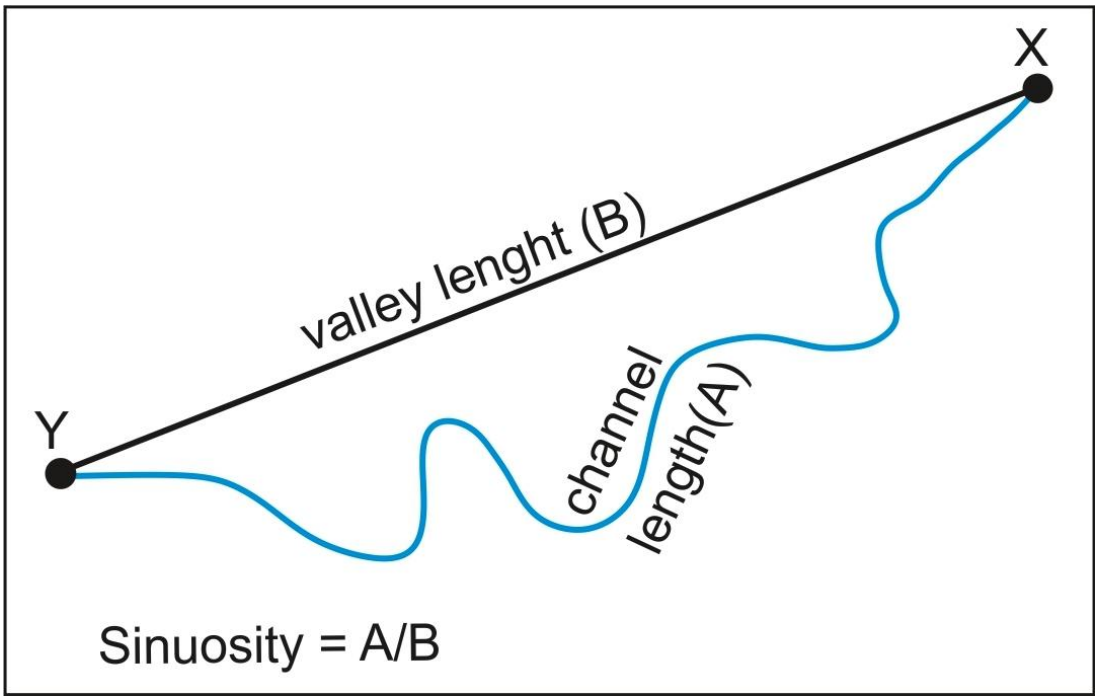

Appendix 3-2: Method of testing different datasets and different moving windows

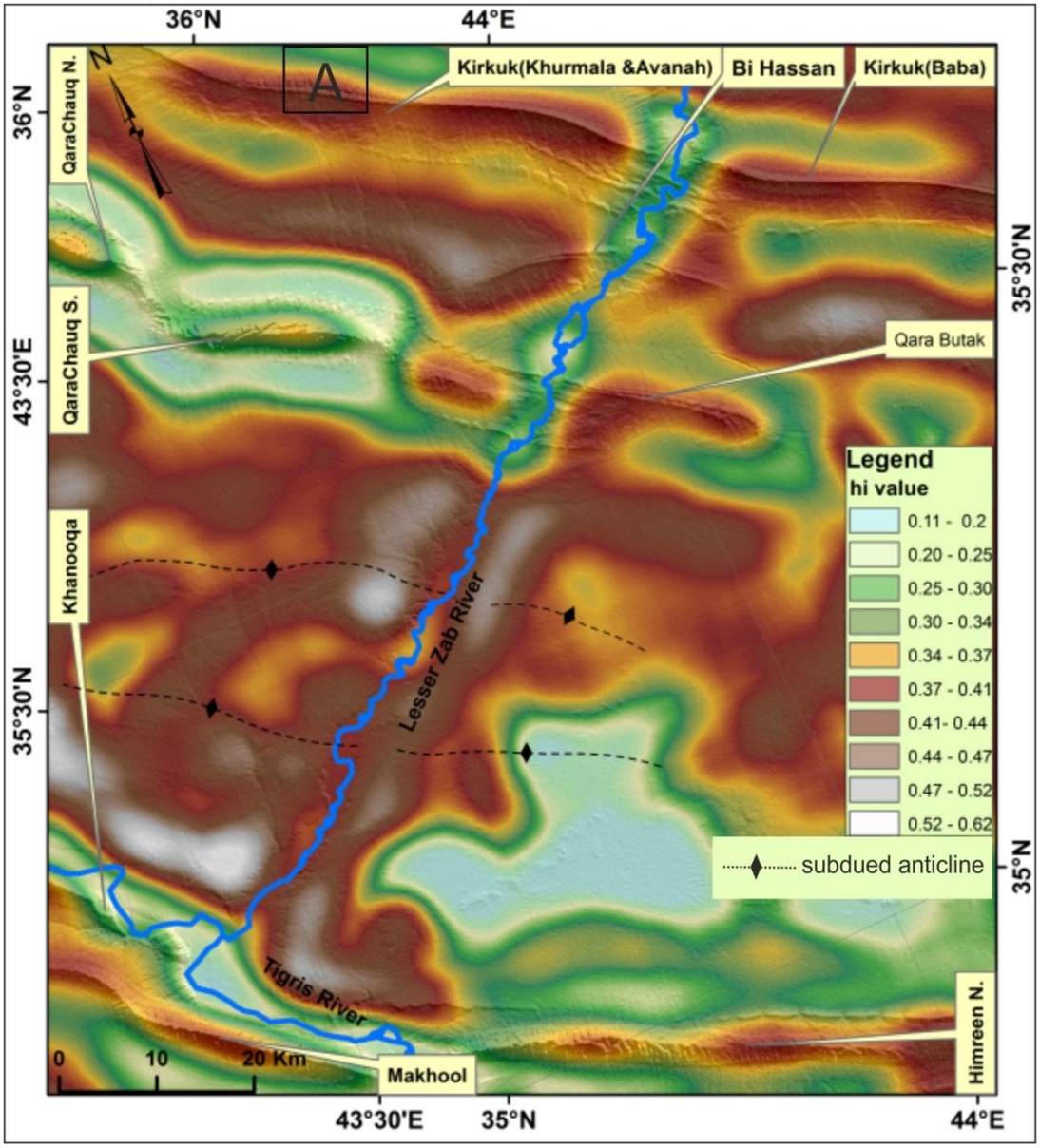

Appendix 3-2A: HI maps of the Kirkuk Embayment using moving window 50 pixels for the SRTM 30 m data

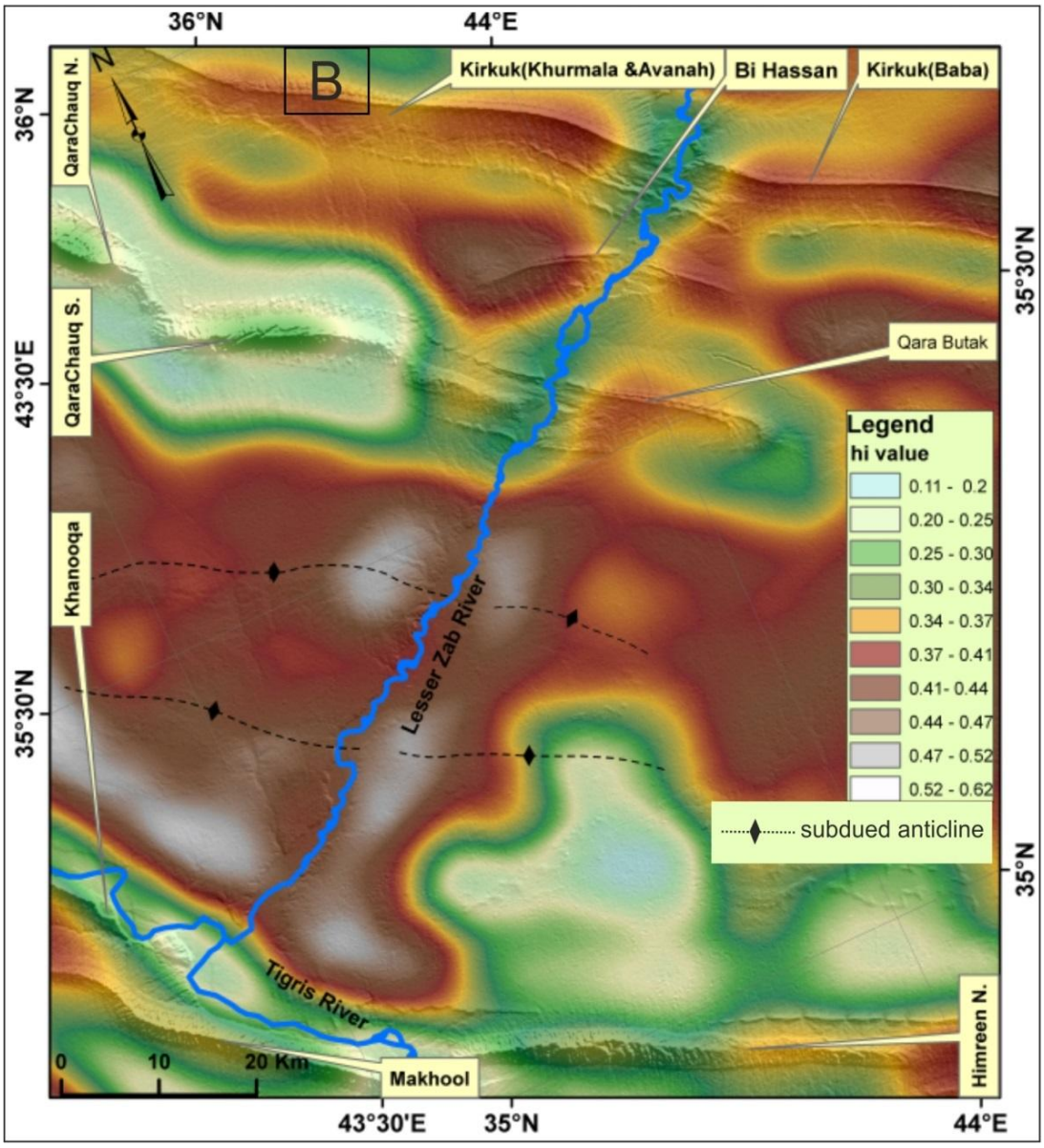

Appendix 3-2B: HI maps of the Kirkuk Embayment using moving window 100 pixels for the SRTM 30 m data

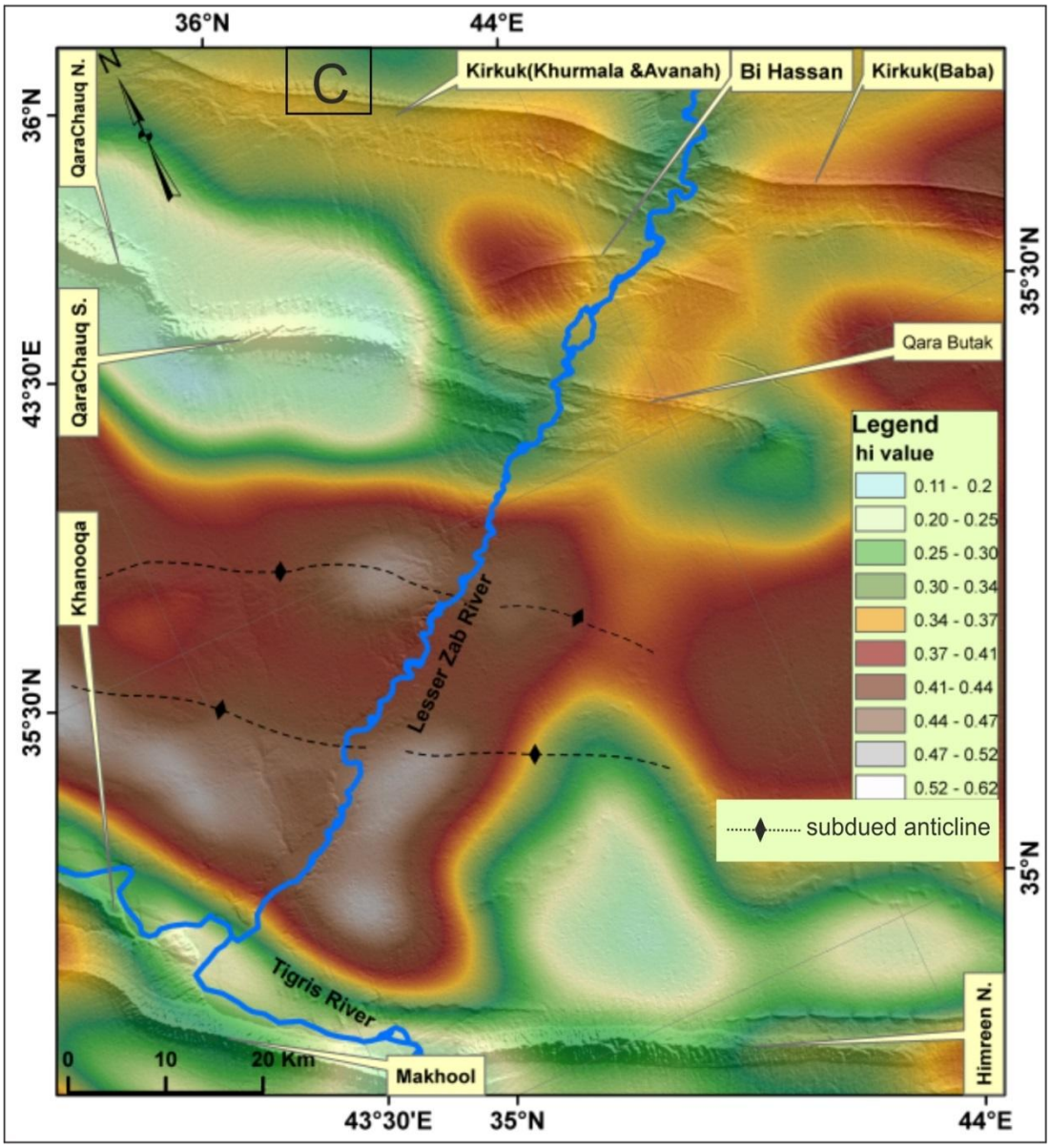

Appendix 3-2C: HI maps of the Kirkuk Embayment using moving window 150 pixels for the SRTM 30 m data

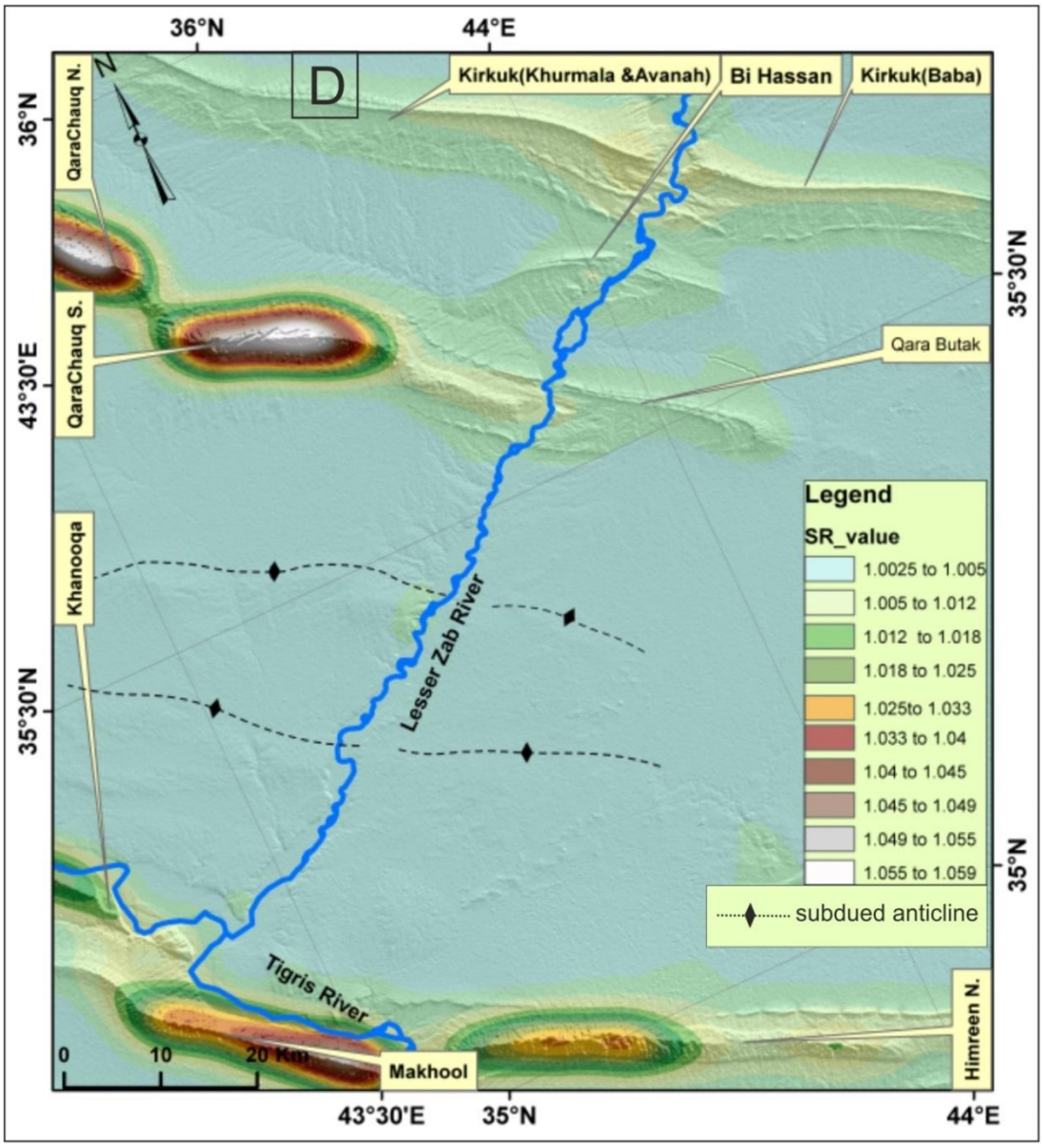

Appendix 3-2D: SR maps of the Kirkuk Embayment using moving window 50 pixels for the SRTM 30 m data

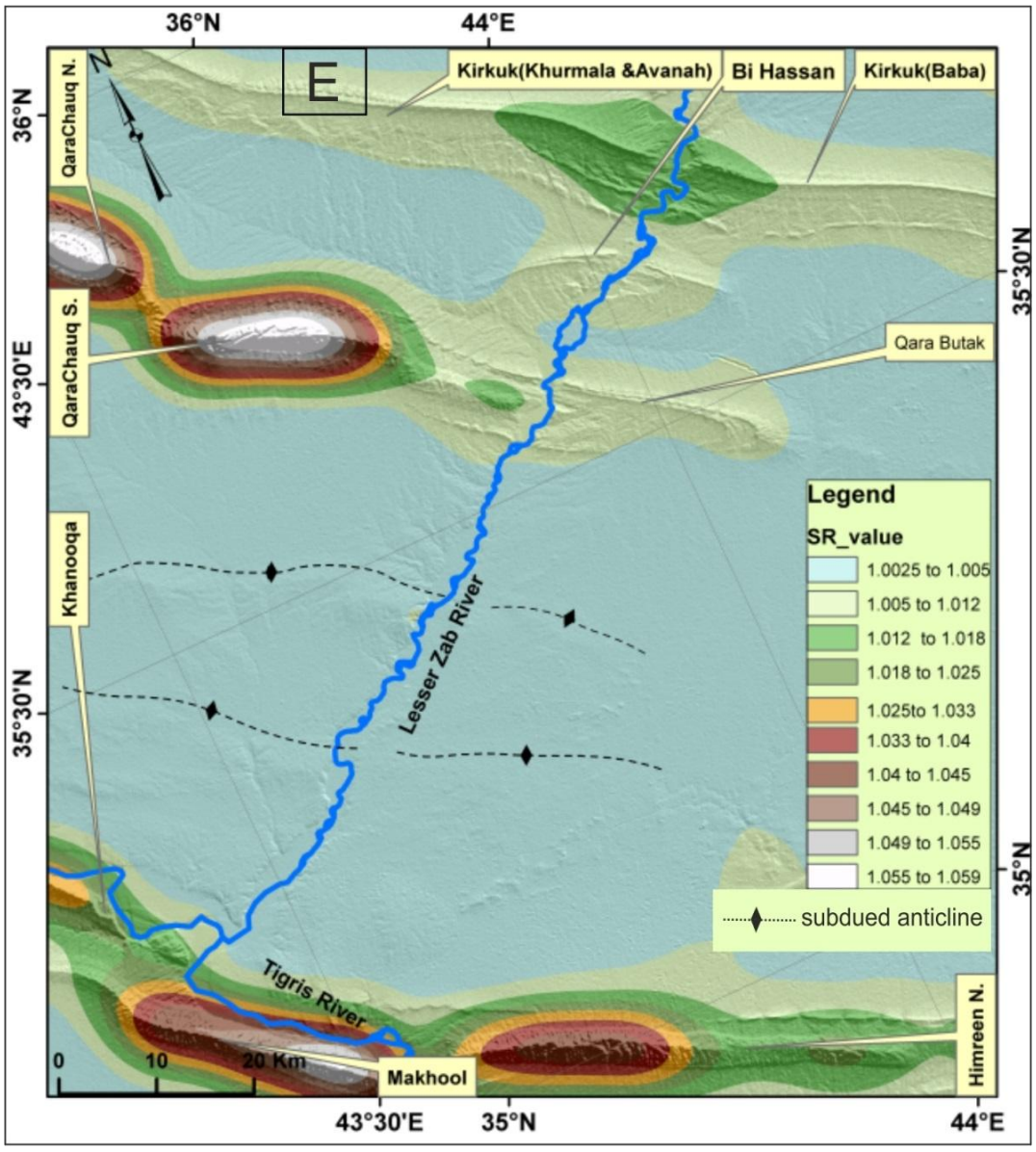

Appendix 3-2E: SR maps of the Kirkuk Embayment using moving window 100 pixels for the SRTM 30 m data

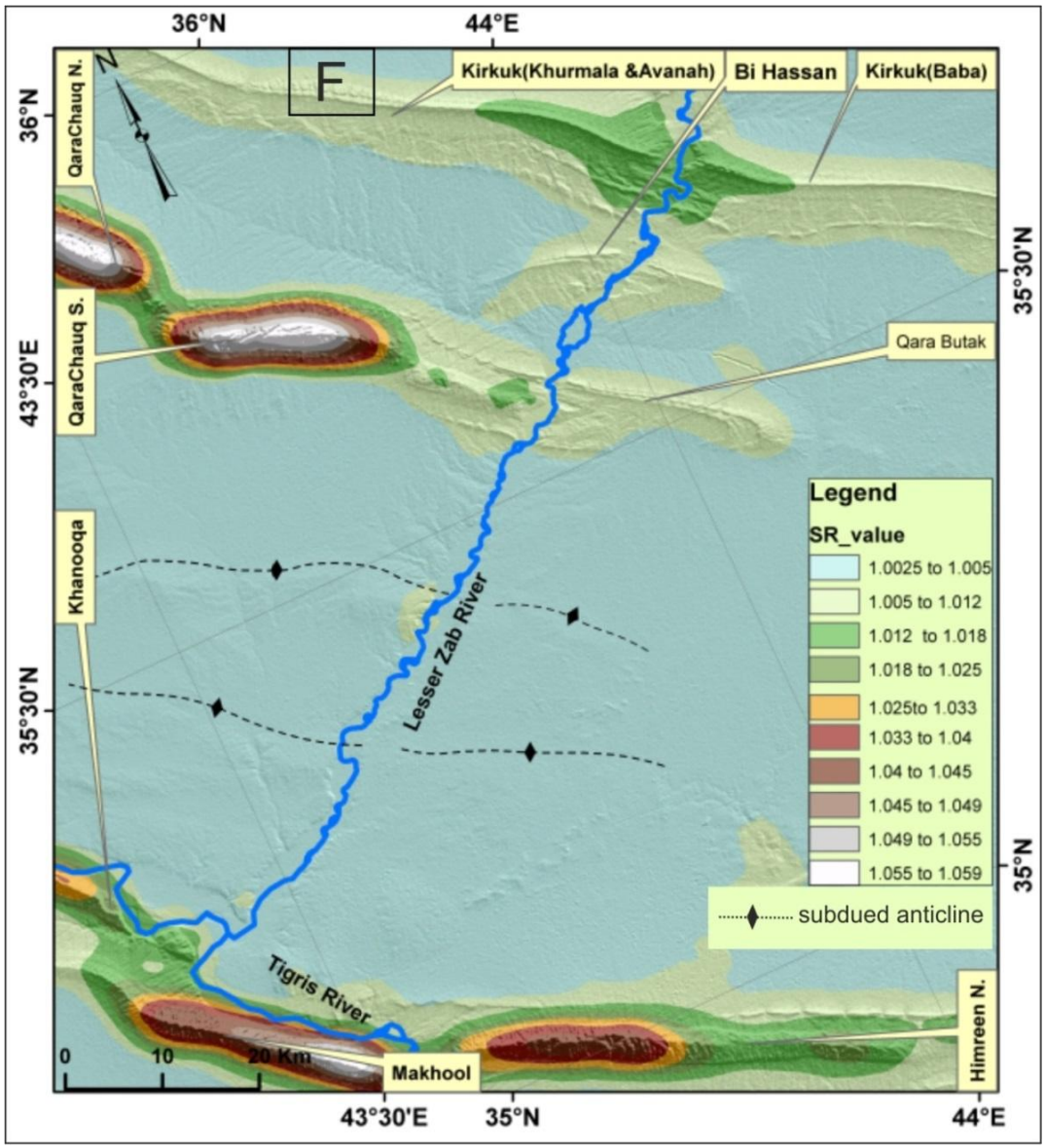

Appendix 3-2F: SR maps of the Kirkuk Embayment using moving window 150 pixels for the SRTM 30 m data

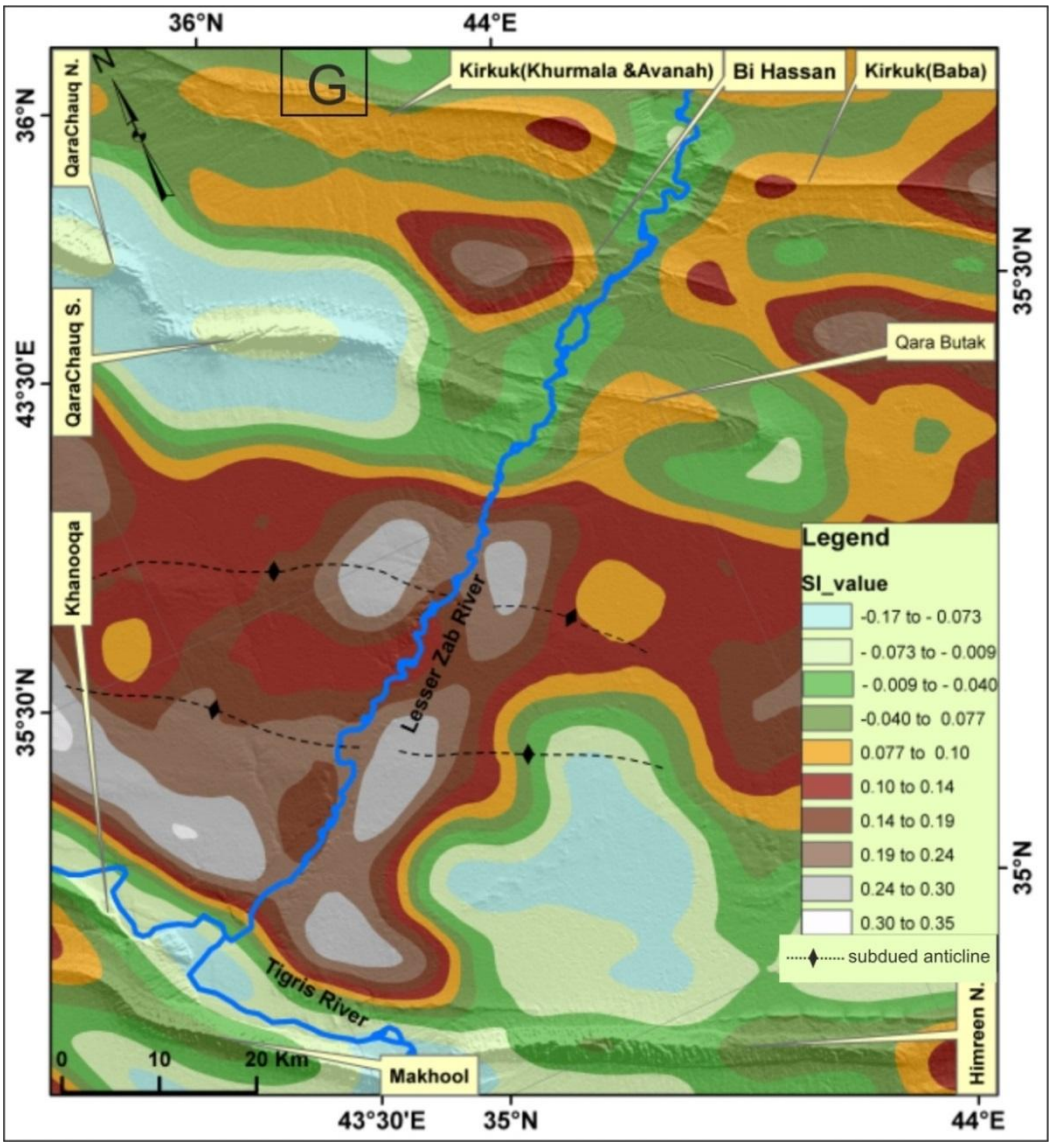

Appendix 3-2G: SI maps of the Kirkuk Embayment using moving window 50 pixels for the SRTM 30 m data

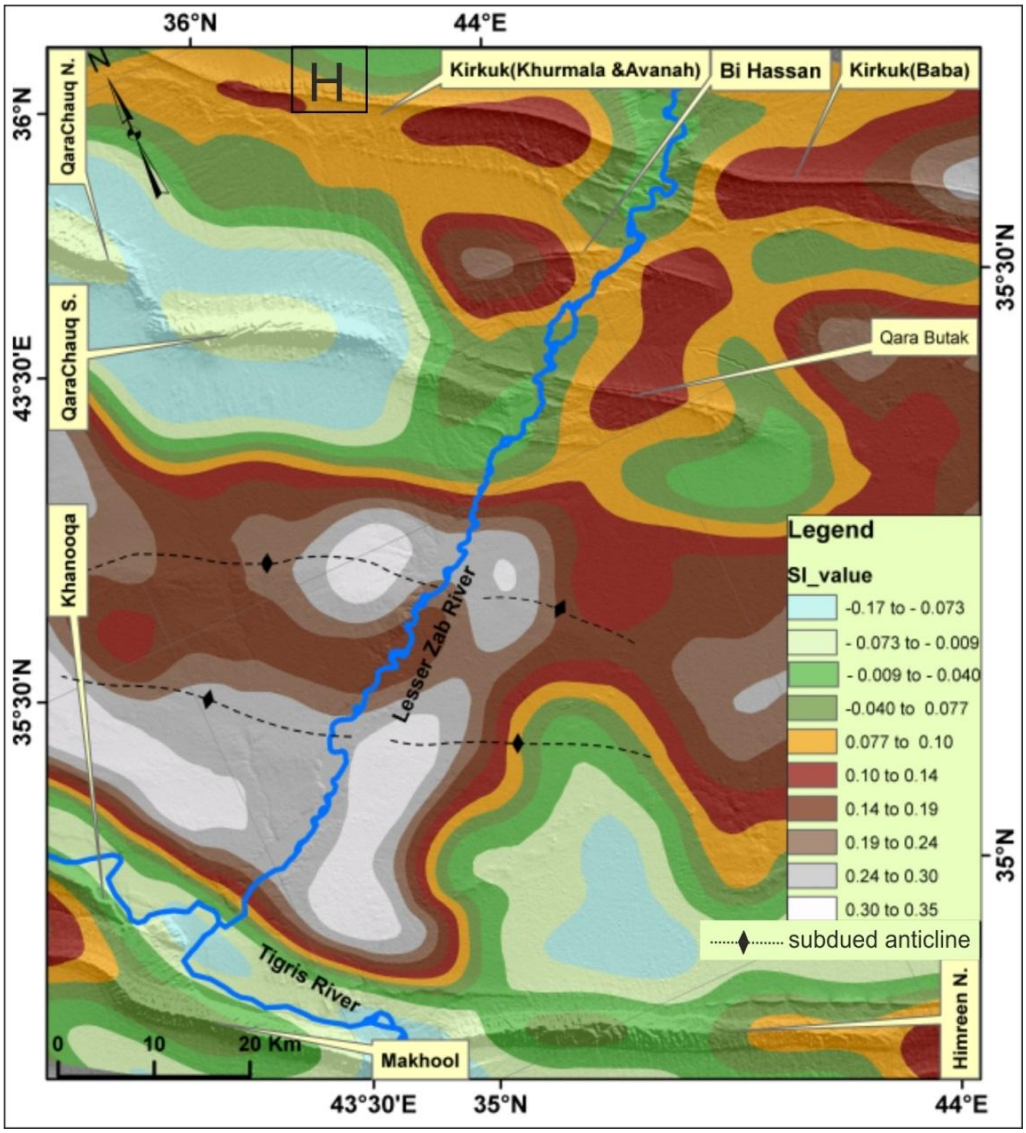

Appendix 3-2H: SI maps of the Kirkuk Embayment using moving window 100 pixels for the SRTM 30 m data

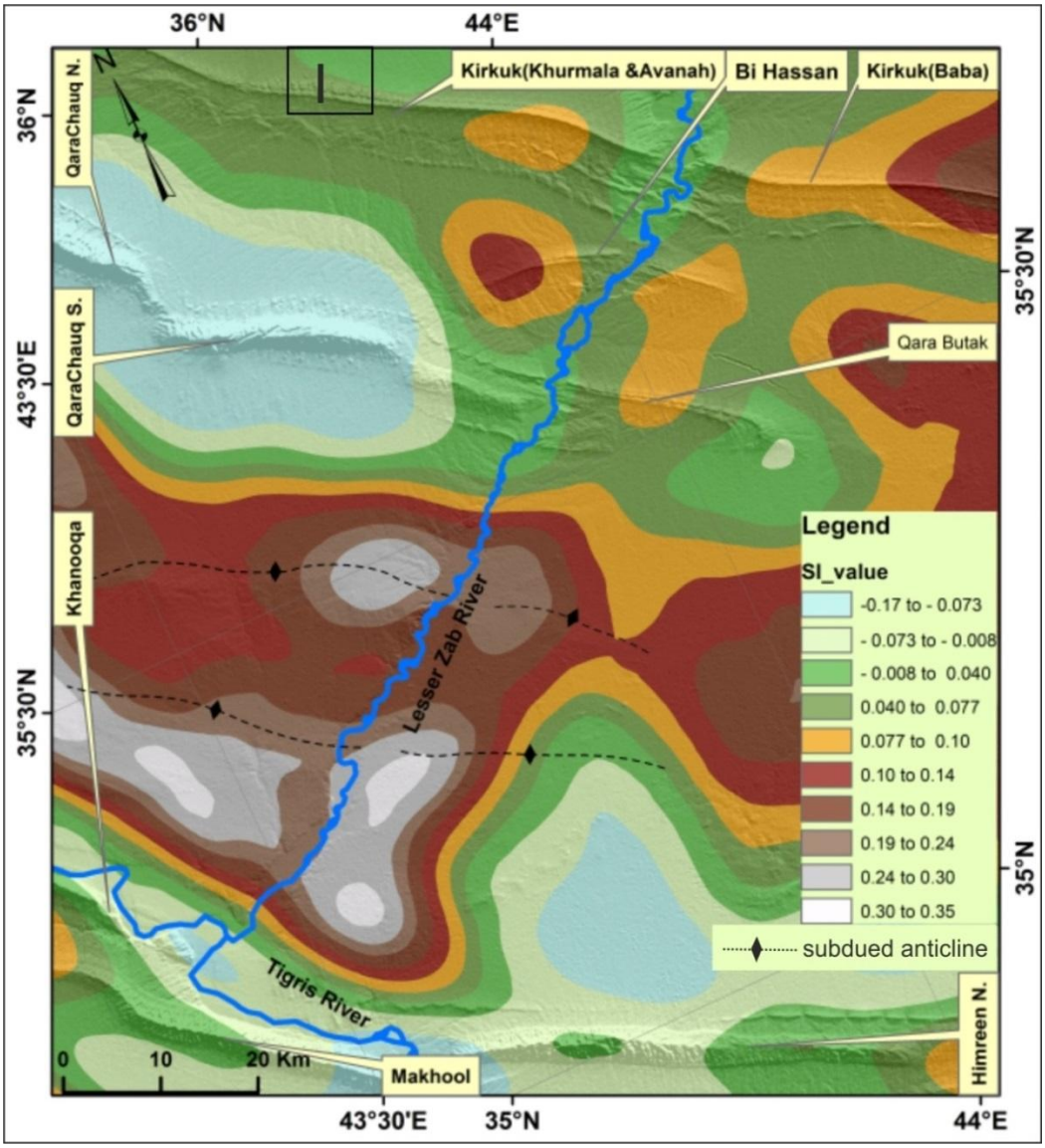

Appendix 3-2I: SI maps of the Kirkuk Embayment using moving window 150 pixels for the SRTM 30 m data

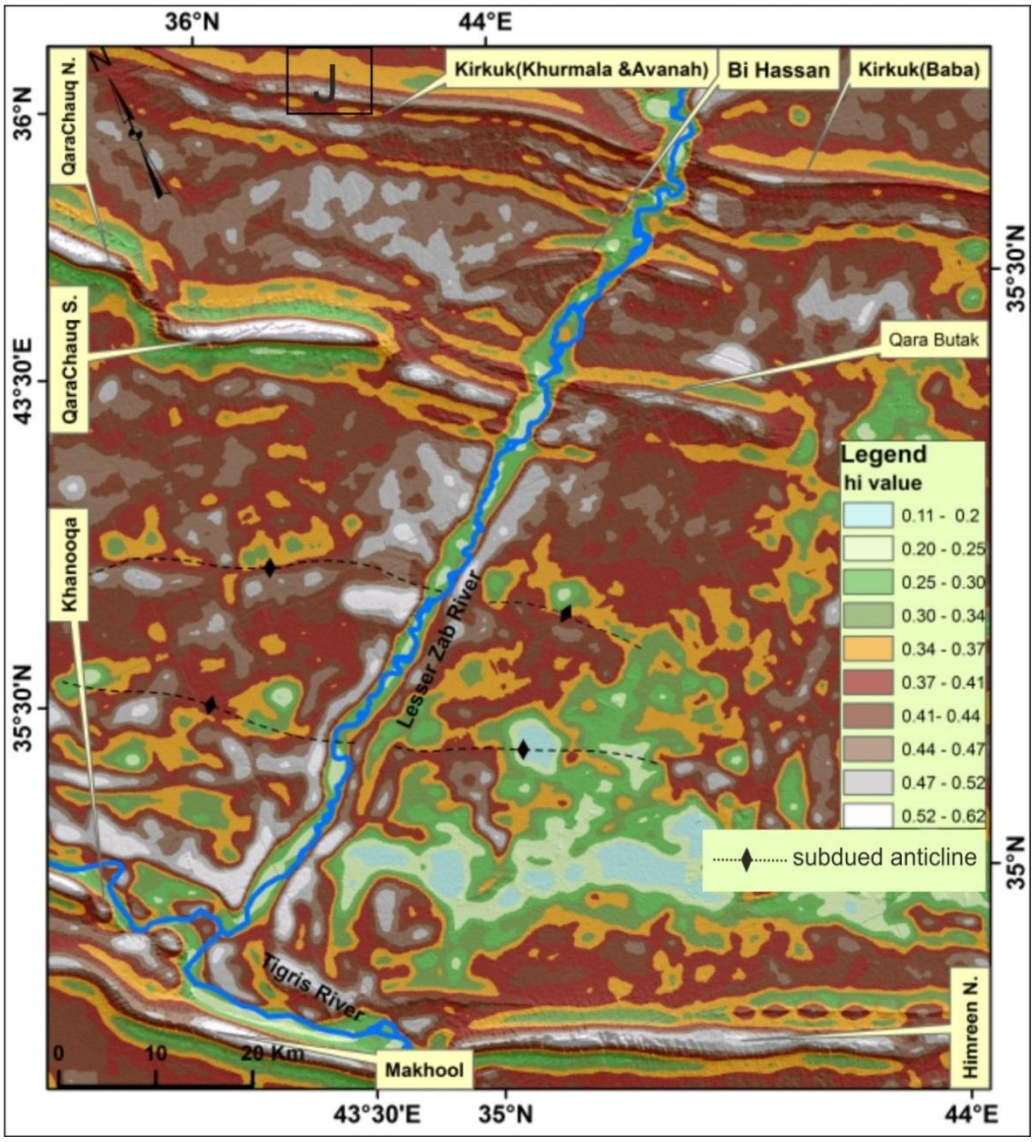

Appendix 3-2J: HI maps of the Kirkuk Embayment using moving window 10 pixels for the SRTM 90 m data

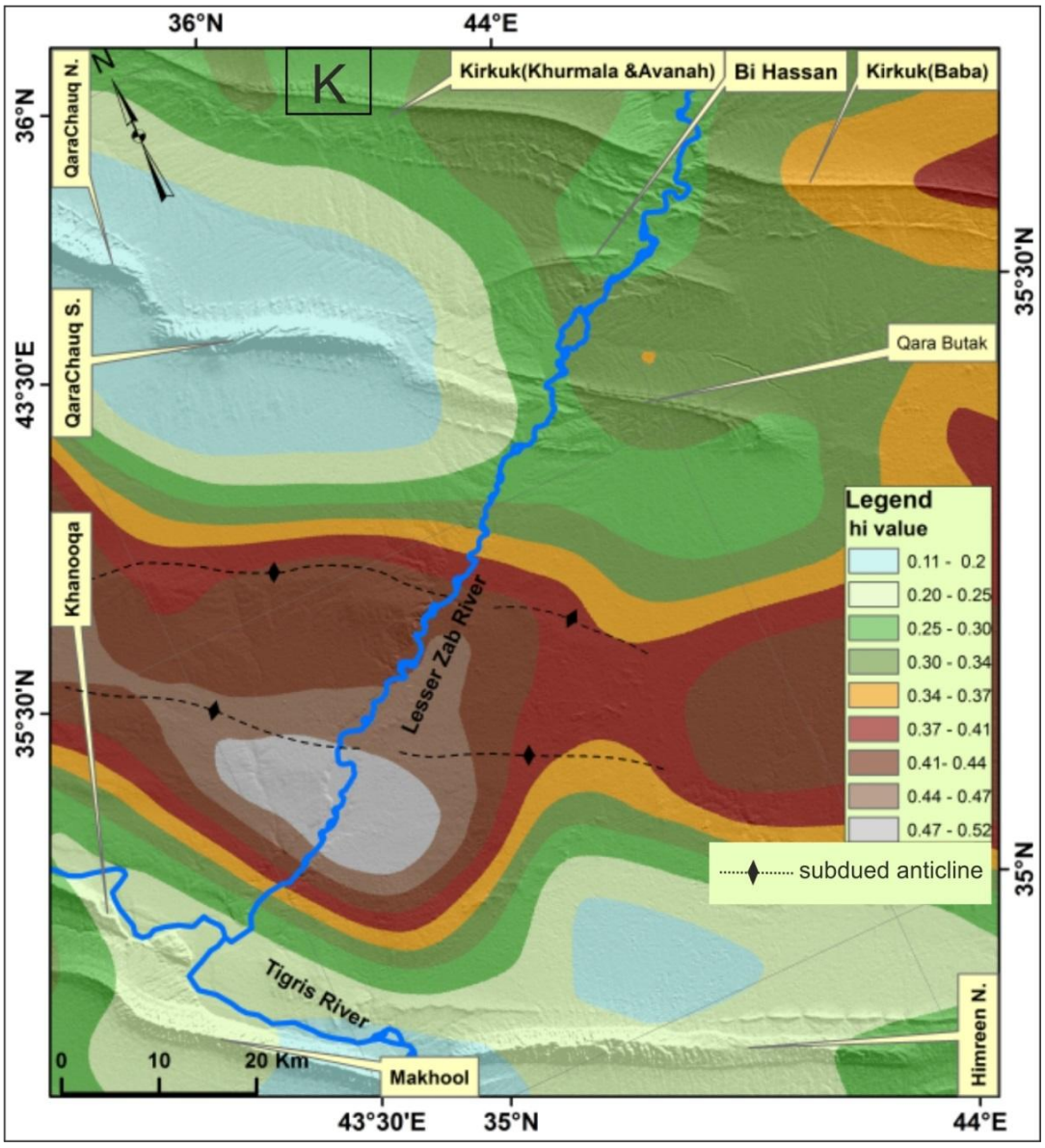

Appendix 3-2K: HI maps of the Kirkuk Embayment using moving window 100, pixels for the SRTM 90 m data

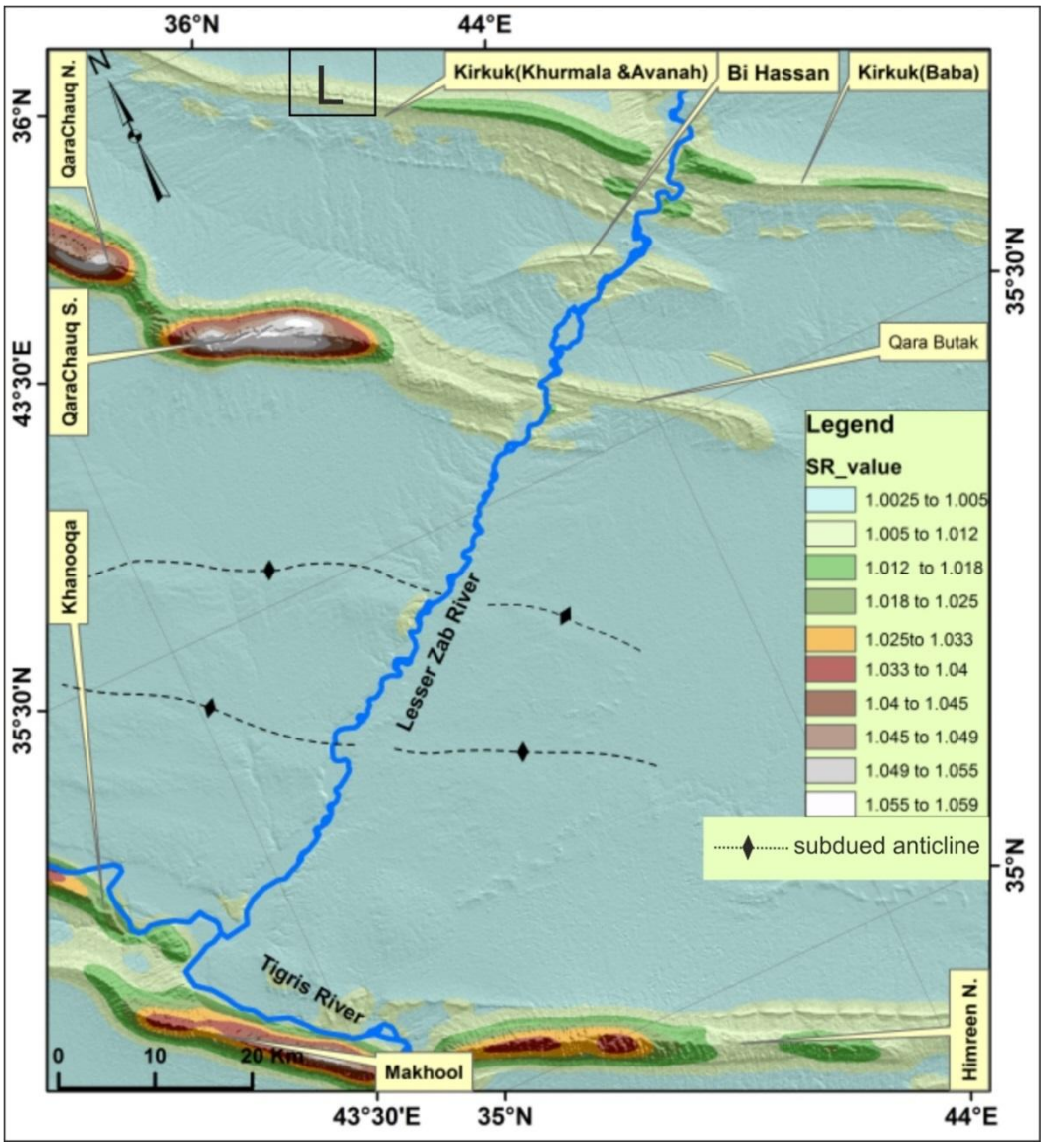

Appendix 3-2L: SR maps of the Kirkuk Embayment using moving window 10 pixels for the SRTM 90 m data

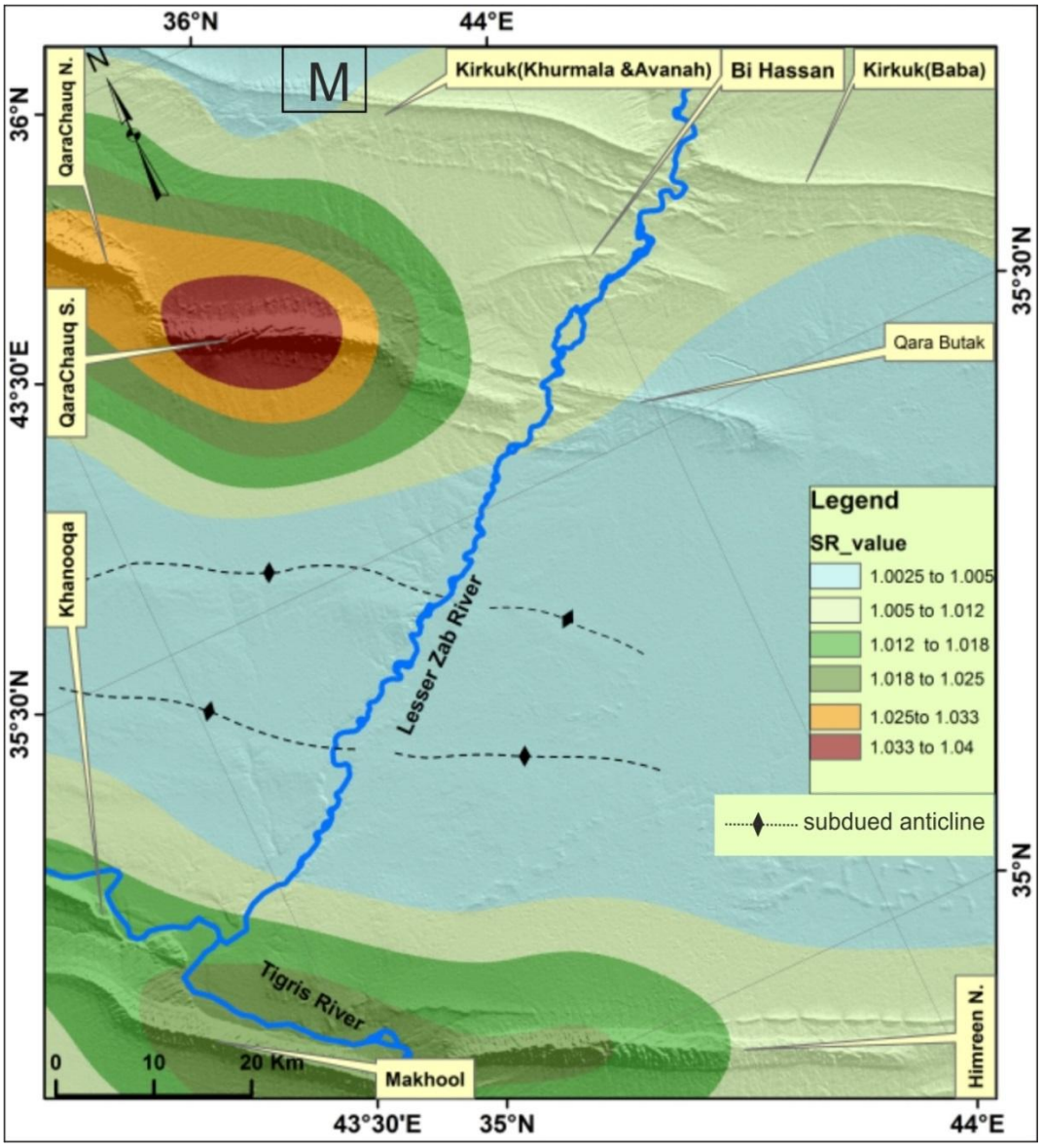

Appendix 3-2M: SR maps of the Kirkuk Embayment using moving window 100 pixels for the SRTM 90 m data

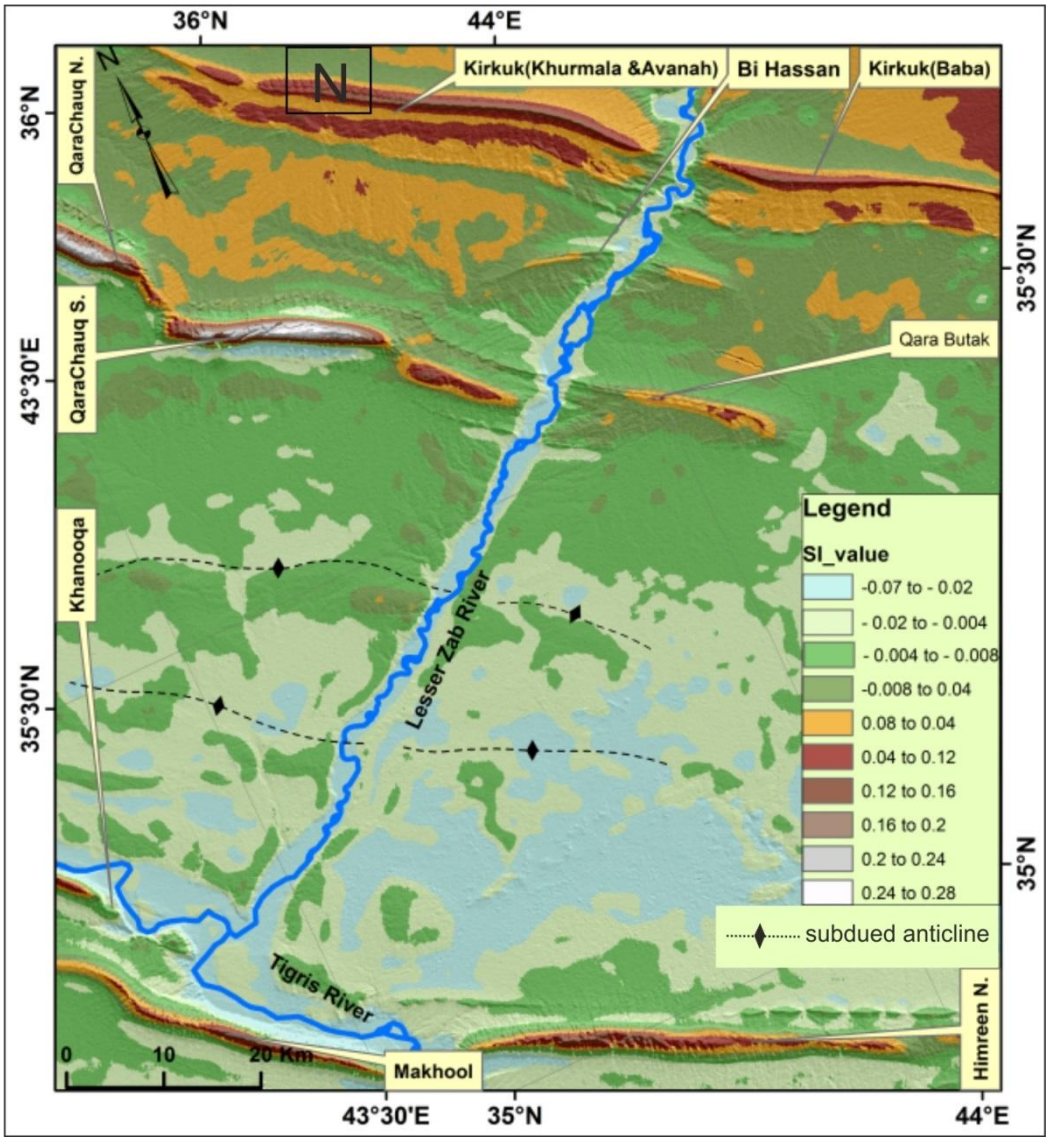

Appendix 3-2N: SI maps of the Kirkuk Embayment using moving window 10 pixels for the SRTM 90 m data

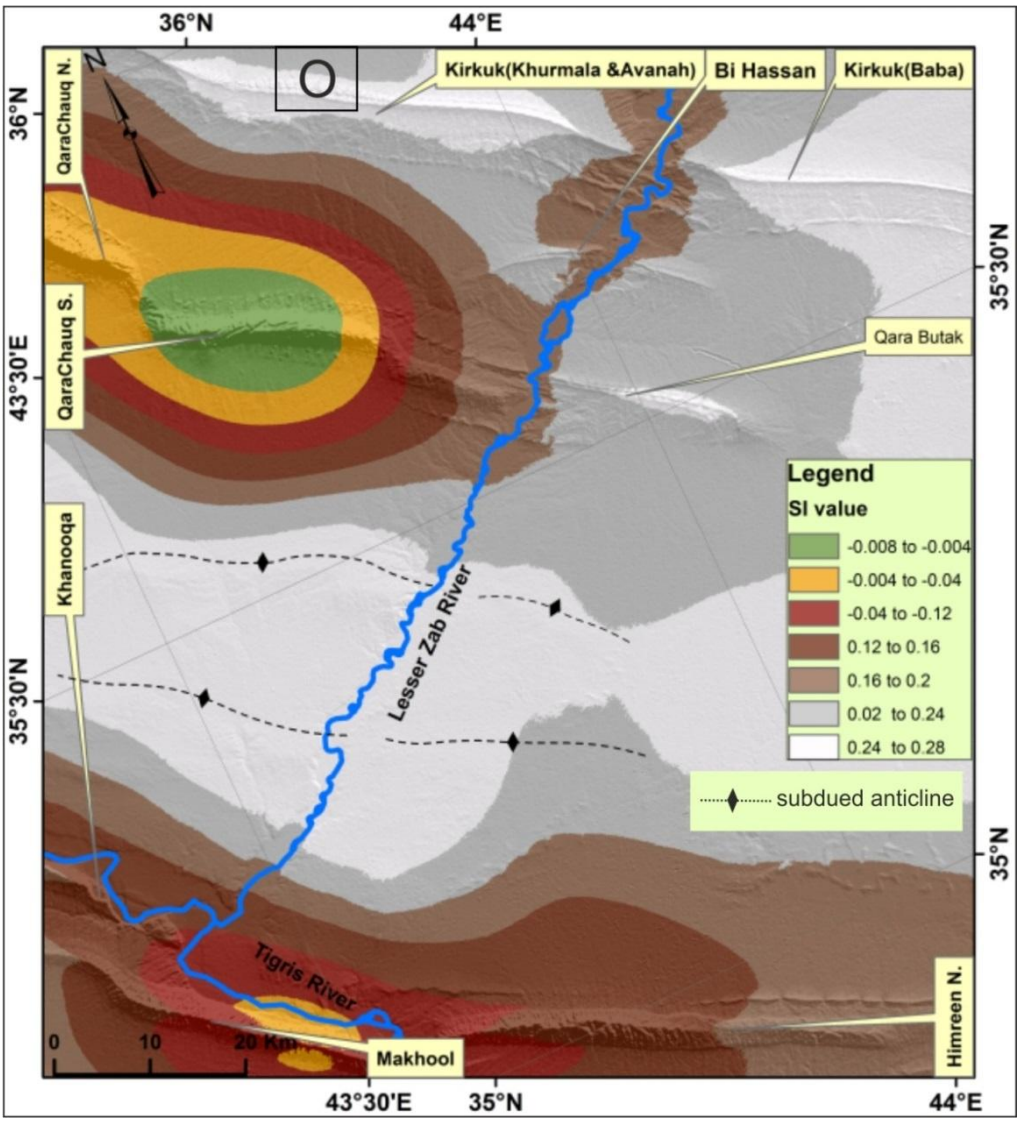

Appendix 3-2O: SI maps of the Kirkuk Embayment using moving window 100 pixels for the SRTM 90 m data

.

Appendix 4: Method of testing mineral identity using SEM.

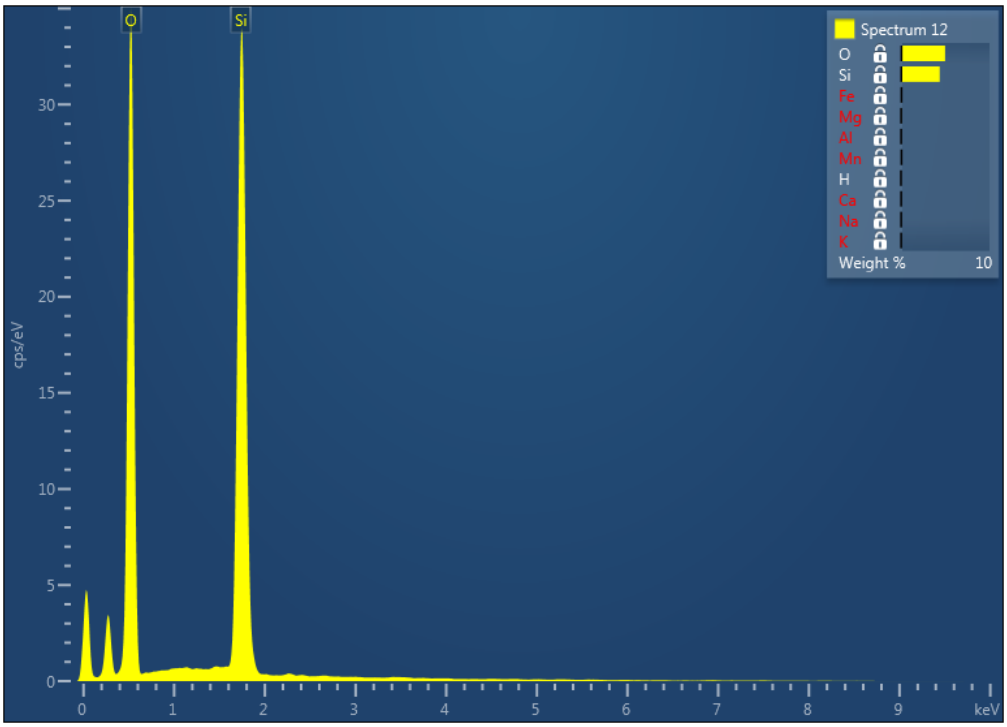

Appendix 4A: SEM spectral analysis shows the identification of polycrystalline quartz grain within lithic fragments in Fig. 5.6. The composition refers to quartz, which is composed of Si and O.

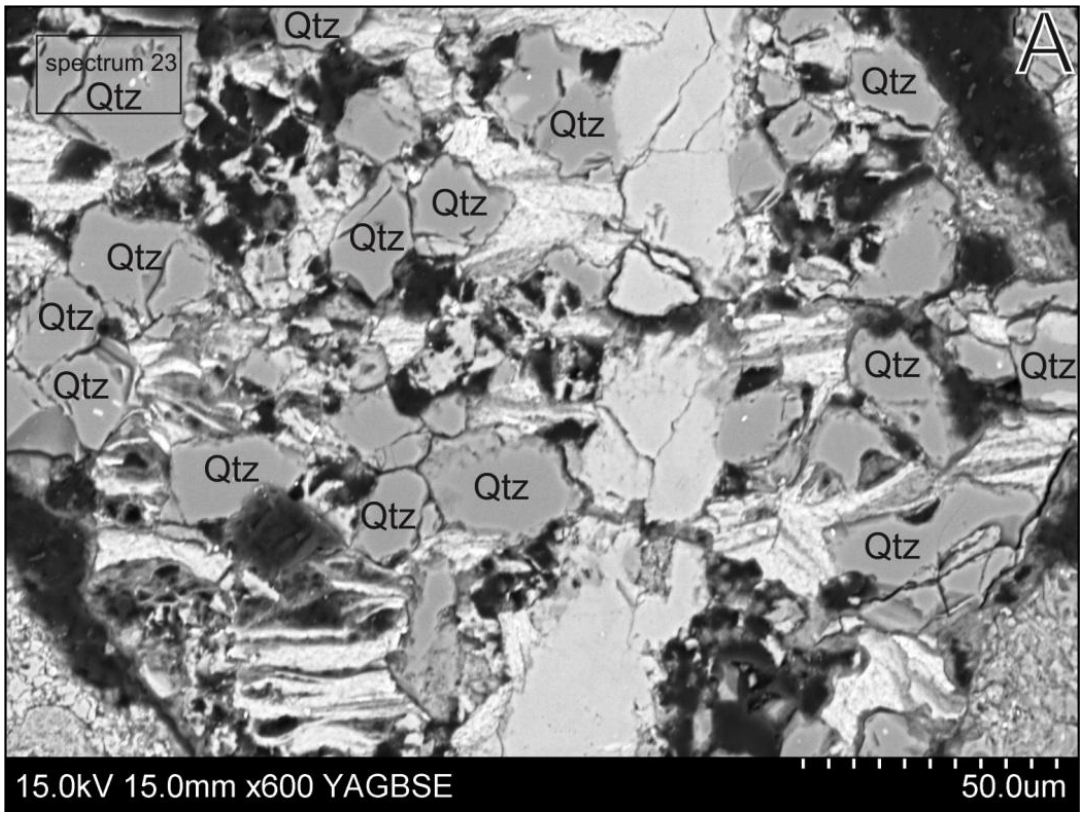

Appendix 4B: SEM plate shows the polycrystalline quartz occurrence within sedimentary fragment of the Bai Hassan Formation in the Erbil area. Qtz = quartz.

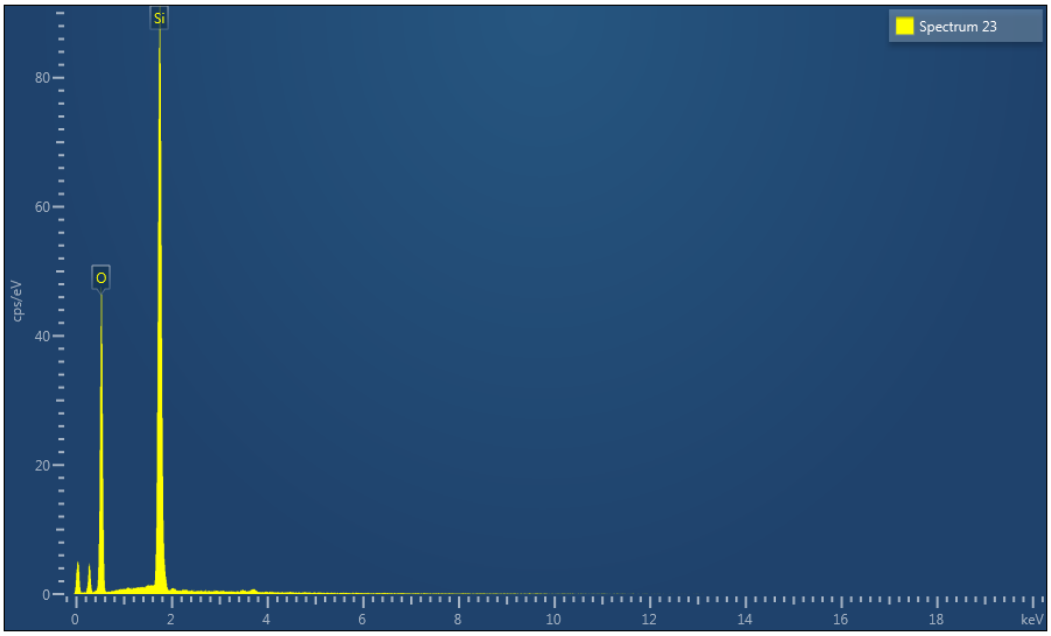

Appendix 4B: SEM spectrum analysis shows the silicon and oxygen elements contained in the grain, noted as spectrum 23 in Appendix 4B.